2008-ISAL-0038 2008

Thèse

A Full-System Finite Element Approach to Elastohydrodynamic Lubrication Problems : Application to Ultra-Low-Viscosity Fluids

Présentée devant
L'Institut National des Sciences Appliquées de Lyon

Pour obtenir
Le grade de Docteur

Formation doctorale : Mécanique
École doctorale : Mécanique, Energétique, Génie civil, Acoustique (MEGA)

Par
Wassim HABCHI
(Ingénieur)

Soutenue le 1er Juillet 2008 devant la Commission d'examen

Jury MM.

Président	D. Dureisseix	Professeur (Université Montpellier II)
Rapporteur	H. P. Evans	Professeur (Cardiff University U.K.)
Co-directeur	D. Eyheramendy	Professeur (E. C. de Marseille)
Examinateur	G. Morales-Espejel	Ingénieur de recherche PhD (SKF ERC – Netherlands)
Rapporteur	D. J. Schipper	Professeur (University of Twente – Netherlands)
Directeur	P. Vergne	Directeur de recherche (CNRS - INSA de Lyon)

Laboratoire de recherche : Laboratoire de Mécanique des Contacts et des Structures
(LaMCoS, INSA – Lyon CNRS UMR 5259)

A Full-System Finite Element Approach to Elastohydrodynamic Lubrication Problems: Application to Ultra-Low-Viscosity Fluids

Abstract

In this thesis, a full-system finite element approach to elastohydrodynamic (EHD) lubrication problems is introduced. EHD lubrication is a full-film regime where the pressure generated in the conjunction is high enough to induce a significant elastic deformation of the contacting bodies. Hence, it involves a strong coupling between hydrodynamic and elastic effects. The non-linear system formed by the Reynolds', linear elasticity and load balance equations is solved using a fully-coupled Newton-Raphson procedure. This approach provides outstanding convergence rates when compared with the semi-system one. A penalty method is used to handle the cavitation problem that arises at the outlet of the contact. Appropriate stabilized formulations are used to extend the solution to the case of highly loaded contacts. The resolution process is then extended to account for non-Newtonian behaviour of the lubricant and for thermal effects. The developed model is used to study the behaviour of EHD contacts lubricated with Ultra-Low-Viscosity Fluids. The use of such fluids as lubricants provides two main advantages: first, the frictional energy dissipation in the contact is reduced and second, in machines that work with a low viscosity operational fluid and a lubricant, the former can be used to fulfil both functions and thus the design and maintenance of such machines would become easier and their performance would be improved.

Keywords: EHD lubrication, fully coupled nonlinear finite elements, ultra-low-viscosity lubricants.

Une Approche Éléments Finis avec Couplage Fort des Problèmes de Lubrification Élastohydrodynamique : Application aux Fluides de Très Faible Viscosité

Résumé

Cette thèse présente un modèle éléments finis avec couplage fort des problèmes de lubrification élastohydrodynamique (EHD). La lubrification EHD consiste en une séparation complète des surfaces en contact par un film complet de lubrifiant dans lequel est générée une pression suffisemment élévée pour engendrer une déformation élastique significative des surfaces. Ainsi, un couplage fort entre les effets hydrodynamiques et les effets élastiques s'établit. Le système non-linéaire formé par les équations de Reynolds, d'élasticité linéaire et d'équilibre des charges est résolu de manière couplée par une approche de type Newton-Raphson. Cette approche permet d'avoir de très bons taux de convergence par rapport à l'approche classique avec couplage faible. Le problème de frontière libre de cavitation à la sortie du contact est traité par le biais d'une méthode de pénalisation. Des formulations de stabilisation appropriées sont utilisées pour étendre la résolution à des cas de contacts fortement chargés. Ensuite, le comportement non-Newtonien du lubrifiant et les effets thermiques sont pris en compte. Le modèle développé est utilisé pour étudier l'utilisation des Fluides de Très Faible Viscosité dans les contacts EHD. L'utilisation de tels fluides en tant que lubrifiants offre deux avantages principaux: tout d'abord, la dissipation d'énergie dans le contact par frottement est réduite et ensuite, dans le cadre de machines qui opèrent avec un fluide de fonction (généralement de faible viscosité) et un lubrifiant, le premier pourrait être utilisé pour remplir les deux fonctions. Cela permettrait une conception et une maintenance plus faciles de la machine en plus d'une amélioration de ses performances.

Mots-Clés: Lubrification EHD, éléments finis nonlinéaires couplés, lubrifiants à très faible viscosité.

Preface

This work was carried out at the "**La**boratoire de **M**écanique des **Co**ntacts et des **S**tructures" (LaMCoS, UMR CNRS 5514) of the "**I**nstitut **N**ational des **S**ciences **A**ppliquées" (INSA) of Lyon.

I wish to express my gratitude to SKF ERC in the Netherlands and the French Ministry of National Education and Scientific Research for financing this study. I thank Pr. E. Ioannides (SKF Group Technical Director) for his kind permission to publish the different papers that stemed from this work. Special thanks go to Dr. G. Morales-Espejel for establishing the link with SKF ERC and for the many helpful discussions we had in the last three years. On a personal level, I would also like to thank him for his kindness and care which were always gratifying.

I am extremely grateful to Dr. P. Vergne for hosting me within his team and advising me throughout this work. My extreme gratitude also goes to Pr. D. Eyheramendy for co-advising this work. On a scientific level, they perfectly combined their knowledge to provide me with a solid backup whenever it was needed. I also wish to thank them for their trust and encouragement without which much of this work wouldn't have seen the light. Finally, on a personal level, it was extremely pleasant for me to work with them for the past three years during which their kindness and great attention helped settle a very healthy working environment.

I would like to thank Pr. H. P. Evans and Pr. D. J. Schipper for their interest in this work and for accepting to review this manuscript. I also thank them along with Pr. D. Dureisseix and Dr. G. Morales-Espejel for being part of the jury.

I wish to express my gratitude to Drs. S. Bair and I. Demirci for their valuable contribution to this work. I also thank all the LaMCoS members and especially the ML2 team for their hospitality and for sharing some special moments. Special thanks go to Pr. G. Bayada, Dr. B. Bou-Said, Pr. G. Dalmaz, Dr. M-H. Meurisse and Pr. Y. Renard for the many helpful discussions. I would also like to thank Dr. N. Bouscharain, Mr. N. Devaux and Mr. G. Roche without whom much of the experimental part in this work wouldn't have been possible. I also thank Dr. N. Fillot for being a very pleasant office partner and sharing my everyday's life joys and problems. I also thank him for the very interesting scientific discussions we had through the years.

I also wish to thank Céline, Fabrice, Titi and the "poker team": Baptiste, Guillaume, Hervé, Nico, Simon and Vincent for the very special moments we had together. Special

thanks go to Baptiste for always “**trying**” to animate the moments we shared. Although it never worked, I guess for many of us, you made us forget our everyday’s worries …

Finally, I wish to thank all my friends and family for their support. Mom and Dad, thank you for making all the sacrifices you made throughout the years so I can get to where I am today. Special thanks go to Mayyouch who has always been there on my side and shared my good and bad moments during the last five years …

Contents

Résumé étendu

Introduction

Le frottement et l'usure font partie intégrante de notre vie de tous les jours. Ces deux phénomènes ont lieu à chaque fois que deux corps rentrent en contact avec un mouvement relatif l'un par rapport à l'autre. Ils s'avèrent essentiels pour entreprendre des activités quotidiennes fondamentales telles que: marcher, brosser ses dents … Mais en général, dans un système mécanique, le frottement et l'usure (bien que des fois essentiels) s'avèrent nocifs à plusieurs niveaux. Le frottement mène à une consommation plus élevée d'énergie dans le système et l'usure à sa dégradation et la réduction de sa durée de vie. Ainsi, dans une machine typique (moteur à combustion, turbine, compresseur …) il est important de controler ces deux phénomènes. D'un point de vue énergétique, réduire le frottement et par conséquent la dissipation d'énergie dans les différents contacts d'un système aide à améliorer son rendement. D'un point de vue fiabilité, éviter la dégradation des surfaces (fatigue, fissurations …) permet de rallonger la durée de vie du mécanisme et d'éviter sa défaillance. L'importance de ces problèmes dans les applications industrielles justifie les efforts qui ont été menés dans le domaine de la Tribologie durant ce dernier siècle.

Un moyen de réduire le frottement dans un contact consiste à le lubrifier. En d'autres termes, séparer les surfaces en contact par un film de lubrifiant, ce dernier pouvant être liquide, gazeux, voire même solide. La mise en place et la préservation du film requiert une génération de pression dans ce dernier. Quand celle-ci est assurée par un système externe (tel un compresseur par exemple), la lubrification est dite « hydrostatique », tandis que si elle est produite par le mouvement relatif des surfaces en contact, la lubrification est dite « hydrodynamique ». Dans un contact lubrifié, les forces de frottement sont nettement moins importantes que dans un contact sec car le mouvement relatif des surfaces est accomodé par le cisaillement du film de lubrifiant. Une bonne compréhension et maîtrise de ces contacts est essentielle pour la conception des composants mécaniques afin d'établir des conditions opératoires optimales et de rallonger leur durée de vie.

En général, on définit 3 régimes de lubrification, suivant l'ordre de grandeur du coefficient de frottement correspondant (Courbe de Stribeck, voir Figure 0.1) :

- **Lubrification limite :** une partie majeure de la charge à laquelle est soumis le contact est supportée par le contact direct entre les aspérités des surfaces. Ce régime se distingue par des coefficients de frottement relativement élevés.

- **Lubrification mixte :** la charge est supportée à la fois par le contact direct des aspérités et par le film lubrifiant. Le coefficient de frottement correpondant est plus faible que celui du régime limite.

- **Lubrification complète :** les surfaces en contact sont séparées par un film complet de lubrifiant. Les coefficients de frottement sont relativement faibles.

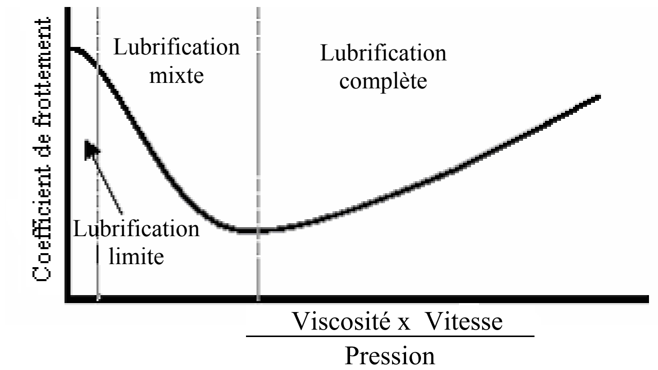

Figure 0.1: Courbe de Stribeck présentant les différents regimes de lubrification

Cette étude concerne le régime de lubrification complète. On distingue 2 types de lubrification:

- **Lubrification Hydrodynamique** qui se manifeste quand la pression générée dans le contact n'induit pas de déformation élastique des surfaces en contact. Cela se produit typiquement dans les contacts conformes, caractérisés par des larges surfaces de contact et ainsi des pressions faibles. Les paliers hydrodynamiques sont représentatifs de ce type de lubrification (Voir Figure 0.2).

- **Lubrification Elastohydrodynamique (EHD)**, comme son nom l'indique, se produit quand la pression générée dans le film lubrifiant est suffisemment élevée pour induire une déformation élastique significative des surfaces en contact. Ces déformations ont une influence importante sur la géométrie du film et peuvent même être plus importantes que l'épaisseur de ce dernier. D'autre part, les propriétés rhéologiques du lubrifiant sont largement affectées par les pressions élevées générées dans le film (la viscosité peut varier de plusieurs ordres de grandeur). C'est typiquement le cas des contacts non-conformes qui sont rencontrés par exemple dans les engrenages, les roulements à rouleaux cylindriques ou aussi les roulements à billes (Voir Figure 0.2).

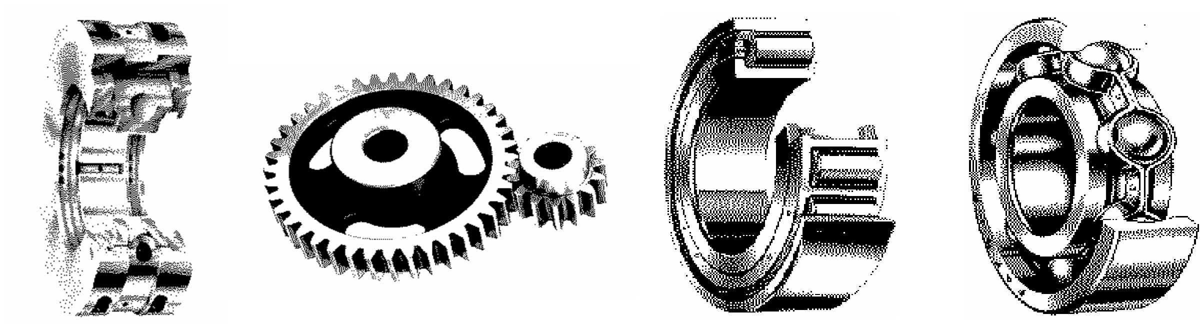

(a) (b) (c) (d)

Figure 0.2: Exemples de lubrification hydrodynamique: (a) palier hydrodynamique et de lubrification élastohydrodynamique (b) engrenages, (c) roulement à rouleaux cylindriques et (d) roulement à bille

L'étude envisagée dans cette thèse concerne surtout ce dernier type de lubrification. Pour étudier ces contacts, il n'est pas nécessaire de considérer la géométrie complète souvent assez complexe du système. Puisque l'épaisseur de film et la taille du contact sont généralement faibles comparés aux rayons de courbure locaux des surfaces en contact, la géométrie des surfaces dans la zone de contact peut très bien être approximée par des paraboloides. Cette approximation permet de simplifier énormément la géométrie du contact, qui se réduit au contact entre un paraboloide et une surface plane.

En général, on distingue deux types de contacts EHD :

- **Contacts linéiques :** les éléments en contact sont considérés infiniment longs dans une des directions principales. En fait, les rayons de courbure des paraboloides dans cette direction sont infinis. Dans le cas d'un contact sec non-chargé, les surfaces se touchent suivant une ligne. Si une charge est appliquée, la zone de contact prend la forme d'une bande infiniment longue à cause des déformations élastiques des surfaces. Ce genre de contacts a lieu dans les engrenages à dentures droites ou dans les roulements à rouleaux cylindriques par exemple (Voir Figure 0.2).

- **Contacts ponctuels :** l'approximation la plus courante est celle du contact entre deux surfaces paraboliques ayant des rayons de courbure locaux différents dans les directions x et y. La direction x est choisie de telle sorte à coincider avec celle des vitesses des surfaces. Dans le cas d'un contact sec, les deux surfaces se touchent en un point. Quand une charge est appliquée, la forme de la zone de contact dépend du rapport des rayons de courbure des deux surfaces dans les deux directions x et y. En général, c'est une ellipse. C'est pourquoi ce type de contact est aussi appelé **contact elliptique.** Un exemple d'un contact ponctuel est celui du contact entre la bille et la cage d'un roulement à billes (Voir Figure 0.2). Le **contact circulaire** est un cas particulier du contact elliptique où les rayons de courbure des surfaces sont les mêmes dans les deux directions principales x et y.

La lubrification EHD des contacts circulaires fait l'objet du thème principal de cette thèse. Un intérêt particulier est porté à l'utilisation des Fluides de Très Faible Viscosité (FTFV) dans ce genre de contacts. Cette étude est motivée par une demande industrielle de SKF ERC implanté aux Pays-Bas. Cette demande se base sur plusieurs facteurs qui rendent l'utilisation de ces fluides en tant que lubrifiants assez intéressante pour différentes raisons dévelopées ci-dessous.

Intérêts de l'utilisation des FTFV en tant que lubrifiants

Avant de traiter les avantages de l'utilisation des FTFV en tant que lubrifiants, il est important de noter que l'ordre de grandeur de la viscosité de ces fluides est de 10^{-4} Pa.s. Comparés à l'eau ayant une viscosité de 10^{-3} Pa.s, ou à l'air dont la viscosité est de 10^{-5} Pa.s, les FTFV auxquels on s'intéresse ont donc une viscosité comprise entre celle de l'air et celle de l'eau.

Un aspect important de l'utilisation des FTFV en tant que lubrifiants est l'aspect économique. Il s'agit ici d'économie d'énergie, qui est considérée de plus en plus de nos jours comme un problème environnemental. En effet, la dissipation d'énergie par frottement dans un contact lubrifié augmente avec la viscosité du lubrifiant. Fox [31] montre qu'une économie de 4% de consommation de carburant dans un moteur Diesel peut être atteinte rien qu'en jouant sur la viscosité du lubrifiant. Évidemment, les conditions opératoires du contact deviennent plus sévères et les taux d'usure augmentent. Quoiqu'il en soit, un bon fonctionnement du système pourrait être obtenu en procédant à un traitement des surfaces en contact de façon à améliorer leur résistance à l'usure. Une alternative permettant aussi d'éviter la dégradation des surfaces consiste à ajouter un additif anti-usure au lubrifiant de base.

D'un autre côté, beaucoup de systèmes mécaniques fonctionnent avec deux fluides opératoires, chacun ayant un rôle différent. Le premier est le lubrifiant alors que le deuxième (ayant généralement une faible viscosité) peut avoir différentes fonctions suivant le type de machine concerné. Cela pourrait être un fluide de transfert (caloporteur) comme dans une pompe à chaleur ou un système de réfrigération par exemple, ou un combustible comme le gasole dans un moteur à combustion interne ou le liquide cryogénique dans un moteur à propulsion de fusée. Pour un bon fonctionnement de ce genre de machines, il est en général préférable que ces deux fluides ne se mélangent pas. Pour cela, elles sont conçues avec deux systèmes de circulation bien isolés, un pour chaque fluide. Non seulement cela rend leur conception et leur maintenance plus complexes, mais leur taille et leur poids augmentent aussi. Ainsi, il pourrait être intéressant de n'avoir qu'un seul fluide qui puisse remplir les deux fonctions à l'intérieur du système. Cela permettrait une conception et une maintenance moins fastidieuses de la machine, qui comporterait ainsi un seul système de circulation. Sachant que le lubrifiant ne pourrait presque jamais remplir la fonction du second fluide, la seule solution envisageable consiste à utiliser le FTFV en tant que lubrifiant.

Lubrification EHD : aperçu historique

Les premières étapes de la compréhension du phénomène de lubrification datent du 19$^{\text{ème}}$ siècle avec les travaux de Hirn [52] en 1854. Ensuite, en 1883, deux investigations expériementales menées par Beauchamp Tower [111] en Angleterre et Nicoli Petrov [96] en Russie mirent en évidence le fait que les surfaces rigides des solides en contact dans un palier hydrodynamique étaient complètement séparées par un film fluide. Ainsi, il a été établi que les forces de frottement dans de tels mécanismes sont gouvernées par les effets hydrodynamiques et non pas par le contact direct entre les solides. En 1886, Reynolds [99] établit sa fameuse équation qui est désormais la base de toutes les théories de lubrification actuelles. Elle exprime la relation entre la pression à l'intérieur du film lubrifiant, la géométrie et la cinématique des parties en mouvement. La solution de cette équation, basée sur la théorie des écoulements visqueux laminaires, confirme les observations antérieures de Tower et Petrov. Au début du 20$^{\text{ème}}$ siècle, Michell [89] et Kingsburry [75] firent un premier pas vers la compréhension du phénomène de lubrification dans les paliers hydrodynamiques.

Quelques années plus tard, Martin [86] et Gümbel [44] appliquèrent la théorie hydrodynamique au cas des engrenages rigides. Ils furent surpris par le fait que les épaisseurs de film prédites par leur analyse étaient trop petites par rapport à la rugosité des surfaces. Et pourtant, le contact était bien protégé par un film complet de lubrifiant qui séparait les surfaces. Il a fallu attendre 20 ans de plus avant l'apparition des principes fondamentaux de la lubrification élastohydrodynamique avec les travaux de Ertel [24] et Grubin [39]. Introduisant la théorie de Hertz [51] pour la déformation des massifs semi-infinis dans un contact sec ainsi que la loi de Barus [7] pour la variation de la viscosité avec la pression, ils obtinrent des épaisseures de film plus importantes que celles obtenues par Martin et Gümbel pour les mêmes conditions opératoires. Ainsi, les aspects fondamentaux de la lubrification élastohydrodynamique furent révélés.

Pendant la deuxième partie du $20^{ème}$ siècle, la communauté scientifique s'intéressa de plus en plus aux problèmes de lubrification. En même temps, le développement des moyens expérimentaux basés sur des techniques d'interférométrie optique, accompagné d'un énorme progrès dans la résolution numérique des équations aux dérivées partielles grâce à des ordinateurs plus puissants et des algorithmes plus performants, permirent une compréhension plus précise des phénomènes de lubrification. Ces développements ont mené l'évaluation précise de la distribution de l'épaisseur du film de lubrifiant dans un contact EHD.

- **Approche expérimentale**

La validation des travaux théoriques requiert des résultats expérimentaux pour confirmer certaines observations qualitatives telles que la séparation complète des surfaces en contact par un film de lubrifiant ou la distribution de pression à l'intérieur de ce dernier. Ces expériences peuvent être aussi utilisées pour confirmer des observations plus quantitatives telles que la distribution exacte de l'épaisseur de film dans le contact. Au fil des années, plusieurs techniques basées sur des principes physiques différents ont été développées. La plus utilisée reste désormais l'interférométrie optique. Foord et al. [30], Gohar et Cameron [36][37], Wedeven et al [119], Chiu et Sibley [19] ont noté en utilisant cette technique, la forme particulière en « fer à cheval » de la distribution de l'épaisseur de film dans un contact ponctuel (Voir Figure 0.3). De nos jours, cette technique est bien plus développée avec des capteurs optiques d'une résolution nettement meilleure, permettant ainsi de mesurer des épaisseurs de film extrêmement minces de l'ordre de quelques nanomètres, comme le montrent les travaux de Guangteng et al. [42] ou de Cann et al. [12][13][14].

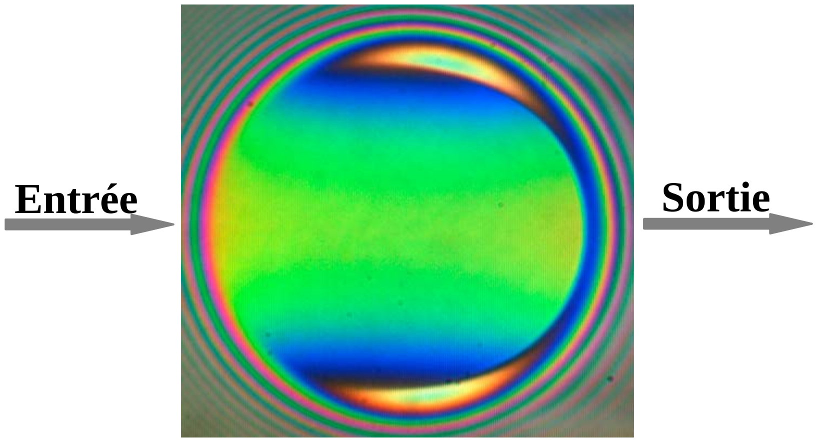

Figure 0.3: Distribution de l'épaisseur de film dans un contact EHD ponctuel obtenue par interférométrie optique

L'interférométrie optique est limitée aux mesures d'épaisseurs de film. Les informations concernant la distribution de pression sont obtenues par le biais d'une technique différente. En effet, Safa et al. [102][103] et Baumann et al. [8] ont effectué des mesures en utilisant des micro-capteurs déposés sous vide sur l'une des surfaces du contact. Suivant le type de capteur, cette technique permet la mesure de pression, épaisseur de film ou aussi de température dans le contact. Plus récemment, une technique de Microspectrométrie Raman a été introduite par Jubault et al. [69] pour mesurer précisemment les distributions de pression dans les contacts lubrifiés.

Le développement parallèle des techniques expérimentales et numériques permet aujourd'hui une comparaison quantitative des distributions de pression et d'épaisseur de film et ainsi la validation des modèles numériques. Le paragraphe suivant expose les différentes méthodes numériques trouvées dans la littérature pour la résolution du problème EHD.

- **Approche numérique**

Petrusevich [97] fut le premier à fournir une solution numérique complète du problème EHD. Il a remarqué la présence de la constriction de l'épaisseur de film à la sortie du contact et celle du pic de pression qui lui est associée (Voir Figure 0.4).

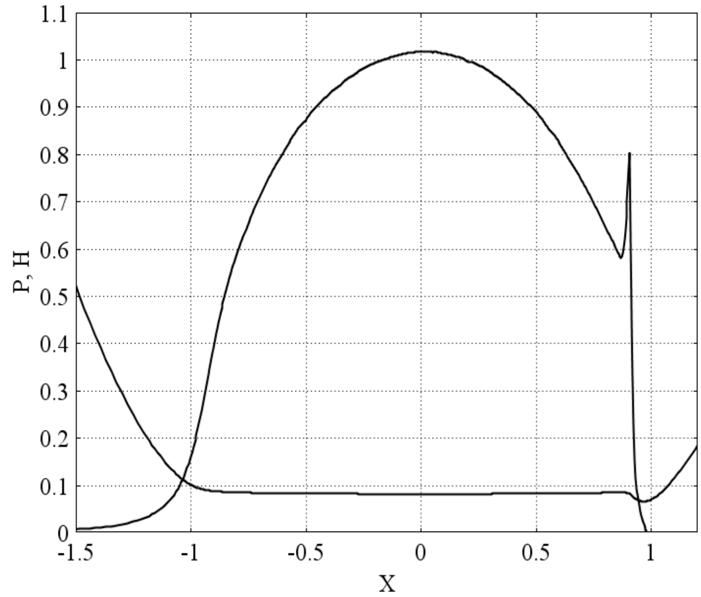

Figure 0.4: Contact EHD linéique: distributions d'épaisseur de film et de pression adimensionnées

Avec le progrès technologique des ordinateurs, les solutions numériques firent leur apparition donnant lieu à plusieurs formules analytiques liant les épaisseurs de film centrales et minimales à différents paramètres adimensionnés du contact. Parmi celles-ci, les plus courantes sont celles de Hamrock et Dowson [46], Nijenbanning et al. [92] et Evans et Snidle [25]. La solution numérique du problème EHD n'est pas facile à atteindre puisqu'elle implique la résolution d'un problème fortement non-linéaire. Ce dernier est défini par trois équations principales : l'équation de Reynolds (qui permet le calcul de la distribution de pression hydrodynamique dans le film lubrifiant pour une géométrie donnée), l'équation d'épaisseur de film (qui résulte de la superposition de la séparation des corps rigides, de la géométrie initiale et de la déformation élastique des surfaces induite par la pression dans le film) et l'équation d'équilibre des charges (permettant de vérifier la convergence globale du schéma numérique). Différentes approches numériques furent développées à cause des difficultés de convergence rencontrées pendant le processus de résolution. Ces difficultés sont, en partie, dues au couplage entre l'équation de Reynolds et celle des déformations élastiques des surfaces. Les différentes approches numériques peuvent être classifiées en deux catégories : les approches avec couplage faible et celles avec couplage fort.

- o **Couplage faible**

Cette approche consiste à résoudre les différentes équations du problème EHD séparément et à établir une procédure itérative entre leurs solutions respectives comme le montre la Figure 0.5. Parmi les premiers à avoir adopter cette approche, on cite Dowson et Higginson [22] dans le cadre d'un contact linéique. Ensuite, suivirent les travaux de Hamrock et Dowson

[45][46][47][48] et de Ranger et al. [98] pour le contact circulaire et plus récemment, Chittenden et al. [18] et Nijenbanning et al. [92] pour le contact elliptique. Ces modèles étaient basés sur ce qu'on appelle la **méthode directe**. En d'autres termes, l'équation de Reynolds est résolue en fonction de la pression pour une géométrie de film donnée. L'inconvénient majeur de ces modèles est la limitation en pression à moins de 1 GPa alors que dans des contacts EHD réels, des pressions de l'ordre de 2 ou 3 GPa peuvent être rencontrées. Afin de s'affranchir de cette limitation, Ertel [24] avait introduit auparavant ce que l'on connait sous le nom de **méthode inverse**. Contrairement à la méthode directe, la méthode inverse consiste à résoudre l'équation de Reynolds en fonction de l'épaisseur de film pour un profil de pression donné. Dowson et Higginson [22] furent les premiers à développer un algorithme pour trouver la solution numérique du problème de contact EHD linéique basé sur la solution inverse de l'équation de Reynolds. Cette approche fut plus tard étendue au cas des contacts circulaires par Evans et Snidle [26]. Malgré la robustesse de cette méthode dans la zone centrale du contact où la méthode directe souffrait de problèmes de stabilité, la solution demeurait instable dans les zones d'entrée et de sortie du contact. Plus tard, Kweh et al. [76] ont introduit une approche hybride qui consistait à utiliser une combinaison des deux méthodes : la méthode directe dans les zones d'entrée et de sortie du contact et la méthode inverse dans la zone centrale. Un algorithme pratiquement similaire a été aussi présenté par Seabra et Berthe [105][106]. Bien que cette approche ait permis l'extension de la solution du problème EHD à des contacts fortement chargés, elle présentait plusieurs inconvénients. En effet, résoudre l'équation de Reynolds en fonction de l'épaisseur de film pour un profil de pression donné requiert la résolution d'une équation cubique qui possède pratiquement trois solutions. Ainsi, il fallait prendre soin de bien choisir la solution appropriée. En plus, la relation employée pour mettre à jour le profil de pression, pour une épaisseur de film donnée, était basée sur l'intuition, son fondement physique n'était pas bien établi.

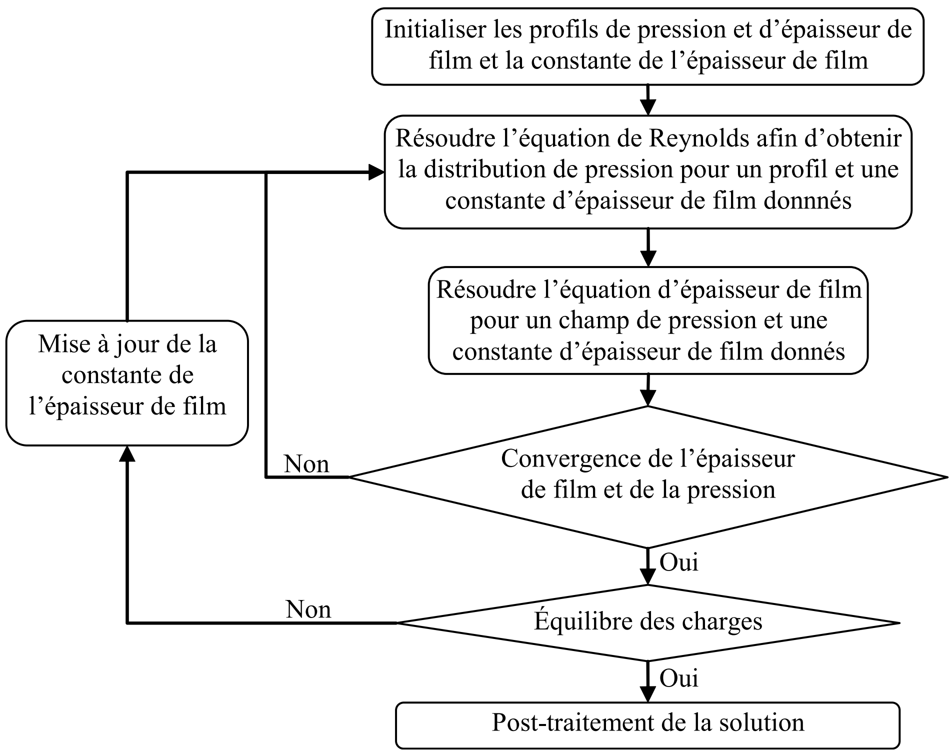

Figure 0.5: Diagramme du schéma d'une approche par couplage faible utilisant une méthode directe

Une avancée majeure dans le domaine fut réalisée par Lubrecht [84][85], qui appliqua les techniques multigrilles au problème de lubrification EHD en utilisant une méthode directe.

Cette technique apporte une nette amélioration au taux de convergence et permet ainsi de réduire les temps de calcul. Elle est basée sur une certaine compréhension du comportement en convergence des processus itératifs de résolution. En effet, les schémas itératifs réussissent à réduire l'erreur dans la solution tant que cette dernière possède une longueur d'onde du même ordre de grandeur que la taille du maillage. Dès que la longueur d'onde de l'erreur devient plus grande que la taille du maillage, le processus itératif devient de plus en plus lent. Afin de surmonter ce problème, il suffit de transférer le processus de résolution sur une grille plus grossière. Ainsi, les techniques multigrilles consistent à faire des allers-retours du processus itératif de résolution entre différents niveaux de grilles. Une réduction encore plus importante des temps de calcul a été réalisée par Brandt et Lubrecht [9] qui introduisirent la technique de Multi-Intégration permettant d'accélérer le processus de calcul intégral des déformations élastiques. Ce travail a été encore amélioré au début des années 90 par Venner [112][113][114] qui étendit le processus de résolution au cas des contacts fortement chargés en appliquant un schéma de relaxation distributive en ligne. Ce travail fournit une alternative efficace à la méthode inverse pour le cas de contacts fortement chargés et constitua ainsi une base pour les travaux numériques dans le domaine de l'EHD pour les années à venir. Ju et al. [68] introduisirent par exemple la méthode de convolution discrète par transformée de Fourier rapide comme alternative pour le calcul de la déformation élastique des surfaces. Wang et al. [117] prétendent que cette dernière est trois fois plus rapide que la méthode de Multi-Intégration.

Les différents travaux cités dans ce paragraphe sont basés sur une discrétisation par différences finies des équations EHD. Bien qu'en général cette méthode limite le processus de discrétisation à des maillages structurés de forme rectangulaire avec des approximations d'ordre faible, c'est la plus utilisée dans la modélisation des problèmes de lubrification. Cela est du au développement des techniques citées précédemment. Une méthode alternative à laquelle il a été accordé beaucoup moins d'attention en EHD est la méthode des éléments finis. Cette dernière permet l'utilisation de maillages non-réguliers non-structurés avec des approximations d'ordre élevé. Un exemple d'application de cette méthode aux problèmes EHD est fourni dans [82][83]. Les auteurs appliquent la méthode directe tout en utilisant une formulation de type Galerkin discontinue afin de stabiliser la solution de contacts linéiques fortement chargés. À la connaissance de l'auteur, cette méthode n'a pas encore été étendue au cas des contacts ponctuels. Malheureusement, l'utilisation d'éléments discontinus mène à des systèmes de plus grande taille. En effet, chaque point de discrétisation peut avoir plusieurs valeurs nodales pour la même variable: une pour chaque élément auquel il appartient. Hughes et ses collaborateurs [60] ont aussi utilisé la méthode des éléments finis en combinant des approches du 1er et du 2nd ordre de l'équation de Reynolds afin d'obtenir une résolution efficace pour les problèmes de contacts EHD linéiques faiblement et fortement chargés. En fait, l'approche de 1er ordre, qui consiste à écrire l'équation de Reynolds sous forme d'une équation différentielle du 1er ordre, est uniquement stable dans la zone de fortes pressions alors que l'approche de 2nd ordre est uniquement stable dans la zone de pressions faibles. Ainsi, les auteurs proposèrent d'utiliser une combinaison de l'approche de 2nd ordre dans les zones d'entrée et de sortie du contact et de celle de 1er ordre dans la zone centrale. Cela mène à un processus de résolution stable indépendemment de la charge appliquée. Malheureusement, l'utilisation de l'approche de 1er ordre limite cette méthode dans tous les cas à une configuration de contact linéique.

Enfin, il est important de noter que, puisque l'approche avec couplage faible présentée dans ce paragraphe se base sur une résolution séparée des équations EHD, une perte d'informations est susceptible de se produire durant le processus itératif établi pour coupler leurs différentes solutions. Cette perte d'information est en général compensée par une sévère sous-relaxation, menant ainsi à un faible taux de convergence du schéma itératif global.

- **Couplage fort**

L'approche couplage fort, comme l'indique son nom, consiste à résoudre les différentes équations simultanément comme le montre le diagramme de la Figure 0.6. Différentes méthodes trouvées dans la littérature pourraient être classées dans cette catégorie. Par exemple, les développements récents en « Computational Fluid Dynamics » (CFD) ou aussi en « Fluide-Structure Interaction » (FSI) ont été appliqués au problème EHD par Hartinger et al. [50] et Yiping et al. [124] respectivement. Ces méthodes sont basées sur une résolution complète des équations de Navier-Stokes couplées aux équations d'élasticité linéaire pour le calcul des déformations élastiques. Cette approche est relativement précise mais présente un inconvénient majeur : les temps de calcul (un calcul typique d'un contact ponctuel pourrait durer plus d'une semaine avec un maillage relativement grossier). Les résultats confirment que les variations de pression dans l'épaisseur du film peuvent être négligées comparé à celles dans le plan du contact. L'avantage principal de ces méthodes est qu'elles permettent une évaluation exacte des fuites latérales du lubrifiant puisque le champ de vitesses complet de l'écoulement est déterminé. De plus, le champ de contraintes dans les corps solides est aussi obtenu. Cela pourrait s'avérer utile pour une étude en fatigue des composants. Mais, à cause des temps de calculs trop longs, de nos jours et jusqu'à ce que les puissances des machines de calcul deviennent bien plus importantes, ces méthodes demeurent peu adoptées.

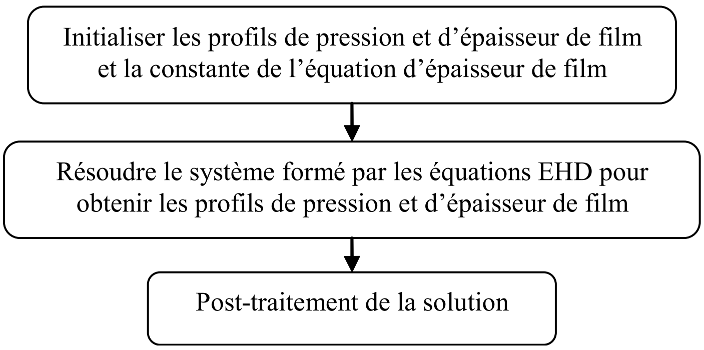

Figure 0.6: Diagramme du schéma d'une approche par couplage fort

Une autre approche assez intéressante consiste à utiliser la méthode de Newton-Raphson. Les premiers à avoir employé cette méthode dans le cadre du problème EHD furent Rhode et Oh [93][101] qui résolvèrent le problème EHD sous la forme d'une seule équation intégro-différentielle en utilisant une approximation par éléments finis. Ce travail révéla l'important potentiel de cette approche caractérisée par des taux de convergence extrêmement rapides. En effet, quelques itérations étaient suffisantes pour obtenir la convegence de la solution. Plus tard, un modèle similaire fut introduit par Okamura [94]. Une version améliorée du modèle d'Okamura fut introduite postérieurement par Houpert et Hamrock [57] pour le cas du contact linéique. Cette méthode fut étendue au cas de contacts elliptiques par Hsiao et al. [58]. À cause de la solution simultanée de toutes les mises à jour des valeurs nodales de pression, l'implémentation de la condition de cavitation s'avère particulièrement compliquée. En effet, pour le contact linéique, la position de la frontière libre est introduite en tant qu'inconnue supplémentaire à déterminer durant le processus de résolution. Puisque cette position consiste en une seule inconnue, cela ne résulte pas en une complication sérieuse des équations. Par contre, pour le contact ponctuel, la position de la frontière libre varie sur le domaine de calcul bidimensionnel. Ainsi, sa détermination mène à un modèle bien plus complexe. En plus, dans tous ces travaux, le calcul des déformations élastiques se base sur une approche de type massif semi-infini. Ainsi, la déformée en chaque point de discrétisation est reliée à tous les autres points de discrétisation du domaine de calcul par le biais du calcul intégral. Cela conduit à une matrice Jacobienne pleine, ce qui requiert des efforts de calcul importants pour son inversion. Enfin, à fortes charges, la matrice Jacobienne devient pratiquement singulière, ce qui rend la solution des contacts fortement chargés difficile à atteindre. La combinaison du traitement compliqué de la frontière libre avec la matrice Jacobienne pleine qui devient pratiquement singulière à fortes charges a mené à l'arrêt du développement de cette méthode pendant un certain temps.

Récemment, Evans et Hughes [27] introduisirent la méthode de « déflection différentielle » qui fournit une équation différentielle (basée sur une approche massif semi-infini) régissant la déformation élastique des corps solides. Cette approche, contrairement à l'approche massif semi-infini directe, a l'avantage d'avoir un caractère plus localisé. En effet, l'opérateur différentiel tend très rapidement vers zéro quand le point d'évaluation de la déformation élastique s'éloigne du point d'application de la force. En pratique, les termes matriciels deviennent de plus en plus négligeables en s'éloignant de la diagonale. Cela donne une matrice Jacobienne moins pleine en appliquant une approche par couplage fort. Les auteurs et leur équipe ont appliqué cette méthode au cas du contact linéique [61], puis ils l'ont étendue au cas plus général du contact ponctuel [55][56]. Néanmoins, le système matriciel avait conservé une largeur de bande relativement importante, et un traitement spécial a du être employé pour résoudre le système d'équations couplées d'une manière efficace.

Finalement, il est important de noter que, puisque l'approche par couplage fort consiste à résoudre les équations EHD simultanément, aucune perte d'informations ne se produit entre leurs solutions respectives. Ainsi, la sous-relaxation n'est plus utile, ce qui explique (en partie) les taux de convergence rapides du processus itératif.

Conclusion

Après cet aperçu bibliographique rapide des modèles numériques du problème EHD, on peut conclure que le solveur EHD « idéal » serait basé sur une résolution de type Newton-Raphson avec couplage fort des différentes équations. Cela permettrait une résolution rapide du problème en seulement quelques itérations sans aucune perte d'information entre les solutions des différentes équations. La discrétisation de ces équations serait réalisée par éléments finis, permettant ainsi l'utilisation de maillages non-réguliers non-structurés ainsi que des approximations d'ordre élevé. Cela mène à une taille de systèmes matriciels réduite où les degrés de liberté (ddl) sont répartis de façon optimale (un maillage fin est utilisé uniquement là où il y en a besoin). Le processus de résolution serait stable pour un vaste domaine de conditions opératoires. Et finalement, la matrice Jacobienne du système correspondant serait creuse et le traitement de la frontière libre relativement simple.

Le but de ce travail est de concevoir ce solveur « idéal » dans le cadre des contacts circulaires avec des surfaces lisses en régime stationnaire. Cette approche n'est en aucun cas restreinte à ce cas de figure et pourra être facilement étendue au cas des contacts linéiques ou elliptiques sous régime transitoire. Mais dans le cadre de ce travail, on s'intéresse uniquement au cas des contacts circulaires en régime stationnaire. Des modèles physiques seront employés pour représenter le comportement rhéologique des lubrifiants. Ensuite, cette approche sera étendue à une modélisation plus proche de la réalité prenant en compte les effets non-Newtoniens et thermiques qui peuvent être importants à des vitesses d'entrainement et / ou de glissement élevées et / ou aussi à des fortes charges. La comparaison avec les modèles numériques existants et avec les résultats expérimentaux est une nécessité afin de s'assurer que le modèle développé ne dévie pas de la réalité. Ainsi, les solutions obtenues dans la partie numérique de ce travail seront dans la mesure du possible comparées aux expérienes. L'approche développée sera utilisée pour étudier l'utilisation des FTFV en tant que lubrifiants dans les contacts EHD circulaires. Cette étude se positionne dans un cadre de développement durable permettant de préserver l'environnement et de décélérer le phénomène de réchauffement climatique. Ces problèmes sont particulièrement difficiles à aborder expérimentalement à cause des très faibles épaisseurs de film rencontrées. Ainsi une étude numérique s'est avérée nécéssaire afin de pouvoir balayer un large domaine de conditions opératoires.

Approche isotherme Newtonienne

Ce chapitre constitue le cœur de cette thèse. Il présente le modèle numérique développé pour résoudre des problèmes de contacts EHD circulaires en considérant une approche isotherme Newtonienne. C’est la base de tout solveur EHD, à partir de laquelle une extension vers une modélisation plus complexe et plus physique pourrait être réalisée.

Comme indiqué dans le chapitre précédent, le but de ce travail est de concevoir le solveur EHD « idéal » robuste sur un large domaine de conditions opératoires, en utilisant une approche de type Newton-Raphson avec couplage fort et une discrétisation par éléments finis. Les modèles basés sur une telle approche dans la littérature souffrent de trois problèmes majeurs: la matrice Jacobienne est pleine, elle devient pratiquement singulière à fortes charges et le traitement du problème de frontière libre s’avère particulièrement difficile à gérer. Ici, on fournit une solution à ces trois problèmes, permettant ainsi de profiter des propriétés de convergence rapide de ce modèle.

La solution du premier problème consiste à introduire une approche alternative à celle de type massif semi-infini pour le calcul des déformations élastiques des corps solides. Cette nouvelle approche consiste à utiliser les équations classiques de l’élasticité linéaire afin de calculer les déformations élastiques d’une structure tridimensionnelle ayant des dimensions relativement grandes comparées à la taille du contact. On montre qu’un cube ayant pour longueur d’arête 60 fois la taille du rayon de contact Hertzien est convenable pour avoir une configuration de type massif semi-infini. Contrairement à l’approche massif semi-infini classique où la déformation en chaque point de discrétisation est calculée par le biais d’une double intégrale sur la zone de contact reliant ce point à tous les autres, ici, le caractère différentiel des équations de l’élasticité linéaire résolues par éléments finis donne un aspect localisé au problème. En effet, chaque point de discrétisation appartenant à un certain nombre d’éléments est uniquement lié aux noeuds appartenant à ces mêmes éléments. Cela permet d’avoir une matrice Jacobienne creuse (plus de 99% des termes sont nuls).

Le deuxième problème est résolu par l’utilisation de formulations éléments finis stabilisées. En effet, l’équation de Reynolds est écrite sous forme d’une équation de Convection / Diffusion avec un terme source fonction de la pression. La convection devient dominante à fortes charges par rapport à la conduction. Or, la méthode des éléments finis avec une formulation de type Galerkin classique est uniquement appropriée à la résolution de problèmes où la conduction est dominante. Dans le cas contraire, cette dernière mène à un caractère oscillatoire de la solution. Ce problème est surmonté par l’utilisation de formulations spécifiques plus complexes, tel que « Streamline Upwind Petrov Galerkin » (SUPG) [11] ou « Galerkin Least Squares » (GLS) [63]. Dans le cas d’un contact linéique, l'utilisation de ces deux méthodes permet de stabiliser complètement la solution. L'avantage des ces dernières est qu'elles sont résiduelles. En effet, les termes rajoutés sont proportionnels au résidu de l'équation résolue. Ainsi pour une solution convergée, les termes rajoutés sont pratiquement nuls et la consistence de l'équation de Reynolds est préservée. D'un autre côté, pour un contact circulaire, ces deux techniques réduisent largement l'amplitude des oscillations sans toutefois obtenir leur disparition complète. Afin d'éliminer complètement ces oscillations, il est nécessaire de rajouter un terme supplémentaire de « Isotropic Diffusion » (ID) [127]. Ce dernier n'est pas résiduel, mais on montre que son effet sur la solution est négligeable.

Enfin, le troisième problème est surmonté par l'introduction d'une méthode de pénalisation consistant à rajouter un terme supplémentaire à l'équation de Reynolds. Ce terme force les pressions négatives vers zéro et permet aussi d'avoir un gradient de pression nul sur la frontière libre ce qui permet de satisfaire la conservation de la masse dans le contact. Cette méthode présente l'avantage d'une implémentation facile et directe.

Désormais, les inconvénients majeurs de cette approche sont surmontés. Les trois équations du problème EHD (Reynolds, élasticité linéaire et équilibre des charges) sont résolues simultanément par le biais de la méthode de Newton-Raphson en utilisant une discrétisation par éléments finis. Les équations de l'élasticité linéaire sont résolues sur la structure tridimensionnelle alors que l'équation de Reynolds est résolue sur une partie bidimensionnelle de la surface de cette structure correspondant à la zone de contact. L'équation d'équilibre des charges est rajoutée directement au système formé par les deux équations précédentes en rajoutant une inconnue supplémentaire correspondant à la séparation initiale des surfaces non-déformées. La complexité de ce modèle est la même que celle du modèle multigrille, considéré jusqu'à présent comme étant le plus performant. D'un autre côté, de par l'utilisation de la méthode des éléments finis qui permet l'usage de maillages non-réguliers non-structurés avec des approximations d'ordre élevé, la taille des systèmes obtenus par cette méthode est nettement inférieure à celle requise par le modèle multigrille. En effet, ce dernier étant basé sur une discrétisation par différences finis des équations correspondantes, un maillage régulier et structuré est exigé. De plus, de par le couplage fort évitant la perte d'informations durant le processus de résolution itératif et l'usage de la méthode de Newton-Raphson connue pour ses propriétés de convergence rapide, la convergence de ce modèle est nettement améliorée par rapport au modèle multigrille. Ainsi, ayant la même complexité que le modèle multigrille mais avec des tailles de systèmes réduites et des taux de convergence plus rapides, notre modèle requiert une capacité mémoire et des temps de calculs moins importants.

Effets non-Newtoniens

Mis à part en théorie, un fluide « parfaitement » Newtonien n'existe pas réellement. Néanmoins, en pratique, un fluide est considéré Newtonien quand il possède une limite Newtonienne relativement élevée. En d'autres termes, il peut supporter des taux de cisaillement élevés avant que sa viscosité ne varie. Mais une fois la limite Newtonienne atteinte, la linéarité du comportement contraintes-déformations est perdue. Dans les applications de lubrification, le lubrifiant peut être soumis à des sollicitations extrêmes. Dans les roulements à billes ou les engrenages par exemple, la vitesse moyenne d'entrainement du lubrifiant peut atteindre 100 m/s alors qu'il traverse le contact en seulement quelques microsecondes. Les gradients de vitesse peuvent atteindre 10^7 s^{-1} et des pressions de l'ordre de 2 ou 3 GPa peuvent être rencontrées. Sous de telles conditions extrêmes, la plupart des fluides ont une réponse bien plus complexe que le simple comportement Newtonien. De nos jours, la composition chimique de plus en plus compliquée des lubrifiants, qui inclue des additifs polymères ou d'autres substances rend leur comportement encore plus difficile à modéliser. Différentes lois constitutives ont été introduites pour représenter ces réponses complexes telle que la loi de Carreau [15] ou le modèle non-linéaire de Maxwell [107][108] qui sont dits de type « shear-thinning ». En effet, la viscosité des fluides obéissant à ces lois diminue avec l'augmentation des contraintes de cisaillement, menant ainsi à une diminution de l'épaisseur de film correspondante. Plus tard, Bair et Winer [5][6] introduisirent un autre type de comportement non-Newtonien nommé « limiting-shear-stress ». Leur analyse se basait sur des expériences de laboratoire utilisant des viscomètres à fort taux de cisaillement. Il est important de noter que la liste des modèles cités ci-dessus n'est pas exhaustive et que bien d'autres modèles peuvent être retrouvés dans la littérature tel que Gecim et Winer [34] qui est de type limiting-shear-stress ou aussi la loi en sinh de Ree-Eyring [28] de type shear-thinning... Le but de ce travail n'est ni de valider, ni de comparer les différents modèles rhéologiques, mais de fournir une approche unique permettant d'utiliser une grande variété de lois constitutives.

Dans les contacts EHD, les taux de cisaillement dans le film lubrifiant sont souvent importants et si ce dernier présente un comportement de type « shear-thinning », sa viscosité peut diminuer de façon significative avec l'augmentation du taux de cisaillement. Ainsi, faire l'hypothèse que le lubrifiant est Newtonien quand il ne l'est pas pourrait être dangereuse pour la conception d'un composant mécanique puisque les épaisseurs de film seront surestimées. Cela pourrait mener à une réduction sévère de sa durée de vie, voire même dans le cas extrême, à sa défaillance. Dans ce chapitre, on s'intéresse à l'influence des effets non-Newtoniens sur la pression, l'épaisseur de film et le frottement dans un contact EHD circulaire en régime isotherme, lubrifié par un fluide ayant un comportement de type shear-thinning. Le modèle numérique est similaire à celui présenté dans le chapitre précédent sauf que l'équation de Reynolds classique est cette fois remplaçée par l'équation de Reynolds généralisée prenant en compte les effets non-Newtoniens. Cette dernière peut aussi s'écrire sous forme d'une équation de Convection / Diffusion avec un terme source en fonction de la pression et le terme de convection devient dominant à fortes charges. Ainsi, les mêmes techniques de stabilisation sont employées pour obtenir la solution de contacts fortement chargés. L'application de ce modèle à des cas typiques de contacts EHD circulaires sous différentes conditions opératoires révèle ce qui suit:

- Globalement, le profil de pression dans le contact n'est pas affecté par les variations du taux de cisaillement. Seul un effet mineur sur le pic de pression peut être observé. Ce dernier perd en hauteur lorsque le cisaillement augmente.
- Les épaisseurs de film et les coefficients de frottement sont réduits de façon significative à cause de la diminution de la viscosité du lubrifiant avec le cisaillement. Ainsi ces deux paramètres tribologiques sont surestimés par une approche Newtonienne simple.
- Une approche non-Newtonienne permet de prédire des épaisseurs de film réalistes, surtout à des conditions opératoires en vitesse faibles ou modérées. Par contre, pour les vitesses élevées et probablement à cause d'effets thermiques qui deviennent importants (même dans la zone d'entrée du contact), les résultats numériques dévient des expériences.
- Finalement, les coefficients de frottement prédits par une approche isotherme non-Newtonienne sont réalistes uniquement à vitesse faible. Cela est probablement du à l'importance des effets thermiques dans la zone centrale du contact.

La comparaison des résultats obtenus avec les expériences permet de valider à la fois le modèle numérique et les modèles rhéologiques employés. Ainsi, on peut conclure que, lorsqu'un fluide non-newtonien est utilisé en tant que lubrifiant, l'approche isotherme non-Newtonienne est efficace pour la détermination d'épaisseurs de film et de coefficients de frottement pour des conditions opératoires en vitesse d'entrainement et / ou de glissement faibles ou modérées. Par contre, à grande vitesse, cette approche n'est plus appropriée. Les effets thermiques sont probablement responsables des différences observées entre les résultats numériques et expérimentaux. Ces effets peuvent être aussi importants dans un contact lubrifié par un fluide Newtonien. Ainsi, le chapitre suivant est dédié à l'étude des effets thermiques dans les contacts EHD circulaires lubrifiés avec un fluide Newtonien ou non-Newtonien.

Effets thermiques

Sous des conditions opératoires extrêmes, l'élévation de température dans un contact EHD peut devenir importante. Cela est susceptible de se produire quand les conditions opératoires combinent plusieurs facteurs tels que des vitesses d'entraînement ou de glissement élevées, une forte viscosité ou piézoviscosité du lubrifiant ou de fortes charges. Cette élévation de température découle de deux sources de chaleur: le cisaillement de la couche mince de lubrifiant et le réchauffement par compression, dû aux variations de pression dans la zone de contact. Les conséquences sur le comportement du contact lubrifié ne peuvent plus être négligées. En effet, comme signalé dans le chapitre précédent, négliger la génération de chaleur dans un contact EHD opérant sous des conditions sévères mène à la surestimation à la fois des épaisseurs de film et des coefficients de frottement. Ceci parce que les variations de température causent une variation de densité et, plus important, de viscosité du lubrifiant à travers le film. L'intérêt porté aux effets thermiques dans les problèmes de lubrification EHD commença avec le travail théorique de Cheng [16][17]. La première solution numérique complète du contact ponctuel fut obtenue par Zhu et Wen [125]. Depuis, plusieurs auteurs proposèrent différentes méthodes pour traiter ce problème en considérant un fluide Newtonien ou non-Newtonien comme Kim et Sadeghi [72], Guo et al. [43] ou aussi Liu et al. [80] qui résolvèrent les équations de l'énergie tridimensionnelles afin de déterminer les variations de température dans le film lubrifiant. Une méthode alternative consiste à réduire le problème de transfer de chaleur tridimensionnel en un problème bidimensionnel en faisant l'hypothèse que la distribution de température à travers l'épaisseur de film a un profil parabolique. Cette approche a été utilisée par plusieurs chercheurs tels que Salehizadeh et Saka [104], Wolff et Kubo [120] et Kazama et al. [71] dans le cadre d'un contact linéique ou aussi Jiang et al. [65], Lee et al. [77] et Kim et al. [73][74] dans le cadre de contacts ponctuels. Par contre, la simplification qui consiste à considérer un profil de température parabolique dans l'épaisseur de film mène à des prédictions de température peu correctes, surtout dans la zone d'entrée du contact, comme le montrent Kazama et al. [71]. Cela est dû à la présence d'effets thermiques convectifs complexes associés à des écoulements inverses importants dans cette zone.

Dans ce chapitre, on propose un modèle pour étudier les effets thermiques dans un contact EHD circulaire lubrifié par un fluide Newtonien ou non-Newtonien. Cette étude est basée sur la résolution des équations de l'énergie tridimensionnelles appliquées aux corps solides et au film lubrifiant. Le modèle numérique est similaire à celui présenté dans les chapitres précédents sauf que l'équation de Reynolds est cette fois remplaçée par l'équation de Reynolds sous sa forme la plus généralisée pouvant prendre en compte à la fois les effets non-Newtoniens et les effets thermiques. Cette dernière peut aussi s'écrire sous forme d'une équation de Convection / Diffusion avec un terme source fonction de la pression et le terme de convection qui devient dominant à forte charge. Ainsi, les mêmes techniques de stabilisation sont employées pour obtenir la solution des contacts fortement chargés.

Des cas typiques sont simulés en régime isotherme et thermique sous des conditions de roulement pur et de roulement-glissement. Les résultats montrent clairement qu'à partir d'une certaine limite en vitesse, il est nécessaire de prendre en compte les effets thermiques pour une bonne estimation des épaisseurs de film, et surtout du frottement. Le « shear-thinning » et l'échauffement ont tous les deux un effet de réduction de l'épaisseur de film quand la vitesse de glissement augmente. Ils modifient aussi les profils de pression et d'épaisseur de film. En effet, il a été montré dans le chapitre 3 que l'effet non-Newtonien tend à diminuer la hauteur du pic de pression sans avoir de répercusion significative sur la forme du profil d'épaisseur de film quand le taux de roulement-glissement augmente. D'un autre côté, les effets thermiques tendent non seulement à diminuer la hauteur du pic mais aussi à l'élargir et le rapprocher de la zone centrale du contact. Cela mène à un changement de la forme du profil d'épaisseur de film, surtout dans la zone de sortie du contact où la forme en « fer à cheval » gagne en largeur sur sa partie centrale et s'amincit sur les bords. Ainsi, elle prend une largeur à peu près constante sur son étendue, comparé au profil isotherme où elle est large sur les bords et mince sur la partie centrale. Tous les résultats sont comparés à des données expérimentales montrant un meilleur accord, par rapport à l'approche isotherme, entre les résultats thermiques et les expériences, surtout à forte vitesse ou taux de glissement. Les comparaisons numériques / expérimentales permettent à la fois de valider l'approche numérique et les modèles rhéologiques employés. Un accord remarquable est obtenu pour les résultats de frottement où l'approche isotherme s'est révélée surestimatrice des coefficients de frottement à forte vitesse. Cela est surtout du aux effets thermiques dans la zone centrale du contact. Ces derniers sont importants même à des vitesses d'entraînement faibles ou modérées quand les taux de glissement sont importants.

FTFV en lubrification

Dans cette partie, le potentiel d'utilisation des FTFV en tant que lubrifiants dans les contacts EHD circulaires est étudié. Comme mentionné dans l'introduction, ces fluides présentent deux aspects intéressants quand ils sont utilisés en tant que lubrifiants. Tout d'abord, à cause de leur faible viscosité, ils mènent à une réduction de la dissipation d'énergie par frottement dans les contacts lubrifiés. D'autre part, d'un point de vue purement pratique, il est bien plus facile de concevoir et maintenir des machines opérant avec un seul fluide jouant à la fois le rôle du lubrifiant et du fluide opérateur (par exemple: moteurs à propulsion, moteurs à combustion interne, pompes à chaleur …). Cette possibilité se situe aussi dans une stratégie de préservation de l'environnement et de développement durable. Par contre, à cause de la viscosité très faible de ces fluides, des épaisseurs de film relativement minces sont susceptibles de se former dans la zone de contact. Le but du travail effectué dans ce chapitre est de déterminer s'il est possible de lubrifier « correctement » avec ce genre de fluides et sous quelles conditions opératoires. Deux FTFV typiques sont considérés. Il est important de noter que ces fluides n'ont jamais été d'intérêt pour la communauté de Tribologie. Ainsi, leurs propriétés rhéologiques sont très peu connues. En fait, ces dernières sont restreintes à des domaines de pressions relativement faibles comparés à ceux rencontrés dans les applications EHD. Pour cela, des mesures de viscosité et de compressibilité ont été réalisées afin de déterminer le comportement rhéologique de ces fluides sur un domaine de pression plus important. Les résultats montrent que ces fluides ont non seulement des faibles viscosités mais aussi des faibles piézoviscosités, de l'ordre de 2 à 5 GPa^{-1}. Par ailleurs, de par leur faible masse et taille moléculaire (de l'ordre de 5 Å), ils présentent un comportement Newtonien sur un large domaine de taux de cisaillement. D'autre part, ils ont une compressibilité relativement élevée et inhabituelle comparé aux lubrifiants classiques qui obéissent souvent à la loi de Dowson & Higginson.

Des calculs ont été mené pour ces deux fluides en utilisant le modèle développé dans le chapitre précédent prenant en compte les effets thermiques. Les calculs ont révélé qu'un régime de vitesses élevées est indispensable pour un bon fonctionnement des contacts lubrifiés avec ces fluides. Les comparaisons avec les expériences permettent à la fois de démontrer la précision du modèle TEHD développé et la validité des modèles rhéologiques employés pour ces fluides. Les essais en roulement-glissement montrent que l'influence des effets thermiques sur les épaisseurs de film sont très faibles à cause de la faible viscosité de ces fluides. Ainsi les épaisseurs de film sont presque constantes en fonction des taux de cisaillement. Ensuite, des formules analytiques d'épaisseur de film spécifiques à chaque fluide sont développées. Ces dernières peuvent être utilisées directement par les ingénieurs sans avoir à exécuter les calculs complets. Dans ce contexte, l'effet de la compressibilité inhabituelle de ces fluides sur les épaisseurs de film est assez important comparé aux applications EHD classiques où les effets hydrodynamiques, générés surtout par la viscosité, sont dominants. En effet, un changement de pente (dans une échelle log-log) des courbes d'épaisseur de film en fonction de la vitesse d'entraînement est observé avec la variation de la charge. Cela est attribué à la compressibilité inhabituelle de ces fluides. Afin de vérifier cette hypothèse, un fluide fictif ayant une viscosité du même ordre de grandeur que celle des fluides étudiés mais une compressibilité de type Dowson & Higginson a été utilisé pour réaliser des calculs d'épaisseur de film. Pour ce fluide, les courbes d'épaisseur sont parfaitement parallèles en fonction de la charge étudiée. Enfin une analyse de traction dans ces contacts a révélé l'importante réduction de la dissipation d'énergie par frottement. Par conséquent, une réduction de la consommation d'énergie dans le système mécanique correpondant peut être obtenue. Pour finaliser cette étude, un point reste à clarifier. En effet, à cause des épaisseurs de film relativement faibles dans ces contacts, la durée de vie du mécanisme correspondant sera probablement réduite. Il reste alors à quantifier quel est le critère le plus important d'un point de vue économique: est-ce la réduction de la dissipation d'énergie par frottement ou bien la réduction de la durée de vie du système? Cette question dépasse l'objectif de cette thèse et elle est par conséquent reportée pour de futures investigations …

Conclusion générale

Dans cette thèse, une approche éléments finis avec couplage fort des problèmes de lubrification EHD a été développée, dans le cadre du contact circulaire avec surfaces lisses. Un modèle d'élasticité linéaire a été introduit pour le calcul des déformations élastiques des corps solides sous la pression générée dans le film de lubrifiant. Cela conduit à une matrice Jacobienne creuse du système non-linéaire global d'équations. Le problème de frontière libre (de cavitation) qui se pose à la sortie du contact a été géré de manière directe par le biais d'une méthode de pénalisation. Le processus de résolution a été étendu au cas des contacts fortement chargés par l'utilisation de formulations éléments finis stabilisées de type « diffusion artificielle ». Le système non-linéaire global d'équations est résolu suivant une procédure de type Newton-Raphson. Cela conduit à des taux de convergence extrêmement rapides (quelques itérations seulement sont requises pour obtenir une solution convergée) surtout comparés aux modèles classiques basés sur une approche de type couplage faible. Il a aussi été montré que la complexité de ce modèle est la même que celle des modèles basés sur une discrétisation par différences finies et une résolution de type multigrille. Par contre, une taille de système nettement plus petite a été obtenue, à cause de l'utilisation de maillages non-réguliers non-structurés permis par la méthode des éléments finis. Ainsi la capacité mémoire requise et les temps de calcul sont réduits.

Tout d'abord, une approche isotherme Newtonienne a été considérée. Cette dernière prédit bien les épaisseurs de film dans un contact EHD pour un fluide Newtonien et des conditions de vitesses faibles ou modérées. Par contre, si le lubrifiant a un comportement de type shear-thinning, les épaisseurs de film sont surestimées. C'est aussi le cas si des conditions de vitesses d'entraînement et / ou de glissement élevées sont considérées. Cela est du à la dissipation thermique importante dans le contact qui tend à réduire la viscosité du lubrifiant.

Ensuite, une approche isotherme non-Newtonienne a été développée en remplaçant l'équation de Reynolds classique par l'équation généralisée. Cette approche conduit à des estimations d'épaisseur de film conformes aux mesures quand un lubrifiant non-Newtonien est considéré. Par contre, bien qu'une estimation du frottement plus proche de la réalité soit obtenue, l'écart demeure significatif avec les résultats expérimentaux à des conditions de vitesses modérées ou élevées.

Enfin, une approche thermique a été développée à la fois pour des lubrifiants à comportement Newtonien ou non-Newtonien. Elle se base sur une résolution complète des équations de l'énergie dans les corps solides et le film de lubrifiant. Cette approche montre un très bon accord entre les épaisseurs de film et les coefficients de frottement calculés et ceux obtenus expérimentalement. En effet, la faible qualité des résultats de frottement obtenus avec l'approche isotherme non-Newtonienne à des fortes vitesses était due à l'augmentation de température dans la zone centrale du contact. Cette dernière n'affecte pas significativement l'épaisseur de film qui se forme dans la zone d'entrée, mais a un effet important sur le frottement à cause de la réduction de viscosité dans cette région.

Le modèle développé a été utilisé pour étudier le potentiel des Fluides de Très Faible Viscosité (FTFV) en tant que lubrifiants dans les contacts EHD circulaires. Il a été montré que des conditions de vitesses élevées sont requises pour un bon fonctionnement de ces contacts. Les courbes de frottement ont révélé l'importante réduction de la dissipation d'énergie par frottement dans ces contacts comparé à ceux lubrifiés avec des lubrifiants classiques.

Dans la mesure du possible, à chaque étape de cette étude, une validation expérimentale des résultats numériques a été réalisée. Cela permet de valider à la fois le modèle numérique et les modèles rhéologiques employés.

Perspectives

En couvrant à la fois l'aspect numérique (la théorie derrière le développement de solveurs EHD efficaces) ainsi que l'aspect ingénierie (l'application des solveurs à des situations d'intérêt pratique) cette thèse est devenue un travail assez étendu. Cependant, malgré les résultats et les réponses fournies dans les différentes parties de ce document, il reste de nombreux sujets à étudier, de questions auxquelles il faut fournir des réponses et de nouvelles problématiques à surmonter.

D'un point de vue numérique, bien que le modèle présenté dans cette thèse se soit montré relativement puissant comparé aux modèles classiques, il est loin d'atteindre sa capacité maximale. En effet, le problème élastique tridimensionnel peut être l'objet d'importantes améliorations en réduisant sa taille grâce à une analyse modale ou à l'application du principe de la sous-structuration statique. Ce dernier réduirait le calcul des déformations élastiques à la zone de contact bidimensionnelle. En réduisant encore plus la taille du modèle, la voie sera libre pour l'étude des surfaces rugueuses sous régime transitoire qui requiert une finesse de maillage bien plus importante que les problèmes traitant de surfaces lisses. En plus, l'utilisation des équations de la mécanique des solides pour calculer les déformations élastiques des surfaces en contact permet d'étudier des configurations difficiles, voire même impossible à étudier avec une approche de type massif semi-infini. On cite par exemple les revêtements de surface, les matériaux moux, la plasticité …

D'un point de vue ingénierie, il serait intéressant d'aborder l'étude étendue des épaisseurs de film et des coefficients de frottement à des charges faibles, modérées et fortes pour différents types de lubrifiant en couvrant un large domaine de conditions opératoires, tout en prenant en compte, dans la mesure du possible, la dépendence des propriétés thermiques des différents matériaux avec la pression et la température. Cela n'a pas été fait durant ce travail à cause d'un manque de données expérimentales, mais un important projet expérimental-numérique est en train de se mettre en place. De telles études requièrent des collaborations entre différentes institutions afin de déterminer avec précision les propriétés thermiques et rhéologiques des lubrifiants. Le but final est de tirer des résultats obtenus des formules analytiques robustes permettant aux ingénieurs de déterminer directement les épaisseurs centrales et minimales de film sans avoir à exécuter les calculs complets. Dans l'idéal, ces formules prendront en compte les effets thermiques et le comportement rhéologique complet du lubrifiant, y compris les effets non-Newtoniens. Enfin, afin de conclure l'analyse du potentiel d'utilisation des FTFV en tant que lubrifiants dans les contacts EHD, il reste à quantifier quel critère est le plus important d'un point de vue économique: est-ce la réduction de la dissipation d'énergie par frottement ou bien la réduction de la durée de vie du système?

Nomenclature

a	Hertzian contact circle's radius
a_V	Volume-temperature variation constant
A_1, B_1, C_1	WLF model parameters
A_2, B_2, C_2	WLF model parameters
α	Pressure-viscosity coefficient
α^*	Equivalent pressure-viscosity coefficient
B, R_0	Doolittle model parameters
β, β', β''	Dimensionless convection tensors for different Reynolds' equations
β_{ch}	Temperature-viscosity coefficient for the Cheng model
β_{DH}	Dowson & Higginson density-temperature coefficient
β_K	Bulk modulus-temperature coefficient
β'_K	Initial pressure rate of change of bulk modulus-temperature coefficient
C	Compliance matrix
d	Depth of solid bodies for thermal problem
D	Dimensionless depth of solid bodies for thermal problem
δ	Elastic deflection of the contacting bodies
$\overline{\delta}$	Dimensionless elastic deflection of the contacting bodies
E_{eq}, υ_{eq}	Equivalent Young's modulus and Poisson's coefficient
E_i, υ_i	Young's modulus and Poisson's coefficient of component *i* respectively
E'	Reduced elastic modulus of the contacting bodies
ε_c	Relative occupied volume-temperature coefficient
ε_{ii}	Normal strain component in the *i*-direction
ε_s	Strain tensor
$\overline{\varepsilon}, \overline{\varepsilon}', \overline{\varepsilon}''$	Dimensionless diffusion coefficients for different Reynolds' equations
η	Generalized Newtonian viscosity
F	External applied load
F_i	Body force in the *i*-direction
G_c, n_c, β_c	Modified carreau model parameters
γ_{ij}	Shear strain component in the *j*-direction in a plane having *i* as a normal
h	Film thickness
$h_c, h_{\min}$	Central and minimum film thickness respectively

$h_{c\min}$	Minimum film thickness on central line in x-direction
h_e	Element size or diameter
h_0	Film thickness constant parameter
H	Dimensionless film thickness
$H_c, H_{\min}$	Dimensionless central and minimum film thickness respectively
$H_{c\min}$	Dimensionless minimum film thickness on central line in x-direction
H^1	Usual Sobolev space of order 1
k, c	Thermal conductivity and heat capacity respectively
K_0	Initial bulk modulus
K_0'	Initial pressure rate of change of bulk modulus
l, l'	Interpolation order of hydrodynamic and elastic problem respectively
m_x, m_y	Mass flow rate in the x and y-directions respectively
M, L	Moes dimensionless parameters
$\vec{n}$	Outward normal vector
$\vec{n}_c$	Outward normal vector to the cavitation boundary
N_{iter}	Number of iterations of the Newton-Raphson procedure
$N_P, N_U, N_{\overline{T}}$	Interpolation functions for P, U and $\overline{T}$ respectively
μ	Viscosity
μ_g	Viscosity value at glass transition temperature
μ_R	Viscosity value at reference state
μ_0	Ambient temperature zero-pressure viscosity
μ_1, μ_2	Low and high shear Newtonian viscosity respectively
$\overline{\mu}$	Dimensionless viscosity
Ω_c	Contact domain
$\partial\Omega_c$	Contact domain's boundary
p	Pressure
p_h	Hertzian pressure
p_R, T_R	Reference pressure and temperature respectively
P	Dimensionless pressure
$P_i, U_i, \overline{T}_i$	Nodal values of P, U and $\overline{T}$ respectively
$P^h, U^h, \overline{T}^h$	Discrete form of P, U and $\overline{T}$ respectively
P^-	Negative part of pressure profile
Pe	Peclet number
$\delta P, \delta U, \delta H_0$	Increment of P, U, and H_0
R	Equivalent radius of curvature
R_{ix}, R_{iy}	Radius of curvature of surface i in the x and y-directions respectively
Re	Reynolds number
$\mathbb{R}$	Real space
ρ	Density
ρ_{id}	Isotropic diffusion parameter
ρ_R	Density value at reference state

$\bar{\rho}$	Dimensionless density
$S_P, S_U, S_{\bar{T}}$	Solution space for P, U and $\bar{T}$ respectively
$S_P^h, S_U^h, S_{\bar{T}}^h$	Discrete form of S_P, S_U and $S_{\bar{T}}$ respectively
SRR	Slide-to-roll ratio
σ	Stress tensor
σ_{ii}	Normal stress component in the i-direction
σ_n	Normal stress component
t	Time
T	Temperature
T_g	Glass transition temperature
T_0	Ambient termperature
τ	Stabilization parameter
$\tau_e, \dot{\gamma}_e$	Equivalent shear stress and shear rate respectively
τ_{ij}	Shear stress component in the j-direction in a plane having i as a normal
u, v, w	Elastic displacement components in the x, y and z-direction respectively
u_f, v_f	Fluid flow velocity components in the x and y-directions respectively
u_i, v_i, w_i	Velocity components of surface i in the x, y and z-direction respectively
u_m	Mean entrainment velocity
U	Elastic displacement vector
U_i	Velocity vector of surface i
V	Volume
V_R	Volume at reference state
V_0	Ambient pressure volume
V_∞	Relative occupied volume
$V_{\infty R}$	Relative occupied volume at reference state
W_{HD}, G_{HD}, U_{HD}	Hamrock & Dowson dimensionless parameters
$W_P, W_U, W_{H_0}, W_{\bar{T}}$	Weighting functions for P, U, H_0 and $\bar{T}$ respectively
$W_P^h, W_U^h, W_{\bar{T}}^h$	Discrete form of W_P, W_U and $W_{\bar{T}}$ respectively
x, y, z	Space dimensions
X, Y, Z	Dimensionless space dimensions
ξ	Penalty term parameter
ξ_0	Penalty term constant parameter
Z_0, S_0	Roelands equation parameters

1 Introduction

Friction and wear are part of our everyday's life. They take place whenever two bodies come into contact with a relative motion with respect to each other. They are essential for undergoing our simple activities such as walking, brushing our teeth… But in general, in a mechanical system, friction and wear (although sometimes essential) appear to be harmful at many levels. Friction leads to a higher energy consumption of the system whereas wear can shorten its' life. Therefore, for any typical machine (combustion engine, turbine, compressor …), it is important to control these two factors. From an energetical point of view, reducing friction and therefore the power dissipation within the different contacts leads to an improved efficiency of the machine. From a reliability point of view, avoiding any surface degradation (fretting, cracks, fatigue …) allows a considerable increase of the system's life while at the same time avoiding its failure. The importance of these problems in industrial applications justifies the considerable efforts that have been carried out in the field of tribology over the last century.

One way to reduce friction in contacts is lubrication. In other words, the contacting surfaces are separated by a lubricant film. The lubricant can be liquid, gaseous or even solid. The build up and preservation of the film require a pressure generation inside it. When this pressure is generated by an external system (like a compressor for example), the lubrication is called "hydrostatic". On the other hand, when it is generated by the relative motion of the contacting surfaces the lubrication is called "hydrodynamic". In a lubricated contact, friction forces are less important than in the dry case because the relative motion of the surfaces is accommodated by the lubricant shear. The good understanding of the behaviour of such contacts is essential for the design of mechanical components in order to establish optimal operating conditions and therefore increase their life.

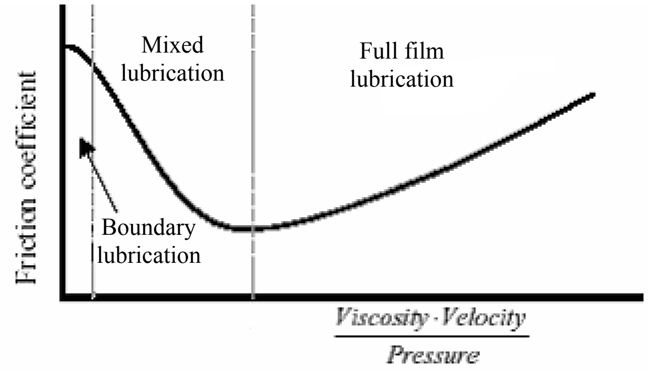

Figure 1.1: Stribeck curve for the different lubrication regimes

In general, three lubrication regimes are defined according to their range of friction coefficients (Stribeck curve, See Figure 1.1):

- **Boundary lubrication:** a major part of the load is supported by the direct contact of the surface asperities. This regime is characterized by a high friction coefficient.

- **Mixed lubrication:** the load is supported by both the direct asperities contact and the lubricant film. The friction coefficient for this regime is lower than for boundary lubrication.

- **Full film lubrication:** the contacting surfaces are separated by a complete lubricant film. Friction coefficients are relatively low.

Our study mainly concerns the full film lubrication regime. When a complete lubricant film separates the contacting surfaces, two different types of lubrication are defined:

- **Hydrodynamic lubrication (HL)** which takes place when the pressure generated within the contact is relatively low and does not enhance a significant elastic deformation of the contacting surfaces. This is typically the case of conformal contacts which are characterized by large contact surfaces and therefore low pressures. Journal bearings are representative of this type of lubrication (See Figure 1.2).

- **Elastohydrodynamic lubrication (EHL)**, as indicated by its name, takes place whenever the pressure generated in the lubricant film is high enough to induce a significant elastic deformation of the contacting surfaces. These deformations have an important influence on the geometry of the lubricant film and their amplitude can be greater than the film thickness. Moreover, the rheological properties of the lubricant are highly affected by the high pressure generation (the viscosity can increase by several orders of magnitude). This is typically the case of non-conformal contacts that can be encountered in spur gears, cylindrical roller bearings, or also ball bearings for example (See Figure 1.2).

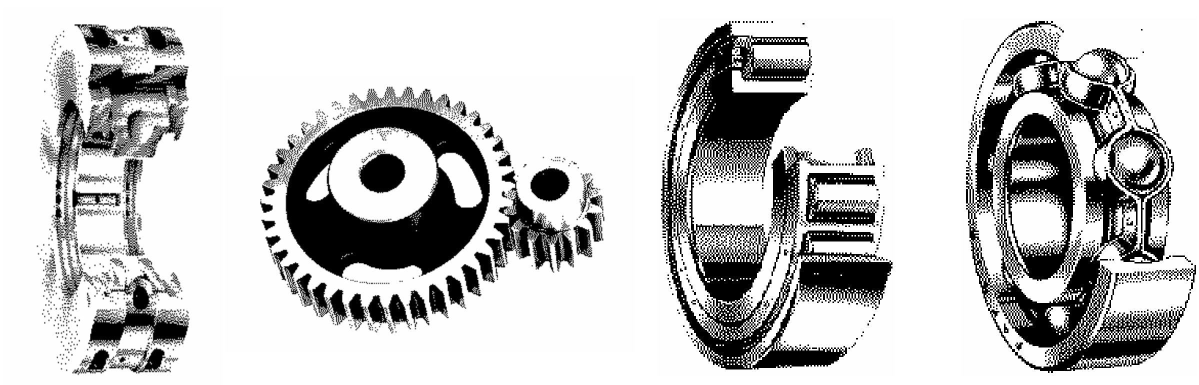

(a) (b) (c) (d)

Figure 1.2: Examples of hydrodynamic lubrication: (a) journal bearing and elastohydrodynamic lubrication: (b) Spur gears, (c) cylindrical roller bearings and (d) ball bearings

The study carried out in this thesis is mainly focused on this last type of lubrication. When studying these contacts, it is not necessary to consider the often rather complex geometry of the contacting machine elements. Since the film thickness and contact width are generally small compared to the local radius of curvature of the running surfaces, the surface geometry in the contact area can be accurately approximated by paraboloids. This approximation allows a simplification of the contact geometry. The latter can be reduced to the contact between a paraboloid and a flat surface.

In general, two types of EHL problems are distinguished:

- **Line contacts:** the contacting elements are assumed to be infinitely long in one of the principal directions. In fact, the radius of curvature of the paraboloids approximating the surfaces in this direction is infinitely large. In the unloaded dry contact situation, the surfaces touch along a straight line. If a load is applied, a strip shaped contact region is formed because of the elastic deformations. Figure 1.3 shows the most widely used approximation of the line contact situation: two parabolically shaped surfaces with local radii of curvature R_1 and R_2 moving with surface velocities u_1 and u_2 respectively. Such contacts take place in spur gears or cylindrical roller bearings for example (See Figure 1.2). The equivalent geometry corresponds to a contact between a cylinder and a plane. The equivalent radius R of the cylinder is given by:

$$\frac{1}{R}=\frac{1}{R_1}+\frac{1}{R_2} \tag{6.1}$$

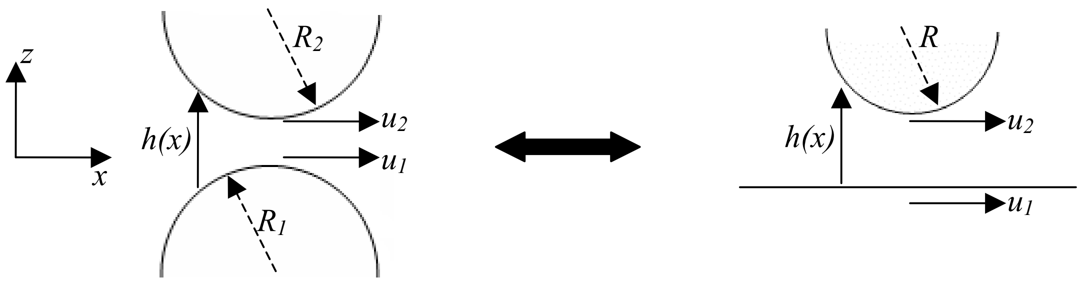

Figure 1.3: EHL line contact and the equivalent reduced geometry

- **Point contacts:** the most widely used approximation of the more general point contact situation corresponds to a contact between two parabolically shaped surfaces with local radii of curvature R_{1x} and R_{2x} in the x-direction and R_{1y} and R_{2y} in the y-direction. The x-direction is chosen to coincide with the direction of the surface velocities u_1 and u_2. In the dry contact situation, both surfaces nominally touch at one point in the unloaded situation. When a load is applied, the shape of the contact region depends on the ratio of the radii of curvature in the x and y-directions of the two bodies. In general, it is an ellipse, and therefore this type of contact is also referred to as an **elliptical contact**. An example of a point contact is the contact between the ball and the inner or outer raceway of a ball bearing (See Figure 1.2). A special case of an elliptical contact is the **circular contact** which occurs if the radii of curvature of the contacting elements in both principal directions are equal. The reduced equivalent geometry of point contacts corresponds to a contact between a single paraboloid with radii of curvature R_x and R_y and a flat surface (See Figure 1.4). R_x and R_y are generally referred to as the reduced radii of curvature in the x and y-direction respectively. They are defined as follows:

$$\begin{aligned} \frac{1}{R_x} &= \frac{1}{R_{1x}} + \frac{1}{R_{2x}} \\ \frac{1}{R_y} &= \frac{1}{R_{1y}} + \frac{1}{R_{2y}} \end{aligned} \tag{6.2}$$

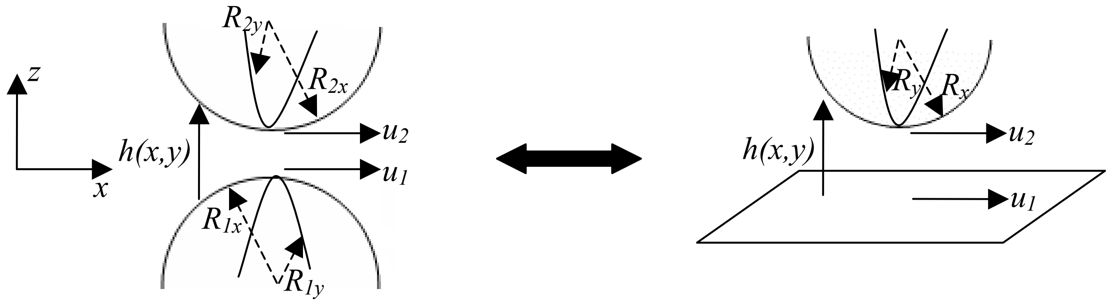

Figure 1.4: EHL point contact and the equivalent reduced geometry

The EHL of circular contacts will be the main topic of this thesis. A particular interest is shown for lubrication with Ultra-Low-Viscosity Fluids (ULVF). This study is motivated by an industrial demand from the SKF Engineering and Research Centre. This demand is based upon many practical reasons that are briefly listed below.

1.1 Why lubricate with ULVF?

Before dealing with the advantages of ULVF in lubrication, we mention that the order of magnitude of the viscosity of these fluids is 10^{-4} Pa.s. Compared to water that has a viscosity of 10^{-3} Pa.s, or air that has a viscosity of 10^{-5} Pa.s, the ULVF fluids that we are interested in, have a range of viscosities varying between those of air and water.

An important aspect of using ULVF as lubricants is the economical issue of energy saving which is also more and more considered nowadays as an environmental issue. As a matter of fact, the energy dissipation in a lubricated contact due to friction forces increases with the viscosity of the lubricant. Fox [31] shows that a 4% economy of fuel consumption in a Diesel engine could be reached by simply reducing the viscosity of the lubricant. Clearly, the contact conditions become more severe and the wear rates of the contacting surfaces increase. Nevertheless, a good functioning of the system can be obtained by applying a surface treatment to the contacting bodies in such a way to increase their resistance to wear. Another alternative to avoid surface degradation consists in adding some anti-wear additives to the lubricant.

On the other hand, many mechanical systems operate with two working fluids, each having a different function. The first one is the lubricant, while the second (that generally has a low viscosity) can have different functions depending on the type of machine. It could be a heat transfer fluid in heat pumps or refrigeration systems for example, or a combustion fluid such as fuel in combustion engines or cryogenic liquids for rocket propulsion engines. For a good functioning of such systems, it is highly preferable that the two working fluids do not mix. This is why these machines are generally designed with two isolated circulation systems, one for each fluid. Not only does this make the design and maintenance of these machines more complicated, but it also leads to an increase of their size and weight. Thus, it would be interesting to have one working fluid that can fulfil the two different functions inside the system. This would allow an easier design and maintenance of the machine that would include only one circulation system. Knowing that a lubricant could almost never fulfil the function of the second working fluid, the only solution would be to use the ULVF as a lubricant.

1.2 EHL, a historical review

The first steps of understanding the lubrication phenomenon go back to the 19th century with the works of Hirn [52] in 1854. Then, in 1883, two experimental investigations lead by Beauchamp Tower [111] in England and Nicoli Petrov [96] in Russia made it clear that the rigid surfaces of the contacting bodies in a hydrodynamic journal bearing were fully separated by a fluid film. Thus, it was demonstrated that the friction forces in such a mechanism are governed by hydrodynamics and not by the direct contact between the solids. In 1886, Reynolds [99] established the famous *Reynolds' equation* which is the basis of all actual lubrication theories. It expresses the relationship between the pressure in the lubricant film, the geometry and the kinematics of the moving parts. The solution of this equation, based on the theory of viscous laminar flows, confirms the observations made by Tower and Petrov. At the beginning of the 20th century, Michell [89] and Kingsburry [75] made a first step towards understanding the phenomenon of lubrication in hydrodynamic journal bearings.

A few years later, Martin [86] and Gümbel [44] applied the hydrodynamic theory to the case of rigid gears. Surprisingly, the results they obtained predicted very small film thicknesses compared to the surface roughness. Nevertheless, the contact was well protected by a full lubricant film that separated the surfaces. It took 20 additional years to witness the appearance of the fundamentals of elastohydrodynamic lubrication with the works of Ertel [24] and Grubin [39]. Introducing Hertz [51] theory for the deformation of semi-infinite elastic bodies under dry contact conditions along with the Barus [7] pressure-viscosity law, they calculated larger film thicknesses compared to those obtained by Martin and Gümbel for the same operating conditions. Thus, the fundamental features of elastohydrodynamic lubrication were revealed.

The second part of the 20th century witnessed an increasing interest of the scientific community in lubrication problems. At the same time, the development of experimental technology based on optical interferometry techniques along with the progress in numerical resolution of partial differential equations due to more powerful computers and more performing algorithms allowed the accurate understanding of lubrication phenomena. These developments lead to a deeper knowledge of the film thickness distribution in an elastohydrodynamic (EHD) contact.

1.2.1 Experimental work

The validation of theoretical works requires experimental results to confirm some qualitative findings such as the full-film separation of the contacting surfaces or the shape of the pressure distribution throughout the film. These experiments can also be used to confirm more quantitative results such as the film thickness distribution. Over the years, several techniques based on different physical principles have been developed. The most popular one is the optical interferometry. Foord et al. [30], Gohar and Cameron [36][37], Wedeven et al [119], Chiu and Sibley [19] noticed by using this technique, the particular horseshoe shape of the film thickness distribution in an EHD point contact (See Figure 1.5). Nowadays, this technique is more developed with much more accurate optical sensors allowing the measurement of very thin film thicknesses reaching the order of a few nanometres as shown in the works of Guangteng et al. [42] and Cann et al. [12][13][14].

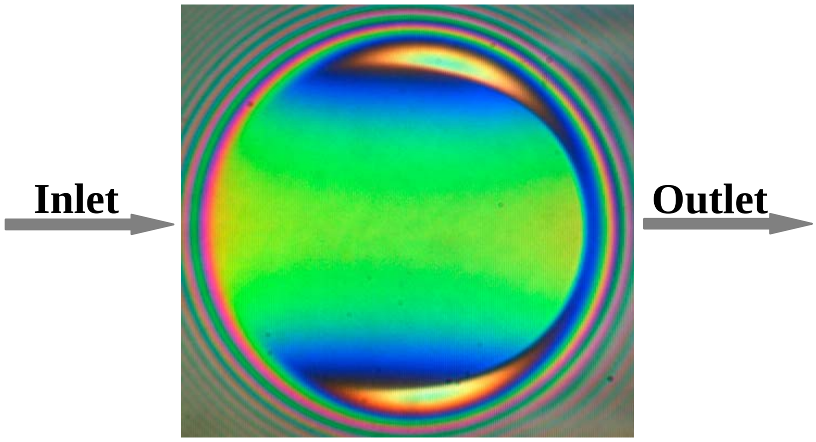

Figure 1.5: Film thickness distribution in an EHL point contact using optical interferometry

Optical interferometry is limited to film thickness measurements. Information regarding the pressure distribution is obtained by a different technique. In fact, Safa et al. [102][103] and Baumann et al. [8] performed measurements using micro transducers, vacuum deposited on one of the running surfaces. Depending on the type of transducer, this technique allows the measurement of pressure, film thickness or also temperature in the conjunction. More recently, a Raman Microspectrometry technique was introduced by Jubault et al. [69] to measure accurate pressure distributions in lubricated contacts.

The parallel development of experimental and numerical techniques allows today the quantitative comparison of pressure and film thickness distributions and thus the validation of numerical models. In the next section, we shall have an overview of the different numerical techniques that have been used in the literature for the modelling of EHL problems.

1.2.2 Numerical work

Petrusevich [97] was the first to provide a full numerical solution of an EHL contact. He noticed the presence of the film thickness constriction and the associated pressure spike at the outlet of the contact (See Figure 1.6).

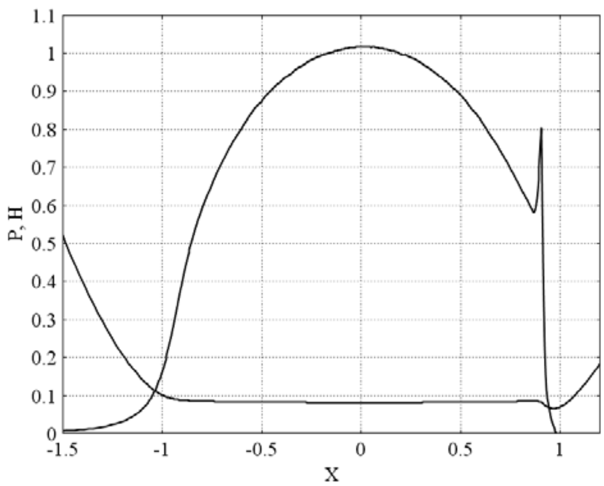

Figure 1.6: Smooth EHD line contact: non-dimensional film thickness and pressure distributions

With the advance of computer technology, numerical solutions emerged giving several analytical formulas linking central and minimal film thicknesses to various non-dimensional parameters in the contact. Among those we cite Hamrock and Dowson [46], Nijenbanning et al. [92] and Evans and Snidle [25]. The numerical solution of the EHD problem is not easy to reach because it involves the resolution of a highly non-linear problem. This problem is defined by three main equations: the Reynolds' equation (allows the computation of the hydrodynamic pressure field in the lubricant film for a given geometry), the film thickness equation (resulting from the superposition of the rigid body separation, the initial geometry and the elastic deformation of the surfaces induced by the pressure in the lubricant film) and the load balance equation (that ensures the global convergence of the numerical scheme). Various numerical approaches emerged because of convergence difficulties encountered during the resolution of the problem. These difficulties are, in part, due to the coupling between the Reynolds' equation and the elastic deformation of the surfaces. The different numerical approaches can be classified within two main categories: the semi-system approach and the full-system approach.

1.2.2.1 Semi-system approach

This approach consists in solving the EHL equations separately and establishing an iterative procedure between their solutions as shown in the flow diagram of Figure 1.7. One of the first to use this approach were Dowson and Higginson [22] for the line contact problem. Then followed the pioneering work of Hamrock and Dowson [45][46][47][48] and Ranger et al. [98] for the circular contact and more recently, Chittenden et al. [18] and Nijenbanning et al. [92] for the elliptical contact. These models were based on what is known as the **direct method** i.e. Reynolds' equation is solved as a function of pressure for a given film geometry. A severe drawback of these models was the pressure limitation to less than 1 GPa whereas in real life EHL contacts, pressures can raise up to 2 or 3 GPa. In order to overcome this limitation, Ertel [24] had introduced earlier the so-called **inverse method**. Contrarily to the direct method, the inverse method consists in solving Reynolds' equation to compute the film thickness for a given pressure profile. Dowson and Higginson [22] were the first to develop an algorithm for the numerical solution of the EHL line contact problem based on the inverse solution of Reynolds' equation. This approach was later extended to circular contacts by Evans and Snidle [26]. Despite the robustness of this method in the contact region where the direct method suffers from stability problems, the solution remains unstable in the inlet and outlet regions of the contact. As a matter of fact, Kweh et al. [76] introduced a hybrid approach which consists in using a combination of both methods: the direct one in the inlet and outlet parts of the contact, and the inverse one in the central contact region. A basically similar algorithm was presented by Seabra and Berthe [105][106]. Although this approach was successful in extending the solution of EHL problems to highly loaded contacts, it suffered from major drawbacks. In fact, solving Reynolds' equation as a function of film thickness for a given pressure profile requires solving a cubic equation which basically has three solutions. Therefore, a good care should be given for the choice of the appropriate solution. Moreover, the relation used for updating the pressure profile, given a certain film thickness, is based on experience and insight. Its physical foundation is not well established.

A major step forward in the field was made by Lubrecht [84][85], who applied multigrid techniques to lubrication problems using the direct method. This technique provides a faster convergence rate of the solution, and therefore, reduced computational times. It is based on a certain understanding of the convergence behaviour of iterative resolution processes. In fact, iterative schemes succeed in smoothing the error of the solution only when the latter has a wavelength of the order of the mesh size. When the wavelength of the error is much larger than the mesh size, the iterative process becomes very slow. A solution to this problem consists in transferring the resolution process to a coarser grid. Thus, Multigrid techniques consist in switching the iterative resolution process back and forth on different grid levels whenever it is required. Further computation time reductions were achieved by Brandt and Lubrecht [9] introducing the so-called Multi-Level Multi-Integration (MLMI) technique for which the computation of the elastic deformation integrals was fastened. This work was further improved at the beginning of the 90's by Venner [112][113][114] who extended this method to the case of highly loaded contacts by applying a distributive line relaxation scheme. This work provided an efficient alternative for the inverse method in the case of highly loaded contacts and laid the foundation in numerical modelling of EHL problems for the years to come. A further development in this approach was the introduction of the so-called Discrete Convolution Fast Fourier Transform (DC-FFT) method for the elastic deformation evaluation by Ju et al. [68]. This method is claimed to be three times faster than the MLMI method according to Wang et al. [117].

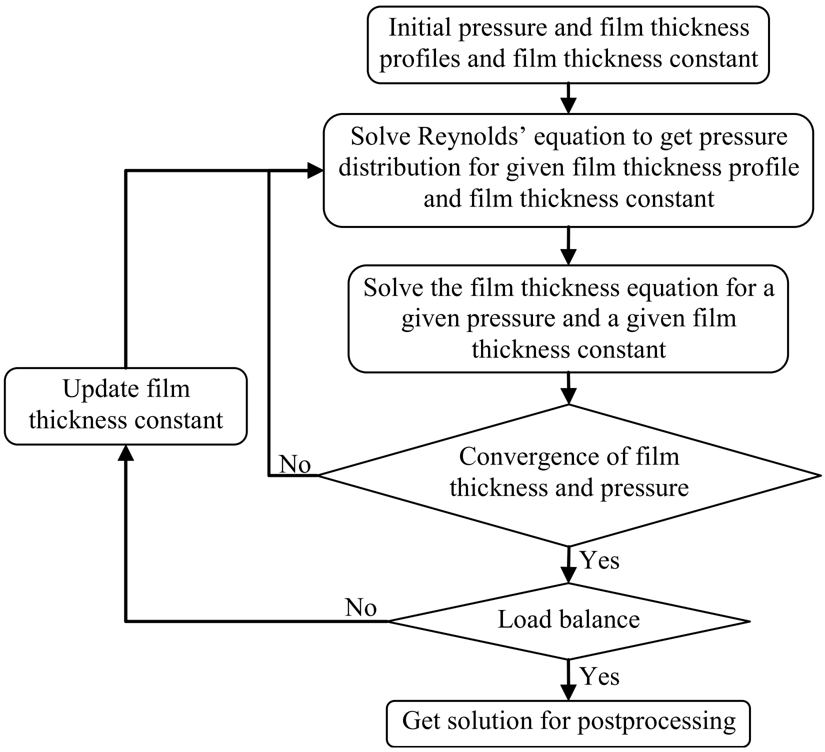

Figure 1.7: Flow diagram of a semi-system approach using the direct method

The different works cited in this section are based on a finite difference discretization of the EHL equations. Although in general this method limits the discretization process to regular structured rectangular meshes using low order approximations, it is the most widely used one in EHL modelling. This is due to the development of the efficient techniques cited above. An alternative method that has been given less attention in EHL is the finite element method. This method enables the use of non-regular unstructured meshing along with high order approximations. An example of the application of this method to EHL problems is given in [82][83]. The authors apply the direct method using a Discontinuous Galerkin formulation in order to stabilize the solution of highly loaded line contacts. To the author's knowledge, this method has not yet been extended to the point contact case. Unfortunately, the use of discontinuous elements leads to larger size systems. In fact, every discretization point may have several nodal values for the same variable: one for every element it belongs to. Hughes and coworkers [60] have also used the finite element method by combining first and second-order Reynolds' approaches in order to get efficient solutions for both lightly and heavily loaded line contacts. In fact, the first-order approach, which consists in writing Reynolds' equation as a first-order differential equation, is only stable in high pressure areas whereas the second-order approach is only stable in low pressure areas. Therefore, the authors proposed to use a combination of the second-order approach in the inlet and outlet areas of the contact whereas in the central area a first-order approach is used. This provides a stable solution for any load case. Unfortunately, the use of the first-order approach limits this method in any case to the line contact problem.

Finally, note that since the semi-system approach presented in this section is based on a separate resolution of the EHL equations, a loss of information occurs during the iterative procedure established to couple the different solutions. This loss of information needs to be compensated by severe underrelaxation, which leads to a slow convergence rate of the iterative process.

1.2.2.2 Full-system approach

The full-system approach, as indicated by its name, consists in solving the different EHL equations simultaneously as shown in the flow diagram of Figure 1.8. Different methods found in the literature can be classified within this category. For example, the recent developments in Computational Fluid Dynamics (CFD) modelling or Fluid-Structure Interaction (FSI) have been applied to EHL problems by Hartinger et al. [50] and Yiping et al. [124] respectively. The latter are based on the resolution of the full Navier-Stokes equations coupled with the linear elasticity equations for the elastic deformation calculation. This approach is quite accurate but is also very time consuming (calculations may last more than one week for typical point contact cases using a relatively coarse mesh). The results clearly confirm that the pressure variation across the film thickness can be neglected compared to the variations in the contact plane. The main advantage of these methods is that the exact amount of side leakage can be evaluated since the complete velocity field in the lubricant film is computed. Moreover, the exact stress field can be obtained in the contacting bodies. This can be useful for a fatigue study of the components. But, because of the large computational efforts, nowadays and until computer power becomes much more developed, these methods will still be of impractical relevance.

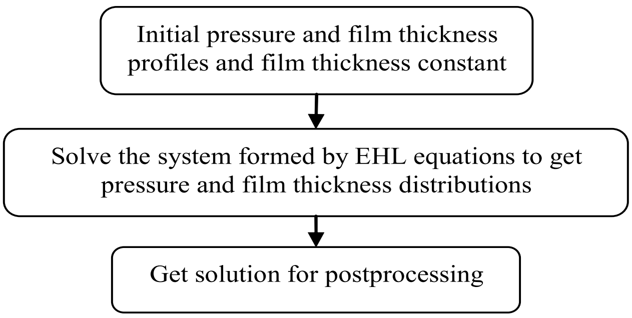

Figure 1.8: Flow diagram for a full-system approach

Another interesting method is the Newton-Raphson method. It was first used by Rhode and Oh [93][101] who solved the EHL problem as one integro-differential equation using a finite element discretization. This work revealed the outstanding potential of this method that ensures the convergence of the solution within only a few iterations. Later on, a similar model was provided by Okamura [94]. An improved version of the model of Okamura was later provided by Houpert and Hamrock [57] for the line contact case. This method was later extended to the case of elliptical contacts by Hsiao et al. [58]. Because of the simultaneous solution of all pressure updates, the implementation of the cavitation condition is rather tedious. In fact, for the line contact case, the location of the exit boundary is introduced as a separate unknown to be solved for in the iterative process. Since this location consists in only a single unknown, this does not result in a serious complication of the equations. However, in the point contact case, the location of the exit boundary varies over the two-dimensional computational domain which results in a more complex model. Moreover, in all these works, the elastic deflection calculation is based on a half-space approach. Therefore the elastic deflection at any discretization point is related to all the other points of the domain by means of the integral calculation. This results in a full Jacobian matrix which requires a huge computational effort in order to invert it. Finally, at heavy loads, the Jacobian matrix becomes practically singular which makes the solution of heavily loaded contacts hard to reach. It is believed that the combination of the tedious treatment of the free boundary problem with the full Jacobian matrix that becomes singular for heavy loads was the main reason behind the cease of development of this method for a while.

Recently, Evans and Hughes [27] introduced the so-called “Differential Deflection” method which provides a differential equation for the elastic deflection problem based on the half-space approach. This approach, contrarily to the direct half-space one, has the advantage of being more localized. In fact, the differential operator quickly tends towards zero when the calculation point of the elastic deflection moves away from the point of application of the force. In practice, the matrix terms become more and more negligible as they move away from the diagonal. This gives a less full matrix when applying a full-system resolution. The authors and their co-workers applied this method to the line contact case [61] and then extended it to the more general point contact case [55][56]. However, the system matrix of the latter still had a large bandwidth, and a special coupled iterative technique had to be used in order to solve the coupled equations efficiently.

Finally, since the full-system approach solves the EHL equations simultaneously, no loss of information occurs between their different solutions. Therefore, underrelaxation is no longer required. This is the main reason behind the outstanding convergence rates of the iterative process.

1.3 Outline of the thesis

After this brief literature review focused on the numerical modelling of EHL problems, one could conclude that the “ideal” EHL solver would be based on a Newton-Raphson full-system resolution of the different equations. This allows a fast solution of the problem within a few iterations without any loss of information occurring between the solutions of the different equations. The discretization of these equations would be realized using finite elements, enabling thus the use of non-regular unstructured meshing along with high order approximations. This leads to smaller size systems where the degrees of freedom (dofs) are optimally distributed (fine meshing is used only where needed). The resolution process would be stable for a wide range of load conditions. And finally, the Jacobian matrix of the corresponding system of equations would be sparse and the treatment of the free boundary problem straightforward. The aim of this thesis is to build this “ideal” EHL solver in the case of steady-state smooth circular contacts. This approach is not restricted to steady-state circular contacts and can be easily extended to the case of line or elliptical contacts under transient regime. But, within the scope of this thesis, only steady-state circular contacts are of interest.

From a physical point of view, appropriate realistic models of lubricants' rheological behaviour are used. Then, this approach is extended to a more physical modelling, taking into account non-Newtonian and thermal effects which can be important at high entrainment and / or sliding speeds and / or also at high load operating conditions. Comparisons with existing numerical models and experimental data are a necessity if one wants to make sure the model does not deviate from reality. Hence, most of the test cases computed in the numerical part of this work have been compared to experimental results. The developed approach is used to study the ULVF lubrication problems which are to be considered more and more seriously in the scope of "decelerating" the global warming phenomenon and preserving the environment. Such problems are quite difficult to handle experimentally because of the very thin films that are encountered. Thus, a numerical approach appears to be necessary if the study is to be carried out over a wide range of operating conditions.

First, chapter 2 describes EHL theory and equations for the steady-state isothermal Newtonian circular contact situation. Reynolds', the film thickness and the load balance equations are given. The different laws describing the variation of the lubricant's viscosity and density with both pressure and temperature are listed. All equations are given in their regular and dimensionless forms.

Then, chapter 3 provides a detailed description of the numerical model established to get a robust EHL solver in the case of a steady-state isothermal circular contact lubricated with a Newtonian fluid. The Reynolds', film thickness and load balance equations are solved simultaneously using a Newton-Raphson scheme. This model uses a new way to take into account the elastic deflection of the contacting surfaces based on the classical linear elasticity equations. The free boundary problem is treated in a straightforward manner using a penalty method. The solution process is then extended to highly loaded contacts by writing Reynolds' equation as a convection / diffusion equation (as a function of pressure) with a source term and using special stabilized finite element formulations. The complexity and convergence properties of this model are then studied and compared to classical finite difference multigrid based ones. A comparative study with the latter is carried out in order to validate the current approach and demonstrate its efficiency. This model provides a solid basis that can be extended towards a more physical modelling of EHL contacts. In this section, line contact results are provided for demonstrative purposes.

Since most lubricants do not behave as Newtonian fluids, chapter 4 is devoted to the extension of the previous model to account for the non-Newtonian behaviour of the lubricant. The solution process is extended to highly loaded contacts using a similar procedure to the one described earlier. A complex rheological modelling is introduced showing that the film thickness comes a lot closer to experimental results than would be predicted by a simple Newtonian approach especially at low or moderate speed operating conditions. However, at high entrainment and / or sliding speeds, they start showing a slight discrepancy with experimental data. This is due to the appearance of significant thermal effects in the **inlet area** of the contact. Friction coefficients are also overestimated by this approach at moderate or high speed operating conditions. This is due to thermal effects, in this case, in the **central area** of the contact. The latter have a significant influence on friction whereas film thicknesses are mostly affected by the temperature increase in the inlet area.

In chapter 5, an extension of the previous model to account for thermal effects in both Newtonian and non-Newtonian lubricant configurations is considered. Again, a numerical stabilization procedure is used to extend the solution to the case of highly loaded contacts. A full 3D modelling of heat convection and conduction within the contact is considered. This approach shows that both film thicknesses and friction coefficients can be accurately estimated over a wide range of speed operating conditions.

In chapter 6, the model described above is used to study the EHL of ULVF in circular contacts. Two typical lubricants are considered. A series of test cases is carried out showing that such lubricated contacts can only work under high speed and moderate load operating conditions. It is also shown that the traction coefficients are relatively low compared to contacts lubricated with a more classical lubricating oil or grease. This confirms the economical aspect of the use of these fluids as lubricants discussed in the first section of this chapter.

Finally, a general conclusion on the numerical modelling of EHL problems and the use of ULVF as lubricants in such contacts is established. As a result of covering both the numerical mathematical side (the theory behind the development of efficient EHL solvers) as well as the engineering side (the application of the solvers to situations of practical interest), this thesis has become quite an extensive work. However, in spite of all the results and answers provided in the different sections of this document, there are still many subjects to be studied, questions that remain unanswered and new issues to be addressed. This is why this document ends with a brief outline of some interesting topics for future research.

2 EHL theory and equations

In this section, a mathematical model describing the steady-state isothermal EHD circular contact situation is established. As mentioned before, the model consists of three equations: The Reynolds'equation that relates the pressure in the lubricant film to the geometry of the conjunction and the velocities of the moving surfaces, the film thickness equation for the computation of the total gap separating the surfaces and finally, the load balance equation requiring that the total generated pressure in the lubricant film balances the externally applied normal load. Because of the high pressures in the lubricant film, the variation of the lubricant properties such as viscosity and density must be taken into consideration. Hence, the model is completed with some relations describing the dependence of both viscosity and density on pressure.

2.1 Reynolds' equation

Reynolds' equation is obtained by applying the full Navier-Stokes equations to thin film flows considering the following simplifying assumptions:

1- Body forces are negligible
2- No slip at the boundary surfaces
3- The lubricant flow is laminar (low Reynolds number)
4- Inertia and surface tension forces are negligible compared to viscous forces
5- The lubricant is Newtonian
6- The film thickness is small compared to the dimensions of the contact
7- The lubricant's viscosity and density are constant across the film thickness

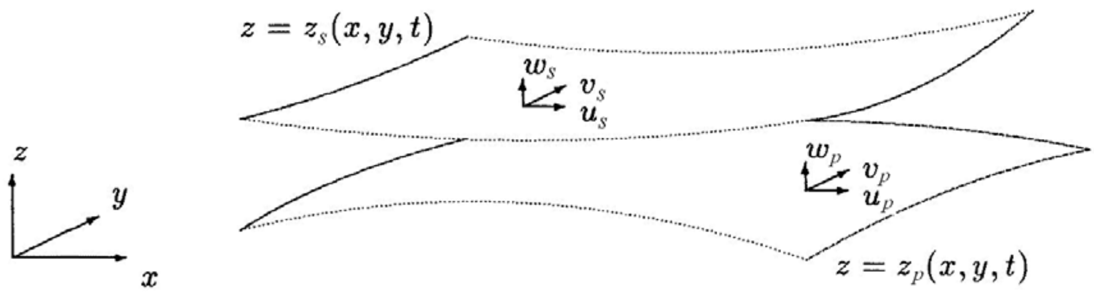

Figure 2.1: Fluid flow between two moving surfaces

Consider the situation displayed in Figure 2.1 corresponding to a flow between two moving surfaces $z = z_p(x, y, t)$ and $z = z_s(x, y, t)$ with surface velocity vectors

$U_p = \{u_p, v_p, w_p\}$ and $U_s = \{u_s, v_s, w_s\}$ respectively. Since circular contacts are considered, the lower and upper surfaces correspond then to the plane and spherical surfaces of the equivalent reduced geometry respectively (See Figure 1.4). The previous assumptions lead to a simplified form of the Navier-Stokes equations. The conservation of momentum equations become:

$$\begin{aligned} \frac{\partial p}{\partial x} &= \frac{\partial \tau_{zx}}{\partial z} \\ \frac{\partial p}{\partial y} &= \frac{\partial \tau_{zy}}{\partial z} \\ \frac{\partial p}{\partial z} &= 0 \end{aligned} \tag{2.1}$$

With:

$$\tau_{zx} = \mu \dot{\gamma}_{zx} = \mu \frac{\partial u_f}{\partial z} \quad \text{and} \quad \tau_{zy} = \mu \dot{\gamma}_{zy} = \mu \frac{\partial v_f}{\partial z} \tag{2.2}$$

Where u_f and v_f are the velocity field components of the lubricant flow in the *x* and *y*-directions respectively. The following no-slip boundary conditions are assumed:

$$\begin{aligned} u_f = u_p, \quad v_f = v_p, \quad w_f = w_p \quad &\text{at } z = z_p(x, y, t) \\ u_f = u_s, \quad v_f = v_s, \quad w_f = w_s \quad &\text{at } z = z_s(x, y, t) \end{aligned}$$

If the lower surface is taken as a reference, in other words, if z_p is considered as the origin of the *z*-axis ($z_p = 0$ and $0 \le z \le h$ with $h = z_s - z_p$ and $w_p = 0$), then the integration of eqs. (2.1) twice with respect to *z* using the associated no-slip boundary conditions gives the velocity field of the lubricant:

$$\begin{aligned} u_f &= \frac{1}{2\mu}\frac{\partial p}{\partial x} z(z-h) + \frac{h-z}{h} u_p + \frac{z}{h} u_s \\ v_f &= \frac{1}{2\mu}\frac{\partial p}{\partial y} z(z-h) + \frac{h-z}{h} v_p + \frac{z}{h} v_s \end{aligned} \tag{2.3}$$

Now, if we consider a steady-state condition, the mass continuity equation for a compressible flow is given by:

$$\frac{\partial m_x}{\partial x} + \frac{\partial m_y}{\partial y} = 0 \tag{2.4}$$

Where: $m_x = \int_0^h \rho u_f \, dz$ and $m_y = \int_0^h \rho v_f \, dz$

Replacing the velocity components by their expressions given in eqs. (2.3), and considering that surface velocities are parallel to the x-axis and do not vary in space, the mass continuity equation becomes:

$$\frac{\partial}{\partial x}\left(\frac{\rho h^3}{\mu}\frac{\partial p}{\partial x}\right)+\frac{\partial}{\partial y}\left(\frac{\rho h^3}{\mu}\frac{\partial p}{\partial y}\right)=12u_m\frac{\partial}{\partial x}\left(\rho h\right) \tag{2.5}$$

Where: $u_m=\dfrac{u_p+u_s}{2}$

In a more compact form eq. (2.5) also reads:

$$\nabla\cdot\left(\varepsilon\nabla p\right)=\frac{\partial\left(\rho h\right)}{\partial x}\quad \text{with}\quad \varepsilon=\frac{\rho h^3}{12u_m\mu} \tag{2.6}$$

Equation (2.6) is known as Reynolds' [99] equation. It describes the pressure variation throughout the lubricant film as a function of the operating conditions for a given film geometry (described by the film thickness h). The left hand side term is known as the "Poiseuille term" with respect to "Poiseuille flows" which are pressure induced flows, whereas the right hand side term is known as the "Couette term" with respect to "Couette flows" which are induced by the surface entrainment of the fluid.

2.2 Film thickness equation

The film thickness equation results from the superposition of a constant known as the rigid body displacement h_0, the initial undeformed geometry and the elastic deformation $\delta\left(x,y\right)$ of the contacting surfaces induced by the pressure generation within the lubricant film:

$$h\left(x,y\right)=h_0+\frac{x^2}{2R_x}+\frac{y^2}{2R_y}+\delta\left(x,y\right) \tag{2.7}$$

Where R_x and R_y are the equivalent radii of curvature in the x and y-direction respectively. The latter were previously described in eqs. (6.2). Since circular contacts are considered, then $R_x=R_y=R$ and the film thickness equation becomes:

$$h\left(x,y\right)=h_0+\frac{x^2+y^2}{2R}+\delta\left(x,y\right) \tag{2.8}$$

The computation of the elastic deflection term $\delta\left(x,y\right)$ is given in details in the next chapter.

2.3 Load balance equation

The external load applied to the contact is totally supported by the lubricant film. Therefore, the equilibrium of forces requires that the total pressure generated in the contact domain Ω_c balances the external applied load F:

$$\int_{\Omega_c} p(x,y)\, d\Omega = F \tag{2.9}$$

This equation is satisfied by adjusting the constant parameter of the film thickness equation h_0.

2.4 Lubricant's properties

In EHD contacts, the important increase of pressure and temperature may lead to a significant variation of the lubricant transport properties. Two properties are of particular interest for the lubricant film build-up: viscosity and density. The viscosity of a typical lubricant can vary by several orders of magnitude with pressure increase whereas the density dependence on pressure is less spectacular. However, it has a direct impact on film thickness. In general, temperature effects are less important than those induced by pressure, but in many cases, not negligible. When a non-Newtonian lubricant is considered, viscosity may also vary with shear stress. In this section, the various laws of variation of viscosity and density for a Newtonian lubricant with both pressure and temperature are listed. Although, up to here, only the isothermal case is considered, it is important to provide the temperature dependence of the lubricant properties because, in practice, the surrounding or ambient temperature T_0 of a system (which is considered to be the lubricant temperature T in an isothermal approach) may be different from the reference temperature T_R used to evaluate these properties.

2.4.1 Density variations

In this section, the density variations with pressure (p) and temperature (T) are considered. Two models are given: the Dowson & Higginson [23] model and the Tait [53] [54] equation of state:

2.4.1.1 Dowson & Higginson

This model is the most used density variation relationship in EHL. It is expressed by the following mathematical expression:

$$\rho(p,T) = \rho_R \left[1 + \frac{0.6\times10^{-9}\, p}{1+1.7\times10^{-9}\, p} - \beta_{DH}\left(T - T_R\right) \right] \tag{2.10}$$

Where $\rho(p,T)$ is the lubricant's density at a given pressure p and temperature T, $\rho_R = \rho\left(p = p_R = 0, T = T_R\right)$ is the zero-pressure density at the reference temperature T_R and β_{DH} is the density-temperature coefficient. This equation is not always accurate and does not have any physical foundation (it is strictly empirical) but it is used because of its simple mathematical form and its non-dependence on the lubricant type.

2.4.1.2 Tait equation of state

The Tait equation of state is written for the volume V relative to the volume at ambient pressure V_0. The density data is obtained by simply inverting it:

$$\frac{V}{V_0} = 1 - \frac{1}{1+K_0^{'}} \ln\left[1 + \frac{p}{K_0}\left(1+K_0^{'}\right)\right] \tag{2.11}$$

The initial bulk modulus K_0 and the initial pressure rate of change of bulk modulus K_0' are assumed to vary with temperature according to:

$$K_0 = K_{0R} \exp\left(-\beta_K T\right) \tag{2.12}$$

$$K_0' = K_{0R}' \exp(\beta_K' T) \tag{2.13}$$

The volume at ambient pressure V_0 relative to the ambient pressure volume V_R at the reference temperature T_R is assumed to depend on temperature according to:

$$\frac{V_0}{V_R} = 1 + a_V\left(T - T_R\right) \tag{2.14}$$

The density relationship to pressure and temperature can be deduced from the previous equations by a simple manipulation:

$$\rho\left(p,T\right) = \rho_R\left(\frac{V_R}{V}\right) = \rho_R\left(\frac{V_R}{V_0}\times\frac{V_0}{V}\right) = \rho_R\left(\frac{1}{V_0/V_R}\times\frac{1}{V/V_0}\right) \tag{2.15}$$

This model is of more physical relevance but is clearly much more complicated than the Dowson & Higginson simple relationship and requires specific characterization and data.

2.4.2 Viscosity variations

In this section, the viscosity variations with pressure and temperature are considered. Four different models are given: Cheng [16], Roelands [100], Modified WLF [123] and the Doolittle [21] free volume model:

2.4.2.1 Cheng

The Cheng relationship is the most widely used viscosity model in EHL. It is not very accurate, especially at high pressures, and does not have any physical foundation. But, its simple mathematical form makes it interesting to use in EHL solvers:

$$\mu\left(p,T\right) = \mu_R \exp\left(\alpha_{ch} p + \beta_{ch}\left(\frac{1}{T} - \frac{1}{T_R}\right) + \gamma_{ch}\frac{p}{T}\right) \tag{2.16}$$

Where $\mu\left(p,T\right)$ is the viscosity at a given pressure p and temperature T, $\mu_R = \mu\left(p = p_R = 0, T = T_R\right)$ is the ambient pressure viscosity at a reference temperature T_R. This model is more known under its isothermal form (with $T = T_R = cst$) called the Barus [7] law:

$$\mu(p) = \mu_R \exp(\alpha p) \qquad \text{with} \qquad \alpha = \alpha_{ch} + \frac{\gamma_{ch}}{T} \tag{2.17}$$

This relationship is restricted to relatively low pressures beyond which, the predicted viscosities are often too high compared to experimental data as pointed out by Vergne [116].

2.4.2.2 Roelands

A more accurate viscosity-pressure-temperature relationship was proposed by Roelands under the following form:

$$\begin{gathered}\mu(p,T) = \mu_R \exp\left\{\left(\ln(\mu_R) + 9.67\right)\left[-1 + \left(1 + 5.1\times10^{-9} p\right)^{Z_0}\left(\frac{T-138}{T_R-138}\right)^{-S_0}\right]\right\} \\ \text{Where:} \quad Z_0 = \frac{\alpha}{\left[5.1\times10^{-9}\left(\ln(\mu_R)+9.67\right)\right]} \\ S_0 = \frac{\beta_{Roe}\left(T_R-138\right)}{\ln(\mu_R)+9.67}\end{gathered} \tag{2.18}$$

This equation can be sufficiently accurate for moderately high pressures beyond which, again some discrepancy with experimental data may be observed as pointed out in [116]. Finally, note that both the Cheng and Roelands models do not have any physical relevance and they are strictly empirical.

2.4.2.3 Modified WLF

A more physical model was initially proposed in the field of polymer physics by William, Landel and Ferry (WLF) [29] based on the time-temperature equivalence principle. The latter stipulates that it is possible to represent the different rheological parameters of a fluid on one and only one "master curve". The latter is associated to a reference temperature corresponding to the glass transition temperature of the fluid T_g. Yasutomi, Bair and Winer [123] later provided a modified version of the WLF model that can be extended to a very wide pressure and temperature domain while keeping the same good accuracy:

$$\begin{gathered}\mu(p,T) = \mu_g \times 10^{\frac{-C_1\cdot\left(T-T_g(p)\right)\cdot F(p)}{C_2+\left(T-T_g(p)\right)\cdot F(p)}} \\ \text{with:} \quad T_g(p) = T_g(0) + A_1 \ln\left(1 + A_2 p\right) \\ F(p) = 1 - B_1 \ln\left(1 + B_2 p\right)\end{gathered} \tag{2.19}$$

A_1, A_2, B_1, B_2, C_1 and C_2 are constants characterizing each fluid and μ_g is the viscosity at the glass transition temperature T_g. The function $T_g(p)$ represents the variation of the glass transition temperature with respect to pressure based on experimental data whereas $F(p)$ represents the variation of the thermal expansion coefficient with pressure. Harrison [49] showed that the WLF model is equivalent to the free volume model which is the basis of the Doolittle formula shown next.

2.4.2.4 Doolittle

Another physical viscosity-pressure-temperature model, based on the free volume principle and valid over a wide range of pressures and temperatures, is defined by the Doolittle relationship:

$$\mu\left(p,T\right)=\mu_R \exp\left[BR_0\left(\frac{\frac{V_\infty}{V_{\infty R}}}{\frac{V}{V_R}-R_0\frac{V_\infty}{V_{\infty R}}}-\frac{1}{1-R_0}\right)\right] \tag{2.20}$$

The relative occupied volume with respect to the reference state is given by the following relationship:

$$\frac{V_\infty}{V_{\infty R}}=1+\varepsilon_c\left(T-T_R\right) \tag{2.21}$$

B and R_0 are constants characterizing a given lubricant, whereas V/V_R is defined by a given equation of state. This model is often associated to the Tait equation of state (See section 2.4.1.2). Together they are known as the Tait-Doolittle free volume density and viscosity model.

The WLF and Tait-Doolittle models are much more accurate than the Dowson & Higginson, Cheng and Roelands models especially at high pressure values. Still, they have been rarely used in EHL modelling because of their complex mathematical formulation and their dependence on several parameters which leads to more tedious experimental characterization.

2.5 Boundary conditions

The solution of differential equations generally depends on the boundary conditions of the system. Up so far, the only differential equation is the Reynolds' equation, it requires a specification of the independent variable p on the boundary $\partial\Omega_c$ of the contact domain Ω_c. Generally, it is admitted that p equals the ambient pressure at the boundary of the contact domain. In practice, it is defined as zero and thus, the pressure solved for corresponds to the pressure rise above the ambient level value:

$$p=0 \quad \text{on } \partial\Omega_c \tag{2.22}$$

Moreover, since the lubricant is assumed to be at liquid state inside the film, pressures lower than the vapour pressure are physically impossible. The fluid will cavitate and the pressure will remain constant and equal to the vapour pressure. Since in most situations the vapour pressure of the lubricant is of the same order of magnitude as the ambient pressure which is very small compared to the contact pressure, the Reynolds' [99] cavitation boundary condition requires that:

$$p \geq 0 \quad \text{on } \Omega_c \quad \text{and} \quad p = \nabla p \cdot \vec{n}_c = 0 \quad \text{on the cavitation boundary} \tag{2.23}$$

Where $\vec{n}_c$ is the outward normal vector to the outlet boundary of the contact also called cavitation boundary. It is clear that determining the exact location of this boundary (specified by the appearance of negative pressures in the solution of Reynolds' equation) is a free boundary problem since the pressure distribution is not known "a priori". This free boundary problem requires a specific treatment that shall be discussed in details in the next chapter. Finally, it is important to note that the first part of eq. (2.23) ensures that the cavitation of the lubricant and the film break-up at the outlet of the contact are taken into account, whereas the second part ensures the mass conservation of the lubricant flow.

2.6 Dimensionless equations and parameters

Writing EHL equations in a dimensionless form offers the advantage of handling independent variables close to unity. This provides a better conditioning and hence an easier resolution of the system of equations. The different equations listed in the current chapter are written in a dimensionless form using the Hertzian dry contact parameters. Hertz's [51] theory gives the pressure profile, the geometry of the contact region and the elastic deformation of the contacting elements in the case of a dry contact between two parabolically shaped elastic bodies. In the case of a circular contact, the Hertzian pressure profile is given by:

$$p(x,y) = \begin{cases} p_h \sqrt{1 - \left(\dfrac{x}{a}\right)^2 - \left(\dfrac{y}{a}\right)^2} & \text{if } \sqrt{x^2 + y^2} \leq a \\ 0 & \text{otherwise} \end{cases} \tag{2.24}$$

Where p_h is the maximum Hertzian pressure given by:

$$p_h = \frac{3F}{2\pi a^2} \tag{2.25}$$

And a denotes the radius of the contact circle:

$$a = \sqrt[3]{\frac{3FR}{2E'}} \tag{2.26}$$

Where F is the external applied load, R the reduced radius of curvature and E' is the reduced elastic modulus of the contacting bodies defined as:

$$E' = \frac{2}{\dfrac{1-\upsilon_p^2}{E_p} + \dfrac{1-\upsilon_s^2}{E_s}} \tag{2.27}$$

Where (E_p, υ_p) and (E_s, υ_s) are the material properties (Young's modulus and Poisson's coefficient) of the planar and spherical surface respectively.

2.6.1 Dimensionless equations

First, let us define the following dimensionless variables:

$$X = \frac{x}{a} \quad Y = \frac{y}{a} \quad P = \frac{p}{p_h} \quad H = \frac{hR}{a^2} \quad \overline{\delta} = \frac{\delta R}{a^2} \quad \overline{\rho} = \frac{\rho}{\rho_R} \quad \overline{\mu} = \frac{\mu}{\mu_R} \tag{2.28}$$

Using these variables, the EHL equations can be written in their dimensionless form. Reynolds' equation (2.6) becomes:

$$\nabla \cdot \left(\overline{\varepsilon} \nabla P\right) - \frac{\partial\left(\overline{\rho} H\right)}{\partial X} = 0 \quad \text{with} \quad \overline{\varepsilon} = \frac{\overline{\rho} H^3}{\overline{\mu}\lambda} \quad \text{and} \quad \lambda = \frac{12 u_m \mu_R R^2}{a^3 p_h} \tag{2.29}$$

Associated to the following boundary conditions:

$$P \geq 0 \text{ on } \Omega_c, \; P = 0 \text{ on } \partial\Omega_c \text{ and } P = \nabla P.\vec{n}_c = 0 \text{ on the cavitation boundary} \tag{2.30}$$

Where $\vec{n}_c$ is the outward normal vector to the cavitation boundary. The film thickness equation becomes:

$$H\left(X,Y\right) = H_0 + \frac{X^2 + Y^2}{2} + \overline{\delta}\left(X,Y\right) \tag{2.31}$$

And finally, the load balance equation in dimensionless form is:

$$\int_{\Omega_c} P\left(X,Y\right) d\Omega = \frac{2\pi}{3} \tag{2.32}$$

The lubricant properties' dimensionless equations are derived from their dimensional form in a straightforward manner by dividing each property by its value at the reference state. The set of equations (2.29) to (2.32) along with the dimensionless lubricant properties' equations defines the system of equations used in practice in EHL solvers in the case of an isothermal circular contact lubricated with a Newtonian lubricant.

2.6.2 Dimensionless parameters

So far, the number of parameters defining an EHL contact almost reaches a dozen between the load, speed, material and lubricant properties parameters. For the sake of simplicity, it would be preferable if this number can be reduced. This is why Hamrock & Dowson [47] used combinations of these parameters to introduce a set of three dimensionless parameters that completely define a typical circular contact EHL problem. Those are the load parameter W_{HD}, the material properties parameter G_{HD} and the speed parameter U_{HD} defined as:

$$W_{HD} = \frac{F}{E'R^2}, \qquad G_{HD} = \alpha E' \qquad \text{and} \qquad U_{HD} = \frac{\mu_0 u_m}{E'R} \tag{2.33}$$

Where $\mu_0 = \mu\left(p = p_R = 0, T = T_0\right)$ and T_0 is the ambient temperature. Moes [90] further reduced the number of dimensionless parameters by combining the three previous parameters to define only two: the load parameter *M* and the material properties parameter *L*, defined as:

$$M = W_{HD}\left(2U_{HD}\right)^{-3/4} \qquad \text{and} \qquad L = G_{HD}\left(2U_{HD}\right)^{1/4} \tag{2.34}$$

The previous two parameters are sufficient to define any EHL circular contact. In other words, if two different contacts have the same values of *M* and *L* (even if all the operating parameters are not the same) they would have the same dimensionless film thickness properties.

2.7 Conclusion

In this chapter, we introduced the theory behind isothermal EHD circular contacts lubricated with a Newtonian lubricant. First, the different equations were listed in their dimensional form: the Reynolds' equation that is deduced from the Navier-Stokes equations by applying some simplifying assumptions, the film thickness equation which reflects the geometry of the contact and the load balance equation which ensures that the correct load is considered. Then different viscosity and density models were listed describing the variations of the lubricant's properties with pressure and temperature. These equations completely describe the lubricant flow within the contact, and in practice, they are solved in their dimensionless form shown in the last section of the chapter.

Now that the mathematical model behind EHL is defined, we move on to describe its resolution. Since this model consists of complex non-linear differential equations, it cannot be solved analytically and a numerical resolution of the system of equations has to be considered. In the next chapters, the numerical models used in this work are described. As a first step, an isothermal Newtonian approach is considered.

3 Isothermal Newtonian approach

This chapter is the core of this thesis. It presents the detailed numerical model developed to solve EHD circular contact problems considering an isothermal Newtonian approach. This is the basis of every EHL solver from which an extension to a more complicated and physical modelling can be achieved.

The goal is to model the contact between two "spherical" surfaces under a prescribed external load (See Figure 1.4). Both contacting bodies are elastic and have constant surface velocities. However, an equivalent geometry is used where only one of the bodies is considered elastic while the other is rigid. The former accommodates the total elastic deflection of both contacting elements. Surface separation is ensured by a complete lubricant film. Thermal effects are neglected and the lubricant is assumed to behave as a Newtonian fluid. Since smooth circular contacts with surface velocities in the x-direction only are considered, the problem is symmetric with respect to the zx plane. This symmetry is taken into account in order to reduce its size.

Remark: Some line contact results are shown (when needed) for demonstrative purposes.

3.1 Introduction

The numerical model developed in this work for the solution of the isothermal EHD circular contact problem is based on a full-system nonlinear finite element resolution of the EHL equations: the Reynolds' equation, the elastic deflection and the load balance equations. As we shall see next, the first two are partial differential equations whereas the last one is an ordinary integral equation. It has been pointed out in the first chapter that models based on such an approach have always suffered from three major drawbacks: the full Jacobian matrix, the fact that it becomes practically singular at heavy loads and the tedious treatment of the free boundary problem. In the following sections, a solution to each of these problems is provided. The first one is avoided by the introduction of a classical finite element model for linear elasticity as an alternative to the half-space approach in the elastic deflection computation. The second problem is solved by using stabilized finite element formulations and the last one by applying a penalty method.

3.2 Elastic deformation

The alternative approach for computing the elastic deformation of the contacting bodies consists in solving the classical linear elasticity equations on a three-dimensional cubic structure with appropriate boundary conditions (See Figure 3.1).

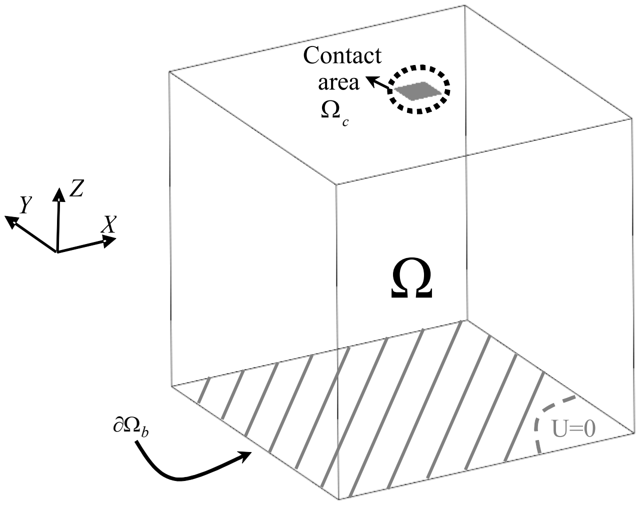

Figure 3.1: Geometry of the EHL problem

Let Ω be the interior domain of the structure, $\partial\Omega$ its boundary, Ω_c the part of the upper boundary that corresponds to the contact domain and $\partial\Omega_c$ its boundary.

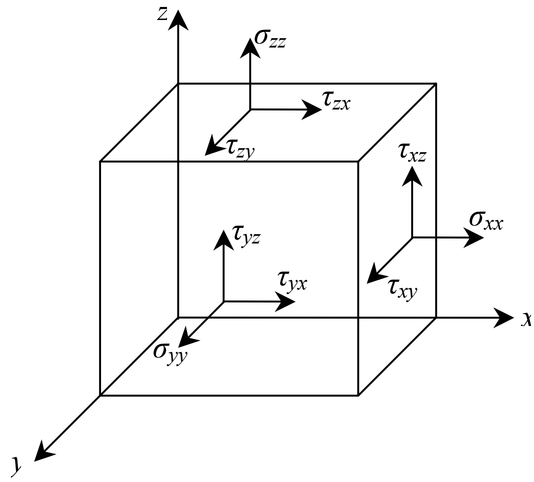

Figure 3.2: Equilibrium of forces on an elemental volume

These equations are derived from the equilibrium of forces on an elemental volume of the material considered (See Figure 3.2):

$$\begin{cases} \dfrac{\partial \sigma_{xx}}{\partial x} + \dfrac{\partial \tau_{xy}}{\partial y} + \dfrac{\partial \tau_{xz}}{\partial z} + F_x = 0 \\ \dfrac{\partial \tau_{xy}}{\partial x} + \dfrac{\partial \sigma_{yy}}{\partial y} + \dfrac{\partial \tau_{yz}}{\partial z} + F_y = 0 \\ \dfrac{\partial \tau_{xz}}{\partial x} + \dfrac{\partial \tau_{yz}}{\partial y} + \dfrac{\partial \sigma_{zz}}{\partial z} + F_z = 0 \end{cases} \tag{3.1}$$

Where F_x, F_y and F_z are body forces in the *x*, *y* and *z*-directions respectively. Neglecting the body forces ($F_x = F_y = F_z = 0$), the system of equations (3.1) can be written as follows:

$$\nabla \cdot \sigma = 0 \quad \text{with} \quad \sigma = \begin{bmatrix} \sigma_{xx} & \tau_{xy} & \tau_{xz} \\ \tau_{xy} & \sigma_{yy} & \tau_{yz} \\ \tau_{xz} & \tau_{yz} & \sigma_{zz} \end{bmatrix} \tag{3.2}$$

The previous equation is solved to find the displacement vector $U = \{u, v, w\}$ on the computational domain Ω by using the generalized Hooke's law to replace the stress tensor σ by its expression as a function of the strain tensor ε_s and the compliance matrix *C*:

$$\sigma = C\varepsilon_s(U) \qquad \text{where} \qquad \varepsilon_s = \begin{bmatrix} \varepsilon_{xx} & \gamma_{xy} & \gamma_{xz} \\ \gamma_{xy} & \varepsilon_{yy} & \gamma_{yz} \\ \gamma_{xz} & \gamma_{yz} & \varepsilon_{zz} \end{bmatrix} \tag{3.3}$$

With: $\varepsilon_{xx} = \dfrac{\partial u}{\partial x}$, $\varepsilon_{yy} = \dfrac{\partial v}{\partial y}$, $\varepsilon_{zz} = \dfrac{\partial w}{\partial z}$, $\gamma_{xy} = \dfrac{\partial u}{\partial y} + \dfrac{\partial v}{\partial x}$, $\gamma_{xz} = \dfrac{\partial u}{\partial z} + \dfrac{\partial w}{\partial x}$ and $\gamma_{yz} = \dfrac{\partial v}{\partial z} + \dfrac{\partial w}{\partial y}$

In practice equation (3.3) is rearranged under the following form (Voigt's notation):

$$\begin{Bmatrix} \sigma_{xx} \\ \sigma_{yy} \\ \sigma_{zz} \\ \tau_{xy} \\ \tau_{yz} \\ \tau_{zx} \end{Bmatrix} = \underbrace{\frac{E}{(1+\upsilon)(1-2\upsilon)} \begin{bmatrix} 1-\upsilon & \upsilon & \upsilon & 0 & 0 & 0 \\ \upsilon & 1-\upsilon & \upsilon & 0 & 0 & 0 \\ \upsilon & \upsilon & 1-\upsilon & 0 & 0 & 0 \\ 0 & 0 & 0 & \frac{1-2\upsilon}{2} & 0 & 0 \\ 0 & 0 & 0 & 0 & \frac{1-2\upsilon}{2} & 0 \\ 0 & 0 & 0 & 0 & 0 & \frac{1-2\upsilon}{2} \end{bmatrix}}_{D} \begin{Bmatrix} \varepsilon_{xx} \\ \varepsilon_{yy} \\ \varepsilon_{zz} \\ \gamma_{xy} \\ \gamma_{yz} \\ \gamma_{zx} \end{Bmatrix} \tag{3.4}$$

Where *D* is the compliance matrix for a homogeneous isotropic material. It is written as a function of the material's Young's modulus *E* and Poisson's coefficient υ. The resolution of eq. (3.2) on the computational domain Ω is associated with the following boundary conditions:

$$\begin{cases} U = 0 & \text{at the bottom boundary } \partial\Omega_b \\ \sigma_n = -P & \text{at the contact area boundary } \Omega_c \\ \sigma_n = 0 & \text{elsewhere} \end{cases} \tag{3.5}$$

Again, these equations are solved in dimensionless form using the dimensionless space coordinates defined earlier: $X = x/a$, $Y = y/a$ and $Z = z/a$. In order to simplify the computational model, an equivalent problem is defined to replace the elastic deformation computation for both contacting bodies under the same pressure distribution. This simplification consists in assuming that one of the bodies is rigid while the other accommodates the total elastic deflection of both surfaces. The material properties of the latter are given by (See Appendix A):

$$E_{eq} = \frac{E_p^2 E_s \left(1+\upsilon_s\right)^2 + E_s^2 E_p \left(1+\upsilon_p\right)^2}{\left[E_p\left(1+\upsilon_s\right)+E_s\left(1+\upsilon_p\right)\right]^2} \times \frac{a}{R\, p_h} \quad \text{and} \quad \upsilon_{eq} = \frac{E_p \upsilon_s \left(1+\upsilon_s\right) + E_s \upsilon_p \left(1+\upsilon_p\right)}{E_p\left(1+\upsilon_s\right)+E_s\left(1+\upsilon_p\right)} \tag{3.6}$$

Note that the dimensionless total elastic deflection of the contacting elements is nothing else but the absolute value of the *Z*-component of the displacement vector *U*:

$$\bar{\delta}\left(X,Y\right) = \left|w\left(X,Y\right)\right| \tag{3.7}$$

<u>Remark</u>: The elastic deformation problem described above is solved using a finite element approximation. Therefore, from a numerical point of view, every discretization point belonging to a certain number of finite elements is only related to its neighbouring points belonging to these elements. This is why the Jacobian matrix of the global non-linear system of equations is sparse.

3.3 The free boundary problem

As pointed out in the previous chapter, a free boundary problem arises at the outlet of the contact. In a semi-system approach it is treated in a straightforward manner by putting to zero all the negative pressures that arise during the iterative resolution process. This ensures a positive pressure distribution on the computational domain Ω_c and a zero pressure and pressure gradient at the free boundary. This satisfies the Reynolds' boundary conditions (2.30). Unfortunately, such a treatment is not possible when using a Newton-Raphson full-system approach because of the simultaneous update of all the unknowns at each iteration. An alternative approach, known as the **penalty method** was introduced to EHL problems by Wu [121]. This approach introduces an additional penalty term to the Reynolds equation (2.29) that becomes (in dimensionless form):

$$\nabla \cdot \left(\bar{\varepsilon}\,\nabla P\right) - \frac{\partial\left(\bar{\rho} H\right)}{\partial X} - \xi \cdot P^- = 0 \tag{3.8}$$

Where ξ is an arbitrary **large** positive number and $P^- = \min\left(P,0\right)$ corresponds to the negative part of the pressure distribution. Note that the penalty term ($-\xi \cdot P^-$) has no effect where $P \geq 0$ and the consistency of Reynolds' equation is preserved. However, in the outlet region of the contact, where $P < 0$, the penalty term dominates eq. (3.8), provided that the arbitrary constant ξ has a sufficiently large value. Hence, the negative pressures are forced towards zero by the presence of the penalty term and the physical constraint that $P \geq 0$ over the entire computational domain is automatically satisfied. Wu also showed that this approach satisfies the Reynolds' boundary conditions and thus the mass flow rate conservation throughout the contact. In addition, this method is very straightforward and easy to implement.

Remark: In practice, negative pressures never become zero, but they get very close to zero (and become negligible) depending on the value of the arbitrary constant ξ. The larger this value is, the closer the negative pressures come to zero (for more details the reader is referred to section 3.7.2).

3.4 Finite element formulation

The full-system approach used in this work consists in solving Reynolds' equation (3.8), the linear elasticity equations (3.2) and the load balance equation (2.32) simultaneously. In Reynolds' equation, the dimensionless film thickness H is replaced by its expression given in eq. (2.31) whereas the dimensionless viscosity $\bar{\mu}$ and density $\bar{\rho}$ are replaced by one of the expressions provided in section 2.4. The Reynolds' and linear elasticity equations are partial differential equations to which a standard Galerkin formulation is applied whereas the load balance equation is an ordinary integral equation that is added directly to the system along with the introduction of an additional unknown H_0. Hence, the unknowns of this model are the pressure distribution P, the elastic deformation of the contacting elements $U = \{u, v, w\}$ and the film thickness constant H_0.

3.4.1 Galerkin formulation

A standard Galerkin formulation is applied to Reynolds' and the linear elasticity equations. The latter is obtained by multiplying each equation by a given weighting function (W_P and W_U respectively) and integrating it over the corresponding domain of application. Finally, integration by parts is applied to the equations revealing thus the boundary terms. For the sake of simplicity, the zero boundary terms are omitted. The load balance equation is also multiplied by a given weighting function W_{H_0} and then added directly to the resultant system of equations which becomes:

Find $(P, U, H_0) \in S_P \times S_U \times \mathbb{R}$ such that $\forall \left(W_P, W_U, W_{H_0}\right) \in S_P \times S_U \times \mathbb{R},$ one has:

$$\begin{cases} \int\limits_{\Omega_c} -\bar{\varepsilon}\, \nabla P \cdot \nabla W_P \, d\Omega + \int\limits_{\Omega_c} \bar{\rho} H \dfrac{\partial W_P}{\partial X} d\Omega - \int\limits_{\Omega_c} \xi \cdot P^- W_P \, d\Omega = 0 \\ \int\limits_{\Omega} -C\varepsilon_s(U) \cdot \varepsilon_s(W_U) \, d\Omega + \int\limits_{\Omega_c} -P \cdot \vec{n}\, W_U \, d\Omega = 0 \\ \int\limits_{\Omega_c} P W_{H_0} d\Omega - \dfrac{2\pi}{3} W_{H_0} = 0 \end{cases} \tag{3.9}$$

Where: $S_P = \left\{P \in H^1(\Omega_c) \,/\, P = 0 \text{ on } \partial\Omega_c\right\}$ and $S_U = \left\{U \in H^1(\Omega) \,/\, U = 0 \text{ on } \partial\Omega_b\right\}$

Note that Reynolds' equation is solved on the two-dimensional contact domain Ω_c whereas the linear elasticity equations are solved on the three-dimensional domain Ω.

3.4.2 Approximated formulation

Let us now write the discrete form of the previous system of equations. Consider $\Omega^h = \left\{ \Omega_1, ..., \Omega_{n_e} \right\}$ a finite element partition of Ω such that: $\bar{\Omega} = \cup_{e=1}^{n_e} \bar{\Omega}_e$, $\bar{\Omega} = \Omega \cup \partial\Omega$, $\bar{\Omega}_e = \Omega_e \cup \partial\Omega_e$ and $\Omega_e \cap \Omega_{e'} = \phi$ if $e \neq e'$. n_e denotes the total number of elements in the partition while $\partial\Omega$ and $\partial\Omega_e$ denote respectively the boundaries of the domain Ω and the element Ω_e. Let Ω_{ce} be the set of elements defined by $\Omega_{ce} = \left\{ \Omega_e \cap \Omega_c / \Omega_{ce} \neq \varnothing \right\}$ and let n_{ce} be the total number of elements belonging to Ω_{ce}. Let $S_P^h \subset S_P$ and $S_U^h \subset S_U$. The discrete functions P^h and U^h defining these spaces have the same characteristics as their analytical equivalents P and U defined in the previous section with the only difference that $P^h \in L^l$ and $U^h \in L^{l'}$ where L^l and $L^{l'}$ are the sets of interpolation polynomials of degrees equal to l and l' respectively defined within each element Ω_e. The approximate functions $P^{h^{(e)}}$ and $U^{h^{(e)}}$ (within an element *e*) of *P* and *U* respectively, are given by:

$$P^{h^{(e)}} = \sum_{i=1}^{n_P} P_i^{(e)} N_{Pi} \quad \text{and} \quad U^{h^{(e)}} = \sum_{i=1}^{n_U} U_i^{(e)} N_{Ui} \tag{3.10}$$

Where $P_i^{(e)}$ and $U_i^{(e)}$ are the nodal values of *P* and *U* respectively, associated to the interpolation functions N_{Pi} and N_{Ui} within the element *e* (n_P and n_U being their respective numbers). The weighting functions W_P and W_U are approximated in a similar way by $W_P^{h^{(e)}}$ and $W_U^{h^{(e)}}$ respectively:

$$W_P^{h^{(e)}} = \sum_{i=1}^{n_P} W_{Pi}^{(e)} N_{Pi} \quad \text{and} \quad W_U^{h^{(e)}} = \sum_{i=1}^{n_U} W_{Ui}^{(e)} N_{Ui} \tag{3.11}$$

Where $W_{Pi}^{(e)}$ and $W_{Ui}^{(e)}$ are the nodal values of W_P and W_U within the element *e* respectively. The discrete form of the system of equations (3.9) is obtained by replacing the field variables *P* and *U* by their discrete equivalents P^h and U^h respectively and the weighting functions W_P and W_U by W_P^h and W_U^h respectively:

Find $\left(P^h, U^h, H_0\right) \in S_P^h \times S_U^h \times \mathbb{R}$ such that $\forall \left(W_P^h, W_U^h, W_{H_0}\right) \in S_P^h \times S_U^h \times \mathbb{R}$, one has:

$$\begin{cases} \int\limits_{\Omega_c^h} -\bar{\varepsilon}\, \nabla P^h \cdot \nabla W_P^h d\Omega + \int\limits_{\Omega_c^h} \bar{\rho} H \dfrac{\partial W_P^h}{\partial X} d\Omega - \int\limits_{\Omega_c^h} \xi \cdot P^{h-} W_P^h d\Omega = 0 \\ \int\limits_{\Omega^h} -C \varepsilon_s \left(U^h\right) \cdot \varepsilon_s \left(W_U^h\right) d\Omega + \int\limits_{\Omega_c^h} -P^h \cdot \vec{n}\, W_U^h d\Omega = 0 \\ \int\limits_{\Omega_c^h} P^h W_{H_0} d\Omega - \dfrac{2\pi}{3} W_{H_0} = 0 \end{cases} \tag{3.12}$$

Again, for the sake of simplicity, the zero boundary integrals have been omitted. The unknowns of the discrete system of equations (3.12) are the nodal values of *P* and *U* and the value of the film thickness constant parameter H_0.

Remark: The finite element method for the solution of partial differential equations can be the subject of several handbooks on its own and it reaches beyond the scope of this thesis. Nevertheless, if the reader is interested in deeper details, he can refer to any of the classical finite element handbooks such as [59], [62] or [126].

3.4.3 Stability issues

The solution of Reynolds' equation is known to be unstable in the central contact area (high pressure region) for highly loaded contacts [22][25][45][84][112]. In this section, we provide a method to cure these instabilities that lead to an oscillatory behaviour of the solution. In fact, let us rewrite the Reynolds' equation in a different way:

$$R(P) = -\nabla \cdot (\bar{\varepsilon}\,\nabla P) + H\frac{\partial\bar{\rho}}{\partial P}\frac{\partial P}{\partial X} + \bar{\rho}\frac{\partial H}{\partial X} = 0 \tag{3.13}$$

Let $\beta = \beta_X$ in the line contact case or $\beta = \begin{bmatrix}\beta_X & \beta_Y\end{bmatrix}$ in the circular contact case with $\beta_X = H\frac{\partial\bar{\rho}}{\partial P}$ and $\beta_Y = 0$. Finally, let $Q = -\bar{\rho}\frac{\partial H}{\partial X}$, then eq. (3.13) can be written:

$$R(P) = \underbrace{-\nabla \cdot (\bar{\varepsilon}\,\nabla P)}_{\text{«Diffusion»}} + \underbrace{\beta \cdot \nabla P}_{\text{«Convection»}} \underbrace{-Q}_{\text{«Source»}} = 0 \tag{3.14}$$

In this section, line contacts are also studied for demonstrative purposes. The penalty term is not mentioned for the sake of simplicity and because it is nil in the region of interest of this section (high pressure region). But keep in mind that this term should be added to eq. (3.14) during the resolution process. Note that eq. (3.14) is the Reynolds' equation in compact notation for both line and circular contacts. For the line contact case, the differential operators are unidirectional in the *X*-direction whereas in the circular contact case they are bidirectional (in the *X* and *Y*-directions).

Equation (3.14) has the form of the classical convection / diffusion equation (applied to *P*) with a source term *Q*. We can clearly identify the diffusion term (left) with a diffusion coefficient $\bar{\varepsilon}$ and the convection term (centre) with the convection operator $\beta \cdot \nabla$. For highly loaded contacts, $\bar{\varepsilon}$ becomes very small. In fact, $\bar{\rho}$ exhibits a slight increase while $\bar{\mu}$ is increased by several orders of magnitude and *H* becomes smaller. Therefore, the convection-like term in eq. (3.14) becomes dominant. It is well known that the standard Galerkin formulation, associated with the finite element method is suitable only when the diffusion term is dominant [11][33][63][64][127]. In fact, the central differencing property of the Galerkin method is well suited only for elliptic problems (dominated by diffusion). When convection becomes dominant, the standard Galerkin formulation is no longer appropriate and gives rise to spurious oscillations in the solution. One way to get rid of these oscillations is obtained by using appropriate stabilized formulations. A various number of these techniques can be found in the literature such as "artificial diffusion" [11] [63] [95] or "Discontinuous

Galerkin" methods [66][67]. In the following, we propose the use of "artificial diffusion" techniques to cure the spurious oscillations of the solution for highly loaded contacts.

3.4.3.1 Line contact

As mentioned earlier, in the case of a highly loaded contact, Reynolds' equation becomes convection-dominated. The solution exhibits an oscillatory behaviour (See Figure 3.3, Left). In order to overcome such a problem Brooks and Hughes [11] introduced the so called Streamline Upwind Petrov Galerkin (SUPG) method. The discrete weak variational form for the SUPG method applied to Reynolds' equation (3.14) is given by:

$$\text{Find } P^h \in S_P^h \text{ such that } \forall W_P^h \in S_P^h, \text{ one has:}$$

$$\int_{\Omega_c^h} \bar{\varepsilon}\, \nabla P^h \cdot \nabla W_P^h d\Omega + \int_{\Omega_c^h} \left(\beta \cdot \nabla P^h - Q\right) W_P^h d\Omega + \sum_{e=1}^{n_{ce}} \int_{\Omega_{ce}} R\left(P^h\right) \tau \left(\beta \cdot \nabla W_P^h\right) d\Omega = 0 \tag{3.15}$$

The first two terms represent the standard Galerkin method applied to Reynolds' equation while the last term represents the additional term that is added to the interior Ω_{ce} of each discretization element. The latter has a stabilizing effect on the spurious oscillations of the solution as can be seen in Figure 3.3 (Centre). The oscillations completely vanish and the pressure profile becomes smooth.

Another interesting technique was proposed by Hughes et al. [63] based on the fact that stabilization terms may be obtained by minimizing the square of the equation's residual. It is called the Galerkin Least Squares (GLS) method. The discrete weak variational form for this method is given by:

$$\text{Find } P^h \in S_P^h \text{ such that } \forall W_P^h \in S_P^h, \text{ one has:}$$

$$\int_{\Omega_c^h} \bar{\varepsilon}\, \nabla P^h \cdot \nabla W_P^h d\Omega + \int_{\Omega_c^h} \left(\beta \cdot \nabla P^h - Q\right) W_P^h d\Omega + \sum_{e=1}^{n_{ce}} \int_{\Omega_{ce}} R\left(P^h\right) \tau \left(\beta \cdot \nabla W_P^h - \nabla \cdot \left(\bar{\varepsilon}\, \nabla W_P^h\right)\right) d\Omega = 0 \tag{3.16}$$

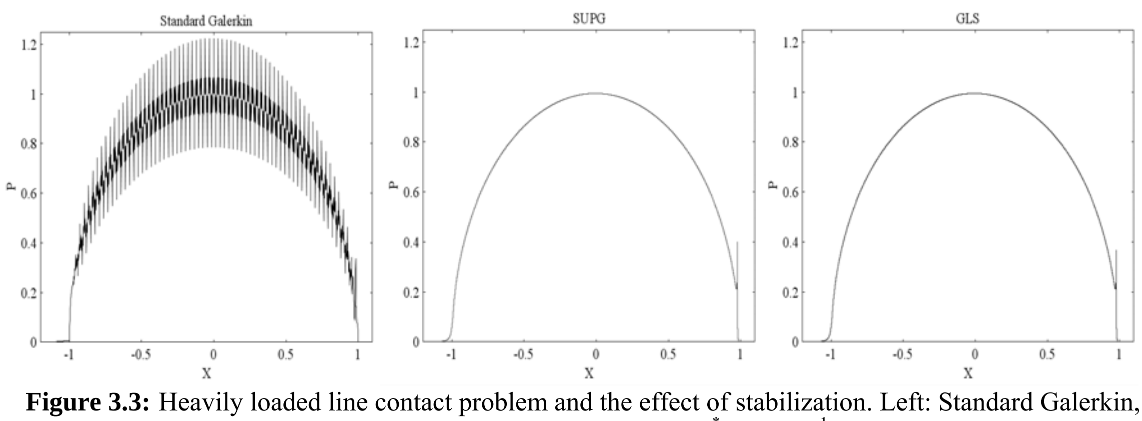

Figure 3.3: Heavily loaded line contact problem and the effect of stabilization. Left: Standard Galerkin, Centre: SUPG, Right: GLS (p_h=3 GPa, μ_R=0.012 Pa.s, α^*=23 GPa^{-1} and u_s=u_p=1m/s)

Once again, we can identify the standard Galerkin formulation in the first two terms and the additional last term that aims at stabilizing the oscillatory behaviour of the solution as can be seen in Figure 3.3 (Right).The most important feature of SUPG and GLS is that both are residual based techniques. In other words, they do not affect the solution of the original problem. Actually, the additional terms vanish at the converged solution ($R \approx 0$) and therefore the consistency of Reynolds' equation is preserved. The definition of the tuning parameter τ remained "intuitive" for a long time. An example of a theoretical formulation was introduced by Hughes [64] in the mid 90's. Since, several formulations have been proposed by various authors. In this work we shall adopt the definition given by Galeão et al. [33] who provided an extension of this parameter to high order approximations:

$$\begin{gathered} \tau = \frac{h_e}{2|\beta| l} \xi(Pe) \\ \text{with: } Pe = \frac{|\beta| h_e}{2 \bar{\varepsilon} l} \text{ and } \xi(Pe) = \coth(Pe) - \frac{1}{Pe} \end{gathered} \tag{3.17}$$

Where h_e and Pe are respectively the characteristic length and the local Peclet number of the element *e*. Pe defines the convection-to-diffusion ratio inside an element *e*. Whenever $Pe > 1$, convection becomes dominant and stability problems mentioned earlier are likely to occur.

Figure 3.3 shows a typical case of a heavily loaded steel-steel line contact with a Hertzian pressure of 3 GPa and a mean entrainment velocity of 1m/s. The lubricant has an ambient pressure viscosity μ_R of 0.012 Pa.s and an equivalent viscosity-pressure coefficient α^* of $23\, GPa^{-1}$. The cylinder's radius is 15 mm. Lagrange quintic elements are used for the hydrodynamic problem and quadratic elements for the elastic part with a mesh density of 400 elements in the Hertzian contact region ($-1 \le X \le 1$).

Remark: Using fifth order elements for the hydrodynamic problem, as an alternative to refining the mesh, allows having a good precision for its solution without inducing any unnecessary increase in the number of dofs of the two-dimensional (line contact case) or three-dimensional (circular contact case) elastic problem.

The total number of dofs in this case is 23000, where only 2000 dofs are dedicated to the hydrodynamic part and the rest to the elastic calculation. This is to be expected since the former is one dimensional while the latter is two dimensional. The Dowson & Higginson formula and the WLF model were used as density-pressure and viscosity-pressure relationships respectively. The WLF constants are: $A_1 = 19.17$ °C, $A_2 = 4.07 \times 10^{-3}$ MPa^{-1}, $B_1 = 0.23$, $B_2 = 0.0249$ MPa^{-1}, $C_1 = 16.04$, $C_2 = 18.18$ °C, $T_g(0) = -73.86$ °C, $\mu_g = 10^{12}$ Pa.s and $T = 40$ °C. The solution exhibits an oscillatory behaviour when a Standard Galerkin formulation is used. On the other hand, the use of SUPG or GLS formulations smoothes out this spurious behaviour.

Remark: A plane strain analysis is employed for the elastic deflection problem in the line contact case. In fact, since the contact is considered infinitely long in the *y*-direction, strain components in this direction are assumed to be zero ($\varepsilon_{yy} = \gamma_{xy} = \gamma_{zy} = 0$).

3.4.3.2 Circular contact

In the case of a heavily loaded circular contact problem, the same behaviour is observed for a standard Galerkin formulation and the solution exhibits serious oscillations in the central area of the contact as can be seen in Figure 3.4 (Left). The SUPG and GLS formulations are the same as those given in eqs. (3.15) and (3.16) respectively. But in this case, both methods only succeed in reducing the amplitude of the oscillations without completely smoothing them out as can be seen in Figure 3.4 (Centre). In the two dimensional case of the convection / diffusion equation, it is of common use to add additional terms to the stabilized SUPG or GLS formulations such as “Isotropic Diffusion (ID)” terms [127]. The latter succeed in smoothing out the remaining oscillations without a significant perturbation in the solution of the original problem. These terms are defined as:

$$ID = \sum_{e=1}^{n_{ce}} \int_{\Omega_{ce}} \rho_{id} \frac{h_e |\beta|}{2l} \nabla P^h \cdot \nabla W_P^h \, d\Omega \tag{3.18}$$

The coefficient ρ_{id} represents the relative amount of “Isotropic Diffusion” with respect to the original method. The terms in eq. (3.18) are added to the stabilized SUPG or GLS formulations given in eqs. (3.15) and (3.16) respectively. This completely smoothes out the remaining oscillations as can be seen in Figure 3.4 (Right).

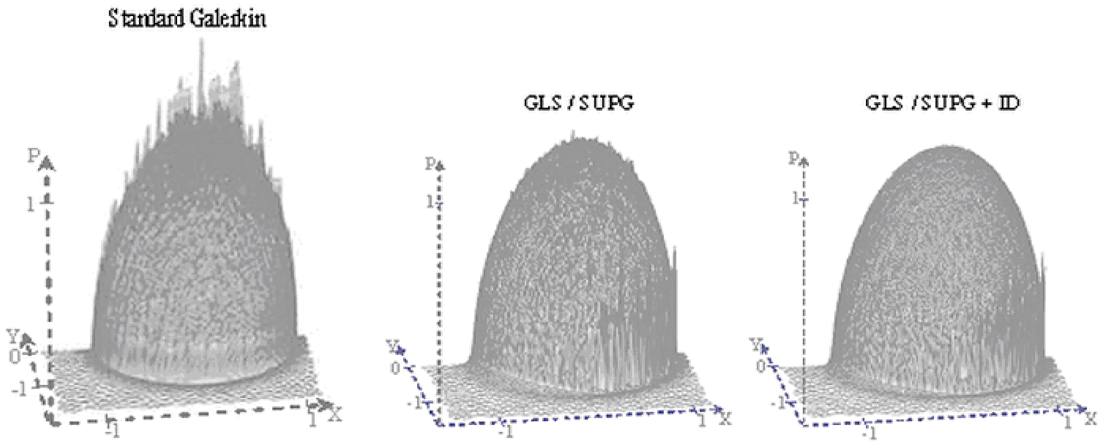

Figure 3.4: Heavily loaded circular contact problem (M=9435, L=9) and the effect of stabilization. Left: Standard Galerkin, Centre: SUPG/GLS, Right: SUPG/GLS+ID

Figure 3.4 shows the case of a heavily loaded steel-steel point contact with a Hertzian pressure of 3 GPa and a mean entrainment velocity of 1 m/s. The same lubricant is used as in the line contact case with the same viscosity-pressure and density-pressure relationships (See previous section). The ball’s radius is 12.7 mm and the corresponding Moes dimensionless parameters are: M=9435 and L=9. Again Lagrange quintic elements are used for the hydrodynamic problem and quadratic elements for the elastic part. The total number of dofs is 75000 where 35000 dofs are dedicated to the hydrodynamic part and the rest to the elastic calculation (note that the difference in the number of dofs between the two parts of the problem is less spectacular than in the case of a line contact). The solution exhibits an oscillatory behaviour when a Standard Galerkin formulation is used. The use of SUPG or GLS formulations reduces these oscillations without completely smoothing them out. And finally, the addition of “Isotropic Diffusion” terms eliminates the remaining oscillations in the solution (ρ_{id} is set to 0.5).

It is important to note that the ID terms are non-residual based and therefore the consistency of the Reynolds equation is lost. But, fortunately, the addition of these terms to the stabilized formulations does not significantly affect the solution of the original problem as can be seen in Figure 3.5. In order to evaluate the effect of these terms on the solution of the circular contact problem, a test case was carried out under the same conditions mentioned earlier with the only difference that the Hertzian pressure is taken to be 0.68 GPa (M=111 and L=9). This allows getting the standard Galerkin solution (the contact is not heavily loaded) in order to compare it to the stabilized GLS formulation with / without addition of "Isotropic Diffusion".

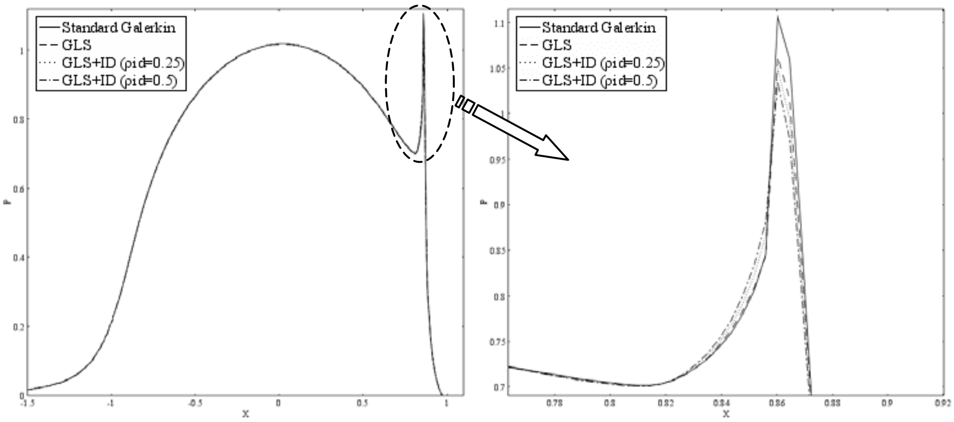

Figure 3.5: Effect of « Isotropic Diffusion » on the dimensionless pressure solution of Reynolds' equation in the case of a circular contact (M=111 and L=9)

Figure 3.5 shows the dimensionless pressure profile along the central line in the X-direction for the case mentioned earlier. Globally, the additional ID terms do not significantly affect the solution (Left). By zooming on the pressure spike's region (Right) we can note that a slight difference can be observed in this region. Finally, note that the more "Isotropic Diffusion" is added, the more the pressure spike is affected. In fact, for $\rho_{id} = 0.5$, the pressure spike deviates from that of the standard Galerkin or GLS solutions more than for $\rho_{id} = 0.25$. The dimensionless central and minimum film thicknesses H_c and H_m along with their corresponding relative deviations for the different formulations with respect to the standard Galerkin solution are reported in Table 3.1:

	H_c	H_m	$(\Delta H/H)_c$	$(\Delta H/H)_m$
Standard Galerkin	0.137462	0.074807	-	-
GLS	0.136897	0.074519	0.41 %	0.38 %
GLS+ID (ρ_{id}=0.25)	0.136752	0.074469	0.52 %	0.45 %
GLS+ID (ρ_{id}=0.5)	0.136608	0.074419	0.62 %	0.52 %

Table 3.1: Effect of « Isotropic Diffusion » on the dimensionless film thickness results in the case of a circular contact (M=111 and L=9)

Table 3.1 clearly confirms that the effect of the additional ID terms on the film thickness results is also negligible and that, again, the more ID is added, the more the solution is affected.

3.5 Newton-Raphson procedure

Now that the stabilized formulations of Reynolds' equation have been defined, after adding the penalty term, they should replace the original Reynolds' equation in system (3.12).

Note that, a unique formulation can be used for both lightly and heavily loaded contacts since the stabilized formulations introduced earlier do not affect the solution of the former.

Remark: The symmetry of the problem is taken into account. Hence, the linear elasticity problem requires a symmetry boundary condition on the symmetry plane *ZX* ($U \cdot \vec{n} = 0 \Leftrightarrow v = 0$ on $\partial\Omega_s$). Similarly, Reynolds' equation requires an additional symmetry boundary condition ($\nabla P \cdot \vec{n} = 0 \Leftrightarrow \partial P / \partial Y = 0$ on $\partial\Omega_{cs}$) and the computed dimensionless load should equal $\pi/3$ instead of $2\pi/3$.

A Newton-Raphson procedure is applied to the non-linear system of equations formed by the stabilized Reynolds equation, the linear elasticity equations and the load balance equation. This system can be rewritten under the following matrix form:

$$\begin{cases} R_{stab}\left(P, U, H_0\right) = 0 \\ J_{21}P + J_{22}U = 0 \\ J_{31}P = F_3 \end{cases} \tag{3.19}$$

Where $\left(P, U, H_0\right)$ is the vector containing the nodal values of P and U, and the constant film thickness parameter H_0 (subscripts and superscripts are dropped for convenience). $R_{stab}\left(P, U, H_0\right)$ denotes the discrete weak form of the non-linear stabilized Reynolds' equation. It is approximated by its linear part $L_{P,U,H_0}R_{stab}\left(\delta P, \delta U, \delta H_0\right)$ at $\left(P, U, H_0\right)$ obtained by a first order Taylor expansion:

$$\begin{aligned} L_{P,U,H_0}R_{stab}\left(\delta P, \delta U, \delta H_0\right) = R_{stab}\left(P, U, H_0\right) + \left.\frac{\partial R_{stab}}{\partial P}\right|_{P,U,H_0} \delta P \\ + \left.\frac{\partial R_{stab}}{\partial U}\right|_{P,U,H_0} \delta U + \left.\frac{\partial R_{stab}}{\partial H_0}\right|_{P,U,H_0} \delta H_0 \end{aligned} \tag{3.20}$$

Let: $J_{11} = \left.\frac{\partial R_{stab}}{\partial P}\right|_{P,U,H_0}$, $J_{12} = \left.\frac{\partial R_{stab}}{\partial U}\right|_{P,U,H_0}$ and $J_{13} = \left.\frac{\partial R_{stab}}{\partial H_0}\right|_{P,U,H_0}$

The elasticity and load balance equations are already linear and therefore they are strictly equivalent to their linear part at $\left(P, U, H_0\right)$. Starting with an initial guess $\left(P^0, U^0, H_0^0\right)$ of the solution, the linearized system of equations to solve at the i^{th} iteration of the Newton procedure is defined by:

$$\text{Find } \left(\delta P^i, \delta U^i, \delta H_0^i\right) \text{ such that: } \begin{cases} L_{P^{i-1},U^{i-1},H_0^{i-1}}R_{stab}\left(\delta P^i, \delta U^i, \delta H_0^i\right) = 0 \\ J_{21} \cdot \left(P^{i-1} + \delta P^i\right) + J_{22} \cdot \left(U^{i-1} + \delta U^i\right) = 0 \\ J_{31} \cdot \left(P^{i-1} + \delta P^i\right) = F_3 \end{cases} \tag{3.21}$$

Where $\left(\delta P^i, \delta U^i, \delta H_0^i\right)$ is an increment vector. The Hertzian pressure and elastic deformation profiles or a previously stored solution are a good estimate for $\left(P^0, U^0\right)$. Replacing $L_{P^{i-1}, U^{i-1}, H_0^{i-1}} R_{stab}\left(\delta P^i, \delta U^i, \delta H_0^i\right)$ by its expression provided in eq. (3.20), the system of equations (3.21) becomes:

$$\begin{bmatrix} J_{11} & J_{12} & J_{13} \\ J_{21} & J_{22} & \varnothing \\ J_{31} & \varnothing & \varnothing \end{bmatrix}^{i-1} \begin{Bmatrix} \delta P \\ \delta U \\ \delta H_0 \end{Bmatrix}^{i} = \begin{Bmatrix} -R_{stab}\left(P, U, H_0\right) \\ -J_{21}P - J_{22}U \\ F_3 - J_{31}P \end{Bmatrix}^{i-1} \tag{3.22}$$

The matrix on the left hand side is the Jacobian matrix where we can identify the coupling terms J_{12}, J_{13}, J_{21} and J_{31}. We remind the reader that in the present approach the Jacobian matrix is sparse (more than 99 % of the terms are zeros), and therefore the computational effort or memory usage required for inverting it are far less important than for a full matrix.

Remark: A semi-system approach does not explicitly take into account the coupling terms. Nevertheless, a weak coupling is established between the Reynolds, linear elasticity and load balance equations by determining the coupling terms for each equation from the last solution of the other two equations. Thus an iterative process is realized between the three equations. This leads to a loss of information that is compensated by underrelaxation and consequently a slow convergence rate of the solution is obtained.

The Newton procedure consists in solving the linearized system of eqs. (3.22) at every iteration i and adding the result $\left(\delta P^i, \delta U^i, \delta H_0^i\right)$ to the vector $\left(P^{i-1}, U^{i-1}, H_0^{i-1}\right)$ obtained at the previous iteration:

$$\begin{Bmatrix} P \\ U \\ H_0 \end{Bmatrix}^{i} = \begin{Bmatrix} P \\ U \\ H_0 \end{Bmatrix}^{i-1} + \begin{Bmatrix} \delta P \\ \delta U \\ \delta H_0 \end{Bmatrix}^{i} \tag{3.23}$$

This procedure is repeated until the convergence of the solution is reached i.e. until the Euclidian norm of the relative residual error vector falls below 10^{-6}. The linearized system of equations is solved using a direct solver. The detailed matrix form of system (3.22) is given in Appendix B.

3.6 Convergence and complexity

As was mentioned earlier, a full-system approach provides a faster convergence rate than a semi-system one. In fact, underrelaxation is no longer needed since no loss of information occurs during the coupling process. A typical line / circular contact case requires roughly between 5 to 20 Newton iterations depending on the smoothness of the solution (e.g.: smooth or severe pressure spike). This is far smaller than the total number of iterations required by a semi-system approach. This result is to be expected, since Newton's method is known to exhibit fast convergence rates when the initial guess for the solution is chosen suitably (quadratic convergence may be expected if consistent linearization is held).

Line Contact		Point Contact	
n	t_{cpu} / Newton iteration (s)	n	t_{cpu} / Newton iteration (s)
5 217 (= n_{ref})	0.347 (= t_{ref})	7 862 (= n_{ref})	2.875 (= t_{ref})
10 441	0.578	17 841	7.765
17 946	1.022	21 873	10.078
21 563	1.094	30 733	15.234
24 405	1.276	46 194	29.344
26 389	1.403	64 977	43.532
42 384	2.158	67 755	50.281

Table 3.2: Calculation time for one Newton iteration as a function of the total number of dofs for typical line / circular contacts

Finally, we studied the complexity of the present model. Table 3.2 gives the calculation time for one Newton iteration (using a 2 GHz processor), for both typical line and circular contact problems, as a function of the total number of dofs *n*. These results are used to plot the overall global complexity of the algorithm as shown in Figure 3.6.

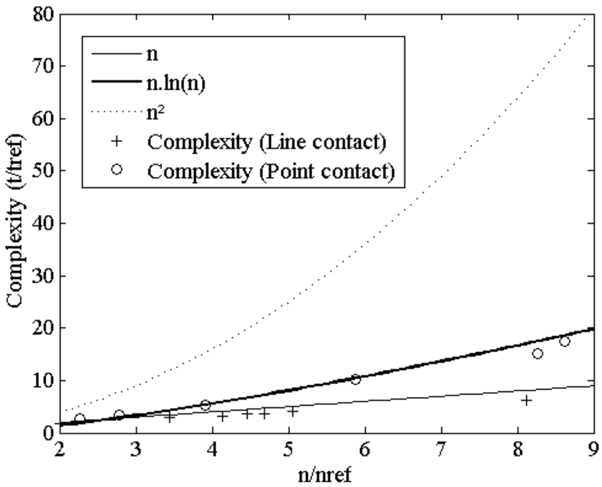

Figure 3.6: Overall complexity of the numerical scheme

Figure 3.6 shows that the complexity of a line contact problem approaches *O(n)* while for a point contact it is *O(n.ln(n))*, where *n* is the total number of dofs in the system. This is the same complexity as multigrid models with a semi-system approach and a finite difference discretization. But in the present approach, a reduced size of the problem is obtained. This is mainly due to the use of the finite element method which enables non-regular non-structured meshing. Therefore, fine meshing is used only where needed as can be seen in Figure 3.7 and Figure 3.9.

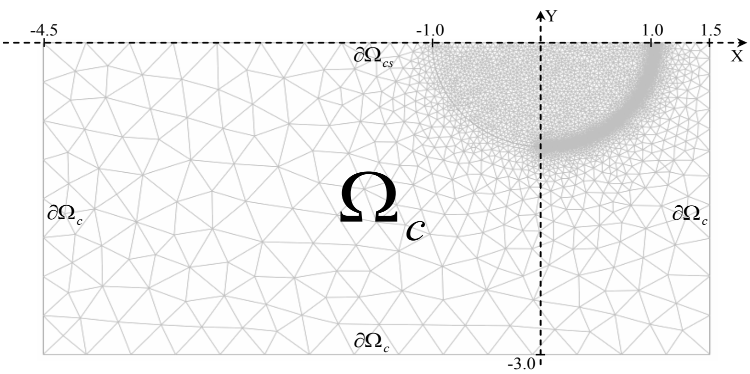

Figure 3.7: Meshing of the contact area Ω_c

Figure 3.7 shows a typical meshing of the contact area Ω_c, delimited by its boundaries $\partial\Omega_c$ and $\partial\Omega_{cs}$, for a circular contact problem. Note that the mesh is coarse in the inlet and outlet regions of the contact where the solution shows small variations. On the other hand, a fine mesh is used in the central (Hertzian) contact area where the pressure gradients are more important. Finally, a finer mesh is used at the outlet of the central contact area where the pressure spike and film thickness constriction are generally observed. Thus a good capture of the severe pressure gradients that occur in this area is obtained. A more quantitative proof of the precision of the current model and its relatively small size compared to finite difference models is provided in the following section.

3.7 Quantitative analysis

In this section, a thorough quantitative analysis of the current model is described. First, the geometrical and mesh properties are studied. Then, the effect of the penalty term on the pressure and film thickness solutions is analyzed. Finally, a comparative study with a finite difference based model (using multigrid techniques) is carried out for a typical circular contact case. The latter validates the current approach and proves its efficiency.

3.7.1 Geometry and mesh considerations

The geometry of the current model is discussed below along with its mesh characteristics. Since the problem is symmetric, only half of the domain is represented in Figure 3.9 where the symmetry boundary $\partial\Omega_s$ splits the cube with respect to the *ZX*-plane.

3.7.1.1 Dimensions of the structure

The size of the 3D structure should be large enough compared to the size of the contact area that extends from *X*=-4.5 to 1.5 and *Y*=-3.0 to 0.0 so that the boundary conditions of eq. (3.5) (that correspond to a semi-infinite media) would stand. This stems from the physical reality of an EHD contact where the size of the contact is very small compared to the size of the contacting bodies. In order to determine the appropriate dimensions of the structure, a test case is carried out with a Hertzian pressure distribution applied in the contact region.

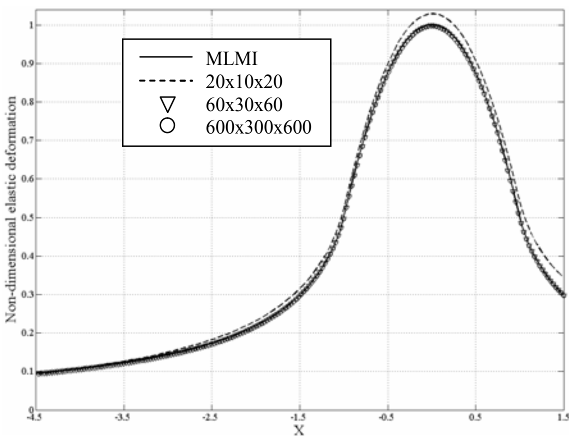

Figure 3.8: Effect of the cube's size on the elastic deformation calculation

Remark: Because of the use of dimensionless variables, the geometry of the contact is independent of the operating conditions. This is one of the reasons behind the use of dimensionless variables and equations.

Figure 3.8 shows the dimensionless elastic deformation in the contact area along the central line in the X direction. The cube's dimensions reported in this figure are dimensionless. It is clear that the size of the cube's side should be at least 60 times the Hertzian contact radius so that the elastic deformation would agree with the solution given by the classical Multi-Level Multi-Integration (MLMI) method [9] applied to a half-space approach. Note that beyond 60x30x60, any increase in the dimensions of the structure would be useless. Therefore, this size will be adopted in our current model. However, even if a 600x300x600 size is taken, the number of degrees of freedom (dofs) remains practically the same because, as we shall see in the next section, in the regions away from the contact, the mesh size is proportional to the dimensions of the structure.

3.7.1.2 Effect of the mesh size

In order to investigate the effect of the mesh size on the precision of the elastic calculation, the same test is run for different mesh cases. The elements' size is kept constant in the contact area (Ω_c) while several mesh coarsenings were tested in the remaining part $(\Omega - \Omega_c)$. Figure 3.9 shows two extreme cases: a normal mesh (left) and an extremely coarse one (right).

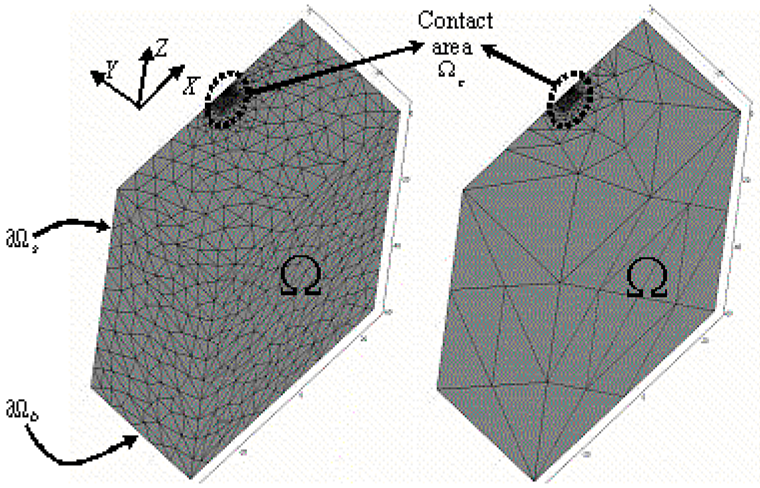

Figure 3.9: Meshes in the regions away from the contact (left: normal, right: extremely coarse)

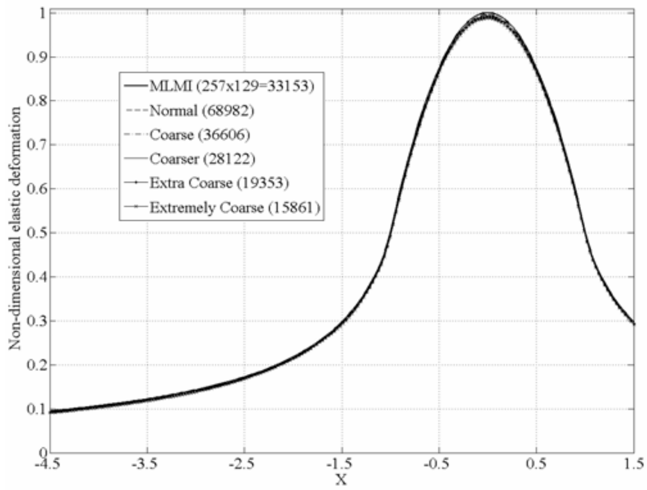

Figure 3.10: Effect of the mesh size on the elastic deformation calculation

Figure 3.10 shows that even for an extremely coarse mesh the loss of precision in the elastic deformation calculation is still negligible especially in the inlet region of the contact where the film thickness is built up. Therefore, in our calculations, this mesh case will be adopted. This leads to a considerable decrease in the size of the system and the computational time. The number of degrees of freedom (dofs) is reported between brackets in the legend of Figure 3.10.

3.7.2 Penalty term analysis

In section 3.3, it was pointed out that the free boundary problem that arises at the outlet of the contact is treated by applying a penalty method. The latter consists in adding to Reynolds' equation a penalyzing term that forces the negative pressures towards zero. In this section, the effect of this term on the pressure and film thickness solutions is analyzed. For this purpose a typical steel-steel ball on plane contact with a load of 100 N, a mean entrainment velocity of 0.8 m/s and a ball radius of 16 mm is considered. The dimensionless Moes parameters for this case are: M=200 and L=10. The lubricant is assumed to be compressible. Its density varies with pressure according to the Dowson & Higginson formula. The Roelands model is used for viscosity-pressure dependence with $\mu_R = 0.04$ Pa.s, $\alpha = 22$ GPa^{-1} and $T=T_R=cst$. The parameter ρ_{id} is taken to be 0.5. Lagrange quintic elements are used for the hydrodynamic problem and quadratic elements for the elastic part. The mesh size is approximately equal to 0.5 in the inlet and outlet regions of the contact and 0.05 in the central area. In practice, the penalty term's parameter ξ in eq. (3.8) is taken as:

$$\xi = \xi_0 \times h_e^2 \tag{3.24}$$

Where ξ_0 is an arbitrary large positive number. The values of the central and minimum film thicknesses, the outlet absicca of the contact (location of the free boundary X_{out}) on the central line in the X-direction and the minimum pressure are listed in Table 3.3 as a function of the value of ξ_0.

ξ_0	H_c	H_m	X_{out} $(Y=0)$	$Min(P)$
10^2	0.082198	0.038382	0.9870	$-3.0092.\ 10^{-2}$
10^4	0.082214	0.039267	1.0403	$-2.5630.\ 10^{-3}$
10^6	0.082215	0.039298	1.0589	$-9.5199.\ 10^{-5}$
10^8	0.082215	0.039298	1.0602	$-6.5941.\ 10^{-5}$

Table 3.3: Effect of the penalty term on the pressure and film thickness solutions

It is clear that a minimum value of ξ_0 is required in order to get converged pressure and film thickness solutions. In fact, note that beyond $\xi_0 = 10^6$, any increase of the value of this parameter is useless and does not lead to any significant changes in the solution. Finally, note that the larger this parameter is, the closer the negative pressures get to zero.

3.7.3 Validation and comparison with FD multigrid based model

A comparative study between the present finite element model and the semi-system finite difference (with multigrid techniques) model is established in order to validate the current approach and demonstrate its efficiency. For this purpose, a representative test case corresponding to a fairly loaded circular contact problem is taken from [115] in order to compare the results and efficiency of both models. The lubricant properties and operating conditions are the same as described in the previous section. The test is carried out for several mesh sizes and the results are reported in Table 3.4. In fact, for the finite difference based model, the mesh diameter h_e is constant throughout the contact domain and equal to 0.046875, 0.0234375 and 0.01171875 for the three cases mentioned in Table 3.4 respectively whereas for the current model, h_e is variable, and approximately equal to 0.5 in the inlet and outlet regions of the contact in the three test cases whereas in the central part of the contact it is approximately equal to 0.15, 0.075 and 0.05 respectively.

Venner & Lubrecht [115]				Current model			
N° dofs	H_c	H_m	N_{iter}	N° dofs	H_c	H_m	N_{iter}
16 770 (128x128 mesh)	0.07887	0.03712	153	18 313	0.080950	0.038818	11
66 306 (256x256 mesh)	0.08093	0.03848	107	39 836	0.081845	0.039165	13
263 682 (512x512 mesh)	0.08144	0.03876	80	76 249	0.082215	0.039298	14

Table 3.4: Comparison of the current model with the Venner & Lubrecht [115] model for a typical circular contact case (M=200 and L=10)

Table 3.4 gives the dimensionless central and minimum film thicknesses obtained by both the Venner & Lubrecht and the current models for the test case described earlier using different mesh densities. The number of iterations N_{iter} required by each model to reach the converged solution is also reported. For the multigrid based model, N_{iter} corresponds to the equivalent number of iterations that would be carried out over the finest mesh level given in the left column. The total number of dofs for the Venner & Lubrecht model is divided by 2 with respect to the number given in [115] because this model does not take into account the symmetry of the problem (e.g.: 66306=(256+1)x(**256/2**+1)x2). Note that even for a total number of 18313 dofs, the solution given by the current model can be considered sufficiently accurate compared to the finest mesh case considered here. Also note, compared to the Venner & Lubrecht model, the much smaller number of iterations that is required to get a converged solution. This reveals the outstanding convergence rate mentioned earlier.

The 3D dimensionless pressure profile for this case is given in Figure 3.11 (Left) and the corresponding plot of the dimensionless pressure and film thickness profiles along the central line in the X-direction are shown in Figure 3.11 (Right).

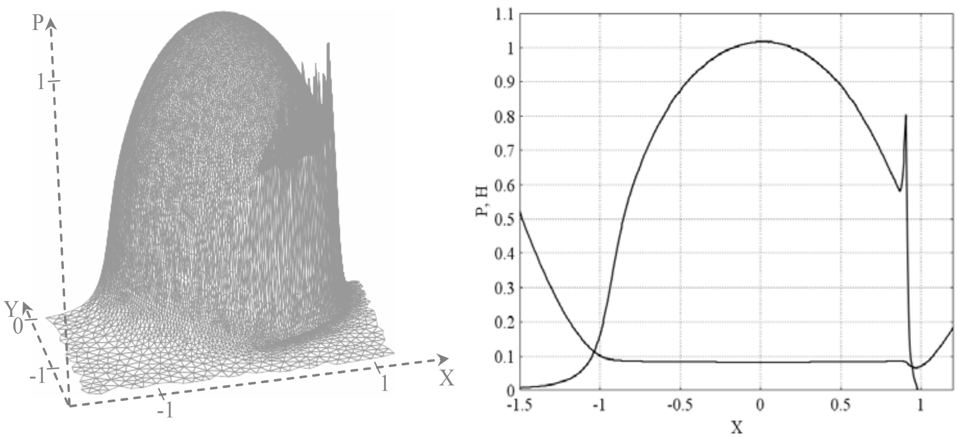

Figure 3.11: Result for M=200 and L=10: 3D dimensionless pressure profile (Left), dimensionless pressure and film thickness profiles along the central line in the X-direction (Right)

This test allows the validation of the method presented in this chapter and confirms that the size of the system of equations to solve can be reduced compared to finite difference based models. Moreover, as we saw earlier, the same complexity as the latter is obtained with faster convergence rates. Therefore, memory storage and computational time are considerably reduced. A typical circular contact resolution takes “roughly” between 1 and 3 minutes on a personal computer with a 2 GHz processor whereas a line contact solution is obtained in less than 10 seconds.

3.8 Conclusion

This chapter presented a finite element resolution of the fully-coupled isothermal elastohydrodynamic circular contact problem. A linear elasticity approach for computing the elastic deformation of the contacting bodies is used. This leads to a sparse Jacobian matrix for the non-linear system of equations to be solved. Suitable stabilization techniques are used to extend the solution to the case of highly loaded contacts and a penalty method is used to handle the free boundary problem efficiently. The complexity of the numerical scheme is shown to be the same as for classical semi-system schemes using for instance Multigrid techniques and a finite difference discretization of the corresponding equations. The use of the finite element method allows the use of variable unstructured meshing and different types of elements / approximations within the same model which leads to a reduced size of the problem. Moreover, the use of the full-system Newton procedure provides faster convergence rates, leading thus to a considerable decrease in the computational time, effort and memory usage.

This model forms the core of the EHL solver from which an extension to a much more physical and practical modelling can be achieved as we shall see in the rest of this thesis. In fact, most real life lubricants do not behave as Newtonian fluids. This is why in the next chapter an extension of this model to account for non-Newtonian effects is developed.

4 Non-Newtonian effects

Besides in theory, an “ideal” Newtonian fluid does not really exist. However, in practice, a fluid is considered Newtonian when it has a relatively high Newtonian limit (it can sustain high shear rates before showing any viscosity variations). But, if the Newtonian limit is reached, the linear (Newtonian) shear-stress / shear-strain dependence is lost. In lubrication applications, the lubricant can be submitted to extremely severe conditions. In ball bearings or spur gears for example, the mean entrainment speed of the lubricant within the conjunction may reach 100 m/s while it goes through the contact in a few microseconds. The velocity gradients may reach 10^7 s^{-1} and pressures up to 2 or 3 GPa may be encountered. Under such extreme conditions, most fluids have a far more complex response than the simple Newtonian one. In addition, the increasingly complex chemical composition of today’s lubricants which include polymer additives and other blends makes their behaviour rather complicated. Different constitutive laws have been introduced throughout the years to represent these complex fluid responses such as Carreau [15] or also the non-linear Maxwell model [107][108] which are considered as shear-thinning models. In fact, the corresponding fluids’ viscosities decrease with the increase of shear stress leading thus to a decrease of the corresponding film thickness. Later on, Bair and Winer [5][6] introduced a different type of non-Newtonian behaviour: limiting-shear-stress. Their analysis was based on primary laboratory experiments using constant pressure stress-strain apparatus and high-shear viscometers. It is important to note that the list of previously cited models is not exhaustive and many others can be found in the literature e.g. Gecim and Winer [34] limiting-shear-stress model, the Ree-Eyring shear-thinning sinh-law [28] ...

In EHL problems, shear stresses in the lubricant film are often important and if the latter has a shear-thinning behaviour, its viscosity may exhibit an important decrease with the increase of shear stress. Hence, assuming that it is Newtonian may be dangerous for the design of a mechanical component because film thicknesses would be overestimated. This could lead to a severe reduction in the life of the component or even, in the extreme case, to its failure. In this chapter, non-Newtonian effects on pressure, film thickness and traction in isothermal EHL circular contacts lubricated with a shear-thinning fluid are studied.

4.1 Lubricant properties

A non-Newtonian lubricant’s density varies with pressure and temperature according to the different models described in section 2.4.1. However, in addition to the variation with pressure and temperature, its viscosity also exhibits a variation with shear stress that varies throughout the lubricant film (the assumption that the viscosity of the lubricant is constant in the film thickness does not hold anymore). Thus, a generalized Newtonian viscosity can be defined by $\eta = f\left(p, T, \tau_e\right)$ such that:

$$\tau_e = \eta\,\dot{\gamma}_e \tag{4.1}$$

Where τ_e and $\dot{\gamma}_e$ are the equivalent shear stress and shear rate inside the lubricant film respectively, defined as:

$$\tau_e = \sqrt{\tau_{zx}^2 + \tau_{zy}^2} \quad \text{and} \quad \dot{\gamma}_e = \sqrt{\dot{\gamma}_{zx}^2 + \dot{\gamma}_{zy}^2} \tag{4.2}$$

Equation (4.1) is a particular case of the non-linear Maxwell model [107][108] where the elastic effects are neglected. In fact, a significant amount of friction is generated in EHL conjunctions such that the shear stresses are usually large enough for the non-linear viscous flow to dominate the strain rate in the lubricant film. The function f could stand for any of the known generalized Newtonian models such as the sinh-law [28], the Carreau [15] model ... In this work, we shall use the Carreau model which takes into account the second Newtonian plateau that can occur at very high shear rates (See Figure 4.1).

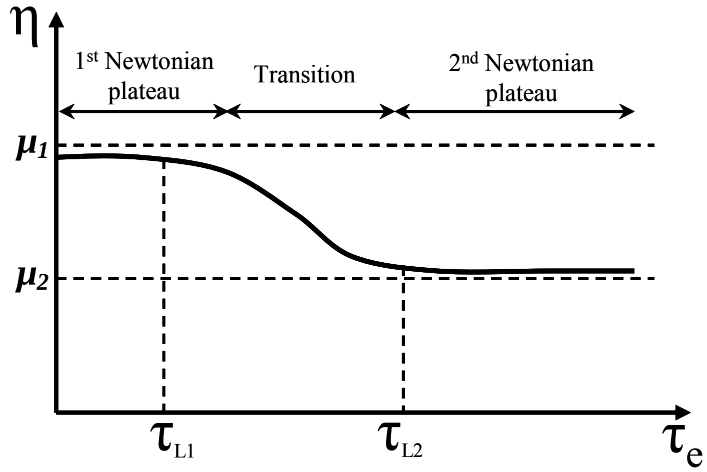

Figure 4.1: Typical behaviour of a shear-thinning lubricant

Despite being a powerful shear-thinning constitutive law, the Carreau model has been seldom used in EHL applications because of its' non reversible form giving the equivalent shear stress as a function of the equivalent shear rate. Recently, a modified version of this equation, well suited for EHL solvers, was provided by Bair [1]. The latter gives a reversed form where the equivalent shear rate is a function of the equivalent shear stress and the rheological parameters. The corresponding generalized Newtonian viscosity is written under the following form:

$$\eta = \mu_2 + \frac{\mu_1 - \mu_2}{\left[1 + \left(\dfrac{\tau_e}{G_c}\right)^{\beta_c}\right]^{\frac{\frac{1}{n_c} - 1}{\beta_c}}} \tag{4.3}$$

Where G_c is the liquid critical shear stress, β_c and n_c are two constant parameters. μ_1 and μ_2 are the low and high shear limiting viscosities respectively. Equation (4.3) is a good approximation of the classical Carreau law for values of n_c ranging from 0.3 to 0.8, which is the range of interest in EHL applications. The variation of η with pressure and temperature is implicitly expressed by the variations of the first and second Newtonian viscosities μ_1 and μ_2 with these parameters according to the relationships given in section 2.4.2. In this chapter, since an isothermal approach is considered, the temperature T throughout the film thickness is assumed to be constant and equal to the ambient (inlet) temperature ($T = T_0 = cst$).

Since the lubricant's viscosity cannot be considered as a constant through the thickness of the lubricant film, a new Reynolds' equation that integrates the viscosity variations in the film thickness has to be introduced.

4.2 Generalized Reynolds' equation

A generalized Reynolds' equation was introduced by Najji [91] for contacts lubricated with a non-Newtonian lubricant. This equation has the advantage of not being restricted to a particular non-Newtonian law and can be used with any model provided that the latter is written as a function of the generalized Newtonian viscosity defined above. Compared to the classical Reynolds' equation, this equation takes into account the viscosity variations in the film thickness. It is obtained in a similar way by integrating the simplified Navier-Stokes equations (2.1) reminded below:

$$\begin{aligned}\frac{\partial p}{\partial x} &= \frac{\partial \tau_{zx}}{\partial z}\\ \frac{\partial p}{\partial y} &= \frac{\partial \tau_{zy}}{\partial z}\\ \frac{\partial p}{\partial z} &= 0\end{aligned} \tag{4.4}$$

The shear stress components are replaced this time by their expressions derived from the projection of eq. (4.1) in the x and y-directions given by:

$$\tau_{zx} = \eta\,\dot{\gamma}_{zx} = \eta\frac{\partial u_f}{\partial z} \quad \text{and} \quad \tau_{zy} = \eta\,\dot{\gamma}_{zy} = \eta\frac{\partial v_f}{\partial z} \tag{4.5}$$

The integration of equations (4.4) twice with respect to z associated to the surface velocity no-slip boundary conditions ($u_f = u_p$, $v_f = w_f = 0$ at $z = z_p$ and $u_f = u_s$, $v_f = w_f = 0$ at $z = z_s$) gives the velocity field of the lubricant:

$$\begin{cases} u_f = \dfrac{\partial p}{\partial x}\left(\displaystyle\int_0^z \frac{z}{\eta}dz - \frac{\eta_e}{\eta_e'}\int_0^z \frac{dz}{\eta}\right) + \eta_e\left(u_s - u_p\right)\displaystyle\int_0^z \frac{dz}{\eta} + u_p \\ v_f = \dfrac{\partial p}{\partial y}\left(\displaystyle\int_0^z \frac{z}{\eta}dz - \frac{\eta_e}{\eta_e'}\int_0^z \frac{dz}{\eta}\right) \end{cases} \tag{4.6}$$

Where: $\dfrac{1}{\eta_e} = \int_0^h \dfrac{dz}{\eta}$, $\dfrac{1}{\eta'_e} = \int_0^h \dfrac{z}{\eta} dz$ and $\dfrac{1}{\eta''_e} = \int_0^h \dfrac{z^2}{\eta} dz$

Note that the shear rate components $\dot{\gamma}_{zx}$ and $\dot{\gamma}_{zy}$ are obtained by deriving these velocity components with respect to z:

$$\begin{cases} \dot{\gamma}_{zx} = \dfrac{1}{\eta}\dfrac{\partial p}{\partial x}\left(z - \dfrac{\eta_e}{\eta'_e}\right) + \dfrac{\eta_e}{\eta}\left(u_s - u_p\right) \\ \dot{\gamma}_{zy} = \dfrac{1}{\eta}\dfrac{\partial p}{\partial y}\left(z - \dfrac{\eta_e}{\eta'_e}\right) \end{cases} \tag{4.7}$$

Finally, replacing u_f and v_f in the mass continuity equation reminded below:

$$\frac{\partial m_x}{\partial x} + \frac{\partial m_y}{\partial y} = 0 \quad \text{with} \quad m_x = \int_0^h \rho u_f dz \quad \text{and} \quad m_y = \int_0^h \rho v_f dz \tag{4.8}$$

by their expressions given in (4.6) gives the generalized Reynolds' equation that reads:

$$\nabla \cdot \left(\varepsilon' \nabla p\right) - \frac{\partial \left[\rho h \left(u_s - \dfrac{\eta_e}{\eta'_e}\left(\dfrac{u_s - u_p}{h}\right)\right)\right]}{\partial x} = 0 \tag{4.9}$$

$$\text{Where: } \varepsilon' = \rho\left(\frac{1}{\eta''_e} - \frac{\eta_e}{\eta'^2_e}\right)$$

For the same practical reasons mentioned in section 2.6, it is preferable to solve this equation in a dimensionless form. Let $\bar{\eta}$ and Z be the dimensionless generalized Newtonian viscosity and space dimension defined as:

$$\bar{\eta} = \frac{\eta}{\mu_R} = \bar{\mu}_2 + \frac{\bar{\mu}_1 - \bar{\mu}_2}{\left[1 + \left(\dfrac{\tau_e}{G_c}\right)^{\beta_c}\right]^{\frac{\frac{1}{n_c} - 1}{\beta_c}}} \quad \text{and} \quad Z = \frac{z}{h} \tag{4.10}$$

Using the dimensionless variables defined in eq. (4.10) along with those mentioned in section 2.6, the generalized Reynolds' equation can be written in a dimensionless form given by:

$$\nabla \cdot \left(\bar{\varepsilon}' \nabla P\right) - \frac{\partial \left[\bar{\rho} H \left(u_s - \dfrac{\bar{\eta}_e}{\bar{\eta}'_e}\left(u_s - u_p\right)\right)\right]}{\partial X} = 0 \tag{4.11}$$

Where: $\bar{\varepsilon}' = \dfrac{\bar{\rho}H^3}{\lambda'}\left(\dfrac{1}{\bar{\eta}_e''} - \dfrac{\bar{\eta}_e}{\bar{\eta}_e'^2}\right)$, $\lambda' = \dfrac{R^2\mu_R}{p_h a^3}$, $\dfrac{1}{\bar{\eta}_e} = \displaystyle\int_0^1 \dfrac{dZ}{\bar{\eta}}$, $\dfrac{1}{\bar{\eta}_e'} = \displaystyle\int_0^1 \dfrac{Z}{\bar{\eta}} dZ$ and $\dfrac{1}{\bar{\eta}_e''} = \displaystyle\int_0^1 \dfrac{Z^2}{\bar{\eta}} dZ$

Note that if the generalized Newtonian viscosity η is replaced by the Newtonian one μ eq. (4.11) becomes the classical Reynolds' equation. Finally, eq. (4.11) can be written in the following form:

$$R'(P) = -\nabla\cdot\left(\bar{\varepsilon}'\nabla P\right) + H\left(u_s - \frac{\bar{\eta}_e}{\bar{\eta}_e'}\left(u_s - u_p\right)\right)\frac{\partial\bar{\rho}}{\partial P}\frac{\partial P}{\partial X} + \bar{\rho}\frac{\partial\left[H\left(u_s - \frac{\bar{\eta}_e}{\bar{\eta}_e'}\left(u_s - u_p\right)\right)\right]}{\partial X} = 0 \tag{4.12}$$

Let: $\beta_X' = H\left(u_s - \dfrac{\bar{\eta}_e}{\bar{\eta}_e'}\left(u_s - u_p\right)\right)\dfrac{\partial\bar{\rho}}{\partial P}$ and $Q' = -\bar{\rho}\dfrac{\partial\left[H\left(u_s - \frac{\bar{\eta}_e}{\bar{\eta}_e'}\left(u_s - u_p\right)\right)\right]}{\partial X}$

Then eq. (4.12) becomes:

$$R'(P) = -\nabla\cdot\left(\bar{\varepsilon}'\,\nabla P\right) + \beta'\cdot\nabla P - Q' = 0 \tag{4.13}$$

Hence, the generalized Reynolds' equation also has the form of a classical convection / diffusion equation (applied to *P*) with a source term Q'. The diffusion coefficient is $\bar{\varepsilon}'$ and the convection tensor is β'.

4.3 Finite element procedure

The system of EHL equations formed by the generalized Reynolds' equation, the linear elasticity and the load balance equations is solved using a similar Newton-Raphson approach as described in chapter 3 (See section 3.5). The finite element formulations for this system are not reminded here. Those are similar to the ones provided in chapter 3 since the generalized Reynolds' equation also has the form of a convection / diffusion equation. The free boundary problem is also treated by applying a penalty method and for heavy loads, the problem exhibits similar instability features as described in the previous chapter. This can be seen in Figure 4.2 where a test case is carried out with a typical shear-thinning lubricant for a steel on glass circular contact with surface velocities of 1m/s for both surfaces and a load of 1000N which corresponds to a maximum Hertzian pressure of 1.66 GPa. Note that, in practice, this case can never be realized on an experimental apparatus because glass would not withstand such a load. The Tait-Doolittle free volume model is used to express the density and viscosity dependence on pressure. The lubricant properties can be found in Table 4.1. It has an equivalent pressure-viscosity coefficient of 18.53 GPa^{-1}. The Moes parameters for this case are *M*=1718 and *L*=7. These are computed using the zero-pressure low-shear limiting viscosity value at ambient temperature.

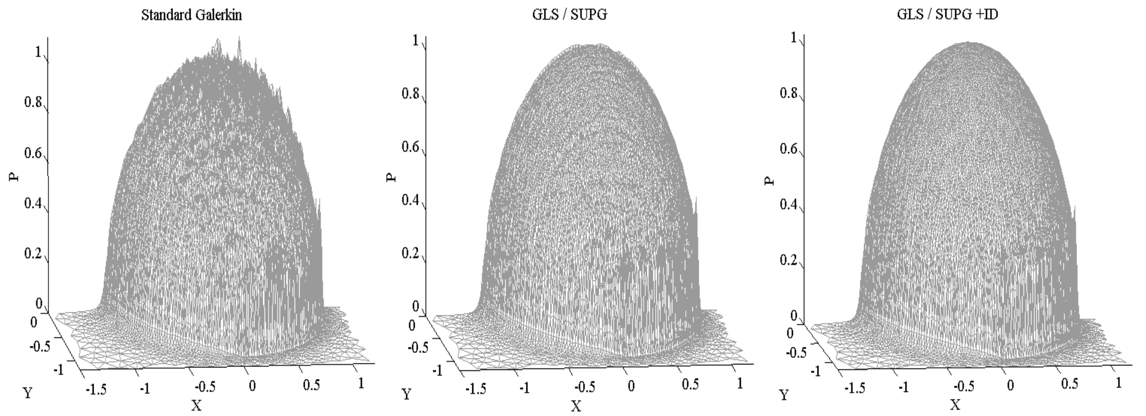

Figure 4.2: Stabilization effects on circular EHD contacts lubricated with a non-Newtonian lubricant (M=1718, L=7, p_h=1.66 GPa)

It is clear that a standard Galerkin formulation leads to an oscillatory behaviour of the solution. The generalized Reynolds' equation can also be written in the convection / diffusion form, and thus, a similar stabilization technique as described in chapter 3 is used to avoid the spurious behaviour of the solution in the central area of the contact. The stabilized formulations are not reminded in this section, those are the same as the ones provided in chapter 3 and for more details the reader is referred to section 3.4.3. Applying GLS or SUPG formulations reduces the amplitude of these oscillations without completely smoothing them out (See Figure 4.2). And finally, adding the ID terms to the GLS or SUPG formulations completely smoothes out the remaining oscillations.

4.4 Global numerical procedure

The same numerical procedure as described in the previous chapter is employed with only a few slight differences. At every Newton resolution, the integral terms in the generalized Reynolds' equation are computed using the solution of the previous resolution. Thus an iterative linearization process is established as shown in the flow diagram of Figure 4.3. This iterative process is repeated until the convergence of the solution is obtained i.e. in this case, until the maximum absolute difference between the pressure solutions at two consecutive resolutions falls below 10^{-3}.

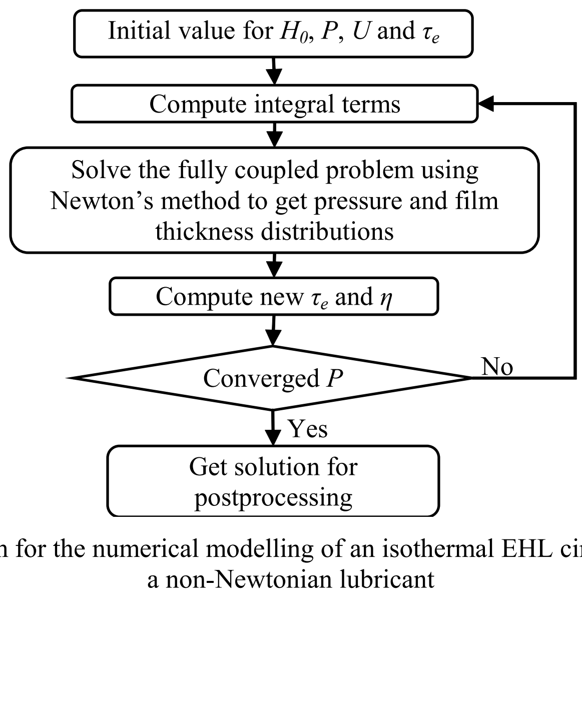

Figure 4.3: flow diagram for the numerical modelling of an isothermal EHL circular contact lubricated with a non-Newtonian lubricant

The cross film integration process is carried out over a meshed lubricant film's geometry using Simpson's quadrature method. The meshing of the lubricant film in the contact plane is similar to that of the contact area Ω_c while the film thickness is partitioned into 10 elements of the same size. The initial values of the pressure profile P and the elastic deflection profile U correspond to those of a dry / Hertzian contact or a suitable previously stored solution. The equivalent shear stress τ_e in the lubricant film is computed using the analytical formulas of eqs. (4.2) and (4.5) where the equivalent shear rates are replaced by their expressions provided in (4.7) and the generalized Newtonian viscosity by its expression given in (4.3). As for the initial value of τ_e, it is obtained by assuming the lubricant is Newtonian and using the initial values of P, U and H_0.

It is clear that the global numerical procedure requires more computational efforts than the one for the Newtonian approach and consequently more cpu time is required. Roughly speaking, for a typical case, the calculations may take between 10 to 20 minutes on a personal computer with a 2 GHz processor.

4.5 Results and validation

In order to reveal the importance of non-Newtonian effects on the behaviour of EHD contacts, two typical shear-thinning lubricants are used to run some test calculations. The first one (Squalane + PIP) is formed by a mixture of Squalane and 15% wt of PolyIsoPrene (PIP). It is representative of the polymer blended multigrade gear and engine oils. The second is a highly viscous PolyAlphaOlefin (PAO 650).

4.5.1 Squalane + PIP

The rheological properties and operating conditions for the Squalane + PIP cases are provided in Table 4.1. The former are taken from [2].

Lubricant properties		Material properties	Operating conditions
$\mu_{1,R}$=0.0705 Pa.s	B=4.2	E_p=81 GPa	T=T_R=T_0=313 K
$\mu_{2,R}$=0.0157 Pa.s	R_0=0.658	υ_p=0.208	R=12.7 mm
G_c=0.01 MPa	K'_0=11.29	E_s=210 GPa	F=23 N
n_c=0.8	K_0=1.007837 GPa	υ_s=0.3	p_h=0.47 GPa
β_c=2.198			

Table 4.1: Material / lubricant properties and operating conditions for the test cases of Squalane+PIP

Steel-on-glass contacts are considered with a contact load of 23 N which corresponds to a Hertzian pressure of 0.47 GPa. The variations of the lubricant's density and viscosity are represented by the Tait-Doolittle free volume model. The film temperature is considered constant and equal to the ambient temperature of 313 K. Both pure rolling and rolling-sliding cases are considered. For the pure rolling cases, the mean entrainment speed of the contacting surfaces varies from 0.1 to 4.64 m/s whereas for the rolling-sliding cases it is kept constant with a Slide-to-Roll Ratio (SRR) varying from 0 to 0.6 (three different constant mean entrainment velocities are considered: 0.18, 0.74 and 1.47 m/s). The Slide-to-Roll ratio is defined as:

$$SRR = \frac{\text{sliding velocity}}{\text{mean entrainment velocity}} = \frac{u_s - u_p}{\frac{1}{2}\left(u_s + u_p\right)} \tag{4.14}$$

The non-Newtonian effects on pressure, film thickness and traction are studied in the following. Where possible, comparisons of the different results with experimental data are carried out in order to validate both the numerical and rheological models. The experimental measurements are carried out on a ball-on-disk apparatus.

4.5.1.1 Pressure

The dimensionless pressure distributions along the central line in the X-direction for a constant mean entrainment velocity of 1.47 m/s and different slide-to-roll ratios are provided in Figure 4.4. The latter were computed using both a Newtonian and non-Newtonian approach. The Newtonian solution is obtained using the approach described in the previous chapter and approximating the viscosity of the lubricant by its low-shear limiting value.

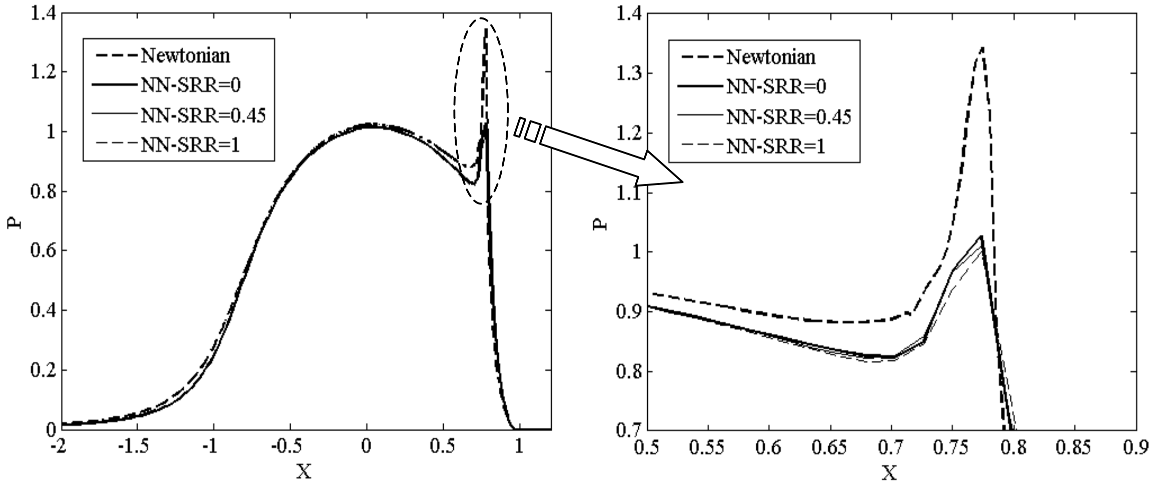

Figure 4.4: Non-Newtonian effects on pressure (u_m=1.47 m/s, p_h=0.47 GPa, M=30 and L=7.8)

Note that when the lubricant is assumed to be Newtonian only one curve is shown for the three different values of the slide-to-roll ratio. This is because, in terms of velocities, the classical Reynolds' equation depends only on the mean entrainment speed which happens to be constant for the three cases shown here. Also note the much higher value of the pressure spike that is predicted by a Newtonian approach compared to the one predicted by the shear-thinning model. On the other hand, when a non-Newtonian approach is considered, it is clear that, globally, the pressure distribution is not affected by the increase of sliding. The only "barely" noticeable difference can be observed in the pressure spike's region. The latter "slightly" loses in height when the SRR is increased.

4.5.1.2 Film thickness

The film thickness curves (for central and minimum film thickness denoted by h_c and h_{min} respectively) under pure rolling regime as a function of the mean entrainment speed are shown in Figure 4.5 along with their experimental equivalent. The Newtonian curves are obtained using the approach described in Chapter 3. It is clear that a Newtonian solution highly overestimates film thicknesses when the lubricant has a shear-thinning behaviour. On the other hand, the non-Newtonian curves show a much better agreement with experimental data. Note that at low speed operating conditions, a very good agreement between the non-Newtonian solution and measurements is obtained whereas a small discrepancy can be observed at high speeds. This is believed to be a consequence of thermal effects which become more important under such operating conditions. This can also be observed in Figure

4.6 where it is shown that for low and moderate mean entrainment speed conditions (0.18 and 0.74 m/s respectively) the agreement between numerical and experimental results is very good for the different values of the SRR considered. However, at high mean entrainment speed (1.47 m/s), a slight discrepancy can be observed.

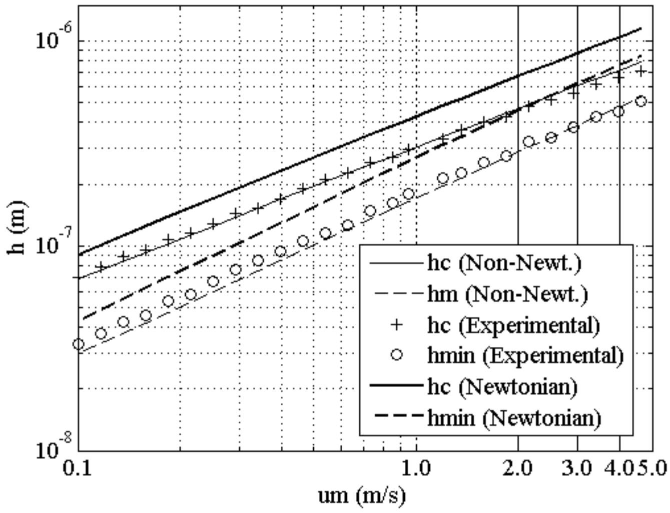

Figure 4.5: Film thickness curves for Squalane + PIP lubricated contacts under pure rolling regime

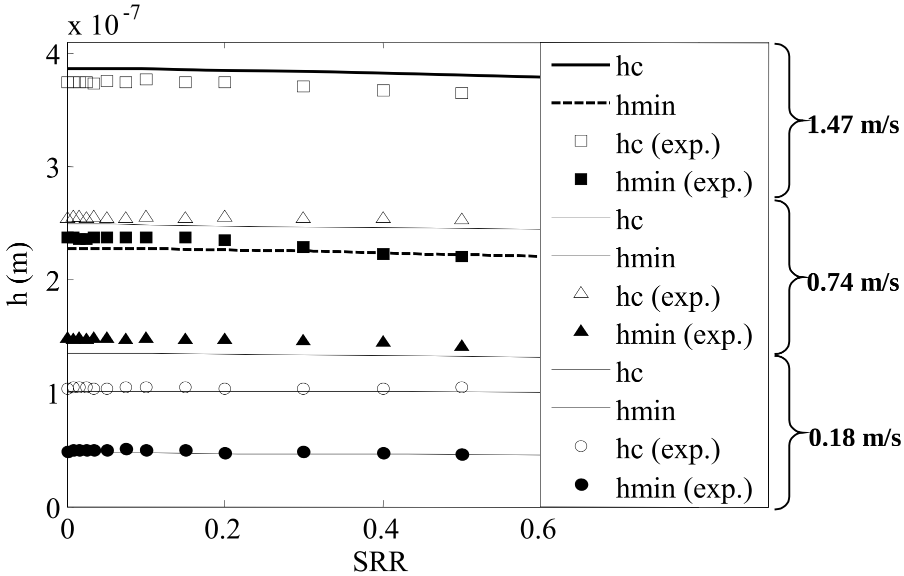

Figure 4.6: Film thickness curves for Squalane + PIP lubricated contacts under rolling-sliding regime

Finally, note the moderate decrease of the film thickness when the SRR is increased. This is characteristic of non-Newtonian lubricants which exhibit a viscosity decrease when sheared. Thus a consequent film thickness reduction is obtained. This feature cannot be observed by a simple Newtonian approach which assumes a constant lubricant viscosity as a function of shear stress. In fact, the latter would have given constant film thicknesses whatever the SRR was. This is to be expected since the classical Reynolds' equation depends only, in terms of velocities, on the mean entrainment speed u_m.

The discrepancy observed in Figure 4.5 between the Newtonian and non-Newtonian film thickness curves under pure-rolling regime is strangely important considering the relatively small decrease in film thickness with the SRR observed in Figure 4.6. This feature is typically an inlet effect. In fact, Figure 4.7 clearly shows that, in the inlet region, the difference in equivalent shear stress τ_e between the pure rolling case and the rolling-sliding cases is very small especially near the solid surfaces. This is because, in this region, due to the important film thickness, the “Poiseuille” component of the equivalent shear stress dominates the “Couette” one. However, in the central area of the contact where the film thickness is much smaller, the “Couette” term is dominant and therefore an important difference in shear stress is observed between the pure-rolling case and the different rolling-sliding ones. This does not significantly affect the film thickness which is known to be built up in the inlet area of the contact but it has an important effect on friction as shall be discussed later.

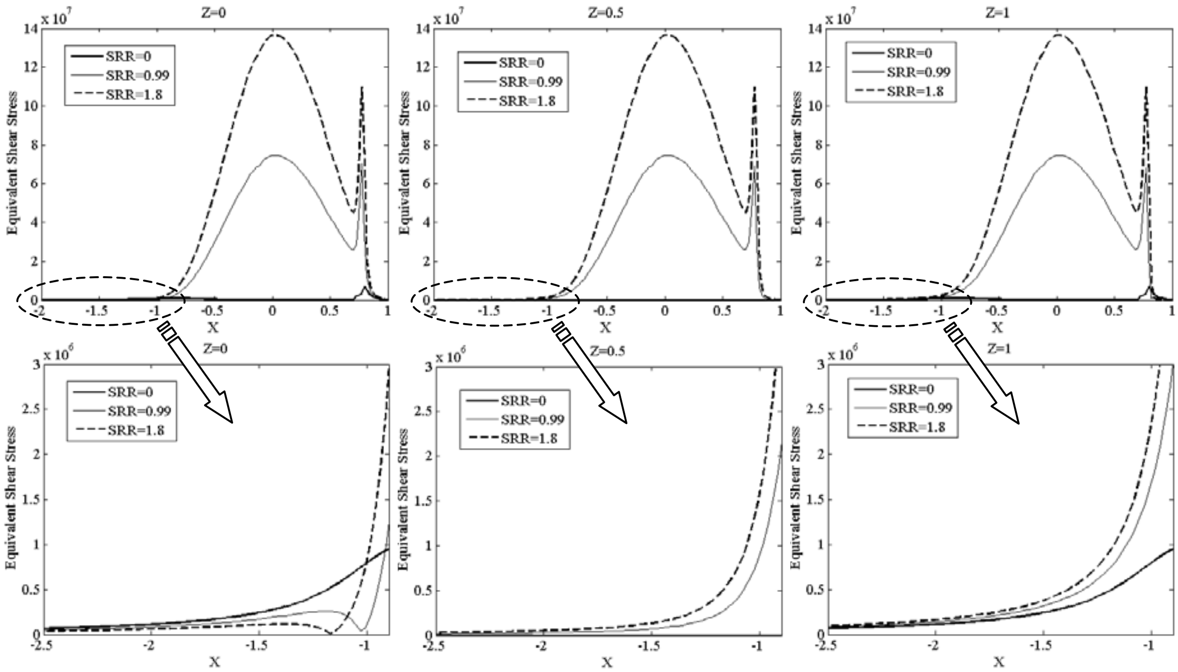

Figure 4.7: Shear stress profiles along the central line of the contact in the x-direction at different Z locations and for different values of the SRR for Squalane + PIP lubrictated contacts (u_m=1.47 m/s)

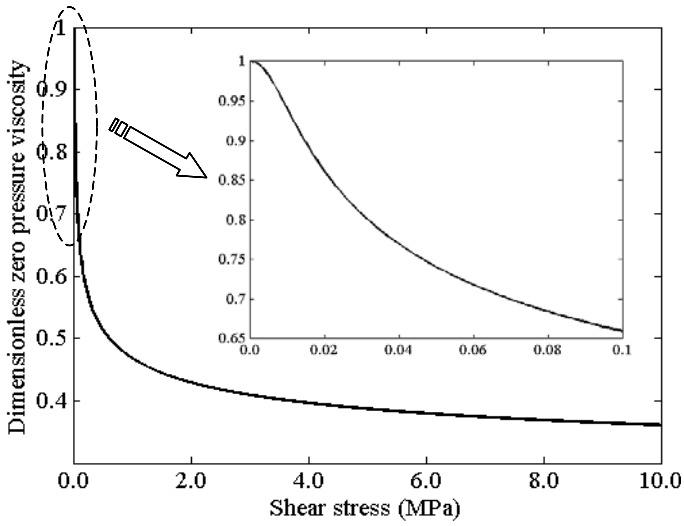

Figure 4.8: Dimensionless zero pressure viscosity variations of Squalane + PIP with shear stress

Also note that, for a value of the equivalent shear stress τ_e of 1 MPa (which is the order of magnitude observed in the inlet area for the pure-rolling and rolling-sliding cases), the viscosity of the Squalane + PIP mixture looses practically more than half its value (See Figure 4.8). This leads to the important film thickness decrease with respect to the Newtonian case where the viscosity is considered to be constant as a function of the equivalent shear stress.

4.5.1.3 Traction

In this section, the traction behaviour of Squalane + PIP lubricated contacts is studied. Figure 4.9 shows the traction curves as a function of the SRR, for two mean entrainment velocities: 0.74 and 1.47 m/s.

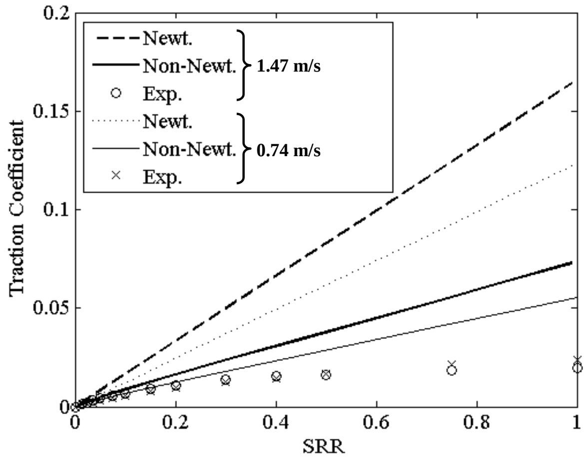

Figure 4.9: Newtonian, non-Newtonian and experimental traction curves for Squalane + PIP lubricated contacts

The traction coefficient in the *x*-direction evaluated at the mid-layer plane of the lubricant film is defined by:

$$\text{Traction Coefficient} = \frac{\int_{\Omega_c} \tau_{zx}\big|_{Z=0.5}\, d\Omega}{F} \tag{4.15}$$

The Newtonian and Non-Newtonian results are provided in Figure 4.9 along with the experimental ones. It is clear that a Newtonian approach highly overestimates friction coefficients in contacts lubricated with a shear-thinning lubricant. The non-Newtonian results are closer to the experimental ones, but still, an important discrepancy is observed when the SRR is increased beyond 0.1. This is believed to be a consequence of thermal effects in the central area of the contact which can be important even at low or moderate entrainment speed when high sliding velocities are considered. This barely affects the film thickness which is known to be mainly built up in the inlet region of the contact, but it has a significant effect on friction coefficients because of the viscosity decrease with the increase of temperature in this area.

4.5.2 PAO 650

The rheological properties and operating conditions for the PAO 650 cases are provided in Table 4.2. The former are taken from [4]. Steel-on-glass contacts are considered with a contact load of 32 N which corresponds to a Hertzian pressure of 0.528 GPa. The variations of the lubricant's density and viscosity are represented by the Tait-Doolittle free volume model. The film temperature is considered constant and equal to the ambient temperature of 348 K. Both pure rolling and rolling-sliding cases are considered. For the pure rolling cases, the mean entrainment speed of the contacting surfaces varies from 0.003 to 0.5 m/s whereas for the rolling-sliding cases it is kept constant with a SRR varying from 0 to 0.5 (three different constant mean entrainment velocities are considered: 0.03, 0.13 and 0.26 m/s).

Lubricant properties		Material properties	Operating conditions
$\mu_{1,R}$=1.42 Pa.s $\mu_{2,R}$=0 Pa.s	B=4.422	E_p=81 GPa	T=T_R=T_0=348 K
G_c=0.031 MPa	R_0=0.6694	υ_p=0.208	R=12.7 mm
n_c=0.74	K'_0=12.82	E_s=210 GPa	F=32 N
β_c=2	K_0=1.4252 GPa	υ_s=0.3	p_h=0.528 GPa

Table 4.2: Material / lubricant properties and operating conditions for the test cases of PAO 650

The non-Newtonian effects on film thickness and traction are studied in the following. Where possible, comparisons of the different results with experimental data are carried out. The experimental measurements are carried out on a ball-on-disk apparatus.

4.5.2.1 Film thickness

The central and minimum film thickness curves under pure rolling regime as a function of the mean entrainment speed are shown in Figure 4.10 along with their experimental equivalent. The Newtonian curves are obtained using the approach described in Chapter 3.

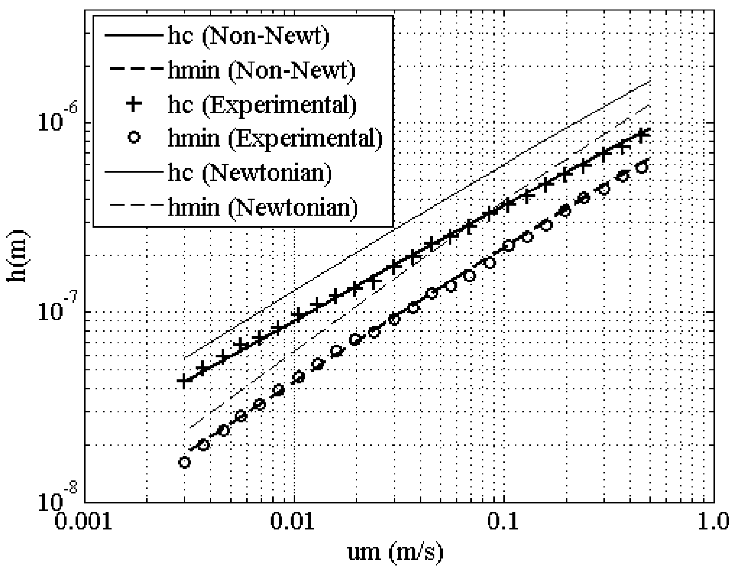

Figure 4.10: Film thickness curves for PAO 650 lubricated contacts under pure rolling regime

Again, it is clear that the Newtonian solution highly overestimates film thicknesses when the lubricant has a shear-thinning behaviour. On the other hand, the non-Newtonian curves show a much better agreement with experimental data. This can also be observed in Figure 4.11 which shows the rolling-sliding film thickness curves for two different mean entrainment speeds (0.03 and 0.13 m/s). A very good agreement between numerical and experimental results is obtained for the different values of the SRR considered. Finally, also note the shear-thinning effect characterized by a moderate decrease of the film thickness when the SRR is increased. This feature cannot be observed by a simple Newtonian approach which assumes a constant lubricant viscosity as a function of shear stress. In fact, for a given mean entrainment speed, the latter predicts constant film thicknesses whatever the SRR was. This is to be expected since the classical Reynolds' equation depends only, in terms of velocities, on the mean entrainment speed u_m.

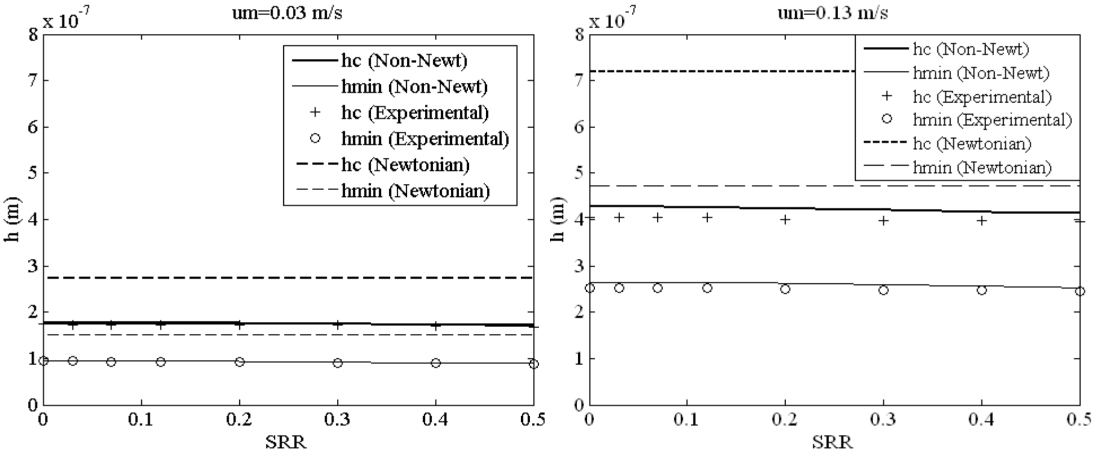

Figure 4.11: Film thickness curves for PAO 650 lubricated contacts under rolling-sliding regime for two different mean entrainment speeds: u_m=0.03 m/s (left) and u_m=0.13 m/s (right)

Note that, in this case, because of the light loads and low entrainment speeds that are considered, the operating conditions can be considered isothermal. This explains the slightly better agreement that is obtained with experimental data compared to the Squalane + PIP test cases.

4.5.2.2 Traction

In this section, the traction behaviour of PAO 650 lubricated contacts is studied. Figure 4.12 shows the traction curves as a function of the SRR, for three mean entrainment velocities: 0.03, 0.13 and 0.26 m/s.

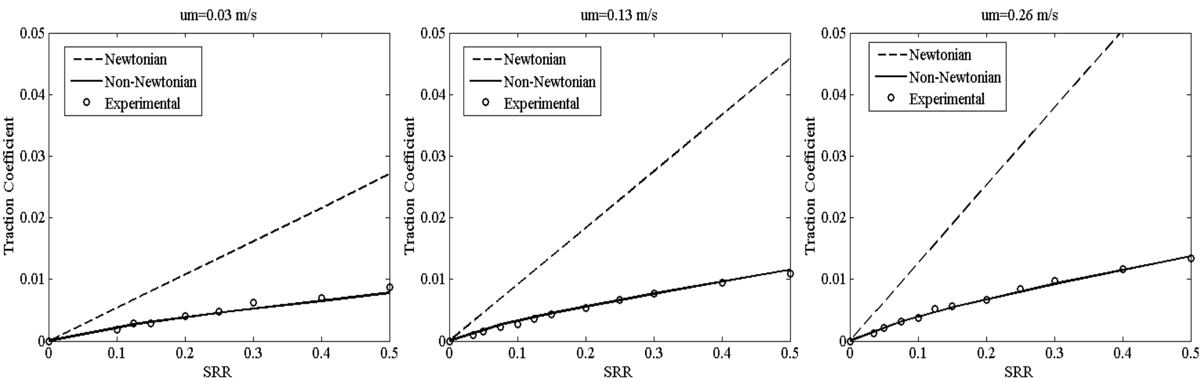

Figure 4.12: Newtonian, non-Newtonian and experimental traction curves for PAO 650 lubricated contacts for three different mean entrainment speeds: u_m=0.03 m/s (left), u_m=0.13 m/s (centre) and u_m=0.26 m/s (right)

The Newtonian and Non-Newtonian results are provided in Figure 4.12 along with the experimental ones. Again, it is clear that a Newtonian approach highly overestimates friction coefficients in contacts lubricated with a shear-thinning lubricant. However, in this case, non-Newtonian results are in perfect agreement with experimental ones. This is because, as stated above, thermal effects are absent since only low speed operating conditions are considered.

4.6 Conclusion

In this chapter, shear-thinning effects on EHL of circular contacts are studied. The classical Reynolds' equation is replaced by a generalized one, taking into account the lubricant's viscosity variations in the film thickness due to shear. These variations are modelled by a powerful shear-thinning model (Carreau) that takes into account the second Newtonian plateau that can occur at very high shear rates. Two typical shear-thinning lubricants (Squalane + PIP and PAO 650) are used to model isothermal EHL contacts under pure rolling and rolling-sliding regimes. Comparisons between numerical and experimental results validate both the employed numerical approach and rheological models. The main observations are summarized below:

- Globally the pressure profile in the contact is not affected by the increase of shear. Only a slight effect can be observed on the pressure spike which looses in height with the increase of the SRR.
- Film thicknesses and friction coefficients are significantly reduced because of the viscosity decrease of the lubricant due to shear. Hence, both are highly overestimated by a simple Newtonian approach.
- A non-Newtonian approach predicts realistic film thicknesses especially at low and moderate speed operating conditions. However, at high speeds, and probably due to thermal effects which become important (even in the inlet area of the contact), some deviation with experiments may be observed.
- Finally, traction results predicted by an isothermal non-Newtonian approach are only realistic at low speed operating conditions. It is believed that this stems from the importance of thermal effects in the central area of the contact.

Thus we can conclude that, when a non-Newtonian lubricant is used, the isothermal non-Newtonian approach is efficient for film thickness and traction calculations at low or moderate entrainment and / or sliding speed operating conditions. However, at high speeds, it is no longer appropriate. It is believed that thermal effects are responsible for the discrepancies observed with experimental results in these cases. These effects can also be important when the contact is lubricated with a Newtonian lubricant. This is why the next chapter is dedicated to the study of thermal effects on EHD circular contacts lubricated with either a Newtonian or a non-Newtonian lubricant.

5 Thermal effects

At severe operating conditions temperature increase in EHD conjunctions may become important. This is more likely to occur when contact conditions combine several factors such as high sliding or mean entrainment speeds, high viscosity or viscosity-pressure dependence of the lubricant and heavy loads. This temperature elevation stems from two heat sources: the shear heating of the lubricant thin layer and the compressive heating due to pressure variations in the contact area. The consequences on the lubricated contact's behaviour cannot be neglected anymore. In fact, as was pointed out in the previous chapter, neglecting the heat generation in EHD contacts working under severe conditions leads to an overestimation of both film thicknesses and traction coefficients. This is because temperature variations cause density, and more importantly, viscosity variations throughout the lubricant film. The interest in thermal effects for EHD lubrication first appeared with the pioneering theoretical work of Cheng [16][17]. The first full numerical solution for the point contact problem was obtained by Zhu and Wen [125]. Since then, several authors proposed different methods to deal with this problem assuming a Newtonian or a non-Newtonian lubricant such as Kim and Sadeghi [72], Guo et al. [43] or also Liu et al. [80] who solved the three dimensional energy equation in order to determine the temperature variations throughout the lubricant film. An alternative method consists in reducing the 3D heat transfer problem to a 2D one by assuming a parabolic temperature distribution across the film thickness. This approach was used by many workers such as Salehizadeh and Saka [104], Wolff and Kubo [120] and Kazama et al. [71] for the line contact case or also Jiang et al. [65], Lee et al. [77] and Kim et al. [73][74] for point contact problems. However, the parabolic temperature profile simplification leads to temperature predictions that are not accurate especially at the inlet of the contact as shown by Kazama et al. [71]. The reason lies in the occurrence of complex thermal convective effects which are associated with important reverse flows in this area.

In the current chapter, some efforts are dedicated to the study of thermal effects on EHD circular contacts lubricated with either a Newtonian or non-Newtonian lubricant. This study is based on the solution of the 3D energy equation applied to the contacting elements and the lubricant film. But before, a new generalized Reynolds' equation is introduced to account for thermal effects.

5.1 Generalized Reynolds' equation with thermal effects

Because of the temperature variations in the contact, not only the viscosity of the lubricant varies in the film thickness but also its density. Hence, the assumption that the latter is constant throughout the film thickness doesn't stand anymore and a new Reynolds' equation has to be introduced to account for these variations. This equation was developed by Yang and Wen [122]. It is derived in a similar way as the classical Reynolds' equation or the generalized one developed in chapters 2 and 4 respectively. In other words, the starting point is again the simplified Navier-Stokes equations reminded below:

$$\begin{aligned}
\frac{\partial p}{\partial x} &= \frac{\partial \tau_{zx}}{\partial z} \\
\frac{\partial p}{\partial y} &= \frac{\partial \tau_{zy}}{\partial z} \\
\frac{\partial p}{\partial z} &= 0
\end{aligned} \tag{5.1}$$

The shear stress components are replaced by their respective expressions:

$$\tau_{zx} = \eta \dot{\gamma}_{zx} = \eta \frac{\partial u_f}{\partial z} \quad \text{and} \quad \tau_{zy} = \eta \dot{\gamma}_{zy} = \eta \frac{\partial v_f}{\partial z} \tag{5.2}$$

The integration of the simplified Navier-Stokes equations twice with respect to z associated to the surface velocity no-slip boundary conditions ($u_f = u_p, v_f = w_f = 0$ at $z = z_p$ and $u_f = u_s, v_f = w_f = 0$ at $z = z_s$) gives the velocity field of the lubricant:

$$\begin{cases}
u_f = \dfrac{\partial p}{\partial x}\left(\displaystyle\int_0^z \frac{z}{\eta} dz - \frac{\eta_e}{\eta'_e} \int_0^z \frac{dz}{\eta} \right) + \eta_e \left(u_s - u_p\right) \displaystyle\int_0^z \frac{dz}{\eta} + u_p \\
v_f = \dfrac{\partial p}{\partial y}\left(\displaystyle\int_0^z \frac{z}{\eta} dz - \frac{\eta_e}{\eta'_e} \int_0^z \frac{dz}{\eta} \right)
\end{cases} \tag{5.3}$$

Note that, so far, the same equations are obtained as in the previous chapter for the isothermal case. This is because up to this point, only viscosity variations in the film thickness are considered. In fact, density variations interfere only in the mass continuity equation:

$$\frac{\partial m_x}{\partial x} + \frac{\partial m_y}{\partial y} = 0 \quad \text{with} \quad m_x = \int_0^h \rho u_f dz \quad \text{and} \quad m_y = \int_0^h \rho v_f dz \tag{5.4}$$

In this case, since density is no longer constant in the film thickness, it cannot be moved out of the integral and replacing the velocity field components in equation (5.4) by their expressions provided in equations (5.3) gives the Generalized Reynolds' equation of Yang and Wen:

$$\nabla \cdot \left(\varepsilon'' \nabla p \right) - \frac{\partial \rho^*}{\partial x} = 0 \tag{5.5}$$

Where:
$$\varepsilon'' = \frac{1}{u_m}\left(\frac{\rho}{\eta}\right)_e, \quad \left(\frac{\rho}{\eta}\right)_e = \frac{\eta_e \rho'_e}{\eta'_e} - \rho''_e, \quad \rho^* = \frac{\left[\rho'_e \eta_e \left(u_s - u_p\right) + \rho_e u_p\right]}{u_m}, \quad \rho_e = \int_0^h \rho \, dz$$
$$\rho'_e = \int_0^h \rho \int_0^z \frac{dz'}{\eta} dz, \quad \rho''_e = \int_0^h \rho \int_0^z \frac{z' dz'}{\eta} dz, \quad \frac{1}{\eta_e} = \int_0^h \frac{dz}{\eta}, \quad \frac{1}{\eta'_e} = \int_0^h \frac{z \, dz}{\eta}$$

Equation (5.5) is the most general form of Reynolds' equation. It is valid for both Newtonian and non-Newtonian lubricants (for a Newtonian lubricant the generalized Newtonian viscosity η is replaced by the Newtonian one μ). It takes into account the variations of both viscosity and density across the film thickness. In fact, the changes in density are due to temperature variations across the lubricant film whereas the changes in viscosity stem from both temperature and (when a generalized Newtonian lubricant is considered) shear rate variations across the film. Moreover, both density and viscosity are allowed to vary with pressure and temperature throughout the contact domain according to the relationships presented in chapter 2. Note that if the temperature in the lubricant film is assumed to be constant and equal to the ambient temperature ($T = T_0 = cst$) equation (5.5) reduces to the generalized Reynolds' equation (4.9), and furthermore, if the generalized Newtonian viscosity η is replaced by the Newtonian one μ, this equation reduces to the classical Reynolds' equation presented in chapter 2.

Using dimensionless variables, equation (5.5) can be written in the following dimensionless form:

$$\nabla \cdot \left(\overline{\varepsilon}'' \, \nabla P \right) - \frac{\partial \left(\overline{\rho}^* H \right)}{\partial X} = 0 \tag{5.6}$$

$$\overline{\varepsilon}'' = \left(\frac{\overline{\rho}}{\overline{\eta}} \right)_e \frac{H^3}{\lambda''} \qquad \left(\frac{\overline{\rho}}{\overline{\eta}} \right)_e = \frac{\overline{\eta}_e \overline{\rho}'_e}{\overline{\eta}'_e} - \overline{\rho}''_e \qquad \lambda'' = \frac{u_m R^2 \mu_R}{a^3 p_h}$$

Where:

$$\overline{\rho}^* = \frac{\left[\overline{\rho}'_e \overline{\eta}_e \left(u_s - u_p \right) + \overline{\rho}_e u_p \right]}{u_m} \qquad \overline{\rho}_e = \int_0^1 \overline{\rho} \, dZ$$

$$\overline{\rho}'_e = \int_0^1 \overline{\rho} \int_0^Z \frac{dZ'}{\overline{\eta}} dZ \qquad \overline{\rho}''_e = \int_0^1 \rho \int_0^Z \frac{Z' dZ'}{\overline{\eta}} dZ$$

$$\frac{1}{\overline{\eta}_e} = \int_0^1 \frac{dZ}{\overline{\eta}} \qquad \frac{1}{\overline{\eta}'_e} = \int_0^1 \frac{Z \, dZ}{\overline{\eta}}$$

Finally, let $\rho_0 = \overline{\rho}\left(P, T = T_0 \right)$ be the two dimensional function defined on the contact domain Ω_c and describing the density variations over the latter with respect to pressure considering a constant temperature $T = T_0$. Equation (5.6) can be written as follows:

$$\begin{aligned} R''\left(P \right) &= -\nabla \cdot \left(\overline{\varepsilon}'' \, \nabla P \right) + \frac{\partial \left[\rho_0 \left(\dfrac{\overline{\rho}^*}{\rho_0} \right) H \right]}{\partial X} = 0 \\ &= -\nabla \cdot \left(\overline{\varepsilon}'' \, \nabla P \right) + \left(\frac{\overline{\rho}^*}{\rho_0} \right) H \frac{\partial \rho_0}{\partial P} \frac{\partial P}{\partial X} + \rho_0 \frac{\partial \left[\left(\dfrac{\overline{\rho}^*}{\rho_0} \right) H \right]}{\partial X} = 0 \end{aligned} \tag{5.7}$$

Let: $\beta''_X = \left(\dfrac{\overline{\rho}^*}{\rho_0}\right) H \dfrac{\partial \rho_0}{\partial P}$ and $Q'' = -\rho_0 \dfrac{\partial \left[\left(\dfrac{\overline{\rho}^*}{\rho_0}\right) H\right]}{\partial X}$

Then eq. (5.7) becomes:

$$R''(P) = -\nabla \cdot \left(\overline{\varepsilon}'' \nabla P\right) + \beta'' \cdot \nabla P - Q'' = 0 \tag{5.8}$$

Hence, the generalized Reynolds' equation with thermal effects also has the form of a classical convection / diffusion equation (applied to *P*) with a source term Q''. The diffusion coefficient is $\overline{\varepsilon}''$ and the convection tensor is β''.

5.2 Thermal model

Temperature variations in the contact are modelled by applying the 3D energy equation to both the contacting elements and the lubricant film. This equation stems from the equilibrium of energy (conservation of heat fluxes) on an elemental volume (See Figure 5.1).

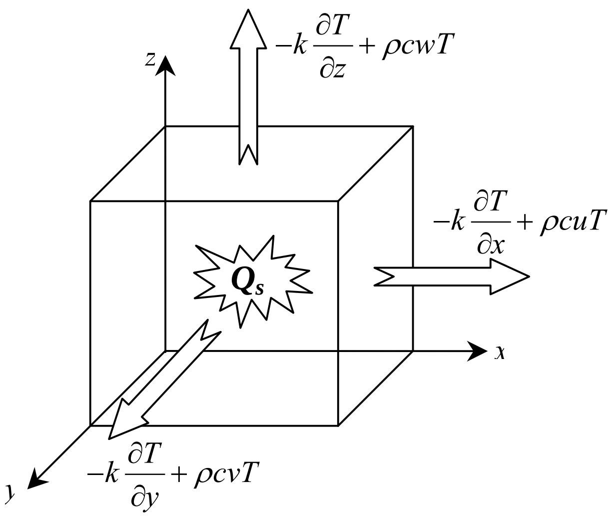

Figure 5.1: Equilibrium of heat fluxes on an elemental volume

Considering that heat transfer mainly occurs by conduction and convection (radiation is neglected), the heat balance applied to the elemental volume under steady-state regime gives:

$$-\frac{\partial}{\partial x}\left(k\frac{\partial T}{\partial x}\right) - \frac{\partial}{\partial y}\left(k\frac{\partial T}{\partial y}\right) - \frac{\partial}{\partial z}\left(k\frac{\partial T}{\partial z}\right) + \rho c\left(u\frac{\partial T}{\partial x} + v\frac{\partial T}{\partial y} + w\frac{\partial T}{\partial z}\right) = Q_s \tag{5.9}$$

Where *u*, *v*, and *w* are the velocity field components of the considered medium, *k* its thermal conductivity, *ρ* its density, *c* its heat capacity and Q_s a given heat source. Equation (5.9) is the general form of the energy equation under steady-state regime. In compact notation, this equation becomes:

$$-\nabla \cdot \left(k \nabla T\right) + \rho c \vec{U} . \nabla T - Q_s = 0 \tag{5.10}$$

Note that equation (5.10) has the form of the classical convection / diffusion equation as a function of T with a source term Q_s. When applied to the solid bodies s and p that have zero velocity components in the y and z-directions ($v_s = v_p = w_s = w_p = 0$) and zero heat source, equation (5.9) gives:

$$\begin{cases} -\dfrac{\partial}{\partial x}\left(k_p \dfrac{\partial T}{\partial x}\right) - \dfrac{\partial}{\partial y}\left(k_p \dfrac{\partial T}{\partial y}\right) - \dfrac{\partial}{\partial z}\left(k_p \dfrac{\partial T}{\partial z}\right) + \rho_p c_p u_p \left(\dfrac{\partial T}{\partial x}\right) = 0 & \text{(Solid } p\text{)} \\ -\dfrac{\partial}{\partial x}\left(k_s \dfrac{\partial T}{\partial x}\right) - \dfrac{\partial}{\partial y}\left(k_s \dfrac{\partial T}{\partial y}\right) - \dfrac{\partial}{\partial z}\left(k_s \dfrac{\partial T}{\partial z}\right) + \rho_s c_s u_s \left(\dfrac{\partial T}{\partial x}\right) = 0 & \text{(Solid } s\text{)} \end{cases} \tag{5.11}$$

Finally, when applied to the lubricant film, equation (5.9) gives:

$$-\frac{\partial}{\partial x}\left(k \frac{\partial T}{\partial x}\right) - \frac{\partial}{\partial y}\left(k \frac{\partial T}{\partial y}\right) - \frac{\partial}{\partial z}\left(k \frac{\partial T}{\partial z}\right) + \rho c \left(u_f \frac{\partial T}{\partial x} + v_f \frac{\partial T}{\partial y} + w_f \frac{\partial T}{\partial z}\right) = Q_s \tag{5.12}$$

Where k is the lubricant's thermal conductivity and c its heat capacity. As mentioned earlier, two heat sources are present in the lubricant film: the compression of the fluid and its shear. These heat sources are described by the following mathematical expressions:

$$Q_{comp} = -\frac{T}{\rho}\frac{\partial \rho}{\partial T}\left(u_f \frac{\partial p}{\partial x} + v_f \frac{\partial p}{\partial y}\right) \quad \text{and} \quad Q_{shear} = \eta \left[\left(\frac{\partial u_f}{\partial z}\right)^2 + \left(\frac{\partial v_f}{\partial z}\right)^2\right] \tag{5.13}$$

Many authors such as, for example, Lin et al. [79], Kim et al. [74], Guo et al. [43] and Cheng [17] show that heat convection in the film thickness and conduction in the film plane can be neglected compared to the convection in the film plane and conduction in the film thickness respectively. This is a consequence of the relatively small dimension of the lubricant film in the thickness direction (z) compared to the other two directions (x and y). Hence, equation (5.12) reduces to:

$$-\frac{\partial}{\partial z}\left(k \frac{\partial T}{\partial z}\right) + \rho c \left(u_f \frac{\partial T}{\partial x} + v_f \frac{\partial T}{\partial y}\right) = Q_{comp} + Q_{shear} \tag{5.14}$$

The geometrical domains of solids p and s are taken as infinite layers with a finite thickness d sufficiently large to have a zero temperature gradient in the medium's depth. The origin of the global coordinates system is located at the centre of the Hertzian contact area on the plane's surface. The energy equations for the solids s and p are associated to the following boundary conditions:

$$T(x_{in}, y, z) = T_0, \quad T(x, y, -d) = T_0, \quad T(x, y, h+d) = T_0 \tag{5.15}$$

At the outlet boundaries, no boundary condition is required for the hyperbolic energy equations of solids s and p. Similarly, equation (5.14) requires a boundary condition in the inlet where $u_f \geq 0$ while for negative values of u_f the boundary condition is unnecessary:

$$T(x_{in}, y, z) = T_0 \quad \text{if} \quad u_f(x_{in}, y, z) \geq 0 \tag{5.16}$$

On the two lubricant-solid interfaces, heat flux continuity boundary conditions must be satisfied to ensure an energetic equilibrium of the system:

$$\begin{cases} k\left.\dfrac{\partial T}{\partial z}\right|_{z=0^+} = k_p\left.\dfrac{\partial T}{\partial z}\right|_{z=0^-} \\ k\left.\dfrac{\partial T}{\partial z}\right|_{z=h^-} = k_s\left.\dfrac{\partial T}{\partial z}\right|_{z=h^+} \end{cases} \tag{5.17}$$

Again, for practical reasons, all these equations are written and solved in their dimensionless form obtained using the dimensionless variables provided previously along with new ones defined as:

$$\overline{T} = \frac{T}{T_0},\quad D = \frac{d}{a} \quad \text{and} \quad Z = \begin{cases} z/h & \text{in the lubricant domain} \\ z/a & \text{in the solid bodies' domains} \end{cases} \tag{5.18}$$

Thus, the dimensionless energy equations for solids s and p and the lubricant film are:

$$\begin{cases} -\dfrac{\partial}{\partial X}\left(\dfrac{k_p}{a}\dfrac{\partial \overline{T}}{\partial X}\right) - \dfrac{\partial}{\partial Y}\left(\dfrac{k_p}{a}\dfrac{\partial \overline{T}}{\partial Y}\right) - \dfrac{\partial}{\partial Z}\left(\dfrac{k_p}{a}\dfrac{\partial \overline{T}}{\partial Z}\right) + \rho_p c_p u_p\left(\dfrac{\partial \overline{T}}{\partial X}\right) = 0 & \text{(Solid } p\text{)} \\ -\dfrac{\partial}{\partial X}\left(\dfrac{k_s}{a}\dfrac{\partial \overline{T}}{\partial X}\right) - \dfrac{\partial}{\partial Y}\left(\dfrac{k_s}{a}\dfrac{\partial \overline{T}}{\partial Y}\right) - \dfrac{\partial}{\partial Z}\left(\dfrac{k_s}{a}\dfrac{\partial \overline{T}}{\partial Z}\right) + \rho_s c_s u_s\left(\dfrac{\partial \overline{T}}{\partial X}\right) = 0 & \text{(Solid } s\text{)} \\ -\dfrac{\partial}{\partial Z}\left(\dfrac{kR^2T_0}{H^2a^3}\dfrac{\partial \overline{T}}{\partial Z}\right) + \rho_R\overline{\rho}\, cT_0\left(u_f\dfrac{\partial \overline{T}}{\partial X} + v_f\dfrac{\partial \overline{T}}{\partial Y}\right) = & \\ \qquad -\dfrac{\overline{T}}{\overline{\rho}}\dfrac{\partial \overline{\rho}}{\partial \overline{T}} p_h\left(u_f\dfrac{\partial P}{\partial X} + v_f\dfrac{\partial P}{\partial Y}\right) + \dfrac{\overline{\eta}\mu_R R^2}{H^2a^3}\left[\left(\dfrac{\partial u_f}{\partial Z}\right)^2 + \left(\dfrac{\partial v_f}{\partial Z}\right)^2\right] & \text{(Lubricant film)} \end{cases} \tag{5.19}$$

In compact notation, the previous system of equations becomes:

$$\begin{cases} -\nabla\cdot\left(\dfrac{k_p}{a}\nabla\overline{T}\right) + \rho_p c_p \vec{U}_p\cdot\nabla\overline{T} = 0 & \text{(Solid } p\text{)} \\ -\nabla\cdot\left(\dfrac{k_s}{a}\nabla\overline{T}\right) + \rho_s c_s \vec{U}_s\cdot\nabla\overline{T} = 0 & \text{(Solid } s\text{)} \\ -\nabla\cdot\left(\vec{k}\cdot\nabla\overline{T}\right) + \rho_R\overline{\rho}\, cT_0\vec{U}_f\cdot\nabla\overline{T} = \overline{Q}_{comp} + \overline{Q}_{shear} & \text{(Lubricant film)} \end{cases} \tag{5.20}$$

Where:

$$\vec{U}_p = \{u_p \quad 0 \quad 0\},\quad \vec{U}_s = \{u_s \quad 0 \quad 0\},\quad \vec{U}_f = \{u_f \quad v_f \quad 0\}$$

$$\vec{k} = \begin{bmatrix} 0 & 0 & 0 \\ 0 & 0 & 0 \\ 0 & 0 & kR^2T_0/H^2a^3 \end{bmatrix}$$

$$\bar{Q}_{comp} = -\frac{\bar{T}}{\bar{\rho}}\frac{\partial \bar{\rho}}{\partial \bar{T}} p_h \left(u_f \frac{\partial P}{\partial X} + v_f \frac{\partial P}{\partial Y} \right) \quad \text{and} \quad \bar{Q}_{shear} = \frac{\bar{\eta}\mu_R R^2}{H^2 a^3}\left[\left(\frac{\partial u_f}{\partial Z} \right)^2 + \left(\frac{\partial v_f}{\partial Z} \right)^2 \right]$$

In dimensionless form, the corresponding boundary conditions become:

$$\begin{cases} \bar{T}\left(X_{in},Y,Z\right)=1, \quad \bar{T}\left(X,Y,-D\right)=1, \quad \bar{T}\left(X,Y,1+D\right)=1 & \text{(Solids } s \text{ and } p\text{)} \\ \bar{T}\left(X_{in},Y,Z\right)=1 \quad \text{if} \quad u_f\left(X_{in},Y,Z\right)\geq 0 & \text{(Lubricant film)} \end{cases} \tag{5.21}$$

Finally, the heat flux continuity equations on the two solid-lubricant interfaces become:

$$\begin{cases} \left.\dfrac{kR}{Ha}\dfrac{\partial \bar{T}}{\partial Z}\right|_{Z=0^+} = k_p \left.\dfrac{\partial \bar{T}}{\partial Z}\right|_{Z=0^-} \\ \left.\dfrac{kR}{Ha}\dfrac{\partial \bar{T}}{\partial Z}\right|_{Z=1^-} = k_s \left.\dfrac{\partial \bar{T}}{\partial Z}\right|_{Z=1^+} \end{cases} \tag{5.22}$$

The systems of equations (5.19), (5.21) and (5.22) completely describe the temperature variations in the contacting elements and the lubricant film. This problem is also symmetric with respect to the *XZ*-plane and this symmetry is taken into account in order to reduce its size. This implies adding a symmetry boundary condition on the symmetry plane given by:

$$\begin{cases} -\dfrac{k_p}{a}\nabla\bar{T}\cdot\vec{n} + \rho_p c \vec{U}_p \bar{T}\cdot\vec{n} = 0 & \text{(Solid } p\text{)} \\ -\dfrac{k_s}{a}\nabla\bar{T}\cdot\vec{n} + \rho_s c \vec{U}_s \bar{T}\cdot\vec{n} = 0 & \text{(Solid } s\text{)} \\ -k\left\{ \dfrac{1}{a}\dfrac{\partial \bar{T}}{\partial X} \quad \dfrac{1}{a}\dfrac{\partial \bar{T}}{\partial Y} \quad \dfrac{R}{Ha^2}\dfrac{\partial \bar{T}}{\partial Z} \right\}\cdot\vec{n} + \bar{\rho}\rho_R c \vec{U}_f \bar{T}\cdot\vec{n} = 0 & \text{(Lubricant film)} \end{cases} \tag{5.23}$$

Taking into consideration that the normal vector to the symmetry plane $\vec{n} = \{0 \quad 1 \quad 0\}$ and that $v_s = w_s = v_p = w_p = w_f = 0$ and that v_f is also zero on the *XZ*-plane, the system of equations (5.23) reduces to:

$$\begin{cases} -\dfrac{k_p}{a}\dfrac{\partial \bar{T}}{\partial Y} = 0 & \text{(Solid } p\text{)} \\ -\dfrac{k_s}{a}\dfrac{\partial \bar{T}}{\partial Y} = 0 & \text{(Solid } s\text{)} \\ -\dfrac{k}{a}\dfrac{\partial \bar{T}}{\partial Y} = 0 & \text{(Lubricant film)} \end{cases} \tag{5.24}$$

The set of differential equations describing temperature variations in the contact associated to the set of boundary conditions provided above are solved using a finite element approximation of the temperature field. The finite element procedure is described in details in the following section.

Remark: The thermal expansion of the solid bodies *p* and *s* is neglected in the current analysis.

5.3 Finite element procedure

In this section, the finite element procedure for both the EHL and thermal models is described:

5.3.1 EHL model

The system of EHL equations formed by the generalized Reynolds' equation with thermal effects, the linear elasticity and the load balance equations is solved using a similar Newton-Raphson approach as described in chapter 3 (See section 3.5). The finite element formulations for this system are not reminded here. Those are similar to the ones provided in chapter 3 since the generalized Reynolds' equation with thermal effects also has the form of a convection / diffusion equation. The free boundary problem is treated by applying a penalty method and for heavy loads, the solution of the generalized Reynolds' equation with thermal effects exhibits similar instability features as described in chapters 3 and 4. The same stabilization techniques are used to avoid them (based on a convection / diffusion form of Reynolds' equation). This can be seen in Figure 5.2 where a test case is carried out for a steel on glass circular contact lubricated by Squalane + PIP with surface velocities of 1m/s for both surfaces and a load of 1000N which corresponds to a maximum Hertzian pressure of 1.66 GPa. Note that, in practice, this case can never be realized on an experimental apparatus because glass would not withstand such a load. The Tait-Doolittle free volume model is used to express the density and viscosity dependence on pressure and temperature. The lubricant's properties are given in Table 5.1, it has an equivalent pressure-viscosity coefficient of 18.53 GPa^{-1}.

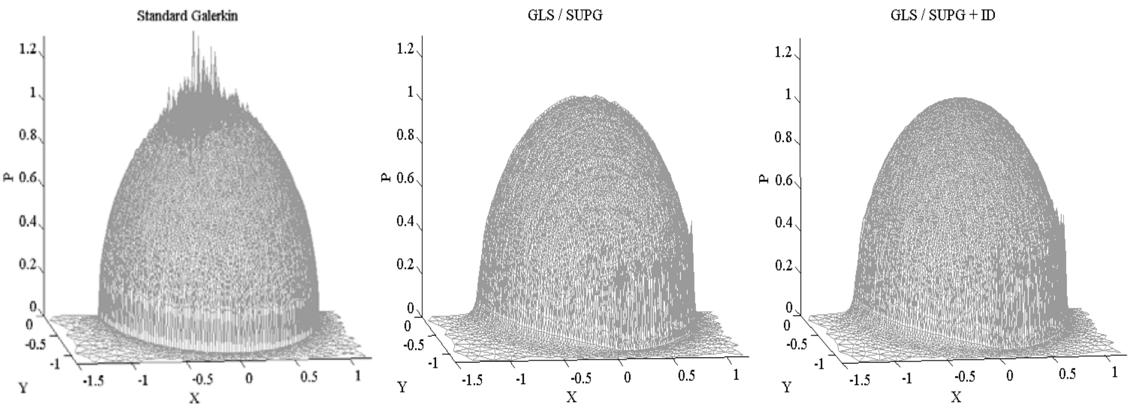

Figure 5.2: Stabilization effects on circular thermal EHD contacts (M=1718, L=7, p_h=1.66 GPa)

The stabilized formulations will not be reminded in this section, these are the same as those provided in chapter 3 and for more details the reader is referred to section 3.4.3. Again, it is clear that a standard Galerkin formulation leads to an oscillatory behaviour of the solution. Applying GLS or SUPG formulations reduces the amplitude of these oscillations without completely smoothing them out. And finally, adding the ID terms to the GLS or SUPG formulations completely smoothes out the remaining oscillations.

5.3.2 Thermal model

In section 5.2, it was mentioned that the geometrical domains of solids *p* and *s* correspond to infinite layers with a finite thickness sufficiently large to have a zero temperature gradient at the depth *D*. In practice, the geometrical domain of the lubricant film extends like for solids *p* and *s* from $-4.5 \le X \le 1.5$ and $-3 \le Y \le 0$ while its height $Z \in [0,1]$ (See Figure 5.3). The height of solids *p* and *s* is *D*. Kaneta et al. [70] and Wang et al. [118] suggest that, in most cases, a depth *D* of 3.15 is enough to ensure a zero temperature gradient in the regions far from the contact surface.

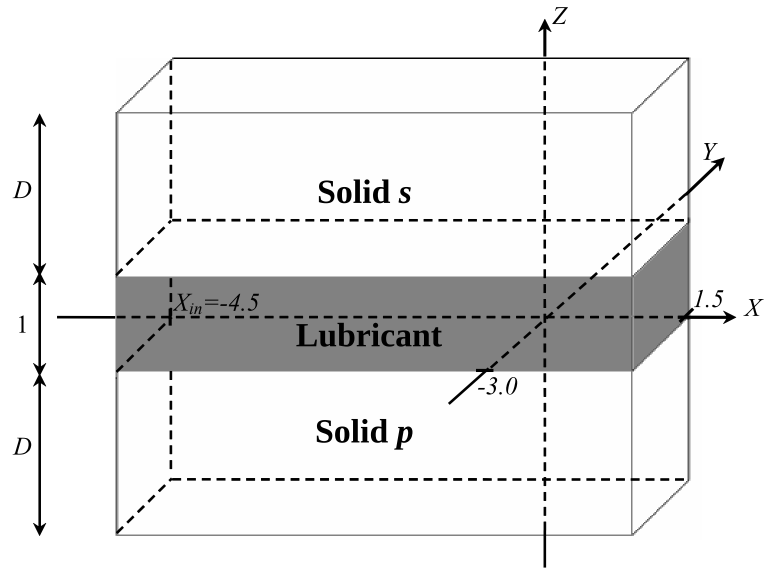

Figure 5.3: Geometrical domain for the thermal problem

Let $\Omega = \{\Omega_s \cup \Omega_p \cup \Omega_f\}$ be the geometrical domain of the thermal problem defined by the assembly of the geometrical domains of solids *s* and *p* and the lubricant film with an external boundary $\partial\Omega = \{\partial\Omega_s \cup \partial\Omega_p \cup \partial\Omega_f - \partial\Omega_{fs} - \partial\Omega_{fp}\}$. $\partial\Omega_{fs}$ and $\partial\Omega_{fp}$ are the interface boundaries between the lubricant film and solids *s* and *p* respectively. The Galerkin formulation of the system of equations (5.20) is given by:

Find $\overline{T} \in S_{\overline{T}}$ such that $\forall W_{\overline{T}} \in S_{\overline{T}}$, one has:

$$\begin{cases} \int\limits_{\Omega_p} \frac{k_p}{a} \nabla \overline{T} \cdot \nabla W_{\overline{T}} d\Omega - \int\limits_{\Omega_p} \rho_p c_p \overline{T} \vec{\overline{U}}_p \cdot \nabla W_{\overline{T}} d\Omega + \int\limits_{\partial\Omega_p} \left(-\frac{k_p}{a} \nabla \overline{T} + \rho_p c_p \overline{T} \vec{\overline{U}}_p \right) \cdot \vec{n} \; W_{\overline{T}} d\Omega = 0 \\ \int\limits_{\Omega s} \frac{k_s}{a} \nabla \overline{T} \cdot \nabla W_{\overline{T}} d\Omega - \int\limits_{\Omega s} \rho_s c_s \overline{T} \vec{\overline{U}}_s \cdot \nabla W_{\overline{T}} d\Omega + \int\limits_{\partial\Omega_s} \left(-\frac{k_s}{a} \nabla \overline{T} + \rho_s c_s \overline{T} \vec{\overline{U}}_s \right) \cdot \vec{n} \; W_{\overline{T}} d\Omega = 0 \\ \int\limits_{\Omega_f} \left(\vec{\overline{k}} \cdot \nabla \overline{T} \right) \cdot \nabla W_{\overline{T}} d\Omega + \int\limits_{\Omega_f} \rho_R \overline{\rho} c T_0 \overline{T} \vec{\overline{U}}_f \cdot \nabla W_{\overline{T}} d\Omega \\ \qquad + \int\limits_{\partial\Omega_f} \left(-\vec{\overline{k}} \cdot \nabla \overline{T} + \rho_R \overline{\rho} c T_0 \overline{T} \vec{\overline{U}}_f \right) \cdot \vec{n} \; W_{\overline{T}} d\Omega = \int\limits_{\Omega_f} \left(\overline{Q}_{comp} + \overline{Q}_{shear} \right) W_{\overline{T}} d\Omega \end{cases} \tag{5.25}$$

Where: $S_{\overline{T}} = \left\{ \overline{T} \in H^1(\Omega) \;/\; \overline{T} = 1 \text{ on the inlet boundaries of } \Omega \right\}$

In practice, these equations are solved in their discrete form. Consider $\Omega^h = \left\{\Omega_1, \, ... \, , \Omega_{n_e}\right\} = \Omega_{pe} \cup \Omega_{se} \cup \Omega_{fe}$ a finite element partition of Ω (See Figure 5.4) such that: $\overline{\Omega} = \cup_{e=1}^{n_e} \overline{\Omega}_e$, $\overline{\Omega} = \Omega \cup \partial\Omega$, $\overline{\Omega}_e = \Omega_e \cup \partial\Omega_e$ and $\Omega_e \cap \Omega_{e'} = \phi$ if $e \neq e'$. n_e denotes the total number of elements in the partition such that $n_e = n_e^p + n_e^s + n_e^f$ while $\partial\Omega$ and $\partial\Omega_e$ denote respectively the boundaries of the domain Ω and the element Ω_e. Unstructured non-regular tetrahedral meshing is employed with a fine mesh only where required. Let $S_{\overline{T}}^h \subset S_{\overline{T}}$ such that the discrete function $\overline{T}^h$ defining this space has the same characteristics as its analytical equivalent $\overline{T}$ with the only difference that $\overline{T}^h \in L^l$ where L^l is the set of interpolation polynomials of degree l defined within each element Ω_e. The discrete functions $\overline{T}^{h^{(e)}}$ of $\overline{T}$ and $W_{\overline{T}}^{h^{(e)}}$ of $W_{\overline{T}}$ within an element *e* are expressed by:

$$\overline{T}^{h^{(e)}} = \sum_{i=1}^{n_{\overline{T}}} \overline{T}_i^{(e)} N_{\overline{T}i} \text{ and } W_{\overline{T}}^{h^{(e)}} = \sum_{i=1}^{n_{\overline{T}}} W_{\overline{T}i}^{(e)} N_{\overline{T}i} \tag{5.26}$$

Where $\overline{T}_i^{(e)}$ and $W_{\overline{T}i}^{(e)}$ are the nodal values of $\overline{T}$ and $W_{\overline{T}}$ respectively, associated to the interpolation functions $N_{\overline{T}i}$ within the element *e*. $n_{\overline{T}}$ being the number of degrees of freedom for temperature in the element *e*.

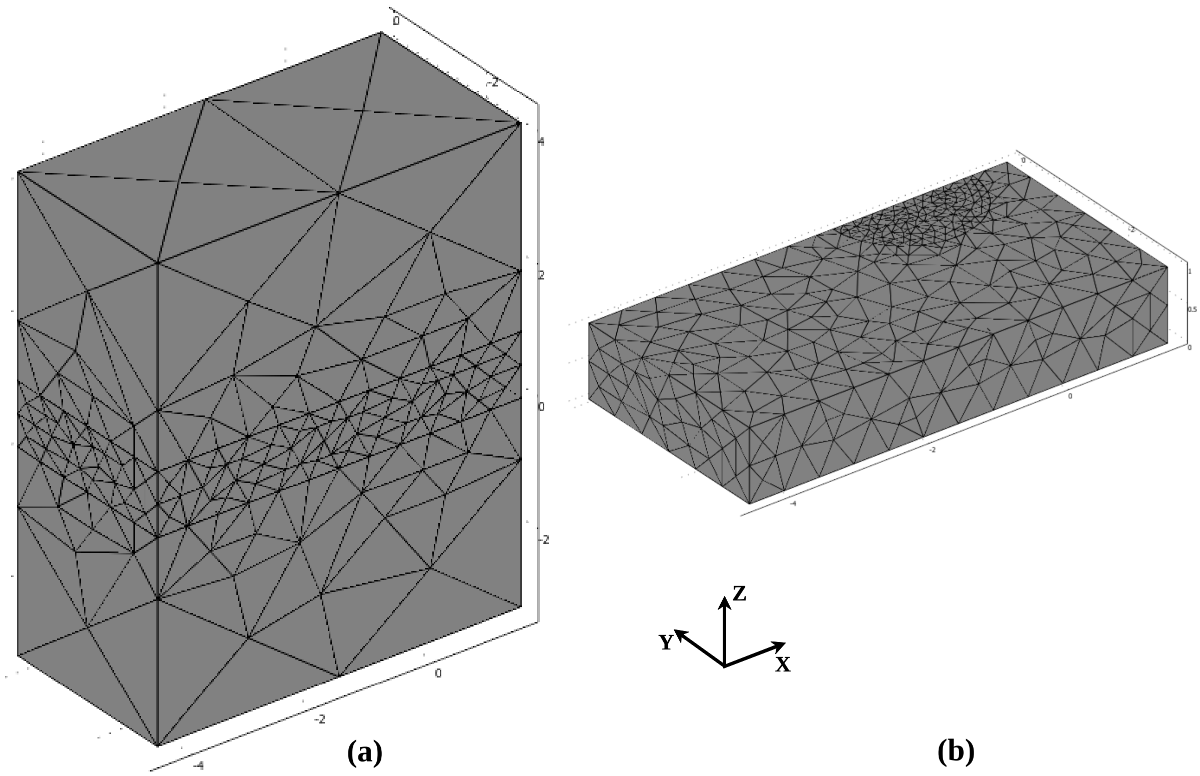

(a) (b)

Figure 5.4: Meshing of the thermal problem's geometry (a) solid bodies and lubricant film (b) lubricant film

The discrete form of the system of equations (5.25) is obtained by replacing the field variable $\overline{T}$ and the weighting function $W_{\overline{T}}$ by their discrete equivalents $\overline{T}^h$ and $W_{\overline{T}}^h$:

Find $\overline{T}^h \in S_{\overline{T}}^h$ such that $\forall W_{\overline{T}}^h \in S_{\overline{T}}^h$, one has:

$$\begin{cases} \int\limits_{\Omega_{pe}^h} \frac{k_p}{a} \nabla \overline{T}^h \cdot \nabla W_{\overline{T}}^h d\Omega - \int\limits_{\Omega_{pe}^h} \rho_p c_p \overline{T}^h \vec{U}_p \cdot \nabla W_{\overline{T}}^h d\Omega \\ \qquad + \int\limits_{\partial\Omega_{pe}^h} \left(-\frac{k_p}{a} \nabla \overline{T}^h + \rho_p c_p \overline{T}^h \vec{U}_p \right) \cdot \vec{n} \; W_{\overline{T}}^h d\Omega = 0 \\ \int\limits_{\Omega_{se}^h} \frac{k_s}{a} \nabla \overline{T}^h \cdot \nabla W_{\overline{T}}^h d\Omega - \int\limits_{\Omega_{se}^h} \rho_s c_s \overline{T}^h \vec{U}_s \cdot \nabla W_{\overline{T}}^h d\Omega \\ \qquad + \int\limits_{\partial\Omega_{se}^h} \left(-\frac{k_s}{a} \nabla \overline{T}^h + \rho_s c_s \overline{T}^h \vec{U}_s \right) \cdot \vec{n} \; W_{\overline{T}}^h d\Omega = 0 \\ \int\limits_{\Omega_{fe}^h} \left(\vec{k} \cdot \nabla \overline{T}^h \right) \cdot \nabla W_{\overline{T}}^h d\Omega + \int\limits_{\Omega_{fe}^h} \rho_R \overline{\rho} c T_0 \overline{T}^h \vec{U}_f \cdot \nabla W_{\overline{T}}^h d\Omega \\ \qquad + \int\limits_{\partial\Omega_{fe}^h} \left(-\vec{k} \cdot \nabla \overline{T}^h + \rho_R \overline{\rho} c T_0 \overline{T}^h \vec{U}_f \right) \cdot \vec{n} \; W_{\overline{T}}^h d\Omega = \int\limits_{\Omega_{fe}^h} \left(\overline{Q}_{comp} + \overline{Q}_{shear} \right) W_{\overline{T}}^h d\Omega \end{cases} \tag{5.27}$$

Note that the boundary integrals at the interior elements cancel out with each other and only the exterior boundary integrals remain. These are replaced (where needed) by their corresponding expressions given by the boundary conditions. The unknowns of the previous system of equations are the nodal values $\overline{T}_i$ of the temperature field. The solution of the thermal problem exhibits instability features at high Peclet numbers. This may occur for example at high speed operating conditions as shown in Figure 5.5. The latter shows a typical example of a temperature distribution through the contacting solids and the lubricant film on the central line of the contact in the z-direction obtained for a contact operating at high speeds. It corresponds to a circular glass on steel contact, lubricated with Squalane + PIP with a load of 23 N and surface velocities $u_p = 5$ m/s and $u_s = 15$ m/s .

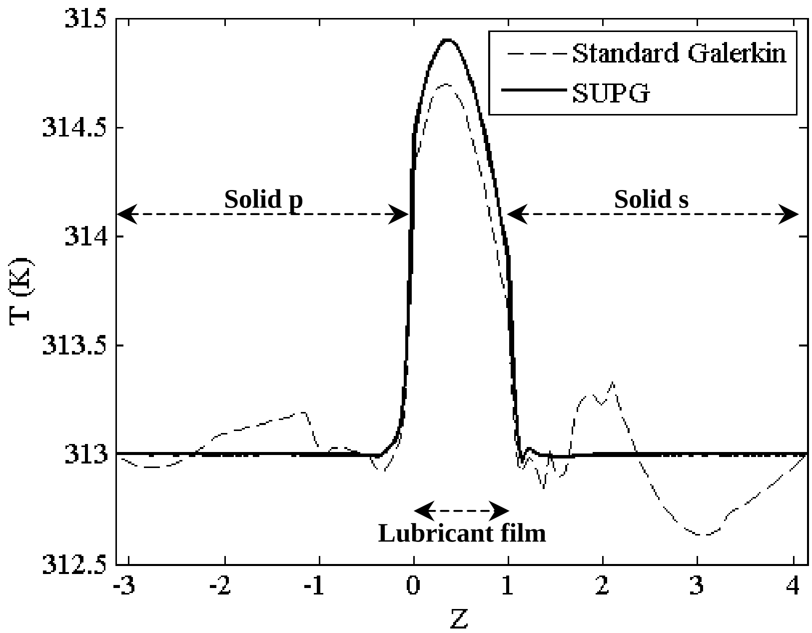

Figure 5.5: Stabilization effects on the solution of the energy equations applied to the contacting elements and lubricant film of an EHD circular contact

The standard Galerkin formulation leads to a spurious behaviour of the solution whereas the SUPG formulation completely smoothes out the oscillations. In this case, no additional ID terms are required. The SUPG formulation is the same as described in chapter 3. For more details, the reader is referred to section 3.4.3.

5.4 Global numerical procedure

The global numerical procedure for thermal EHL (TEHL) modelling is much more complex than for the isothermal case. The starting point consists in defining initial values for P, U, H_0, T and τ_e. The initial values for the pressure profile P and the elastic deflection profile U correspond to those of a dry / Hertzian contact or a suitable previously stored solution. The equivalent shear stress τ_e in the lubricant film is computed using the analytical formulas of eqs. (5.2) where the equivalent shear rates are replaced by their analytical expressions obtained by deriving the lubricant's velocity field components with respect to z and the generalized Newtonian viscosity by its expression given in (4.3). As for the initial value of τ_e, it is obtained by assuming the lubricant is Newtonian and using the initial values of P, U, T and H_0. The initial temperature field is taken to be constant and equal to the ambient temperature T_0 throughout the contacting solids and the lubricant film.

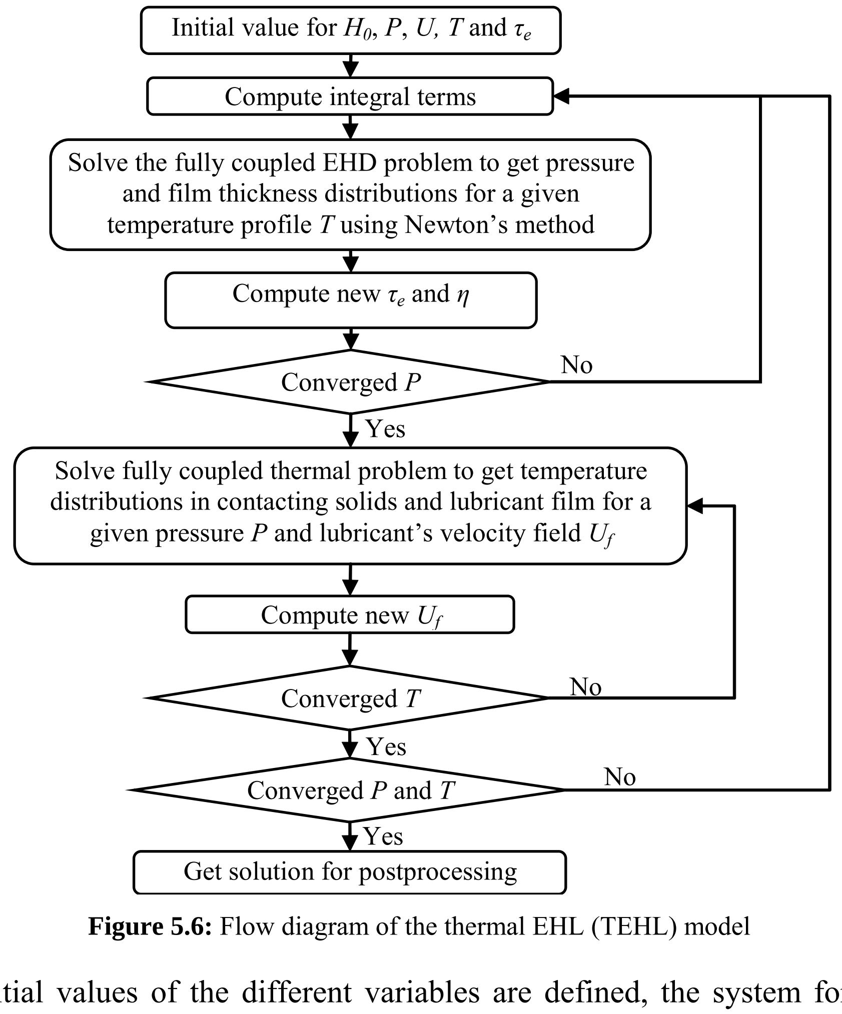

Figure 5.6: Flow diagram of the thermal EHL (TEHL) model

After the initial values of the different variables are defined, the system formed by the generalized Reynolds' equation with thermal effects, the linear elasticity and the load balance equations is solved using a Newton-Raphson procedure. At every Newton resolution, the integral terms in the generalized Reynolds' equation with thermal effects are computed using the solution of the previous resolution (the cross film integration process is similar to that described in section 4.4). Thus an iterative procedure is introduced. It is repeated until the convergence of the solution is obtained i.e. in this case, until the maximum absolute difference between the pressure solutions at two consecutive resolutions falls below 10^{-3}. Then, the system formed by the energy equations of the contacting elements and the lubricant film is solved. The three equations are solved simultaneously for a given pressure profile P and lubricant's velocity field $\vec{U}_f$. The latter is computed for a given viscosity distribution obtained using the last pressure and temperature solutions. Thus, an iterative procedure is established. The new value of the lubricant's velocity field is computed using the new pressure and temperature distributions. The latter is then injected in the energy equations for a new resolution. This is repeated until the convergence of the temperature solution is obtained i.e. in this case, until the maximum relative difference between the temperature solutions at two consecutive iterations falls below 10^{-3}.

Finally, since the temperature solution is obtained for a given pressure distribution and vice versa, a final test is realized to check that the effects of the variations of any of the two solutions on the other one has become negligible i.e. to ensure the convergence of the global algorithm with respect to the coupling procedure. The same convergence criteria as listed above are employed.

The global numerical procedure is described in the flow chart of Figure 5.6. More computational efforts and consequently cpu time are required than for an isothermal approach. In fact, for a typical case, the calculations may take "roughly" between 30 to 60 minutes on a personal computer with a 2 GHz processor.

5.5 Exploration and validation of the model

In this section, a series of test cases under both isothermal and thermal conditions was carried out in order to validate the current approach and reveal the importance of thermal effects on both Newtonian and non-Newtonian lubricated contacts. The Newtonian case is briefly discussed whereas more attention is given to the non-Newtonian case where several results are developed and analyzed. The results are compared with experimental data which allows the validation of both the numerical and rheological models. Isothermal results are obtained using the procedures presented in chapters 3 and 4.

5.5.1 Newtonian lubricant

First, we shall deal with the case of a liquid with a high Newtonian limit, owing to a low (92 Kg/Kmol) molecular weight: Glycerol. This liquid is not expected to shear-thin in the inlet region of the contact [3]. The rheological properties and operating conditions for this fluid are given in Table 5.1. The rheological properties have been derived from [10] and [20] whereas the thermal properties can be found in [78]. Both viscosity and density of Glycerol have relatively low pressure dependence. Therefore, the simple Cheng equation is appropriate to define the viscosity-pressure-temperature relationship. As for the density-pressure-temperature dependence, the Tait equation of state is used.

Both isothermal and thermal results were obtained for pure rolling and rolling-sliding conditions for a contact between a steel ball and a glass plane. For the pure rolling case the mean entrainment velocity covers the range of 0.3 to 4.75 m/s while for the rolling-sliding conditions it keeps a constant value of 0.38 m/s with a slide-to-roll ratio varying from 0 to 1.8. This case was deliberately chosen to correspond to a lightly loaded contact (p_h=0.5 GPa) in order to show that thermal effects are not restricted to highly loaded contacts and high speeds and sliding velocities. These can have a relative importance even for lightly loaded contacts with moderate speed conditions.

Lubricant properties		Material properties		Operating conditions
μ_R=0.2803 Pa.s	c=2400 J/Kg.K	ρ_p=2510 Kg/m^3	ρ_s=7850 Kg/m^3	T_0=T_R=313 K
α_{ch}=5.4 GPa^{-1}	K_{0R}=12.43 GPa	k_p=1.114 W/m.K	k_s=46 W/m.K	R=12.7 mm
β_{ch}=7468.75 K	β_K=0.0035 K^{-1}	c_p=858 J/Kg.K	c_s=470 J/Kg.K	F=30 N
γ_{ch}=0 GPa^{-1}.K	K'_{0R}=4.5432	E_p=81 GPa	E_s=210 GPa	p_h=0.5 GPa
ρ_R=1260 Kg/m^3	β'_K=0.0018 K^{-1}	υ_p=0.208	υ_s=0.3	
k=0.29 W/m.K	a_v=5.2x10^{-4} °C^{-1}			

Table 5.1: Lubricant properties and operating conditions for the Newtonian test cases

Figure 5.7 shows the central and minimum film thickness curves as a function of the mean entrainment velocity under pure rolling conditions. Note that, in this case, isothermal and thermal results are almost the same up to 1 m/s. Beyond this speed, the two solutions diverge from each other due to thermal effects which become important at high speeds, even under pure rolling regime. Also note the good agreement between the numerical results and experimental data. At low speed (here, less than 1 m/s), both isothermal and thermal results show a very good agreement with the experimental results, while at high speed, the isothermal results show some discrepancy with experiments. On the other hand, thermal results are in good agreement with experimental ones under any operating conditions. Finally, note the change in the slope of the thermal film thickness curves beyond the speed limit of 1 m/s. This is characteristic of the appearance of thermal thinning.

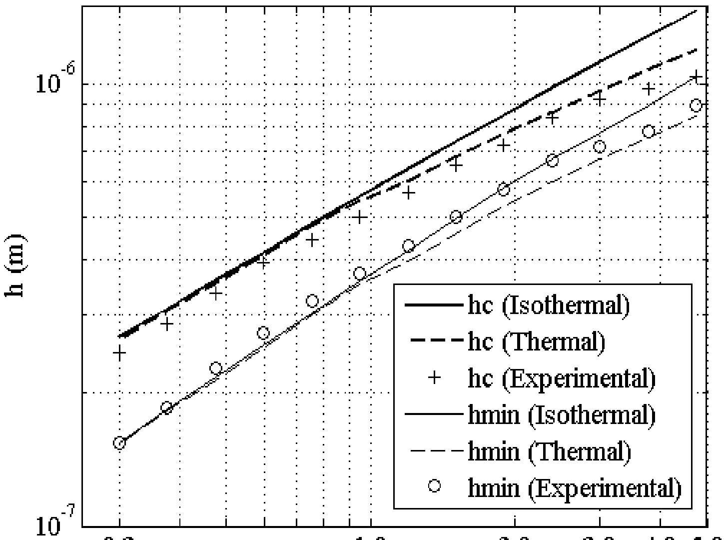

Figure 5.7: Film thickness as a function of the mean entrainment velocity for the Glycerol case under pure rolling conditions (p_h=0.5 GPa)

Figure 5.8 shows the central and minimum film thickness curves for a constant mean entrainment velocity ($u_m = 0.38$ m/s) as a function of the slide-to-roll ratio. An isothermal approach predicts a constant film thickness with respect to the SRR. This is to be expected since the classical Reynolds equation depends only, in terms of velocities, on the mean entrainment speed. On the other hand, a thermal approach shows a clear decrease in the film thickness when the SRR increases. This is because when the sliding velocity becomes important, shear heating acts on reducing the viscosity of the lubricant which leads to a decrease in the film thickness. This is observed in both thermal and experimental results which exhibit a better agreement compared to isothermal and experimental ones.

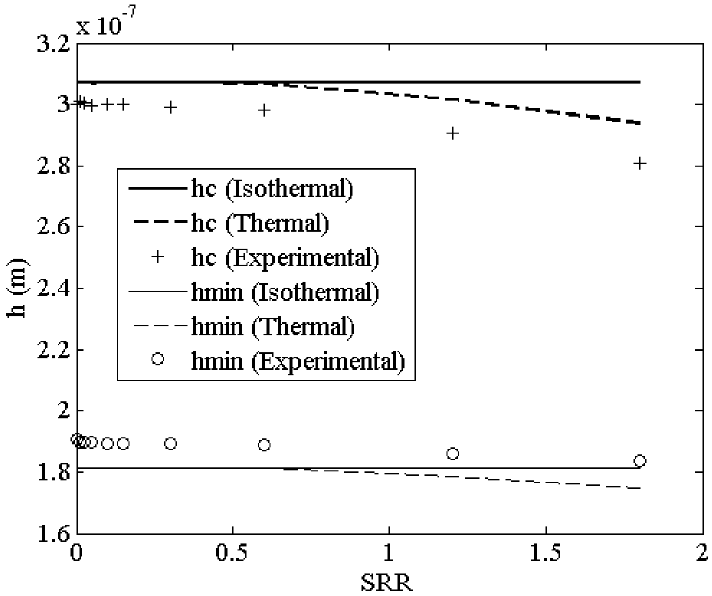

Figure 5.8: Film thickness as a function of the slide-to-roll ratio for the Glycerol case with a constant mean entrainment velocity (u_m=0.38 m/s, p_h=0.5 GPa, M=36.8 and L=2.3)

Finally, note that the "slight" remaining differences between experimental and numerical results may be due (in part) to two different phenomena: first, the proper thermal signature of the experimental apparatus which depends on the design and environment of the latter and second, Glycerol has a high water absorption potential from the surrounding ambient air which may cause its viscosity to vary with room humidity both during viscosity and film thickness measurements.

5.5.2 Non-Newtonian lubricant

For the non-Newtonian case, the Squalane + PIP mixture is used again under the same operating conditions of the previous chapter. This allows the separation of thermal effects from non-Newtonian ones since both often have the same consequences. This separation is impossible to obtain experimentally since both phenomena are intimately related. However, numerically, non-Newtonian effects can be isolated by simply studying the isothermal case and thermal effects can be extracted by comparing the thermal solution to the isothermal one.

Lubricant properties		Material properties	Operating conditions
$\mu_{1,R}$=0.0705 Pa.s	a_v=7.52x10^{-4} °C^{-1}	ρ_p=2510 Kg/m^3	T_R=T_0=313 K
$\mu_{2,R}$=0.0157 Pa.s	K'_{0R}=11.29	k_p=1.114 W/m.K	R=12.7 mm
G_c=0.01 MPa	β'_K=0 K^{-1}	c_p=858 J/Kg.K	F=23 N
n_c=0.8	K_{0R}=8.375 GPa	E_p=81 GPa	p_h=0.47 GPa
β_c=2.198	β_K=0.006765 K^{-1}	υ_p=0.208	
B=4.2	ρ_R=818 Kg/m^3	ρ_s=7850 Kg/m^3	
R_0=0.658	k=0.13 W/m.K	k_s=46 W/m.K	
ε_c=-9.599x10^{-4} °C^{-1}	c=1700 J/Kg.K	c_s=470 J/Kg.K	
		E_s=210 GPa	
		υ_s=0.3	

Table 5.2: Material / lubricant properties and operating conditions for the test cases of Squalane + PIP

The rheology of Squalane + PIP is much more complex than Glycerol and requires more advanced rheological models for an accurate determination of the changes in viscosity and density with respect to the variations in pressure, temperature and shear stress. The rheological properties and operating conditions are reminded in Table 5.2. The rheological properties are taken from [3] whereas the thermal properties can be found in [78]. The Tait-Doolittle free volume model is used for viscosity and density-pressure-temperature dependence and the Carreau model for viscosity-shear stress dependence. The high-shear limiting viscosity at ambient pressure $\mu_{2,R}$ is considered to be the ambient pressure viscosity of pure Squalane.

Results are obtained for pure rolling and rolling-sliding conditions for a contact between a steel ball and a glass plane. For the pure rolling case the mean entrainment velocity covers the range of 0.1 to 4.64 m/s while for the rolling-sliding conditions it keeps a constant value of 1.47 m/s with a varying slide-to-roll ratio (SRR). Thermal effects on pressure, film thickness and traction are investigated.

5.5.2.1 Temperature

Before discussing pressure, film thickness and traction results, it is interesting to have a look at the temperature variations in the lubricant film which are, in part, responsible for the reduction in viscosity that leads to a decrease in both film thickness and traction. Figure 5.9 shows the temperature variation (*DT*) profiles across the film thickness at different *X* locations on the central line in the *x*-direction for four different values of the SRR (-0.45, 0.45, -1 and 1).

Temperature variations are more important in the case of |SRR|=1 than for |SRR|=0.45, revealing thus the higher heat generation due to shear heating. We can also see that in the two cases, temperature on the plane's surface is higher than on the sphere's one. This is to be expected since the plane is made out of glass which has much lower thermal diffusivity ($k/\rho c$) and effusivity ($\sqrt{k\rho c}$) than steel. So, if the two surfaces had the same velocity the ball's surface is expected to have a lower temperature because steel has a higher ability to exchange energy with its surrounding than glass. However, up to a certain limit, as long as heat conduction is the dominant factor in the thermal behaviour of the contact, this is still true even if the surface velocity of the glass plane was higher than that of the steel ball (this happens to be the case here for SRR<0). And for positive values of the SRR, since the surface velocity of the ball is higher than that of the plane, and knowing that steel has a higher volumetric heat capacity (ρc) than glass, then heat removal from the ball by convection is also more important than for the plane. This makes the difference in surface temperature between the two bodies more pronounced than for SRR<0. Also note the slightly higher temperature increase for negative values of the SRR compared to their equivalent positive ones. This is because, for negative values of the SRR, the surface velocity of the steel ball is the lower one. Hence, less heat is removed by convection from the contact area. Finally, note the increase in the temperature of the lubricant as it enters the contact until it reaches its maximum in the central area before decreasing as the lubricant goes out of the contact. In this outlet region, for positive values of the SRR, a reverse in the orientation of the temperature variation parabola is observed. This reveals the importance of the compressive cooling effect that occurs in this area where an important negative pressure gradient is encoutered.

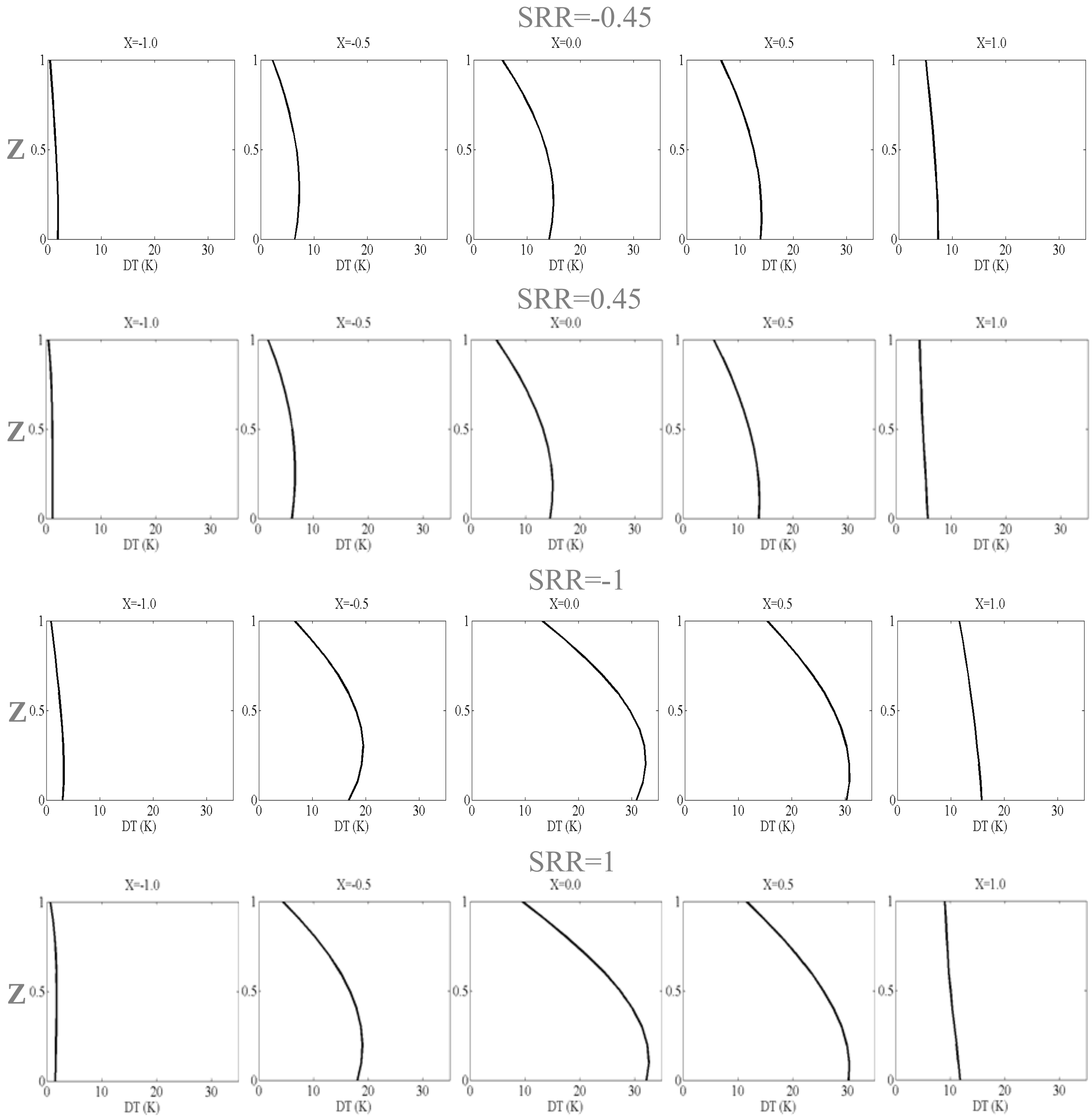

Figure 5.9: Temperature profiles across the film thickness at different X locations on the central line in the x-direction for four different values of the SRR (-0.45, 0.45, -1 and 1) with Squalane + PIP used as lubricant (u_m=1.47 m/s, p_h=0.47 GPa, M=30 and L=7.8)

Next, the effects of these variations in temperature on pressure, film thickness and traction results are investigated.

5.5.2.2 Pressure

In this section, the combined effects of temperature and non-Newtonian behaviour of the lubricant on pressure are studied. And mostly, by comparison with the corresponding isothermal results provided in section 4.5.1.1, temperature effects can be isolated. Figure 5.10 shows that when thermal effects are taken into account, globally, the pressure distribution exhibits a weak decrease in the central contact area when the SRR is increased. Since the load balance should be satisfied, this is generally compensated by a small increase of the pressure in the width of the contact. This was observed in experiments by Jubault et al. [69]. It is also shown in Figure 5.11 where we can note a pressure increase in the contact width in the y-direction with the increase of the SRR.

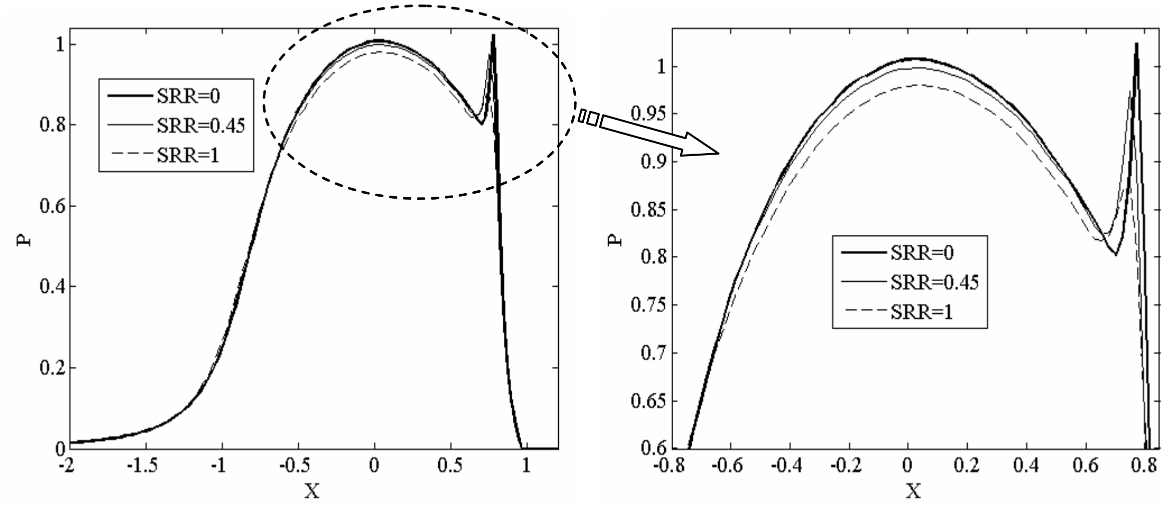

Figure 5.10: Combined non-Newtonian and thermal effects on pressure for the Squalane + PIP case (u_m=1.47 m/s, p_h=0.47 GPa, M=30 and L=7.8)

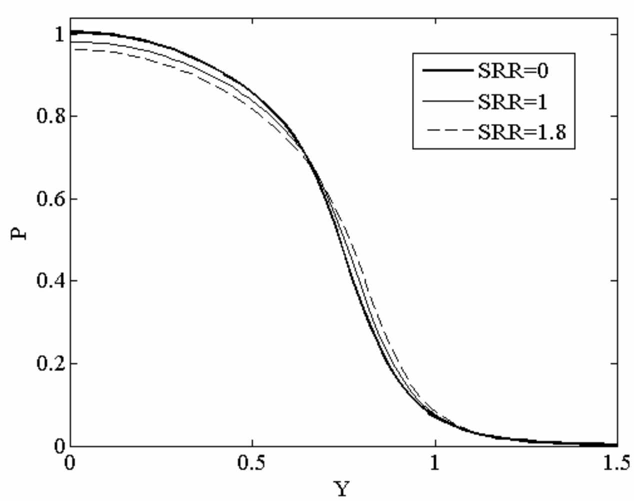

Figure 5.11: Combined thermal and non-Newtonian effects on the width of the contact for the Squalane + PIP case (u_m=1.47 m/s, p_h=0.47 GPa, M=30 and L=7.8)

Concerning the pressure spike, not only does it loose in height due to shear-thinning when the SRR is increased, but, due to thermal effects, it also gains in width and moves towards the centre of the contact. This has a direct consequence on the shape of the film thickness profile especially in the horseshoe area at the outlet of the contact. The variations in the film thickness shape are discussed more into details in the following section.

5.5.2.3 Film thickness

For pure rolling tests, the central and minimum film thickness curves for isothermal, thermal and experimental results are shown in Figure 5.12. As for the Newtonian case, up to a given velocity limit (in this case 2 m/s) isothermal and thermal results are practically the same. Beyond this value, the two curves slightly diverge from each other revealing thus the appearance of important shear heating. Note the exceptional agreement between thermal and experimental results.

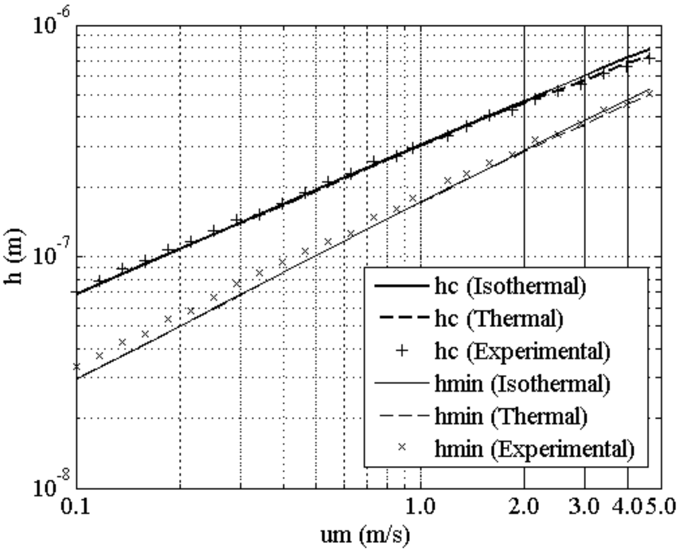

Figure 5.12: Film thickness curves as a function of the mean entrainment velocity under pure rolling conditions for the Squalane + PIP case (p_h=0.47 GPa)

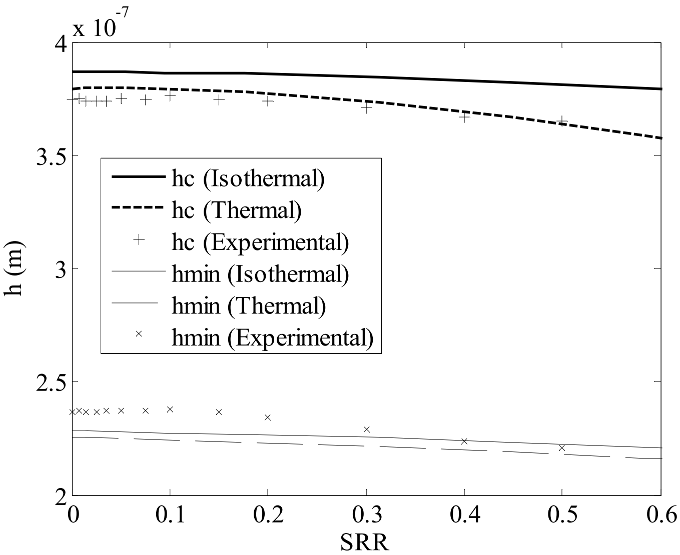

Figure 5.13: Film thickness curves as a function of the SRR for a constant mean entrainment velocity for the Squalane + PIP case (u_m=1.47 m/s , p_h=0.47 GPa, M=30 and L=7.8)

Figure 5.13 shows the film thickness curves as a function of the SRR. The film thickness continuously decreases with the increase of the SRR for both isothermal and thermal approaches. This decrease is more important in the thermal case since the combined non-Newtonian and thermal effects are superposed, and both have a thinning effect on the film thickness. Also note, especially in the case of central film thicknesses, the good agreement between thermal and experimental results.

In Figure 5.14, in addition to the central and minimum film thicknesses, the minimum film thickness on the central line in the x-direction h_{cmin} curves for both isothermal and thermal approaches are shown. In the thermal case, when the SRR is increased, h_{cmin} approaches the global minimum film thickness h_{min}. Therefore, the horseshoe shape at the outlet of the contact which originally has large ends and a narrow central region, gains in width on its central part and starts having an almost constant width. The change in shape of the horseshoe due to thermal effects was also observed in the experiments of Jubault et al. [69].

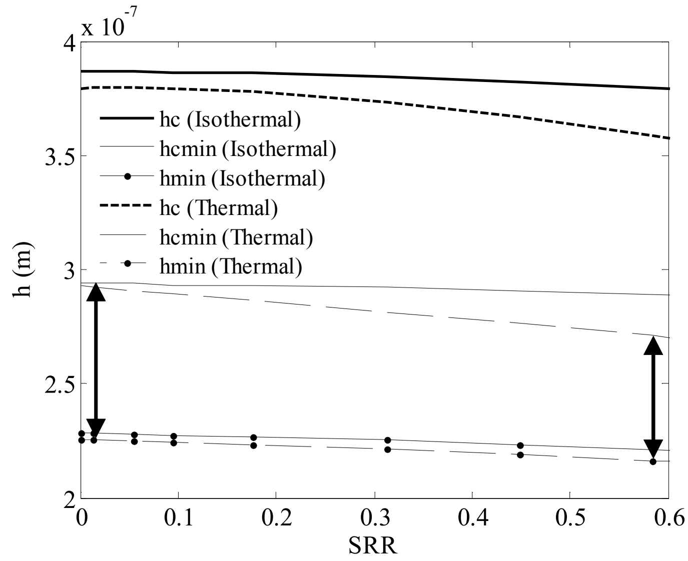

Figure 5.14: Thermal effects on the global film thickness shape for the Squalane + PIP case (u_m=1.47 m/s, p_h=0.47 GPa, M=30 and L=7.8)

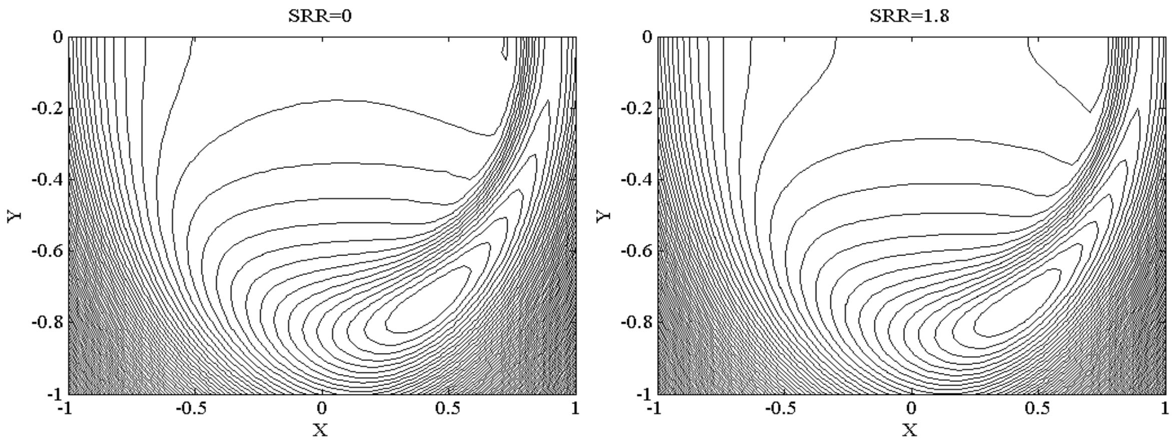

Figure 5.15: Isothermal film thickness contour plots as a function of the SRR for the Squalane + PIP case (u_m=1.47 m/s, p_h=0.47 GPa, M=30 and L=7.8)

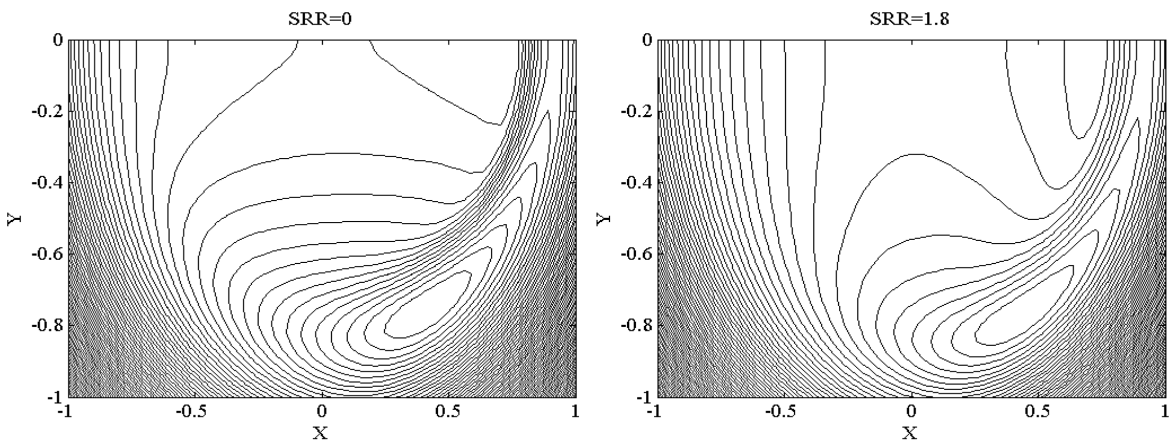

Figure 5.16: Thermal film thickness contour plots as a function of the SRR for the Squalane + PIP case (u_m=1.47 m/s, p_h=0.47 GPa, M=30 and L=7.8)

By examining Figure 5.16, one can see in the contour plots for the thermal cases that when the SRR grows, the horseshoe looses in width on its end parts and becomes larger on its central part. Thus, it comes closer to having a global constant width. This could not be observed by a simple isothermal approach where the difference between h_{cmin} and h_{min} is almost constant whatever the slide-to-roll ratio was (See Figure 5.14). This is also observed on the isothermal contour plots in Figure 5.15 where the horseshoe has practically the same shape for the different slide-to-roll ratios.

Finally, note that the “slight” remaining differences between experimental and numerical results may be due (in part) to the proper thermal signature of the experimental apparatus which depends on the design and environment of the latter.

5.5.2.4 Traction

Figure 5.17 shows the isothermal, thermal and experimental traction curves as a function of the slide-to-roll ratio for two different constant mean entrainment velocities of 0.74 m/s and 1.47 m/s. It is clear that an isothermal approach, as was pointed out in the previous chapter, is not appropriate for estimating friction in an EHL contact at high speed operating conditions. In fact, it overpredicts friction coefficients whereas a thermal approach shows a good agreement with experimental data.

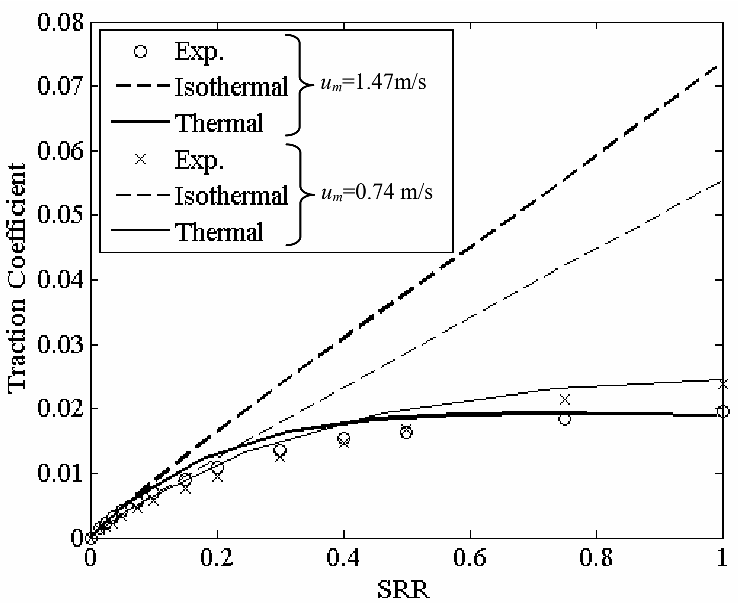

Figure 5.17: Traction curves as a function of the SRR for two different mean entrainment velocities of 0.74 m/s (M=50 and L=6.5) and 1.47 m/s (M=30 and L=7.8) for the Squalane + PIP case (p_h=0.47 GPa)

The discrepancy between the isothermal and experimental results is mainly due to thermal effects in the central area of the contact which are important even at low or moderate speed operating conditions (See Figure 5.9). Although, in such cases, this might have a relatively mild importance on the film thickness which is built up at the inlet of the contact, it has a significant effect on friction coefficients because of the viscosity decrease with the increase of temperature in this area.

Finally, note that the isothermal curves predict a higher traction coefficient for the higher mean entrainment velocity whatever the SRR was. This does not reflect the physical reality since the experimental points (and the thermal curves) show that this is true only up to a certain value of the SRR (here ≈ 0.5). Beyond this value, the tendency is inverted and the friction coefficient for the higher mean entrainment velocity becomes lower. This reveals the appearance of important thermal effects at high speed operating conditions. In this case, beyond SRR ≈ 0.5 and for u_m =1.47 m/s, the latter have more influence on the traction coefficient than frictional shear whereas for u_m =0.74 m/s, frictional shear is dominant.

5.6 Conclusion

In this chapter, the modelling of temperature variations in EHD circular contacts lubricated with either Newtonian or shear-thinning lubricants is presented. A generalized Reynolds' equation that takes into account thermal effects is presented. The same stabilization techniques that were presented in chapter 3 can be used to extend the solution to highly loaded contacts. Temperature variations are computed by applying the energy equation to the contacting bodies and the lubricant film. This equation can be written under the form of a pure convection / diffusion equation and at high Peclet numbers, a SUPG formulation is used to get a stable solution.

Some typical test cases were simulated under isothermal and thermal operating regimes for both pure rolling and rolling-sliding conditions. It is shown that beyond a certain limit of speed operating conditions, it is necessary to take into account shear heating for a good estimation of film thickness and, more importantly, friction. Both shear-thinning and thermal effects have a film-thinning effect when the sliding velocity is increased. They also modify pressure and film thickness distributions. In fact, it was shown in chapter 4 that shear-thinning effects tend to decrease the height of the pressure spike without any significant change in the shape of the film thickness distribution when the slide-to-roll ratio is increased. As for thermal effects, not only do they act on decreasing the height of the pressure spike, but, they also provide a gain in its width and its approach towards the centre of the contact. This leads to a change in the film thickness profile, especially in the outlet region where the horseshoe shape becomes wider at its central part and less large at its ends. Thus, it has an almost constant width compared to the isothermal shape where the horseshoe is large at the ends and narrow in the central region. All the results were compared to experimental data showing a better agreement between thermal results and experiments especially at high speeds or sliding velocities. Comparisons between numerical and experimental results validate both the employed numerical approach and rheological models. A remarkable agreement was obtained for friction results where the isothermal approach was shown to overestimate traction coefficients in the contact at high speed operating conditions. This is mainly because of thermal effects in the central area of the contact which are important even at low or moderate mean entrainment speed operating conditions when high sliding velocities are considered.

6 ULVF as lubricants

In this section, the potential use of ULVF as lubricants is studied. As mentioned in section 1.1, such fluids present two important aspects in engineering applications when they are used as lubricants. First, due to their low viscosity, they lead to reduced energy dissipation by friction in lubricated contacts. Second, from a practical point of view, it is much easier to design and maintain machines operating with only a single fluid serving as a lubricant and an operating fluid (e.g.: propulsion engines, car engines, heat pumps …). All in all, this falls within a strategy of preserving the environment and trying to decelerate the global warming phenomenon. However, because of the very low viscosity of these fluids, thin lubricant film layers are expected to be built up in the contact area. The aim of this work is to investigate wether it is possible or not to lubricate “correctly” with such fluids and under what range of operating conditions. The underlying motivation of this study stems from an interest in the topic shown by SKF Engineering and Research Centre in the Netherlands. However, this subject is classified as confidential and thus the real engineering application and some specific details are not revealed in this thesis. Still, this does not prevent from going through a thorough scientific investigation of the problem. Two typical ULVFs are considered. In the following, they are referred as “Fluid A” and “Fluid B”. It is worth noting that such fluids have almost never been of interest for the tribological community. Furthermore, their rheological properties are poorly known. In fact, these are restricted to a small range of pressure conditions compared to the range of interest in EHL applications. This is why some measurements are carried out in order to determine both the viscosity and density of “Fluid A” and “Fluid B” at a more important pressure range. The results are reported in Appendix C.

6.1 How about inertia effects?

Generally, in liquid flows, when low viscosity fluids are considered or also when high velocities take place, inertia effects might become important and cannot be considered as negligible anymore. The appearance of these effects is characterized by high values of the Reynolds number associated to the flow. The latter expresses the ratio of inertia forces over viscous forces and is written in general under the following form:

$$\mathrm{Re} = \frac{Inertia\ forces}{Viscous\ forces} = \frac{\rho\, V\, L}{\mu} \tag{6.1}$$

Where: ρ: Fluid's density $\quad$ V: Characteristic velocity of the flow

μ: Fluid's viscosity $\quad$ L: Characteristic length of the flow

When the value of Reynolds' number is below a given critical value ($\mathrm{Re} < \mathrm{Re}_c$), the corresponding flow is considered laminar and inertia effects negligible. However, when the Reynolds' number exceeds the critical value, inertia effects become important and these have a significant influence on the flow characteristics. If it is further increased, turbulent regime may appear beyond a certain limit.

Inertia effects are rarely encountered in tribological applications because of the "relatively" small characteristic lengths (film thicknesses) of the corresponding flows and the generally high viscosity of classical lubricants. However, in journal bearings lubricated by a low viscosity lubricant or also in gas bearings working under high speed operating conditions inertia effects might become important and a turbulent regime might even arise [32]. In such cases, the simplifying assumptions of the classical lubrication theory are not valid anymore (pressure is not constant over the film thickness, the normal velocity becomes of the same order of magnitude as the rest of the velocity components …). Hence, the classical Reynolds equation is not representative of the lubricant flow within the contact anymore. The latter has to be replaced by the generalized Reynolds equation with inertia effects or even the Navier-Stokes equations if a turbulent regime is encountered. Since very low viscosity fluids are considered in this section, one might wonder if inertia effects have to be considered or not, especially that high speed operating conditions are probably required in order to have a sufficient film thickness that prevents the direct contact between asperities. In order to clarify this point, an order of magnitude analysis is carried out for a typical EHD circular contact lubricated with a ULVF. The characteristic length which corresponds to the film thickness is considered to be 100 nm, the characteristic velocity which in this case corresponds to the mean entrainment speed is taken as 10 m/s. Typical values for the zero-pressure density and viscosity of a ULVF are 1500 Kg/m^3 and 5.10^{-4} Pa.s. The value of the critical Reynolds' number for a flow between two parallel plates $\mathrm{Re}_c \approx 2000 - 2500$. This is the closest configuration to a typical EHL circular contact. Thus the Reynolds' number that corresponds to an EHD circular contact lubricated with a typical ULVF is estimated as follows:

$$\mathrm{Re} = \frac{\rho\, V\, L}{\mu} = \frac{1500 \times 10 \times 10^{-7}}{5 \cdot 10^{-4}} = 3 \ll \mathrm{Re}_c \approx 2000 - 2500$$

Note that the "safer" zero-pressure value of the viscosity has been used in this case. The latter is far smaller than the actual value that is encountered within the contact (especially in the central area). This way, the analysis is valid for both the inlet and central regions of the contact. It is clear that the value of the typical Reynolds' number for ULVF lubricated contacts is far smaller than the critical value. Hence, the flow within the corresponding conjunctions can be considered laminar and inertia effects negligible. The classical lubrication theory that has been used so far is still valid in this case.

6.2 Is it possible to use ULVF as lubricants?

In this section, a thorough investigation is carried out in order to reveal wether it's possible or not to use ULVFs as lubricants and under what operating conditions. "Fluid A" and "Fluid B" are considered for this analysis. Owing to their small molecular weight (100-150 Kg/Kmol) and size (<5 Å) both fluids have a Newtonian behaviour. The TEHL model developed in the previous chapter is used. Film thickness computations are carried out for both pure rolling and rolling-sliding conditions. The mesh diameter is approximately equal to 0.5 in the inlet and outlet regions of the contact and 0.075 in the central area. Lagrange quintic elements are again used for the hydrodynamic problem and quadratic elements for the elastic one. The total number of dofs is about 40 000. The properties of the different materials that are used in this chapter are listed in Table 6.1. The pure rolling cases are run for a steel ball on a glass plane configuration whereas the rolling-sliding cases are run for steel-on-steel contacts. The ball's radius is taken as R=12.7 mm. For "Fluid A", the ambient temperature T_0=10 °C whereas for "Fluid B", $T_0 = T_R$ = -0.5°C. Figure 6.1 and Figure 6.2 show the central and minimum film thickness curves respectively as a function of the mean entrainment speed for both fluids under pure rolling conditions and for different values of the load.

Steel	Glass	Fluid A	Fluid B
E=210 GPa	E=81 GPa	k=0.077 W/m.K	k=0.011 W/m.K
υ=0.3	υ=0.208	c=1019 J/Kg.K	c=815 J/Kg.K
k=46 W/m.K	k=1.114 W/m.K	ρ_R=1465.2 Kg/m^3	ρ_R=1379.5 Kg/m^3
c=470 J/Kg.K	c=858 J/Kg.K	μ_R=0.465 mPa.s	μ_R=0.268 mPa.s
ρ=7850 Kg/m^3	ρ=2510 Kg/m^3	T_R=24.5 °C	T_R=-0.5 °C

Table 6.1: Properties of Steel, Glass, "Fluid A" and "Fluid B"

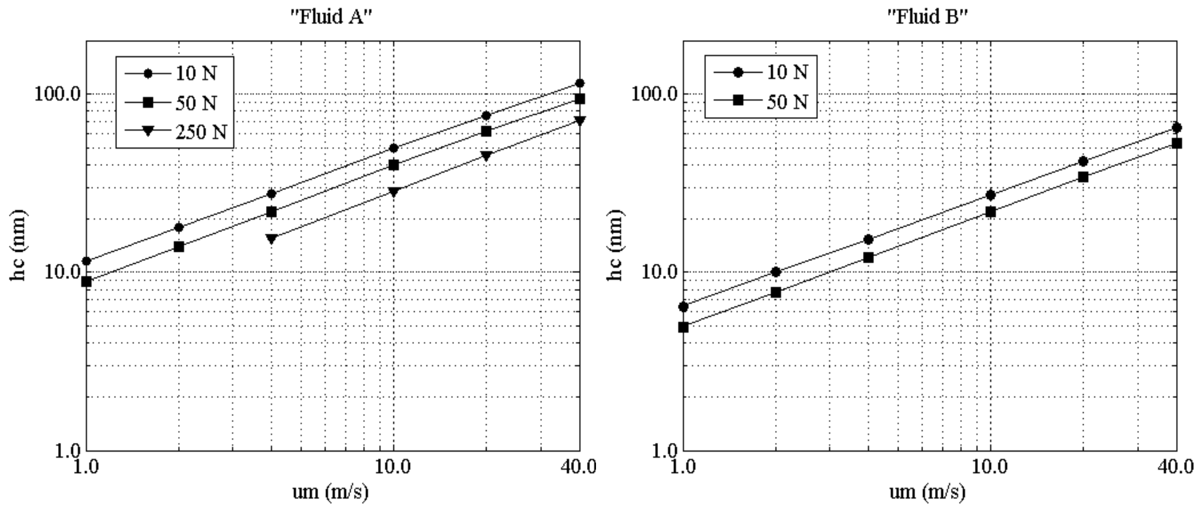

Figure 6.1: Central film thickness curves for a steel-on-glass contact on a log-log scale as a function of the mean entrainment speed for "Fluid A" (left) and "Fluid B" (right) (F=10 N / p_h=0.36 GPa, F=50 N / p_h=0.61 GPa, F=250 N / p_h=1.05 GPa)

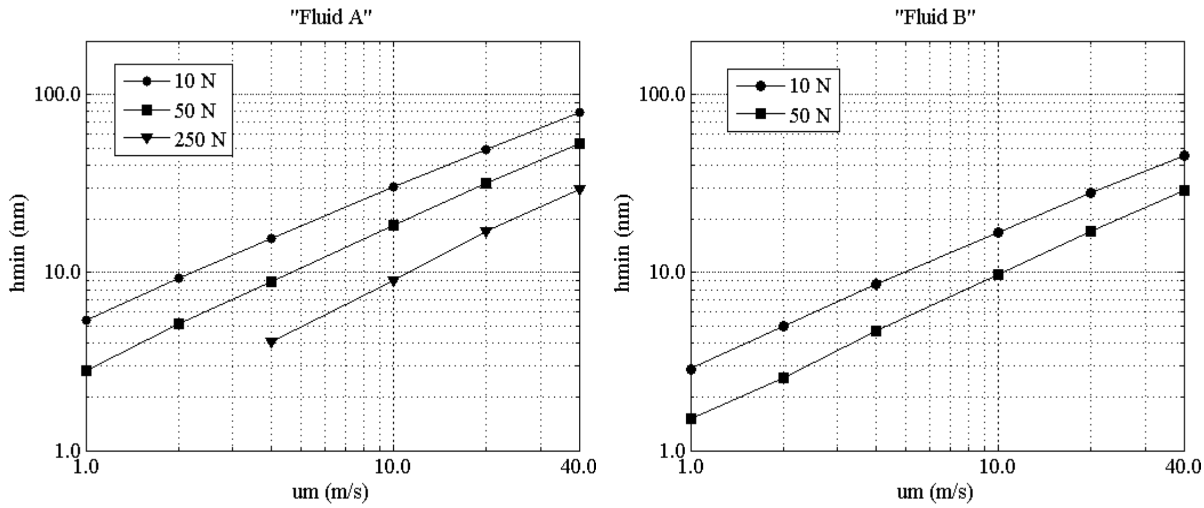

Figure 6.2: Minimum film thickness curves for a steel-on-glass contact on a log-log scale as a function of the mean entrainment speed for "Fluid A" (left) and "Fluid B" (right) (F=10 N / p_h=0.36 GPa, F=50 N / p_h=0.61 GPa, F=250 N / p_h=1.05 GPa)

Note that, in practice, the 250 N load case can never be realized on an experimental apparatus because glass would not withstand such a load. It is considered that beyond 10 molecular layers (5 nm), the theory of continuum mechanics that has been used throughout this work is valid. In fact, Granick [38] noticed that for *n*-dodecane, which has a relatively more important molecular size and weight than the considered ULVF, the bulk properties of the lubricant flow were the same as those predicted by a continuum approach down to 4 nm. This is confirmed by the observations of Georges et al. [35] who showed that this was true for *n*-dodecane and *n*-hexadecane down to 2.5 and 4.4 nm respectively. In EHL applications, the same observations were made by Guangteng and Spikes [40][41] and also Matsuoka and Kato [87][88] who showed that the continuum approach is valid down to approximately 10 molecular layers. When thinner films are considered, the analysis becomes more complex since it involves additional parameters that are neglected by the continuum approach such as surface tensions, solvation forces, chemical reactions … In this case alternative methods are introduced to study such contacts e.g. Tichy [109][110]. Hence, the reader should be aware that the less than 5 nm film thicknesses that are presented in Figure 6.2 have no physical relevance. Moreover, even the best finished surfaces have a surface roughness of a few nanometers and therefore a direct contact between asperities is likely to occur. Thus, a simple EHL analysis would not stand anymore and a “mixed lubrication” analysis would have to be considered when film thicknesses fall below the 5 nm limit.

In order to answer the question that is addressed in the title of this section, it is considered that a minimum surface separation of 10 nm is sufficient to ensure reasonably “safe” functioning of a high-quality ball bearing. Note that, generally, high speed operating conditions (up to 10 or 20 m/s) are required for a “safe” film separation especially for “Fluid B” which has a lower viscosity than “Fluid A”. Moreover, as the load is increased, the minimum required entrainment speed increases. Note that thermal effects on the film thicknesses are negligible even at very high speed operating conditions. In fact, the curves in Figure 6.1 and Figure 6.2 are “straight lines” in the log-log scale without any change in slope even at very high speeds. This is because of the ultra small viscosity of these fluids. This feature can also be seen in Figure 6.3 and Figure 6.4 which show the central and minimum film thickness variations with the sliding velocity. It is clear that even under pure sliding conditions (SRR=2), the decrease in the film thickness due to thermal effects is very small. The reader is reminded that both “Fluid A” and “Fluid B” are considered as Newtonian and thus, do not exhibit viscosity variations with shear stress.

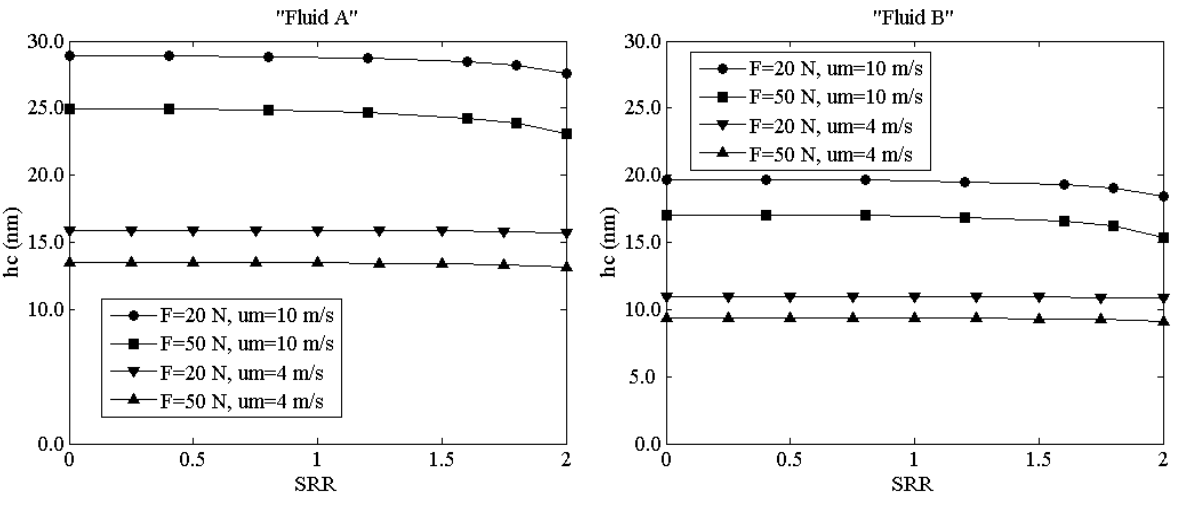

Figure 6.3: Central film thickness curves for steel-on-steel contacts as a function of the SRR for “Fluid A” (left) and “Fluid B” (right) (F=20 N / p_h=0.68 GPa, F=50 N / p_h=0.93 GPa)

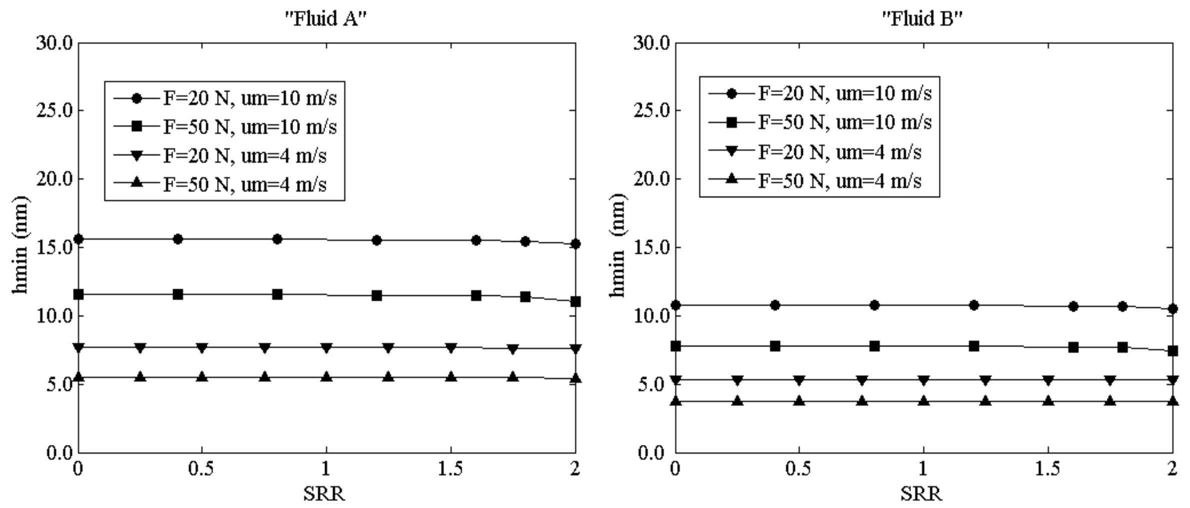

Figure 6.4: Minimum film thickness curves for a steel-on-steel contact as a function of the SRR for "Fluid A" (left) and "Fluid B" (right) (F=20 N / p_h=0.68 GPa, F=50 N / p_h=0.93 GPa)

Finally, note that the film thicknesses generated by "Fluid A" are generally higher than those by "Fluid B". This is to be expected since the former has a higher viscosity than the latter.

6.3 Experimental validation

In order to validate both the numerical approach and the rheological models that have been used in this chapter, a few film thickness measurements have been carried out using a steel-on-glass ball-on-disk apparatus. The measurements were realized for "Fluid A" under pure-rolling regime, considering a load of 30 N (p_h=0.52 GPa) on a range of speed conditions that goes from 1 to 2 m/s. Accurate higher speed measurements are difficult to reach because of the very low viscosity of the lubricant which prevents its good return into the contact area, leading thus to some starvation problems. The central and minimum film thickness results are reported in Figure 6.5.

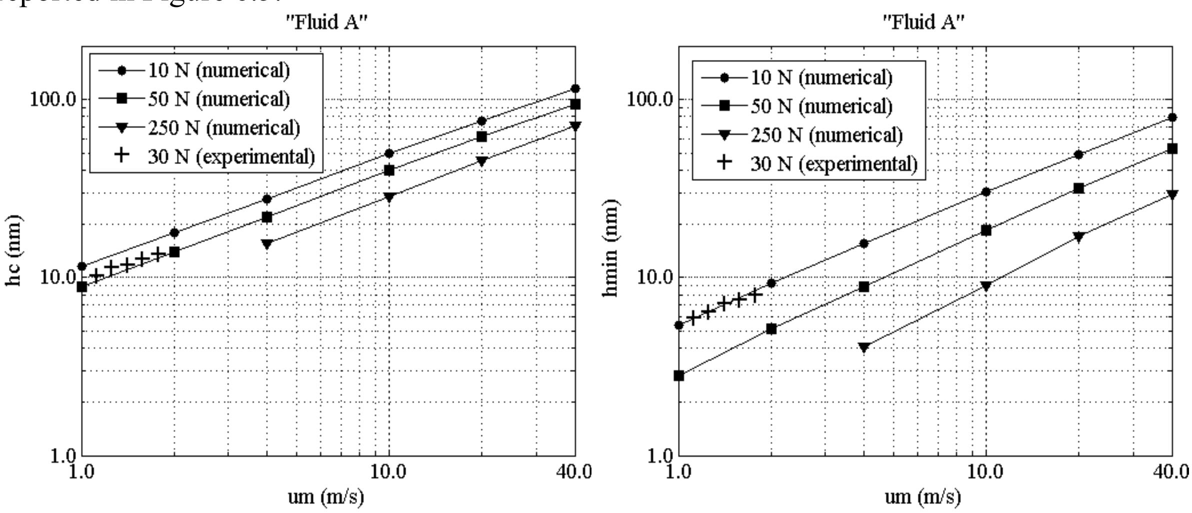

Figure 6.5: Experimental validation of steel-on-glass film thickness results for "Fluid A"

The agreement between experimental data and numerical results can be considered more than satisfactory, considering that the resolution of the former is of a few nanometers.

6.4 Film thickness formulae for ULVF

Because of the small viscosity, the weak viscosity-pressure dependence of ULVF and the fairly high loads that are studied in this chapter, one might expect that the *elastic-isoviscous* asymptote that was introduced by Venner [112] for cases of large values of M and L=0 would be appropriate to estimate the film thickness generated by these fluids in EHD contacts (M and L are the Moes parameters that were introduced in section 2.6.2). This formula was developed for central film thickness and has the following mathematical expression:

$$h_c = 1.96\, R \sqrt{2U_{HD}}\, M^{-1/9} \tag{6.2}$$

Figure 6.6 shows the central film thickness curves for the pure-rolling steel-on-glass cases mentioned in section 6.2 as predicted by numerical resolution and by the *elastic-isoviscous* asymptote in equation (6.2) for both "Fluid A" and "Fluid B".

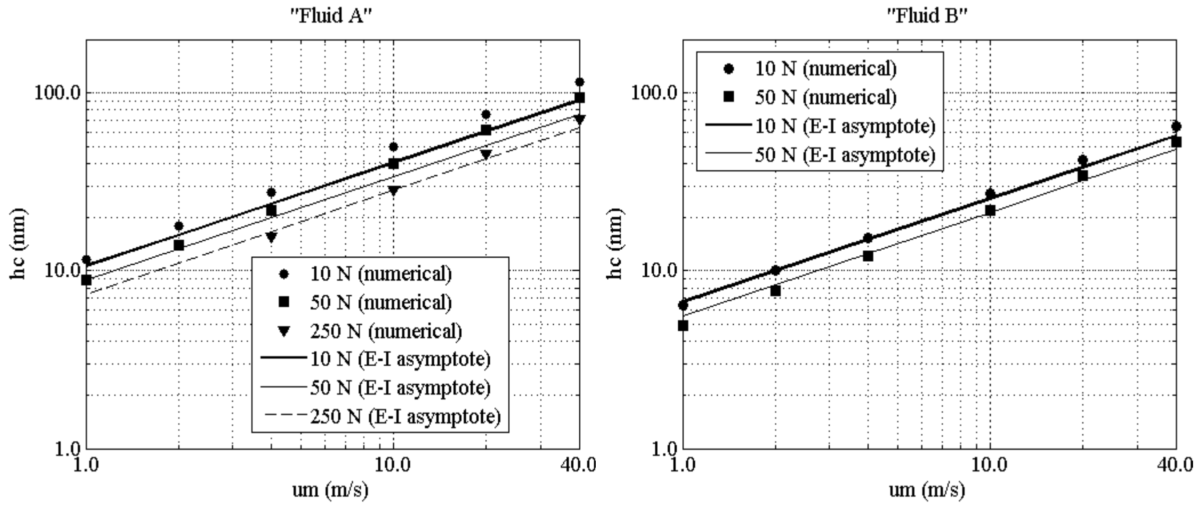

Figure 6.6: Comparison of central film thickness curves for steel-on-glass contacts under pure-rolling regime predicted by TEHL numerical resolution and the *elastic-isoviscous* asymptote for "Fluid A" (left) and "Fluid B" (right) (F=10 N / p_h=0.36 GPa, F=50 N / p_h=0.61 GPa, F=250 N / p_h=1.05 GPa)

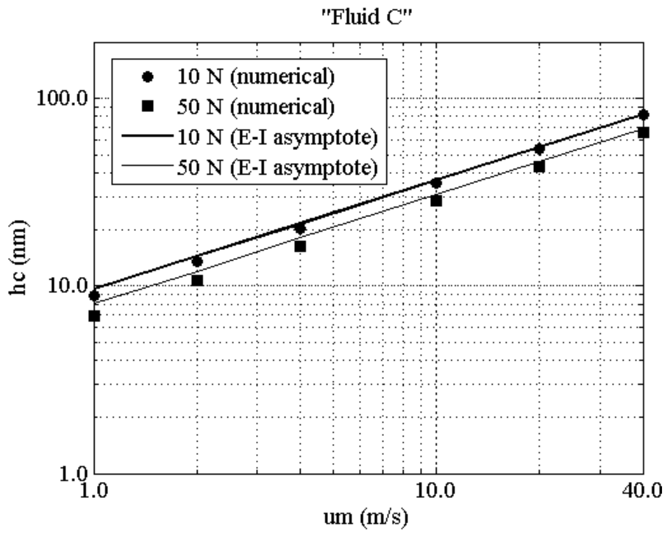

Figure 6.7: Comparison of central film thickness curves for steel-on-glass contacts under pure-rolling regime predicted by TEHL numerical resolution and the *elastic-isoviscous* asymptote for "Fluid C" (F=10 N / p_h=0.36 GPa, F=50 N / p_h=0.61 GPa)

The *elastic-isoviscous* asymptote fits reasonably well the numerical results especially for "Fluid B". However, for "Fluid A", the fit is less accurate. This is because the latter has a higher pressure-viscosity coefficient and is thus further from the *isoviscous* extreme. Moreover, the unusual density-pressure dependence of these fluids leads to unusual film thicknesses that cannot be predicted by classical formulae. In fact, if for the same operating conditions a less viscosity-pressure dependent fluid ("Fluid C") is considered with $\alpha = 0.5 \text{ GPa}^{-1}$, $\mu_R = 0.5 \text{ mPa.s}$ and a Dowson & Higginson-like compressibility, the fit between numerical results and the *elastic-isoviscous* asymptote would be much more accurate as can be seen in Figure 6.7. Hence some specific formulae have to be developed to predict central and minimum film thickness in EHD contacts lubricated by ULVF. Because of the different compressibility of "Fluid A" and "Fluid B", specific formulae have to be introduced for each fluid.

The numerical results for "Fluid A" and "Fluid B" were fitted to the following mathematical expressions for central and minimum film thickness:

$$\begin{aligned}
&\text{"Fluid A" : } \begin{cases} h_c = 2.9401\ R\sqrt{2U_{HD}}\ M^{-0.1541} L^{0.0526} \\ h_{\min} = 3.7607\ R\sqrt{2U_{HD}}\ M^{-0.3155} L^{0.0013} \end{cases} \\
&\text{"Fluid B" : } \begin{cases} h_c = 2.6815\ R\sqrt{2U_{HD}}\ M^{-0.1405} L^{0.1087} \\ h_{\min} = 4.1150\ R\sqrt{2U_{HD}}\ M^{-0.3255} L^{0.0568} \end{cases}
\end{aligned} \tag{6.3}$$

The fit between the previous formulae and numerical results for both fluids is shown in Figure 6.8 and Figure 6.9:

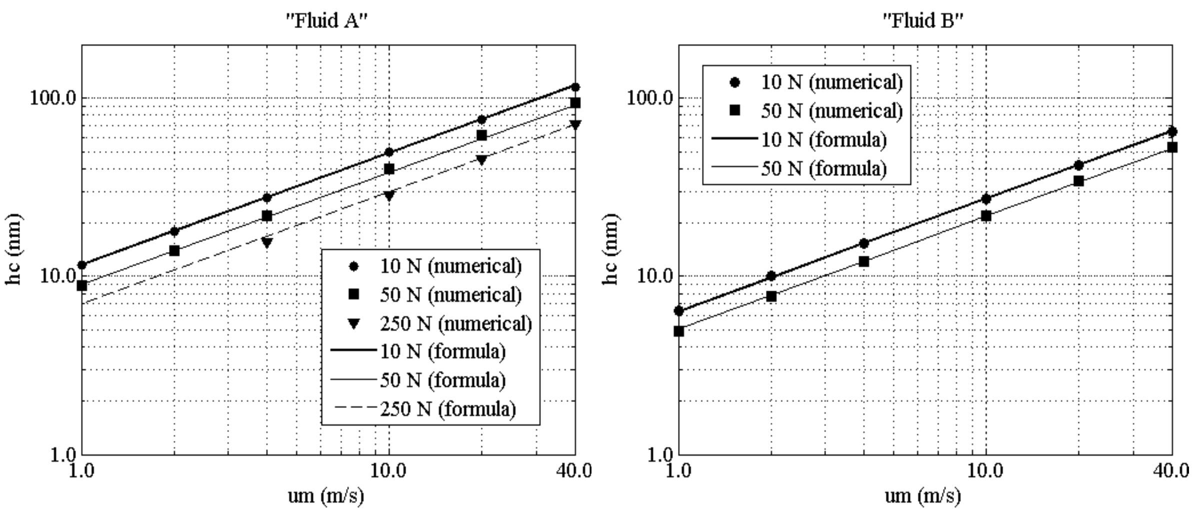

Figure 6.8: Comparison of central film thickness curves for steel-on-glass contacts under pure-rolling regime predicted by TEHL numerical resolution and analytical formulae for "Fluid A" (left) and "Fluid B" (right) (F=10 N / p_h=0.36 GPa, F=50 N / p_h=0.61 GPa, F=250 N / p_h=1.05 GPa)

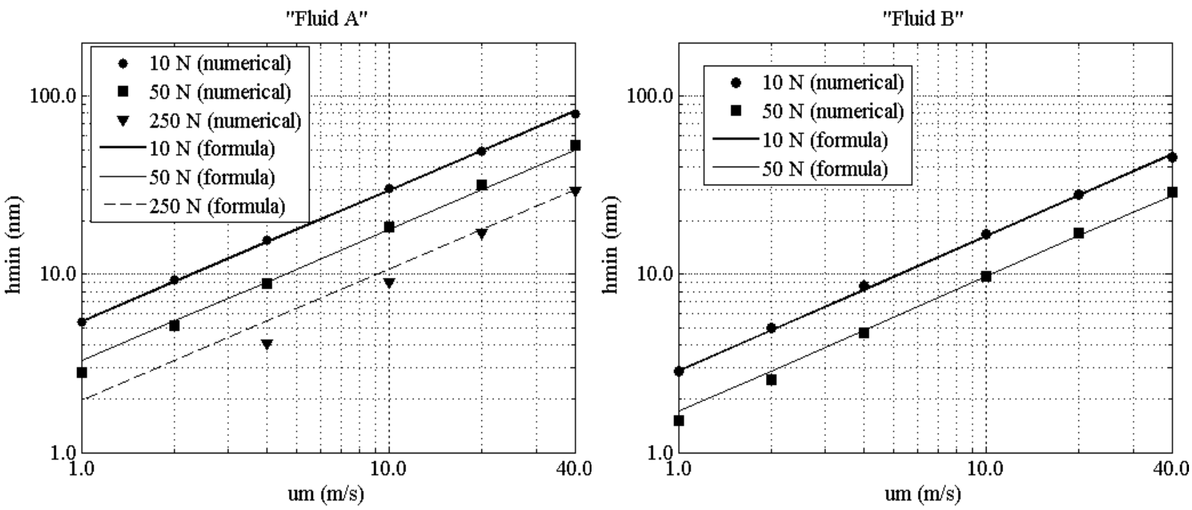

Figure 6.9: Comparison of minimum film thickness curves for steel-on-glass contacts under pure-rolling regime predicted by TEHL numerical resolution and analytical formulae for "Fluid A" (left) and "Fluid B" (right) (F=10 N / p_h=0.36 GPa, F=50 N / p_h=0.61 GPa, F=250 N / p_h=1.05 GPa)

Finally, although the *elastic-isoviscous* asymptote shows a good fit with the numerical results for "Fluid C", the latter is restricted to central film thicknesses. This is why a curve fit procedure was applied to the results of "Fluid C" giving the mathematical expressions below for central and minimum film thicknesses. The fit between these formulae and numerical results is shown in Figure 6.10.

$$\text{"Fluid C"}: \begin{cases} h_c = 2.2318\ R\sqrt{2U_{HD}}\ M^{-0.1362}L^{0.0198} \\ h_{\min} = 2.6759\ R\sqrt{2U_{HD}}\ M^{-0.2525}L^{0.0297} \end{cases} \tag{6.4}$$

As expected, the central film thickness formula is quite close to the *elastic-isoviscous* asymptote given in eq. (6.2) with an almost nill L exponent and fairly close M exponent and constant term.

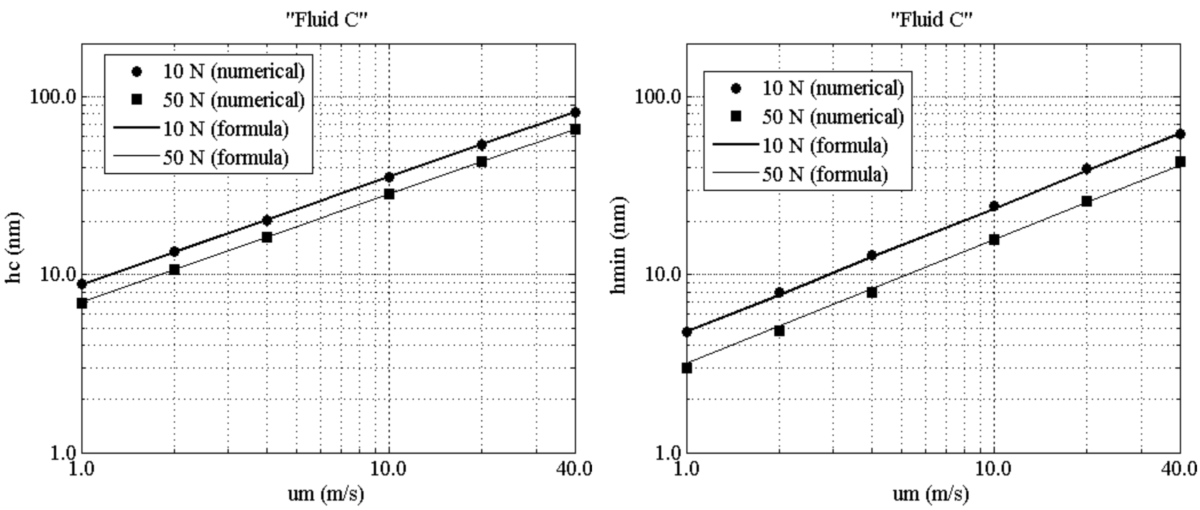

Figure 6.10: Comparison of central (left) and minimum (right) film thickness curves for steel-on-glass contacts under pure-rolling regime predicted by TEHL numerical resolution and analytical formulae for "Fluid C" (F=10 N / p_h=0.36 GPa, F=50 N / p_h=0.61 GPa)

Finally, it is clear that a very good agreement is obtained on the considered range of operating conditions between numerical results and the specific analytical formulae for the three considered fluids. Hence, the latter can be used by engineers to estimate sufficiently accurate central and minimum film thicknesses generated by “Fluid A”, “Fluid B” and “Fluid C” in EHD contacts without having to run the complete numerical resolution.

6.5 Economical issues

As was pointed out earlier, an attractive feature in the use of ULVF as lubricants is the economical aspect. In fact, due the low viscosity of these fluids, frictional losses in the contact area are much smaller than those generated by classical lubricants. In order to quantify this, the traction curves corresponding to the rolling-sliding steel-on-steel cases mentioned in section 6.2 are shown in Figure 6.11.

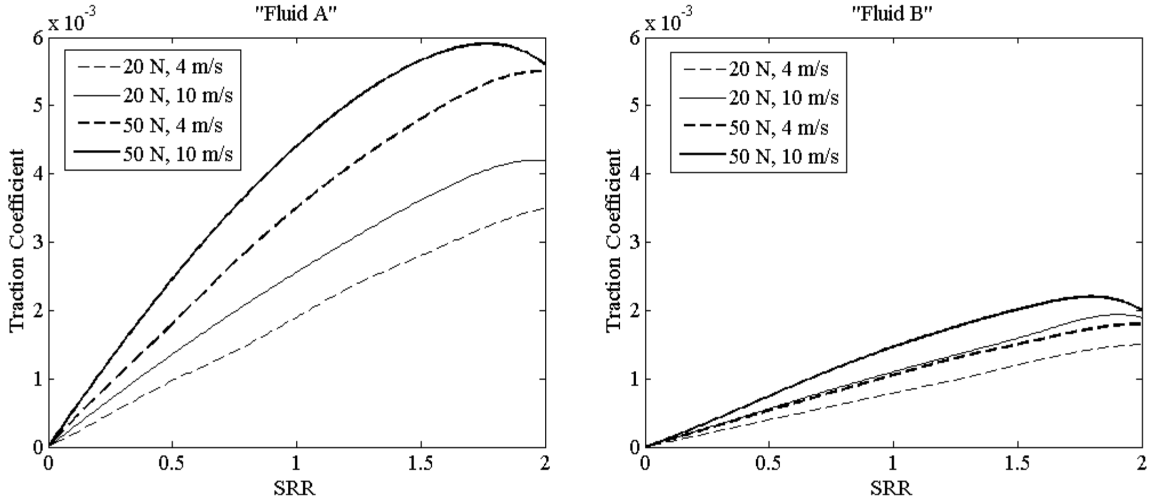

Figure 6.11: Traction curves for “Fluid A” (left) and “Fluid B” (right) for steel-on-steel contacts working under rolling-sliding conditions (F=20 N / p_h=0.68 GPa, F=50 N / p_h=0.93 GPa)

Note the relatively small values of the friction coefficients generated by the use of both fluids even under pure sliding conditions (SRR=2). The latter never exceed 6 ‰. This value is in most cases 10 times smaller than what would be obtained with a classical lubricant. Since energy dissipation by friction within a mechanical system is proportional to the friction coefficient, then the former is expected to be reduced by a factor of 10 when a ULVF fluid is used for lubrication.

6.6 Conclusion

A thourough investigation of the use of ULVF in EHD circular contacts was carried out in this chapter. Two typical ULVFs were considered. A series of test cases were carried out to compute central and minimum film thicknesses generated by these fluids in EHD contacts under a wide range of operating conditions. It was found that high speed regimes are favourable for a “safe” operation of systems lubricated with such fluids. Comparisons with experimental data showed the accuracy of both the numerical TEHL approach and the rheological models that were used. Then, specific film thickness formulae were developed for each fluid. These can be used directly by engineers in order to estimate sufficiently accurate film thicknesses without having to run the full calculations. In this context, the high compressibility of “Fluid A” and “Fluid B” has a significant impact on film thicknesses compared to ususal EHL applications where hydrodynamic effects, generated mostly by viscosity, are dominant. A traction analysis showed the important reduction of frictional dissipation in these contacts. The latter leads to a reduced energy consumption in the corresponding mechanical system. However, in order to complete this analysis, an additional question has to be addressed. In fact, one has to wonder which is more economically important: the reduction in energy consumption of the system or the reduction in the bearing's life because of the smaller film thicknesses that are encountered? This question reaches beyond the scope of this thesis and shall be reported for future investigations…

General conclusion

In this thesis a full-system finite element approach to elastohydrodynamic lubrication problems has been introduced with an emphasis on the smooth circular contact case. A linear elasticity model has been used to compute the elastic deformation of the contacting solids due to pressure generation in the lubricant film. This leads to a sparse Jacobian matrix of the global non-linear system of equations. The free boundary (cavitation) problem that arises at the outlet of the contact was treated in a straightforward manner by means of a penalty method. The resolution process was extended to the case of highly loaded contacts by using "artificial diffusion" finite element stabilized formulations. The global non-linear system of equations is solved by means of a Newton procedure. This provides outstanding convergence rates (only a few iterations are required to get a converged solution) especially when compared to classical semi-system based models. The current model has been shown to have the same complexity as finite difference multigrid based ones but a much smaller size due to non-regular unstructured meshes which stem from the use of the finite element method. Thus, reduced memory storage and computational times are obtained.

First, an isothermal Newtonian approach was considered. The latter predicts fairly well the film thickness in EHL conjunctions provided that the lubricant has a Newtonian behaviour and that moderate speeds and sliding velocities are considered. However, if a shear-thinning lubricant is considered, film thicknesses are overestimated. This is also the case if high speed and / or high sliding velocity operating conditions are considered. This is due to the important thermal dissipation that occurs in the contact and acts to reduce the lubricant's viscosity.

Then an isothermal non-Newtonian approach was developed by replacing the classical Reynolds' equation by the generalized one. This approach provides a much better estimation of film thicknesses when a shear-thinning lubricant is considered. However, although a closer-to-reality estimation of friction is obtained, an important discrepancy with experimental results is still observed at moderate or high speed operating conditions.

Finally, a thermal approach was developed for both Newtonian and non-Newtonian lubricants. It is based on a full resolution of the energy equations in the contacting solids and the lubricant film. This approach shows a very good film thickness and friction agreement with experimental data. In fact, the low quality friction results that were observed at high speed operating conditions for the isothermal non-Newtonian approach were due to the temperature increase in the central area of the contact. The latter does not significantly affect the film thickness which is known to be built-up in the inlet area, but it has an important effect on friction because of the viscosity decrease in this region.

The developed model was used to study the potential use of ULVF as lubricants in EHD circular contacts. It was shown that high speed operating conditions are required for such contacts to operate “safely”. The traction curves highlighted the important reduction of energy dissipation due to friction in such contacts compared to those lubricated with classical lubricants.

All in all, at every step of this study, whenever it was possible, experimental validation of the numerical results was realized. This is the only way to make sure the developed numerical approach and the employed rheological models provide realistic film thickness and traction results.

Recommendations for future work

As a result of covering the numerical side (the theory behind the development of efficient EHL solvers) as well as the engineering side (the application of the solvers to situations of practical interest), this thesis has become quite an extensive work. However, in spite of all the results and answers provided in the different sections of this document, there are still many subjects to be studied, questions that remain unanswered and new issues to be addressed.

From a numerical point of view, although the model presented in this thesis shows to be rather powerful compared to classical models, its' full power is far from being achieved. In fact, the three-dimensional elasticity problem can be subject to serious reduction in its size by applying either a model reduction by modal analysis or the static-condensation principle. The latter would reduce the elastic deformation calculation to the two-dimensional contact area Ω_c. Reducing the size of the model would open the way for studying rough surface problems and including real surface roughness under transient regime which require much finer meshing than smooth surface contacts. In addition, the use of structural mechanics equations to compute the elastic deflection of the contacting surfaces enables the study of configurations that are hard, if not impossible, to treat with a half-space approach e.g. coatings, soft materials, plasticity …

From an engineering point of view, it would be interesting to carry out an extensive investigation of film thickness and friction under light, moderate and heavy loads for different types of lubricants over a wide range of operating conditions, taking into account, as far as possible, the pressure and temperature dependence of the lubricant's thermal properties. This hasn't been done in this work for the lack of experimental data, but an important experimental-numerical project is currently taking place. Such studies require collaborations between different institutions in order to get accurate rheological and thermal properties of lubricants. The final aim would be to extract from the obtained results some robust analytical formulas that can be used directly by engineers without having to run the complete calculations. Ideally, these would take into account thermal effects and the complete rheological behaviour of the lubricant including non-Newtonian effects. Finally, to complete the analysis of the potential use of ULVF as lubricants, it is important to determine which is more economically important: the reduction in energy consumption of the system or the reduction in the bearing's life because of the smaller film thicknesses that are encountered.

Appendix A : Equivalent elastic problem

In this appendix, the theory behind the equivalent elastic problem is described. This problem is introduced in order to avoid solving the elastic deflection problem twice, under the same loading conditions, on the same geometry, using the respective material properties of solids p and s. The equivalent material properties are obtained using the half space theory. The latter states that the displacement $\delta(x,y,z)$ of a point (x,y,z) produced by a concentrated point force F acting normally to the surface $z=0$ at the origin (See Figure A.1) is given, according to Love [81], by:

$$\delta(x,y,z)=\frac{F}{4\pi\mu}\frac{z^2}{r^3}+\frac{(\lambda+2\mu)F}{4\pi\mu(\lambda+\mu)}\frac{1}{r} \tag{A.1}$$

Where λ and μ are the Lamé constants and $r=\sqrt{x^2+y^2+z^2}$. The Lamé constants are related to Young's modulus E and Poisson's coefficient υ according to:

$$\lambda=\frac{E\upsilon}{(1+\upsilon)(1-2\upsilon)} \quad \text{and} \quad \mu=\frac{E}{2(1+\upsilon)} \tag{A.2}$$

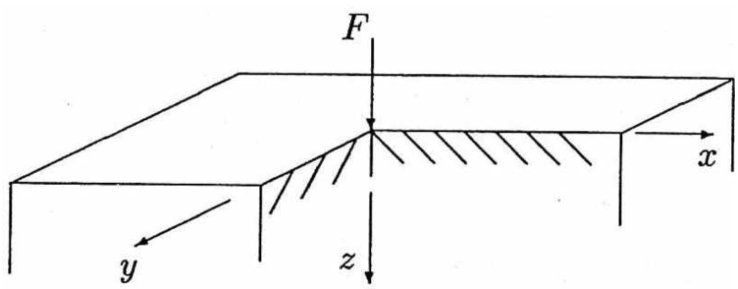

Figure A.1: Point loading of an elastic half space

Then, the equivalent displacement $\delta_{eq}(x,y,z)$ of the two solids p and s under the same concentrated point force F acting normally to the surface $z=0$ at the origin is given by:

$$\delta_{eq}(x,y,z)=\delta_p(x,y,z)+\delta_s(x,y,z) \tag{A.3}$$

Replacing every term by its expression given by equation (A.1), this equation becomes:

$$\frac{F}{4\pi\mu_{eq}}\frac{z^2}{r^3}+\frac{\left(\lambda_{eq}+2\mu_{eq}\right)F}{4\pi\mu_{eq}\left(\lambda_{eq}+\mu_{eq}\right)}\frac{1}{r}=\frac{F}{4\pi\mu_p}\frac{z^2}{r^3}+\frac{\left(\lambda_p+2\mu_p\right)F}{4\pi\mu_p\left(\lambda_p+\mu_p\right)}\frac{1}{r}+\frac{F}{4\pi\mu_s}\frac{z^2}{r^3}+\frac{\left(\lambda_s+2\mu_s\right)F}{4\pi\mu_s\left(\lambda_s+\mu_s\right)}\frac{1}{r}$$

After simplification, the previous equation becomes:

$$\frac{1}{\mu_{eq}}\left[\frac{z^2}{r^2}+2\left(1-\upsilon_{eq}\right)\right]=\frac{1}{\mu_p}\left[\frac{z^2}{r^2}+2\left(1-\upsilon_p\right)\right]+\frac{1}{\mu_s}\left[\frac{z^2}{r^2}+2\left(1-\upsilon_s\right)\right] \tag{A.4}$$

Any couple of material properties $\left(\mu_{eq},\upsilon_{eq}\right)$ that satisfies equation (A.4) can be used to define the equivalent elastic problem. In this work, we consider the particular case where:

$$\frac{1}{\mu_{eq}}=\frac{1}{\mu_p}+\frac{1}{\mu_s} \tag{A.5}$$

Replacing the Lamé constant μ by its expression given in (A.2), equation (A.5) becomes:

$$\frac{1+\upsilon_{eq}}{E_{eq}}=\frac{1+\upsilon_p}{E_p}+\frac{1+\upsilon_s}{E_s} \tag{A.6}$$

Equation (A.4) becomes after simplification and replacing $1/\mu_{eq}$ by its expression given in (A.5) and the Lamé constant μ by its expression given in (A.2):

$$\frac{1-\upsilon_{eq}^2}{E_{eq}}=\frac{1-\upsilon_p^2}{E_p}+\frac{1-\upsilon_s^2}{E_s} \tag{A.7}$$

Thus, solving the system of equations formed by (A.6) and (A.7), one gets the equivalent material properties E_{eq} and υ_{eq}:

$$E_{eq}=\frac{E_p^2E_s\left(1+\upsilon_s\right)^2+E_s^2E_p\left(1+\upsilon_p\right)^2}{\left[E_p\left(1+\upsilon_s\right)+E_s\left(1+\upsilon_p\right)\right]^2}\quad\text{and}\quad\upsilon_{eq}=\frac{E_p\upsilon_s\left(1+\upsilon_s\right)+E_s\upsilon_p\left(1+\upsilon_p\right)}{E_p\left(1+\upsilon_s\right)+E_s\left(1+\upsilon_p\right)} \tag{A.8}$$

Remark: For the particular case of the two contacting elements being made out of the same material $\left(E,\upsilon\right)$, the equivalent material properties are $E_{eq}=E/2$ and $\upsilon_{eq}=\upsilon$. Therefore, the total elastic deflection would be twice the elastic deflection of each body.

Finally, by multiplying the equivalent Young's Modulus by a/R the dimensionless displacement vector is obtained directly and dividing it by p_h allows the use of the dimensionless pressure distribution as a pressure load in the contact area. Hence, the equivalent material properties become:

$$E_{eq} = \frac{E_p^2 E_s \left(1+\upsilon_s\right)^2 + E_s^2 E_p \left(1+\upsilon_p\right)^2}{\left[E_p \left(1+\upsilon_s\right) + E_s \left(1+\upsilon_p\right)\right]^2} \times \frac{a}{R\, p_h} \quad \text{and} \quad \upsilon_{eq} = \frac{E_p \upsilon_s \left(1+\upsilon_s\right) + E_s \upsilon_p \left(1+\upsilon_p\right)}{E_p \left(1+\upsilon_s\right) + E_s \left(1+\upsilon_p\right)} \tag{A.9}$$

Replacing the material properties in the geometry of the elastic problem by those given in (A.9) gives directly the total dimensionless elastic displacement of both contacting bodies. This avoids running the same calculation twice. Of course, this approach limits the analysis in any case to systems with a half-space configuration (i.e.: the size of the contact should be small compared to the size of the contacting elements). This is fairly enough in the scope of this thesis which mainly concerns circular contacts in ball bearings. However, if a half-space configuration cannot be considered anymore (e.g.: soft materials as joints …), one has to run the calculation twice, using the real geometries of the contacting elements, and then sum the elastic displacements of both bodies in order to get the total deflection.

In order to validate the equivalent problem's theory, a test case is carried out with a dry glass-on-steel circular contact with a Hertzian pressure distribution applied in the contact region.

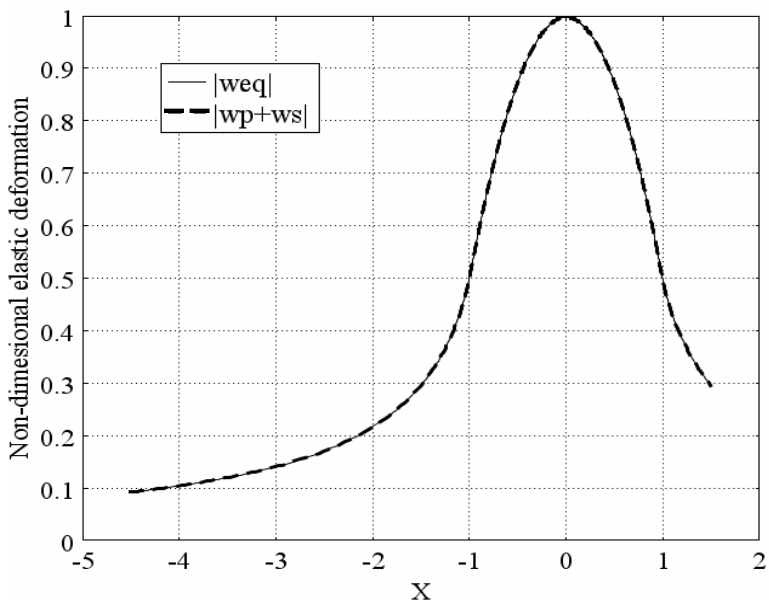

Figure A.2: Total elastic deflection of a dry glass-on-steel circular contact

Figure A.2 shows the non-dimensional elastic deflection curves on the central line in the X-direction obtained by both the equivalent problem defined in this section and the sum of the elastic displacements of the two contacting elements. It is clear that the two curves show a perfect match, revealing thus the equivalence between the two approaches.

Appendix B : EHL equations in matrix form

In this section, the detailed matrix form of the different EHL equations is provided. The Reynolds' equation is considered in its convection / diffusion form with a source term:

$$R\left(P,U,H_0\right) = -\nabla \cdot \left[\varepsilon\left(P,U,H_0\right)\nabla P\right] + \beta\left(P,U,H_0\right)\cdot\nabla P - Q\left(P,U,H_0\right) = 0 \qquad \text{(B.1)}$$

As was shown throughout this document, this form is suitable for all Reynolds' equations used in this work: the classical one, the generalized one and the generalized one with thermal effects. The penalty term and the stabilizing terms are not added here for simplicity, but the reader is reminded that these are to be added to the previous equation. The weak form of equation (B.1) is given by:

$$\begin{aligned}&\text{Find } P \in S_P \text{ such that } \forall W_P \in S_P, \text{ one has:}\\ &\int_{\Omega_c} \varepsilon \nabla P \cdot \nabla W_P d\Omega + \int_{\Omega_c} \beta \cdot \nabla P \; W_P d\Omega - \int_{\Omega_c} Q W_P d\Omega = 0\end{aligned} \qquad \text{(B.2)}$$

As was pointed out in chapter 3, equation (B.2) is approximated by its linear part which reads:

$$\begin{aligned}&\int_{\Omega_c}\left(\varepsilon \nabla \delta P \cdot \nabla W_P + \frac{\partial \varepsilon}{\partial P}\delta P \nabla P \cdot \nabla W_P + \frac{\partial \varepsilon}{\partial U}\delta U \nabla P \cdot \nabla W_P + \frac{\partial \varepsilon}{\partial H_0}\delta H_0 \nabla P \cdot \nabla W_P\right) d\Omega\\ &+\int_{\Omega_c}\left(\beta \cdot \nabla \delta P \; W_P + \frac{\partial \beta}{\partial P}\delta P \cdot \nabla P \; W_P + \frac{\partial \beta}{\partial U}\delta U \cdot \nabla P \; W_P + \frac{\partial \beta}{\partial H_0}\delta H_0 \cdot \nabla P \; W_P\right) d\Omega\\ &-\int_{\Omega_c}\left(\frac{\partial Q}{\partial P}\delta P W_P + \frac{\partial Q}{\partial U}\delta U \, W_P + \frac{\partial Q}{\partial H_0}\delta H_0 \, W_P\right) d\Omega =\\ &\qquad -\left[\int_{\Omega_c} \varepsilon \nabla P \cdot \nabla W_P d\Omega + \int_{\Omega_c} \beta \cdot \nabla P \; W_P d\Omega - \int_{\Omega_c} Q W_P d\Omega\right]\end{aligned} \qquad \text{(B.3)}$$

On the other hand, the elasticity and load balance equations are already linear and therefore they are strictly equivalent to their linear part. The linearized system of equations (3.22) to solve at the k^{th} iteration of the Newton procedure is reminded below:

$$\begin{bmatrix} J_{11} & J_{12} & J_{13} \\ J_{21} & J_{22} & \varnothing \\ J_{31} & \varnothing & \varnothing \end{bmatrix}^{k-1} \begin{Bmatrix} \delta P \\ \delta U \\ \delta H_0 \end{Bmatrix}^{k} = \begin{Bmatrix} -R\left(P,U,H_0\right) \\ -J_{21}P - J_{22}U \\ F_3 - J_{31}P \end{Bmatrix}^{k-1} \tag{B.4}$$

Where:
$$\begin{Bmatrix} \delta P \\ \delta U \\ \delta H_0 \end{Bmatrix} = \begin{Bmatrix} \left.\begin{matrix} \delta P_1 \\ \vdots \\ \delta P_{n_P} \end{matrix}\right\} n_P \text{ unknowns} \\ \left.\begin{matrix} \delta u_1 \\ \delta v_1 \\ \delta w_1 \\ \vdots \\ \delta u_{n_U} \\ \delta v_{n_U} \\ \delta w_{n_U} \end{matrix}\right\} 3 \text{ x } n_U \text{ unknowns} \\ \left.\delta H_0 \right\} 1 \text{ unknown} \end{Bmatrix}$$

The different components of the Jacobian matrix defined in system (B.4) are given by:

$$J_{11} = \int_{\Omega_{ce}} \left(B_P^T \, \varepsilon \, B_P + B_P^T \nabla P \frac{\partial \varepsilon}{\partial P} G_P + G_P^T \beta^T B_P + G_P^T \nabla P^T \frac{\partial \beta}{\partial P} G_P - G_P^T \frac{\partial Q}{\partial P} G_P \right) d\Omega$$

$$J_{12} = \int_{\Omega_{ce}} \left(B_P^T \, \nabla P \frac{\partial \varepsilon}{\partial U} G_U + G_P^T \nabla P^T \frac{\partial \beta}{\partial U} G_U - G_P^T \frac{\partial Q}{\partial U} G_U \right) d\Omega$$

$$J_{13} = \int_{\Omega_{ce}} \left(B_P^T \, \nabla P \frac{\partial \varepsilon}{\partial H_0} + G_P^T \nabla P^T \frac{\partial \beta}{\partial H_0} - G_P^T \frac{\partial Q}{\partial H_0} \right) d\Omega$$

$$J_{21} = \int_{\Omega_{ce}} -G_U^T \, n^T \, G_P \, d\Omega \quad \text{and} \quad J_{22} = \int_{\Omega_e} B_U^T \, D \, B_U \, d\Omega$$

$$J_{31} = \int_{\Omega_{ce}} G_P W_{H_0} \, d\Omega$$

And the right-hand-side terms are defined as follows:

$$R\left(P,U,H_0\right) = \int_{\Omega_{ce}} \left(B_P^T \, \varepsilon \nabla P + G_P^T \beta^T \, \nabla P - G_P^T Q \right) d\Omega \qquad F_3 = \frac{\pi}{3} W_{H_0}$$

Where:

$$\nabla P = \begin{bmatrix} \dfrac{\partial P}{\partial X} \\ \dfrac{\partial P}{\partial Y} \end{bmatrix} \qquad \beta = \begin{bmatrix} \beta_X \\ \beta_Y \end{bmatrix} \qquad n = \begin{bmatrix} n_x & n_y & n_z \end{bmatrix}$$

$$B_U = \begin{bmatrix} \frac{\partial N_{U1}}{\partial X} & 0 & 0 & \frac{\partial N_{U2}}{\partial X} & 0 & 0 & \cdots & \frac{\partial N_{Un_U}}{\partial X} & 0 & 0 \\ 0 & \frac{\partial N_{U1}}{\partial Y} & 0 & 0 & \frac{\partial N_{U2}}{\partial Y} & 0 & \cdots & 0 & \frac{\partial N_{Un_U}}{\partial Y} & 0 \\ 0 & 0 & \frac{\partial N_{U1}}{\partial Z} & 0 & 0 & \frac{\partial N_{U2}}{\partial Z} & \cdots & 0 & 0 & \frac{\partial N_{Un_U}}{\partial Z} \\ \frac{\partial N_{U1}}{\partial Y} & \frac{\partial N_{U1}}{\partial X} & 0 & \frac{\partial N_{U2}}{\partial Y} & \frac{\partial N_{U2}}{\partial X} & 0 & \cdots & \frac{\partial N_{Un_U}}{\partial Y} & \frac{\partial N_{Un_U}}{\partial X} & 0 \\ \frac{\partial N_{U1}}{\partial Z} & 0 & \frac{\partial N_{U1}}{\partial X} & \frac{\partial N_{U2}}{\partial Z} & 0 & \frac{\partial N_{U2}}{\partial X} & \cdots & \frac{\partial N_{Un_U}}{\partial Z} & 0 & \frac{\partial N_{Un_U}}{\partial X} \\ 0 & \frac{\partial N_{U1}}{\partial Z} & \frac{\partial N_{U1}}{\partial Y} & 0 & \frac{\partial N_{U2}}{\partial Z} & \frac{\partial N_{U2}}{\partial Y} & \cdots & 0 & \frac{\partial N_{Un_U}}{\partial Z} & \frac{\partial N_{Un_U}}{\partial Y} \end{bmatrix}$$

$$G_U = \begin{bmatrix} N_{U1} & 0 & 0 & N_{U2} & 0 & 0 & \cdots & N_{Un_U} & 0 & 0 \\ 0 & N_{U1} & 0 & 0 & N_{U2} & 0 & \cdots & 0 & N_{Un_U} & 0 \\ 0 & 0 & N_{U1} & 0 & 0 & N_{U2} & \cdots & 0 & 0 & N_{Un_U} \end{bmatrix}$$

$$B_P = \begin{bmatrix} \frac{\partial N_{P1}}{\partial X} & \frac{\partial N_{P2}}{\partial X} & \cdots & \frac{\partial N_{Pn_P}}{\partial X} \\ \frac{\partial N_{P1}}{\partial Y} & \frac{\partial N_{P2}}{\partial Y} & \cdots & \frac{\partial N_{Pn_P}}{\partial Y} \end{bmatrix} \qquad G_P = \begin{bmatrix} N_{P1} & N_{P2} & \cdots & N_{Pn_P} \end{bmatrix}$$

$$D = \frac{E}{(1+\upsilon)(1-2\upsilon)} \begin{bmatrix} 1-\upsilon & \upsilon & \upsilon & 0 & 0 & 0 \\ \upsilon & 1-\upsilon & \upsilon & 0 & 0 & 0 \\ \upsilon & \upsilon & 1-\upsilon & 0 & 0 & 0 \\ 0 & 0 & 0 & \frac{1-2\upsilon}{2} & 0 & 0 \\ 0 & 0 & 0 & 0 & \frac{1-2\upsilon}{2} & 0 \\ 0 & 0 & 0 & 0 & 0 & \frac{1-2\upsilon}{2} \end{bmatrix}$$

$$\frac{\partial \varepsilon}{\partial U} = \begin{bmatrix} \frac{\partial \varepsilon}{\partial u} & \frac{\partial \varepsilon}{\partial v} & \frac{\partial \varepsilon}{\partial w} \end{bmatrix} \qquad \frac{\partial Q}{\partial U} = \begin{bmatrix} \frac{\partial Q}{\partial u} & \frac{\partial Q}{\partial v} & \frac{\partial Q}{\partial w} \end{bmatrix}$$

$$\frac{\partial \beta}{\partial P} = \begin{bmatrix} \frac{\partial \beta_X}{\partial P} \\ \frac{\partial \beta_Y}{\partial P} \end{bmatrix} \qquad \frac{\partial \beta}{\partial U} = \begin{bmatrix} \frac{\partial \beta_X}{\partial u} & \frac{\partial \beta_X}{\partial v} & \frac{\partial \beta_X}{\partial w} \\ \frac{\partial \beta_Y}{\partial u} & \frac{\partial \beta_Y}{\partial v} & \frac{\partial \beta_Y}{\partial w} \end{bmatrix} \qquad \frac{\partial \beta}{\partial H_0} = \begin{bmatrix} \frac{\partial \beta_X}{\partial H_0} \\ \frac{\partial \beta_Y}{\partial H_0} \end{bmatrix}$$

The different derivative terms of ε, β and Q with respect to P, U and H_0 are computed analytically. These depend on the density-pressure and viscosity-pressure relationships that are employed.

As stated throughout this thesis, two-dimensional Lagrange quintic (21 nodes) elements are used for the hydrodynamic part whereas three-dimensional tetrahedral Lagrange quadratic (10 nodes) elements are used for the elastic part (See Figure B.1). Hence, $n_P = 21$ and $n_U = 10$.

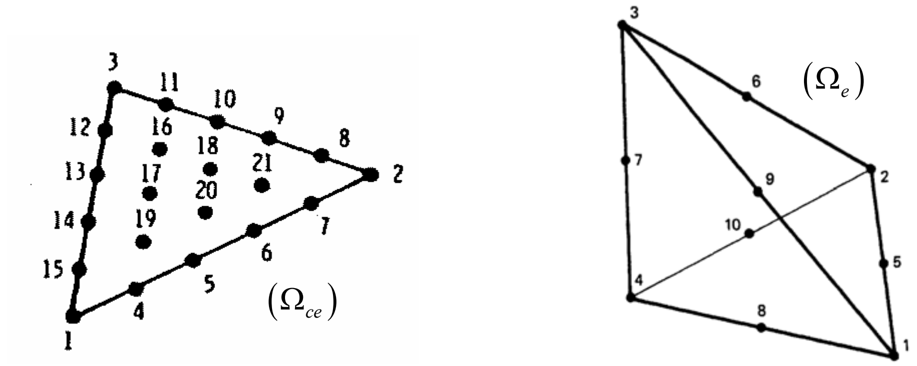

Figure B.1: Two-dimensional triangular Lagrange quintic (21 nodes) element (left) and three-dimensional tetrahedral Lagrange quadratic (10 nodes) element (right)

The system of equations (B.4) as described in this section is elementary i.e. it corresponds to one element. The global system of equations is assembled the usual way by expanding the different elementary systems. For more details the reader is referred to any finite element handbook such as [59], [62] and [126].

<u>Remark</u>: If $\Omega_e \cap \Omega_c = \varnothing$, then the integral terms over Ω_{ce} in the elementary matrix of Ω_e are nill and thus the lines that correspond to Reynolds' and the load balance equations are zero. These are not included in the global matrix system. Otherwise $\Omega_e \cap \Omega_c = \Omega_{ce}$ which happens to be one of the faces of the 3D tetrahedral element that corresponds to Ω_e (the same mesh is used for both the hydrodynamic and elastic problems). In this case, no zero lines are encountered in the elementary matrix.

Finally, the reader is reminded that the penalty and stabilizing terms haven't been added for simplicity. These are to be added to the matrix form of Reynolds' equation in a similar way as the other terms. Also note that the energy equations of the thermal problem described in chapter 5 also have a convection / diffusion form and therefore their matrix form is similar to that of Reynolds' equation described above.

Appendix C : Viscosity and density of ULVF

Visosity and density measurements over wide pressure and temperature ranges were carried out for the two typical ULVF considered in this work: “Fluid A” and “Fluid B”. The results are reported below:

C.1 Viscosity measurements

Pressure-viscosity data is measured using a high-pressure falling body viscometer designed to sustain pressures up to 0.6 GPa. The temperature can vary from -20 to 130°C and its viscosity domain covers a typical range of 0.2×10^{-3} to $5\times10^{+3}$ Pa.s.

Pressure (MPa)	Viscosity (mPa.s)		
	-16 °C	**-0.9 °C**	**24.5 °C**
0.1	0.772	0.633	0.465
25	0.994	0.810	0.578
50	1.207	0.965	0.675
100	1.584	1.239	0.854
150	2.049	1.549	1.024
200	2.559	1.903	1.218
300	4.098	2.767	1.683
400	6.568	4.227	-

Table C.1: Viscosity values of “Fluid A” as a function of pressure for three different temperatures (-16, -0.9 and 24.5 °C)

Pressure (MPa)	Viscosity (mPa.s)	
	-32.5 °C	**-0.5 °C**
0.1	0.416	0.268
25	0.471	0.299
50	0.517	0.326
100	0.617	0.368
150	0.718	0.408
200	0.863	0.458
300	-	0.560

Table C.2: Viscosity values of “Fluid B” as a function of pressure for two different temperatures (-32.5 and -0.5 °C)

An ultrasonic detector (emitter-receiver) is used to monitor the falling body. It allows recording its position in the high pressure vessel against time. The viscosity of the fluid is proportional to the inverse of the falling body’s velocity. Using this ultrasonic technique, the experiments are carried out in order to account for the longitudinal propagation speed variations as a function of pressure for each temperature investigated. After this preliminary step, different falling bodies are used to measure viscosity at different temperatures and pressures. They are made out of different material (i.e. different densities) and present different gaps with respect to the internal diameter of the high-pressure cell that is equal to 16 mm. Using several falling bodies, it becomes possible to obtain the relative viscosity increase over a large pressure domain. The measurements are carried out for three different temperatures (-16, -0.9 and 24.5 °C) on a pressure domain ranging from atmospheric pressure to 400 MPa. The ambient pressure value of the viscosity is taken from ref. [78]. The results for "Fluid A" and "Fluid B" are listed in Table C.1 and Table C.2 respectively.

Note the low viscosity of these fluids which is by several orders of magnitude smaller than that of classical lubricants. The viscosity data is fitted to the Cheng model using a least-squares technique. The results are presented in Figure C.1 showing a good agreement between the experimental data and the analytical model for the considered range.

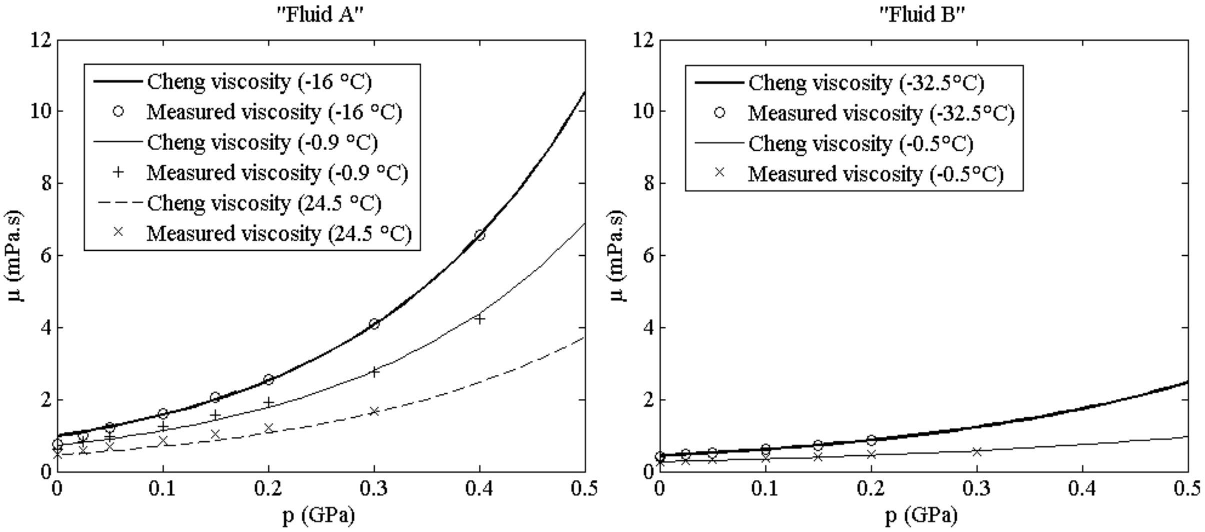

Figure C.1: "Fluid A" (left) and "Fluid B" (right) viscosity data fit to the Cheng model

The values of the different parameters of the Cheng model for "Fluid A" are: $\alpha_{ch} = 0.409\ \text{GPa}^{-1}$, $\beta_{ch} = 1396.34\ \text{K}$ and $\gamma_{ch} = 1118.62\ \text{GPa}^{-1}\cdot\text{K}$. The reference temperature T_R is taken as 24.5 °C and thus the reference viscosity $\mu_R = 0.465\ \text{mPa}\cdot\text{s}$. As for "Fluid B", the Cheng parameters are: $\alpha_{ch} = -4.567\ \text{GPa}^{-1}$, $\beta_{ch} = 959.02\ \text{K}$ and $\gamma_{ch} = 1940.72\ \text{GPa}^{-1}\cdot\text{K}$. The reference temperature T_R is taken as -0.5 °C and thus the reference viscosity $\mu_R = 0.268\ \text{mPa}\cdot\text{s}$. Note that, globally, "Fluid B" has a lower viscosity than "Fluid A".

C.2 Density measurements

The density measurements for both fluids were carried out on a range of pressures and temperatures varying from the ambient value to 1.25 GPa and 10 to 70°C respectively. The data was fitted to appropriate mathematical expressions. Their corresponding behaviour is shown in Figure C.2. The latter shows the compressibility curve of "Fluid A", "Fluid B" and the one for classical lubricants which often obey reasonably well the Dowson & Higginson formula. It is clear that both ULVFs used here have a relatively different density variation with respect to pressure compared to classical lubricants. In fact, "Fluid A" has a quasi-linear pressure dependence and beyond ≈ 300 MPa it has a much higher compressibility than classical lubricants. On the other hand, "Fluid B" has an even higher compressibility with a very high slope for the 0-100 MPa range. Beyond this range, it also has a quasi-linear pressure dependence with a slightly smaller slope than "Fluid A".

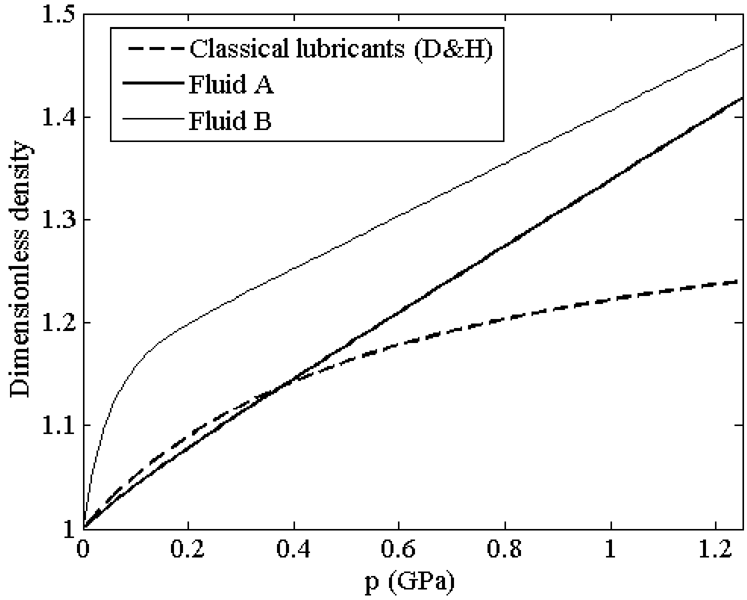

Figure C.2: Compressibilty of "Fluid A" and "Fluid B" compared to classical lubricants

Finally, it is worth noting that (like most classical lubricants) both "Fluid A" and "Fluid B" have a linear density dependence on temperature.

Publications

The work presented in this document has lead so far to several journal papers and has been presented in different conferences that are listed below in chronological order:

Journal papers:

- **W. Habchi**, I. Demirci, D. Eyheramendy, G. Morales-Espejel and P. Vergne – A Finite Element Approach of Thin Film Lubrication in Circular EHD Contacts. *Tribol. Int.*, 2007, vol. 40, pp. 1466-1473.
- **W. Habchi**, D. Eyheramendy, P. Vergne and G. Morales-Espejel – A Full-System Approach of the Elastohydrodynamic Line/Point Contact Problem. *ASME J. Tribol.*, 2008, vol. 130, 021501.
- **W. Habchi**, D. Eyheramendy, S. Bair, P. Vergne and G. Morales-Espejel – Thermal Elastohydrodynamic Lubrication of Point Contacts Using a Newtonian/Generalized Newtonian Lubricant. *Tribol. Lett.*, 2008, vol. 30 (1), pp. 41-52.
- **W. Habchi**, D. Eyheramendy, P. Vergne and G. Morales-Espejel – Stabilized Fully-Coupled Finite Elements for elastohydrodynamic Lubrication Problems. *Submitted to IJNME*.

Conferences:

- **W. Habchi**, I. Demirci, D. Eyheramendy, G. Morales-Espejel and P. Vergne – A Finite Element Approach of Thin Film Lubrication in Circular EHD Contacts. *Proc. 33rd Leeds-Lyon Symp. Tribol.*, 2006, Leeds (UK).
- **W. Habchi**, D. Eyheramendy, S. Bair, P. Vergne and G. Morales-Espejel – A Finite Element Approach of the Fully Coupled Elastohydrodynamic Problem. *Proc. STLE/ASME IJTC*, 2007, San Diego (USA).
- **W. Habchi**, D. Eyheramendy, P. Vergne and G. Morales-Espejel – Stabilized Finite Elements for Elastohydrodynamic Lubrication Problems. *Proc. 6th Int. Conf. Engnrng. Comp. Techn.*, 2008, Athens (Greece).
- **W. Habchi**, D. Eyheramendy, P. Vergne and G. Morales-Espejel – Friction and Film Thickness in Heavily Loaded Circular Contacts Operating Under Thermal Elastohydrodynamic Regime. *Proc. 35th Leeds-Lyon Symp. Tribol.*, 2008, Leeds (UK).

References

[1] Bair S. - A Rough Shear-Thinning Correction for EHD Film Thickness. *STLE Trib. Trans.*, 2004, vol. 47, pp. 361-365.

[2] Bair S. – Reference Liquids for Quantitative Elastohydrodynamics: Selection and Rheological Characterization. *Tribology Letters*, 2006, vol. 22, pp. 197-206.

[3] Bair S. - High-Pressure Rheology for Quantitative Elastohydrodynamics, *Elsevier Science*, Amsterdam, 2007.

[4] Bair S., Vergne P. and Querry M. – A Unified Shear-Thinning Treatment of Both Film Thickness and Traction in EHD. *Tribology Letters*, 2005, vol. 18, pp. 145-152.

[5] Bair S. and Winer W. O. – Shear Strength Measurements of Lubricant at High Pressure. *ASME J. Lubr. Techn.*, 1979, vol. 101, pp. 251-257.

[6] Bair S. and Winer W. O. – A Rheological Model for Elastohydrodynamic Contacts Based on Primary Laboratory Data. *ASME J. Lubr. Techn.*, 1979, vol. 101, pp. 258-265.

[7] Barus C. – Isothermal, Isopiestics and Isometrics Relative to Viscosity. *Am. J. Sci.*, 1893, vol. 45, pp. 87-96.

[8] Baumann H., Von Frey D. and Haller R. – Druck und Temperaturverteilungen in EHD-Kontakten. *Tribologie und Schmierungstechnik*, vol. 2, pp. 84-96, 1988.

[9] Brandt A. and Lubrecht A. A. – Multilevel Matrix Multiplication and Fast Solution of Integral Equations. *J. Comput. Phys.*, 1990, vol. 90 (2), pp. 348-370.

[10] Bridgman P. W. - The Physics of High Pressure, *Dover*, New York, 1970.

[11] Brooks A. N. and Hughes T. J. R. - Streamline-Upwind/Petrov-Galerkin Formulations for Convective Dominated Flows with Particular Emphasis on the Incompressible Navier-Stokes Equations. *Comp. Meth. Appl. Mech. Engnrg.*, 1982, vol. 32, pp.199-259.

[12] Cann P. M., Hutchinson J. and Spikes H. A. – The Development of a Spacer Layer Imaging Method (SLIM) for Mapping Elastohydrodynamic Contacts. *STLE Tribology Transactions*, 1996, vol. 39, pp. 915-921.

[13] Cann P. M. and Spikes H. A. – Film Thickness Measurements of Greases under Normally Starved conditions. *NLGI Spokesman*, 1992, vol. 56, pp. 21-26.

[14] Cann P. M. and Spikes H. A. – Thin Film Optical Interferometry in the Study of Grease Lubrication in a Rolling Point Contact. *Acta Tribologica*, 1994, vol. 2, n° 1, pp. 45-50.

[15] Carreau P. J. - Rheological Equations from Molecular Network Theories. *Trans. Soc. Rheol.*, 1972, vol. 16 (1), pp. 99-127.

[16] Cheng H. S. and Sternlicht B. - A Numerical Solution for the Pressure, Temperature and Film Thickness Between Two Infinitely Long, Lubricated Rolling and Sliding Cylinders, Under Heavy Loads, *ASME J. Basic. Eng.*, 1965, vol. 87, pp. 695-707.

[17] Cheng H. S. - A Refined Solution to the Thermal-Elastohydrodynamic Lubrication of Rolling and Sliding Cylinders. *ASLE Trans.*, 1965, vol. 8, pp. 397-410.

[18] Chittenden R. J., Dowson D., Dunn J. F. and Taylor C. M. – A Theoretical Analysis of the Isothermal Elastohydrodynamic Lubrication of concentrated contacts. II: General Case with Lubricant Entrainment along either Principal Axis of the Hertzian Contact Ellipse or at some Intermediate angle. *Proceedings of the Royal Society of London*, 1985, vol. A 397, pp. 271-294.

[19] Chiu Y. P. and Sibley L. B. – Contact Shape and Non-Newtonian Effects in Elastohydrodynamic Point Contact. *ASLE Transactions*, 1972, vol. 28, pp. 48-60.

[20] Cook R. L., King H. E., Herbst C. A. and Herschback D. R. - Pressure and Temperature Dependent Viscosity of Two Glass Forming Liquids: Glycerol and Dibutyl Phthalate, *J. Chem. Phys.*, 1994, vol. 100 (7), pp. 5178-5189.

[21] Doolittle A. K. - Studies in Newtonian Flow II, The Dependence of the Viscosity of Liquids on Free-Space, *J. Appl. Phys.*,1951, vol. 22, pp. 1471-1475.

[22] Dowson D. and Higginson G. R. – A Numerical Solution of the Elastohydrodynamic Problem. *J. Mech. Eng. Sci.*, 1959, vol. 1, n° 1, pp. 6-15.

[23] Dowson D. and Higginson G. R. – Elastohydrodynamic Lubrication. The Fundamental of Roller and Gear Lubrication, *Oxford, Pergamon* (1966).

[24] Ertel A. M. – In Russian (Hydrodynamic Lubrication Based on New Principles). *Akad. Nauk SSSR Prikadnaya Mathematica i Mekhanika*, 1939, vol. 3, n° 2, pp. 41-52.

[25] Evans H. P. and Snidle R. W. – The Isothermal Elastohydrodynamic Lubrication of Spheres. *ASME J. of Lubr. Techn.*, 1981, vol. 103, pp. 547-557.

[26] Evans H. P. and Snidle R. W. – Inverse Solution of Reynolds' Equation of Lubrication under Point Contact Elastohydrodynamic conditions. *ASME J. of Lubr. Techn.*, 1981, vol. 103, pp. 539-546.

[27] Evans H. P. and Hughes T. G. – Evaluation of Deflection in Semi-Infinite Bodies by a Differential Method. *Proc. IMechE J. Mech. Engnrng. Sc.*, 2000, Part C, vol. 214, pp. 563-584.

[28] Eyring H. - Viscosity, Plasticity and Diffusion as Examples of Absolute Reaction Rates. *J. Chem. Phys.*, 1936, vol. 4, pp. 283-291.

[29] Ferry J. D. – Viscoelastic Properties of Polymers. *John Wiley & Sons Inc.*, New York, 1961.

[30] Foord C. A., Hammam W. E. and Cameron A. – Evaluation of Lubricants using Optical Elastohydrodynamics. *ASLE Transactions*, 1968, vol. 11, pp.31-43.

[31] Fox I. E. – Numerical Evaluation of the Potential for Fuel Economy Improvement due to Boundary Friction Reduction within Heavy-Duty Diesel Engines. *Tribology International*, 2005, vol. 38, pp. 265-275.

[32] Frêne J., Arghir M. and Constantinescu V. – Combined Thin-Film and Navier-Stokes Analysis in High Reynolds Number Lubrication. *Tribology International*, 2006, vol. 39, pp. 734-747.

[33] Galeão A. C., Almeida R. C., Malta S. M. C. and Loula A. F. D. - Finite Element Analysis of Convection Dominated Reaction-Diffusion Problems. *Appl. Num. Math.*, 2004, vol. 48, pp. 205-222.

[34] Gecim B. and Winer W. O. – Lubricant Limiting Shear Stress Effect on EHD Film Thickness. *ASME J. of Lubr. Techn.*, 1980, vol. 102, pp. 213-221.

[35] Georges J. M., Millot S., Loubet J. L. and Tonck A. – Drainage of Thin Liquid Films Between Relatively Smooth Surfaces. *J. Chem. Phys.*, 1993, vol. 98, pp. 7345-7360.

[36] Gohar R. – Oil Film Thickness and Rolling Friction in Elastohydrodynamic Point Contact. *ASME J. of Lubr. Techn.*, 1971, vol. 93, pp. 371-382.

[37] Gohar R. and Cameron A. – The Mapping of Elastohydrodynamic Contacts. *ASLE Transactions*, 1967, vol. 10. pp. 215-225.

[38] Granick S. – Motions and Relaxations of Confined Liquids. *Science*, 1991, vol. 253, n° 5026, pp. 1374-1379.

[39] Grubin A. N. and Vinogradova I. E. – In Russian (Investigation of the contact of machine components), Moscow: Kh. F. Ketova, 1949, *Central Scientific Research Institute for Technology and Mechanical Engineering*, vol. 30.

[40] Guangteng G. and Spikes H. A. – Boundary Film Formation by Lubricant Base Fluids. *Tribology Transactions*, 1996, vol. 39, n° 2, pp. 448-454.

[41] Guangteng G. and Spikes H. A. – Fractionation of Liquid Lubricants at Solid Surfaces. *Wear*, 1996, vol. 200, pp. 336-345.

[42] Guangteng G., Cann P. M. and Spikes H. A. – A Study of Parched Lubrication, *Wear*, 1992, vol. 153, pp. 91-105.

[43] Guo F., Yang P. and Qu S. - On the Theory of Thermal Elastohydrodynamic Lubrication at High Slide-Roll Ratios – Circular Glass-Steel Contact Solution at Opposite Sliding. *ASME J. of Tribol.*, 2001, vol. 123, pp. 816-821.

[44] Gümbel L. – Uber geschmierte Arbeitsräder. *Z. Ges. Turbinenwiesen*, 1916, n° 13, p. 357.

[45] Hamrock B. J. and Dowson D. – Isothermal Elastohydrodynamic Lubrication of Contacts, Part I – Theoretical Formulation. *ASME J. of Lubr. Techn.*, 1976, vol. 98, n° 2, pp. 223-229.

[46] Hamrock B. J. and Dowson D. – Isothermal Elastohydrodynamic Lubrication of Point Contacts, Part II – Ellipticity Parameter Results. *ASME J. of Lubr. Techn.*, 1976, vol. 98, n° 3, pp. 375-383.

[47] Hamrock B. J. and Dowson D. – Isothermal Elastohydrodynamic Lubrication of Point Contacts, Part III – Fully Flooded Results. *ASME J. of Lubr. Techn.*, 1977, vol. 99, n° 2, pp. 264-276.

[48] Hamrock B. J. and Dowson D. – Isothermal Elastohydrodynamic Lubrication of Point Contacts, Part IV – Starvation Results. *ASME J. of Lubr. Techn.*, 1977, vol. 99, n° 1, pp. 15-23.

[49] Harrison G. – The Dynamic Properties of Supercooled Liquids. *Academic Press Inc. Ltd*, London, 1976.

[50] Hartinger M., Gosman D., Ioannides S. and Spikes H. – Two- and Three-Dimensional CFD Modelling of Elastohydrodynamic Lubrication. *Proc. 34th Leeds-Lyon Symp. Trib.*, 2007 (Lyon, France).

[51] Hertz H. – Uber die Berührung fester Elastischer Körper. *J. reine und angew. Math.*, 1881, vol. 92, pp. 156-171.

[52] Hirn G. - Sur les principaux phénomènes qui présentent les frottements Médiats. *Bull. Soc. Ind. Mulhouse*, 1854, vol. 26, pp. 188-277.

[53] Hirschfelder J. O., Curtiss C. F., and Bird R. B. - Molecular Theory of Gases and Liquids, *Wiley*, New York (1954).

[54] Hogenboom D. L., Webb W. and Dixon J. D. - Viscosity of Several Liquid Hydrocarbons as a Function of Temperature, Pressure and Free Volume, *J. Chem. Phys.*, 1967, vol. 46 (7), pp. 2586-2598.

[55] Holmes M. J. A., Evans H. P., Hughes T.G. and Snidle R. W. – Transient Elastohydrodynamic Point Contact Analysis using a New Coupled Differential Deflection Method. Part I: Theory and Validation. *Proc. IMechE J. Engnrng. Trib.*, 2003, Part J, vol. 217, pp. 289-303.

[56] Holmes M. J. A., Evans H. P., Hughes T.G. and Snidle R. W. – Transient Elastohydrodynamic Point Contact Analysis using a New Coupled Differential Deflection Method. Part II: Results. *Proc. IMechE J. Engnrng. Trib.*, 2003, Part J, vol. 217, pp. 305-321.

[57] Houpert L. G. and Hamrock B. J. – Fast Approach for Calculating Film Thicknesses and Pressures in Elastohydrodynamically Lubricated Contacts at High Loads. *ASME J. of Tribol.*, 1986, vol. 108, pp. 411-420.

[58] Hsiao H. S. S., Hamrock B. J. and Tripp J. H. – Finite Element System Approach to EHL of Elliptical Contacts: Part I – Isothermal Circular Non-Newtonian Formulation. *ASME J. of Tribol.*, 1998, vol. 120, pp. 695-704.

[59] Huebner K. H., Dewhirst D. L., Smith D. E. and Byrom T. G. – The Finite Element Method for Engineers, Fourth Edition. *Wiley*, New York, 2001.

[60] Hughes T. G., Elcoate C. D. and Evans H. P. – A Novel Method for Integrating First- and Second-Order Differential Equations in Elastohydrodynamic Lubrication for the Solution of Smooth Isothermal, Line Contact Problems. *Int. J. Num. Meth. Engnrng.*, 1999, vol. 44, pp. 1099-1113.

[61] Hughes T. G., Elcoate C. D. and Evans H. P. – Coupled Solution of the Elastohydrodynamic Line Contact Problem Using a Differential Deflection Method. *Proc. IMechE J. Mech. Engnrng. Sc.*, 2000, Part C, vol. 214, pp. 585-598.

[62] Hughes T. J. R. – The Finite Element Method: Linear Static and Dynamic Finite element Analysis. *Dover*, New York, 2000.

[63] Hughes T. J. R., Franca L. P. and Hulbert G. M. - A New Finite Element Formulation for Computational Fluid Dynamics: VII. The Galerkin-Least-Squares Method for Advective-Diffusive Equations. *Comp. Meth. Appl. Mech. Engnrg.*, 1989, vol. 73, pp. 173-189.

[64] Hughes T. J. R. - Multiscale Phenomena: Green's Functions, the Dirichlet-to-Neumann Formulation, Subgrid Scale Models, Bubbles and the Origins of Stabilized Methods. *Comp. Meth. Appl. Mech. Engnrg.*, 1995, vol. 127, pp.387-401.

[65] Jiang X., Wong P. L. and Zhang Z. – Thermal Non-Newtonian EHL Analysis of Rib-Roller End Contact in Tapered Roller Bearings. *ASME J. of Tribol.*, 1995, vol. 117, pp. 646-654.

[66] Johnson C., Nävert U. and Pitkäranta J. – Finite Element Methods for Linear Hyperbolic Problems. *Comp. Meth. Appl. Mech. Engnrng.*, 1984, vol. 45, pp. 285-312.

[67] Johnson C. and Pitkäranta J. – An Analysis of the Discontinuous Galerkin Method for a Scalar Hyperbolic Equation. *Math. Comput.*, 1986, vol. 46, pp. 1-26.

[68] Ju Y. and Farris T. N. – Spectral Analysis of Two-Dimensional Contact Problems. *ASME J. of Tribol.*, 1996, vol. 118, pp. 320-328.

[69] Jubault I., Molimard J., Lubrecht A. A., Mansot J. L. and Vergne P. - In Situ Pressure and Film Thickness Measurements in Rolling / Sliding Lubricated Point Contacts. *Tribology Letters*, 2003, vol. 15 (4), pp. 421-429.

[70] Kaneta M., Shigeta T. and Yang P. – Film Pressure Distributions in Point Contacts Predicted by Thermal EHL Analysis. *Tribology International*, 2006, vol. 39, n° 8, pp. 812-819.

[71] Kazama T., Ehret P. and Taylor C. M. – On the Effects of the Temperature Profile Approximation in the Thermal Newtonian Solutions of Elastohydrodynamic Line Contacts. *Proc. IMechE. J. Engnrng. Tribol.*, 2001, Part J., vol. 215, pp. 109-120.

[72] Kim K. H. and Sadeghi F. - Three-Dimensional Temperature Distribution in EHD Lubrication: Part I – Circular Contact, *ASME J. of Tribol.*, 1992, vol. 114, pp. 32-41.

[73] Kim H. J., Ehret P., Dowson D. and Taylor C. M. - Thermal Elastohydrodynamic Analysis of Circular Contacts, Part 1: Newtonian Model, *Proc. IMechE. J. Engnrng. Tribol.,* 2001, Part J., vol. 215, pp. 339-352.

[74] Kim H. J., Ehret P., Dowson D. and Taylor C. M. - Thermal Elastohydrodynamic Analysis of Circular Contacts, Part 2: Non-Newtonian Model, *Proc. IMechE. J. Engnrng. Tribol.,* 2001, Part J., vol. 215, pp. 353-362.

[75] Kingsbury A. – Experiments with an air-lubricated journal. *J. Am. Soc. Nav. Engrs.*, 1897, vol. 9, pp. 267-292.

[76] Kweh C. C., Evans H. P. and Snidle R.W. – Elastohydrodynamic Lubrication of Heavily Loaded Circular Contacts. *Proc. IMechE*, 1989, vol. 203, pp. 133-148.

[77] Lee R. T., Hsu C. H. and Kuo W. F. – Multilevel Solution for Thermal Elastohydrodynamic Lubrication of Rolling-Sliding Circular Contacts. *Tribology International*, 1995, vol. 28, pp. 541-552.

[78] Lide D. R. - CRC Handbook of Chemistry and Physics, 85th edition, *CRC press*, Boca Raton-Florida, 2004-2005.

[79] Lin T. R. and Lin J. F. – Thermal Effects in Elastohydrodynamic Lubrication of Line Contacts Using a Non-Newtonian Lubricant. *Tribology International*, 1991, vol. 24, n° 6, pp. 365-372.

[80] Liu X., Jiang M., Yang P. and Kaneta M. - Non-Newtonian Thermal Analyses of Point EHL Contacts Using the Eyring Model. *ASME J. of Tribol.*, 2005, vol. 127, pp. 70-81.

[81] Love A. E. H. – A treatise on the Mathematical Theory of Elasticity, 4th edition. *Dover*, New York, 1944.

[82] Lu H., Berzins M., Goodyer C. E. and Jimack P. K. – High Order Discontinuous Galerkin Method for Elastohydrodynamic Lubrication Line Contact Problems. *Comm. Num. Meth. Engnrng.*, 2005, vol. 21 (11), pp. 643-650.

[83] Lu H., Berzins M., Goodyer C. E., Jimack P. K. and Walkley M. – Adaptive High-Order Finite Element Solution of Transient Elastohydrodynamic Lubrication Problems. *Proc. IMechE J. Engnrng. Trib.*, 2006, Part J., vol. 220, pp. 215-225.

[84] Lubrecht A.A. – The Numerical Solution of the Elastohydrodynamically Lubricated Line and Point Contact Problem Using Multigrid Techniques. *PhD Thesis*, University of Twente, Enschede, The Netherlands, 1987.

[85] Lubrecht A.A., ten Napel W. E. and Bosma R. – Multigrid, an Alternative Method for Calculating Film Thickness and Pressure Profiles in Elastohydrodynamically Lubricated Line Contacts. *ASME, J. of Tribol.*, 1986, vol.108, pp. 551-556.

[86] Martin H. M. – Lubrication of gear teeth. *Engineering (London)*, 1916, vol. 102, pp. 119-121.

[87] Matsuoka H. and Kato T. – An Ultrathin Liquid Film Lubrication Theory – Calculation Method of Solvation Pressure and its Application to the EHL Problem. *ASME J. of Tribol.*, 1997, vol. 119, pp. 217-226.

[88] Matsuoka H. and Kato T. – Experimental Study of Ultrathin Liquid Lubrication Film Thickness at the Molecular Scale. *Proc. IMechE J. Engnrng. Trib.*, 1997, Part J, vol. 211, pp. 139-150.

[89] Michell A. – Lubrication of plane surfaces. *Zeit. Math. Phys.*, 1905, vol. 52, n° 2, pp.123-137.

[90] Moes H. – Optimum Similarity Analysis with Applications to Elastohydrodynamic Lubrication. *Wear*, 1992, vol. 159, pp. 57-66.

[91] Najji B., Bou-Said B. and Berthe D. – New Formulation for Lubrication with Non-Newtonian Fluids. *ASME J. of Tribol.*, 1989, vol.111, pp. 29-33.

[92] Nijenbanning G., Venner C. H. and Moes H. – Film Thickness in Elastohydrodynamically Lubricated Elliptic Contacts. *Wear*, 1994, vol. 176, pp. 217-229.

[93] Oh K. P. and Rohde S. M. – Numerical Solution of the Point Contact Problem Using the Finite Element Method. *Int. J. Num. Meth. Engnrng.*, 1977, vol.11, pp. 1507-1518.

[94] Okamura H. – A Contribution to the Numerical Analysis of Isothermal Elastohydrodynamic Lubrication. *Proc. 9th Leeds-Lyon Symp. Trib.*, 1982 (Leeds, UK).

[95] Oñate E. – Derivation of Stabilized Equations for Numerical Solution of Advective-Diffusive Transport and Fluid Flow Problems. *Comp. Meth. Appl. Mech. Engnrng.*, 1998, vol. 151, pp. 233-265.

[96] Petrov N. P. – In Russian (Friction in machine and effect of the lubricant). *Inzh. Zh., St-Peterb.*, 1883, vol. 1, pp.71-140.

[97] Petrusevich A. I. – In Russian (Fundamental Conclusions from the Hydrodynamic Contact Theory of Lubrication). *Izv. Akad. Nauk. SSSR (OTN)*, 1951, vol. 2, p. 209.

[98] Ranger A. P., Ettles C. M. and Cameron A. – The Solution of the Point Contact Elastohydrodynamic Problem. *Proc. Roy. Soc. London*, 1975, vol. 346 (A), pp. 229-244.

[99] Reynolds O. – On The Theory of the Lubrication and its Application to Mr Beauchamp Tower's Experiments, Including an Experimental Determination of the Viscosity of Olive Oil. *Phil. Trans. R. Soc.*, 1886, vol. 177, pp.157-234.

[100] Roelands C. J. A. - Correlational Aspects of the Viscosity-Temperature-Pressure Relationship of Lubricating Oils, *PhD Thesis*, Technische Hogeschool Delft, The Netherlands (1966).

[101] Rohde S. M. and Oh K. P. – A Unified Treatment of Thick and Thin Film Elastohydrodynamic Problems by Using Higher Order Element Methods. *Proc. Roy. Soc. London*, 1975, Part A, vol. 343, pp. 315-331.

[102] Safa M. M. A. – Elastohydrodynamic Studies Using Thin Film Transducers. *PhD Thesis*, Imperial College of Science and Technology, London, 1982.

[103] Safa M. M. A., Anderson J. C. and Leather J. A. – Transducers for Pressure, Temperature and Oil Film Thickness Measurement in Bearings. *Sensors and Actuators*, vol. 3, pp. 119-128, 1982.

[104] Salehizadeh H. and Saka N. – Thermal Non-Newtonian Elastohydrodynamic Lubrication of Rolling Line Contacts. *ASME J. of Tribol.*, 1991, vol. 113, pp. 481-491.

[105] Seabra J. and Berthe D. – Elastohydrodynamic Point Contacts. Part I: Formulation and numerical Solution. *Wear*, 1989, vol. 130, pp. 301-318.

[106] Seabra J. and Berthe D. – Elastohydrodynamic Point Contacts. Part II: Influence of Surface Speeds, Surface Waviness and Load on the Contact Behaviour. *Wear*, 1989, vol. 130, pp. 319-335.

[107] Tevaarrwerk J. L. and Johnson K. L. – A Simple Non-Linear Constitutive Equation for Elastohydrodynamic oil Films. *Wear*, 1975, vol. 35, pp. 345-356.

[108] Tevaarrwerk J. L. and Johnson K. L. – The Influence of Fluid Rheology on the performance of Traction Drives. *ASME J. of Lubr. Techn.*, 1979, vol. 101, pp. 266-274.

[109] Tichy J. A. – Modeling of Thin Film Lubrication. *STLE Tribol. Trans.*, 1995, vol. 38, pp. 108-118.

[110] Tichy J. A. – A Surface Layer Model for Thin Film Lubrication. *STLE Tribol. Trans.*, 1995, vol. 38, pp. 577-582.

[111] Tower B. - First Report on Friction Experiments (Friction of Lubricated Bearings). *Proc. Instn. Mech. Engrs.*, 1883, pp. 632-659.

[112] Venner C. H. – Multilevel Solution of the EHL Line and Point Contact Problems. *PhD Thesis*, University of Twente, Enschede, The Netherlands, 1991.

[113] Venner C. H. and ten Napel W. E. – Multilevel Solution of the Elastohydrodynamically Lubricated Circular Contact Problem. Part I: Theory and Numerical Algorithm. *Wear*, 1992, vol. 152, pp. 351-367.

[114] Venner C. H. and ten Napel W. E. – Multilevel Solution of the Elastohydrodynamically Lubricated Circular Contact Problem. Part II: Smooth Surface Results. *Wear*, 1992, vol. 152, pp. 369-381.

[115] Venner C. H. and Lubrecht A. A. - Multilevel Methods in Lubrication. *Tribology Series (37)*, *Elsevier*, Amsterdam, 2000.

[116] Vergne P. – (In French) « Comportement Rhéologique des Lubrifiants et Lubrification: Approches Expériméntales ». *HDR Thesis*, INSA de Lyon, Lyon, France, 2002.

[117] Wang W. Z., Wang H., Liu Y. C., Hu Y. Z. and Zhu D. – A Comparative Study of the Methods for Calculation of Surface Elastic Deformation. *Proc. IMechE J. Engnrng. Trib.*, 2003, Part J., vol. 217, pp. 145-153.

[118] Wang Y., Li H., Tong J. and Yang P. – Transient Thermoelastohydrodynamic Lubrication Analysis of an Involute Spur Gear. *Tribology International*, 2004, vol. 37, pp. 773-782.

[119] Wedeven L. D., Evans D. and Cameron A. – Optical Analysis of Ball Bearing Starvation. *ASME J. of Lubr. Techn.*, 1971, vol. 93, pp. 349-363.

[120] Wolff R. and Kubo A. – The Application of Newton-Raphson Method to Thermal Elastohydrodynamic Lubrication of Line Contacts. *ASME J. of Tribol.*, 1994, vol. 116, pp. 733-740.

[121] Wu S. R. – A Penalty Formulation and Numerical Approximation of the Reynolds-Hertz Problem of Elastohydrodynamic Lubrication. *Int. J. Engnrng. Sci.*, 1986, vol. 24 (6), pp. 1001-1013.

[122] Yang P. and Wen S. - A Generalized Reynolds Equation for Non-Newtonian Thermal Elastohydrodynamic Lubrication. *ASME J. of Tribol.*, 1990, vol. 112, pp. 631-636.

[123] Yasutomi S., Bair S. and Winer W. O. - An Application of a Free-Volume Model to Lubricant Rheology, (1) Dependence of Viscosity on Temperature and Pressure. *ASME J. of Tribol.*, 1984, vol. 106, pp. 291-312.

[124] Yiping H., Darong C., Xianmei K. and Jiadao W. – Model of Fluid-Structure Interaction and its Application to Elastohydrodynamic Lubrication. *Comp. Meth. Appl. Mech. Engnrng.*, 2002, vol. 191, pp. 4231-4240.

[125] Zhu D. and Wen S. - A Full Numerical Solution for the Thermo-Elastohydrodynamic problem in Elliptical Contacts, *ASME J. of Tribol.*, 1984, vol. 106, pp. 246-254.

[126] Zienkiewicz O. C. and Taylor R. L. – The Finite Element Method. Volume1: The Basis, 5th Edition. *Butterworth & Heinemann*, England, 2000.

[127] Zienkiewicz O. C. and Taylor R. L. - The Finite Element Method, Volume 3, Fluid Dynamics, 5th edition", *Butterworth & Heinmann*, England, 2000.

FOLIO ADMINISTRATIF

THESE SOUTENUE DEVANT L'INSTITUT NATIONAL DES SCIENCES APPLIQUEES DE LYON

NOM : HABCHI DATE de SOUTENANCE : 1er Juillet 2008
(avec précision du nom de jeune fille, le cas échéant)

Prénoms : Wassim

TITRE : A Full-System Finite Element Approach to Elastohydrodynamic Lubrication Problems : Application to Ultra-Low-Viscosity Fluids

NATURE : Doctorat Numéro d'ordre : 2008-ISAL-0038

Ecole doctorale : MEGA

Spécialité : Mécanique

Cote B.I.U. - Lyon : T 50/210/19 / et bis CLASSE :

RESUME : Cette thèse présente un modèle éléments finis avec couplage fort des problèmes de lubrification élastohydrodynamique (EHD).La lubrification EHD consiste en une séparation complète des surfaces par un film complet de lubrifiant dans lequel est générée une pression suffisemment élevée pour engendrer une déformation élastique significative des surfaces. Ainsi, un couplage fort entre les effets hydrodynamiques et les effets élastiques s'établit. Le système non-linéiare formé par les équations de Reynolds, d'élasticité linéaire, et d'équilibre des charges est résolu de manière couplée par une approche de type Newton-Raphson. Cette approche permet d'avoir de très bons taux de convergence par rapport à l'approche classique avec couplage faible. Le problème de frontière libre de cavitation à la sortie du contact est traité par le biais d'une méthode de pénalisation. Des formulations de stabilisation appropriées sont utilisées pour étendre la résolution à des cas de contacts fortement chargés. Ensuite, le comportement non-Newtonien du lubrifiant et les effets thermiques sont pris en compte. Le modèle développé est utilisé pour étudier l'utilisation des Fluides de Très Faible Viscosité dans les contacts EHD. L'utilisation des tels fluides en tant que lubrifiants offre deux avantages principaux : tout d'abord, la dissipation d'énergie dans le contact par frottement est réduite et ensuite, dans le cadre de machines qui opèrent avec un fluide de fonction (généralement de faible viscosité) et un lubrifiant, le premier pourrait être utilisé pour remplir les deux fonctions. Cela permettrait une conception et une maintenance plus faciles de la machine en plus d'une amélioration de ses performances.

MOTS-CLES : Lubrification EHD, éléments finis nonlinéiares couplés, lubrifiants à très faible viscosité.

Laboratoire (s) de recherche : Laboratoire de mécanique des Contacts et des Structures (LaMCoS)

Directeur de thèse: Dr. Philippe Vergne

Président de jury : Pr. D. Dureisseix

Composition du jury :

Président	D. Dureisseix	Professeur (Université Montpellier II)
Rapporteur	H.P. Evans	Professeur (Cardiff University U.K.)
Co-directeur	D. Eyheramendy	Professeur (E. C. de Marseille)
	G. Morales-Espejel	Ingénieur de recherche PhD (SKF ERC – Pays-Bas)
Rapporteur	D. J. Schipper	Professeur (University of Twente – Pays-Bas)
Directeur	P. Vergne	Directeur dde recherche (CNRS – INSA de Lyon)